Journal of Polymer Science and Engineering

EnPress Publisher

JPSE

2 2024
Volume 7
Issue 2

https://systems.enpress-publisher.com/index.php/JPSE

Gholamhossein Sodeifian
University of Kashan
Iran

Tulio Hallak Panzera
Federal University of São João del Rei
Brazil

Hassan Mohamed El-Dessouky
University of Sheffield
United Kingdom

Wai Fen Yong
Xiamen University Malaysia
Malaysia

Manoj Kumar Gupta
Motilal Nehru National Institute of Technology
India

Aditya Narayan Singh
Ulsan National Institute of Science and Technology
Korea

Jihong Sun
Beijing University of Technology
China

Kishore Debnath
NIT Meghalaya
India

Jin-Hae Chang
Kumoh National Institute of Technology
Korea

Xiaoxuan Liu
Guangdong University of Technology
China

Murat Ates
Tekirdag Namik Kemal University
Turkey

Micaela Vannini
University of Bologna
Italy

Kinsuk Naskar
Indian Institute of Technology
India

Kalim Deshmukh
University of West Bohemia
Czech Republic

Long Zhang
Changchun University of Technology
China

Jude Onwuegbu Iroh
University of Cincinnati
United States

Sung Ting Sam
Universiti Malaysia Perlis
Malaysia

Ramiro Guerrero-Santos
Centro de Investifacion en Quimica Aplicada
Mexico

Koramala Naveen Kumar
Yeungnam University
Korea

Mohammad Gulham Haider Zaidi
Govind Ballabh Pant University of Agriculture and Technology
India

Jincai Su
Ngee Ann Polytechnic
Singapore

Volume 7 Issue 2·2024

Journal of Polymer Science and Engineering

Editor-in-Chief

Prof. Dr. Nehad Ali Shah

Sejong University, Korea

EnPress Publisher

2024 | Volume 7 | Issue 2

Journal of Polymer Science and Engineering

https://systems.enpress-publisher.com/index.php/JPSE

Contents

Articles

Reviews

Journal of Polymer Science and Engineering 2024, 7(2), 6086.
https://doi.org/10.24294/jpse.v7i2.6086

Article

Calculation of elastic tensile behavior of CF/PA6 composite material disc

Hüseyin Fırat Kayiran

Agriculture and Rural Development Support Institution, Mersin 33190, Turkey; huseyinfirat.kayiran@tkdk.gov.tr

CITATION

Kayiran HF. Calculation of elastic tensile behavior of CF/PA6 composite material disc. Journal of Polymer Science and Engineering. 2024; 7(2): 6086. https://doi.org/10.24294/jpse.v7i2.6086

ARTICLE INFO

Received: 28 April 2024
Accepted: 31 May 2024
Available online: 17 July 2024

Abstract: In this paper, the characteristic behavior of the disc consisting of thermoplastic composite CF/PA6 material was considered. Analysis was made by taking into account the usage areas of the materials and referring to certain temperatures between 30 ℃ and 150 ℃. Composite materials are lightweight; they show high strength. For these reasons, they are preferred in technology, especially in the aircraft and aerospace industry. With this study, the radial and tangential stresses determined within a certain temperature The temperatures were determined and compared with previous studies in the literature. According to the results obtained, it is believed that the thermoplastic composite CF/PA6 disc design can be used in engineering.

Keywords: elastic stress; thermoplastic composite; elastisite modulus; temperature; disc

1. Introduction

The behavior of stresses in the disc based on the CF/PA6 material has been studied numerically. In the study, disk materials were determined by taking into account the optimum temperatures after a literature review. As it is known, composite materials are lightweight; they show high strength. For these reasons, they are preferred in technology, especially in the aircraft and aerospace industry. With this study, the radial and tangential stresses determined within a certain temperature The results obtained were compared with the studies conducted by different authors previously. According to the results obtained, thermoplastic composite CF/PA6 disc design is considered to be usable in engineering. Composite materials consist of two different material compositions and have new properties. Decomposed property. We can see thermoplastics, especially composite materials, everywhere with today's technology. These materials are advantageous in terms of their mechanical properties when combined with the designed parts; the stress sensitivity needs to be known, and they are also bendable and ductile. The numerically obtained results are in accordance with the literature. Materials science is very important in today's technologies. Materials are almost the constitution of machine parts. Knowing the stresses of materials and material parts against temperature is of great importance in the advancement of material technology. In the literature review, it has been seen that stress analyses of different disk materials have been performed, but the adaptation of these studies to the newly used materials today is considered incomplete. The thermal stress behavior of a circular disc used in brakes has been studied by two different methods. The results are shared with the graphs; it has been seen that the margin of error obtained in analytical and numerical results is very small [1]. In another study, the behavior of the preferred discs in automobile braking systems in the friction environment has been studied [2]. In another study, the interpretation and stress behavior of the disks used in railway systems have been investigated by means of a computer program [3]. In another study, the behavior of a circular disk subjected to friction against temperature has been studied [4]. In the other two studies, the stresses occurring on disks with different materials were examined and compared with other results obtained in the literature. It has been clearly observed that the results obtained at the end of the disc materials show different mechanical properties are completely different from each other; the stresses change with temperature [5,6] again in different studies. The mechanical behaviors and thermal conduction occurring in a layered disk modeled in the form of rings have been investigated. In addition, the stresses occurring on disks consisting of different layers have been analyzed [7,8].

2. Materials and methods

The materials of the discs have been specially researched. The plane stress has been treated as zero. The modeled disk is shown in **Figure 1** below [9].

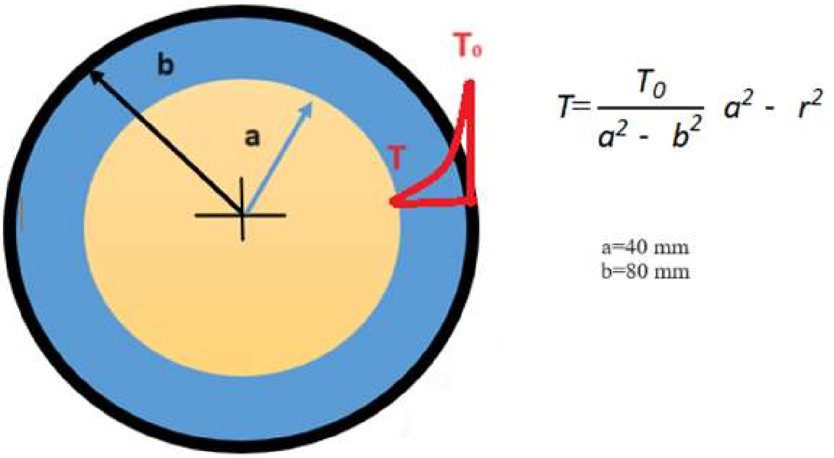

Figure 1. CF/PA6 composite composite disc.

$$\frac{r(d\sigma_r)_i}{dr} + (\sigma_r)_i - (\sigma_\theta)_i = 0 \qquad (i = 1) \tag{1}$$

As can be seen in the formulas; r can be called the disk radius. The different stresses that occur are given below.

$$\varepsilon_r = \frac{du}{dr} = a_{rr}\sigma_r + a_{r\theta}\sigma_\theta \tag{2}$$

$$\varepsilon_{\theta i} = \frac{u}{r} = a_{r\theta}\sigma_r + a_{\theta\theta}\sigma_\theta \tag{3}$$

By establishing a relationship between the general equation and the function F, Equation (4) is derived below.

$$a_{\theta\theta}r^2\frac{d^2F}{dr^2} + a_{\theta\theta}r\frac{dF}{dr} - a_{rr}F = -\alpha_\theta r^2\frac{dT}{dr} + \alpha_r Tr - \alpha_\theta Tr \tag{4}$$

In an environment where the temperature increases parabolically from the inside out; T_0 is the symbol of the first temperature on the disk. Tr symbolizes the temperature that occurs at any regional point on the disk.

$$T = \frac{T_0}{a^2 - b^2}(a^2 - r^2) \tag{5}$$

For the solution of equations in general:

$$\sigma_r = \frac{F}{r} = C_1 r^{k-1} + C_2 r^{-k-1} + Ar^2 + C \tag{6}$$

$$\sigma_{\theta i} = \frac{dF}{dr} = kC_1 r^{k-1} + kC_2 r^{-k-1} + 3Ar^2 + C \tag{7}$$

By reference to the constants A and C "λ" and k, the general stress equations arise.

$$A = \lambda \frac{3(\alpha_\theta - \alpha_r)}{a_{\theta\theta}(9 - k^2)} \tag{8}$$

$$C = \lambda \frac{(\alpha_r - \alpha_\theta) b^2}{a_{\theta\theta}(1 - k^2)} \tag{9}$$

$$\lambda = \frac{T_0}{(b^2 - a^{2)}} \tag{10}$$

$$k^2 = \frac{a_{rr}}{a_{\theta\theta}} \tag{11}$$

$$C_1 = \frac{Aa^{k+3} + Ca^{k+1} - Ab^{k+3} - Cb^{k+1}}{(b^{2k} - a^{2k)}} \tag{12}$$

$$C_2 = -C_1 a^{2k} - Aa^{k+3} - Ca^{k+1} \tag{13}$$

Thermal stresses analysis

The disc with CF/PA6 material is fixed. The inner radius and outer radius of the disk have been determined. The temperature shows a parabolic increase from the inner to the outer part. The disk modeled by the ANSYS finite element program is given in **Figure 2** below.

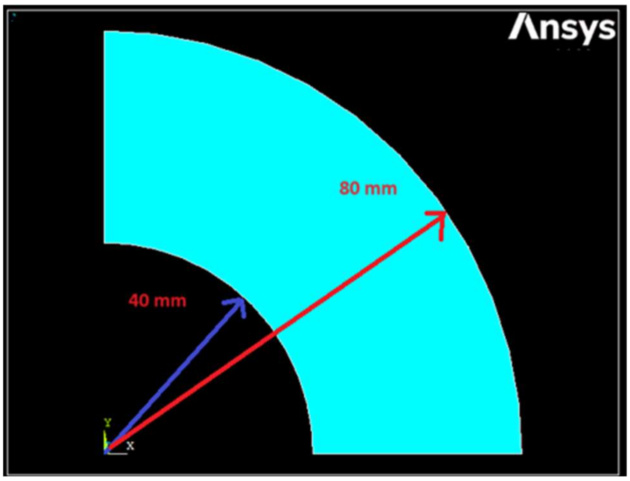

Figure 2. Disk modeling with ANSYS program.

The modulus of elasticity and other properties of CF/PA6 composite material are given in **Table 1**.

Table 1. Mechanical properties of CF/PA6 composite material [10–12].

E_θ	E_r	k	α_r	α_θ	$\upsilon_{\theta r}$
230	15	3.91	8×10^{-6}	2.8×10^{-6}	0.37

The stress values obtained at the end of the numerical analysis of the circular disc with CF/PA6 material are shown in **Table 2** below. Tangential stresses have compression intensity in the inner region and tensile intensity in the outer region.

Table 2. Numerical analysis of circular discs with CF/PA6 material.

Temperature ΔT (°C)	Surface	Tangential Stress (MPa)	Radial Stress (MPa)
30	Inner	4.47	0
	Outer	–7.34	0
60	Inner	8.94	0
	Outer	–14.69	0
90	Inner	13.40	0
	Outer	–22.03	0
120	Inner	17.88	0
	Outer	–29.37	0
150	Inner	22.34	0
	Outer	–36.72	0

Figure 3 below is the stress graph that occurs at the end of the analysis.

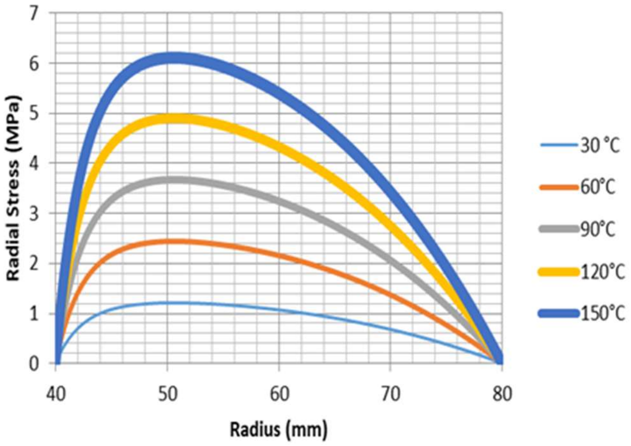

Figure 3. Stress graph of CF/PA6 composite material disc (in the radial direction).

In **Figure 3**, the stresses that occur in the radial direction increase from the inner part of the disk to the outside. It decreases from the middle part towards the end zone.

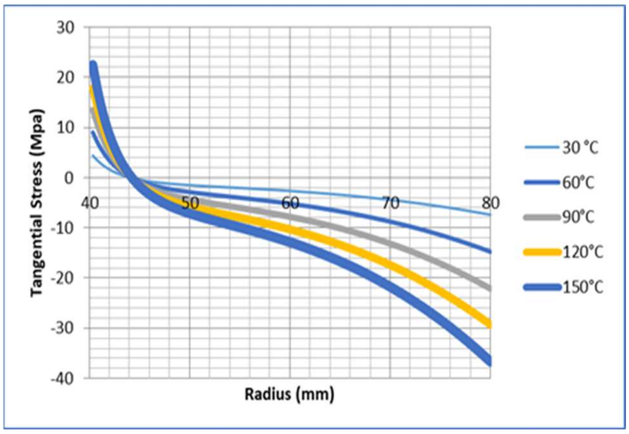

Figure 4. Stress graph of CF/PA6 composite material disc (in the tangential direction).

The radial stresses calculated for the disc modeled with CF/PA6 were determined as zero. The tangential stresses determined for the composite disc with thermoplastic CF/PA6 material are given in **Figure 4**.

Figure 4 is a graph of tangent stresses occurring on a CF/PA6 composite material disk.

As can be seen in **Figure 4**, the tangential stresses are tensile stress in the inner regions of the CF/PA6 material disk and compressive stress towards the outer regions. It differs in stresses depending on the temperature.

In **Figure 5**, the tangential stresses obtained in the inner part of the disk for temperatures of 30 °C and 150 °C occurring in the CF/PA6 material disk are graphically given.

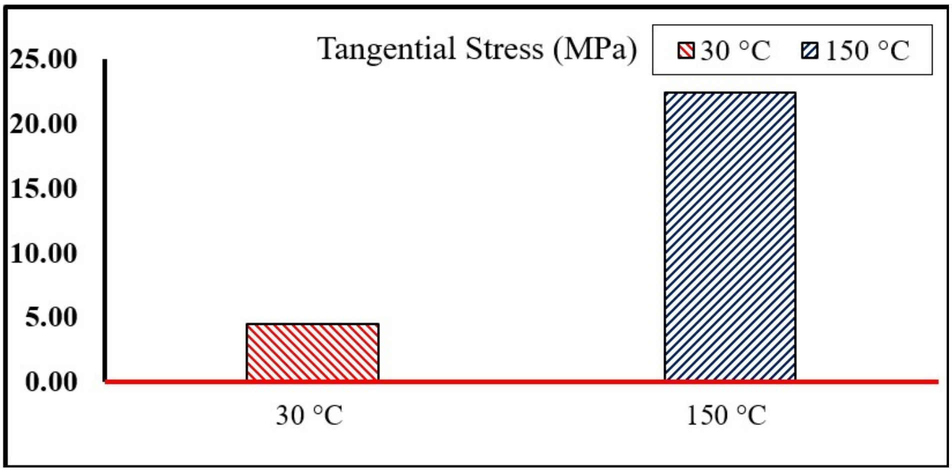

Figure 5. Stresses caused by CF/PA6 material in the inner region of the disk (in the tangential direction).

In **Figure 5**, it was determined that the increase in stress values, which are mathematically calculated in the inner region of the disk, depends on the temperature. 30 °C to 150 °C, the tangential stress value increases by about 5 times.

In **Figure 6**, the stresses obtained on the CF/PA6 material disk in its outer part for temperatures of 30 °C and 150 °C are graphically presented.

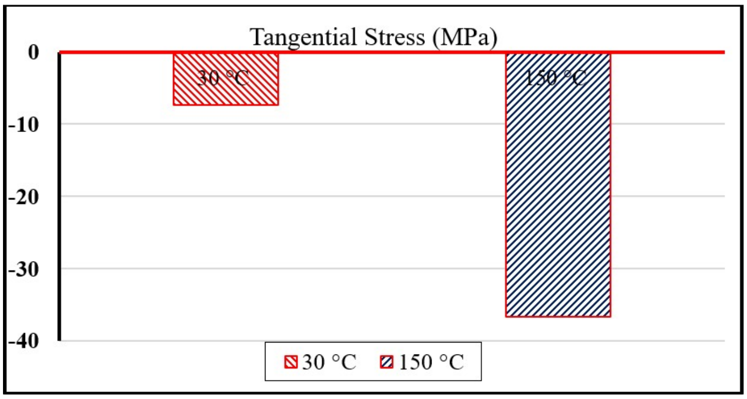

Figure 6. Stresses caused by CF/PA6 material in the outer region of the disk (in the tangential direction).

As the temperature increases from 30 °C to 150 °C, it is observed that the tangential stress value increases by about 5 times in the outer parts.

It is understood that the findings obtained in this study give similar results to some studies. For example, the stresses occurring on an aluminum alloy disk are zero in the innermost and outermost regions of the disk [12]. Its compatibility with other studies is that the analysis results obtained using mathematical programming are considered applicable [13,14].

3. Results and discussion

Mathematical modeling was performed at optimum temperatures for thermoplastic CF/PA6 material disc.

The effect of temperature is in the form that it increases parabolically from the inner surface of the CF/PA6 material disk to the outer surface.

At the end of the model, tangential and radial stresses formed in the disk were determined by means of a mathematical program. The table was created by drawing graphs.

The radial stress component is zero and close to zero on the innermost and outermost surfaces of the disc with CF/PA6 material.

As the temperature increases from 30 °C to 150 °C, there are increases in tangential and radial stresses.

Radial stresses have appeared in the form of pull stress. Radial stresses can reach their highest value in approximately r = 50 mm regions of the CF/PA6 material disc.

Stresses in the tangential direction are calculated first as compressive stress and then as tensile stress.

As the most important result of this study conducted by deriving a mathematical program, it is believed that the CF/PA6 material disk can be selected appropriately at certain temperatures in disk designs.

Conflict of interest: The author declares no conflict of interest.

References

1. Jiregna IT, Lemu HG. Thermal stress analysis of disc brake using analytical and numerical methods. IOP Conference Series: Materials Science and Engineering. 2021; 1201(1): 012033. doi: 10.1088/1757-899x/1201/1/012033
2. Khairnar HP, Phalle VM, Mantha SS. Comparative frictional analysis of automobile drum and disc brakes. Tribology in Industry. 2016; 38(1): 11-23.
3. Deressa KT, Ambie DA. Thermal Load Simulations in Railway Disc Brake: A Systematic Review of Modelling Temperature, Stress and Fatigue. Archives of Computational Methods in Engineering. 2021; 29(4): 2271-2283. doi: 10.1007/s11831-021-09662-y
4. Belhocine A, Abdullah OI. A thermomechanical model for the analysis of disc brake using the finite element method in frictional contact. Journal of Thermal Stresses. 2019; 43(3): 305-320. doi: 10.1080/01495739.2019.1683482
5. Kayiran HF. Numerical analysis of composite disks based on carbon/aramid—epoxy materials. Emerging Materials Research. 2022; 11(1): 155-159. doi: 10.1680/jemmr.21.00052
6. Kayiran HF. Rotating brake discs with carbon laminated composite and e-glass epoxy material: A mathematical modeling. Iranian Polymer Journal. 2022; 32: 457-468. doi: 10.1007/s13726-022-01138-5
7. Manthena VR, Srinivas VB, Kedar GD. Analytical solution of heat conduction of a multilayered annular disk and associated thermal deflection and thermal stresses. Journal of Thermal Stresses. 2020; 43(5): 563-578. doi: 10.1080/01495739.2020.1735975
8. Zhang Z, Zhou D, Fang H, et al. Analysis of layered rectangular plates under thermo-mechanical loads considering

temperature-dependent material properties. Applied Mathematical Modelling. 2021; 92: 244-260. doi: 10.1016/j.apm.2020.10.036

9. Timeshenko S, Goodier, JN. Theory of Elasticity. McGraw-Hill; 1970. pp. 73-75.
10. Sen F, Akyüz BH. Analysis of thermal stresses in a metal matrix composite rotating disk under the influence of temperature. Dicle University, Faculty of Engineering. 2013; 4(1): 51-60.
11. Tahir MM, Wang WX, Matsubara T. A new design of end-tab for the tensile testing of unidirectional thermoplastic composites CF/PA6. In: Proceedings of the 21st International Conference on Composite Materials; 20-25 August 2017; Xi'an, China.
12. MCAM. Available online: https://www.mcam.com/mam/37307/GEPErtalon%C2%AE%20LFX%20PA6_en_US.pdf (accessed on 15 April 2024).
13. Matvienko O, Daneyko O, Valikhov V, et al. Elastoplastic Deformation of Rotating Disk Made of Aluminum Dispersion-Hardened Alloys. Metals. 2023; 13(6): 1028. doi: 10.3390/met13061028
14. Ekhteraei Toussi H, RezaeiFarimani M. Elasto-plastic deformation analysis of rotating disc beyond its limit speed. International Journal of Pressure Vessels and Piping. 2012; 89: 170-177. doi: 10.1016/j.ijpvp.2011.11.001

Journal of Polymer Science and Engineering 2024, 7(2), 7061.
https://doi.org/10.24294/jpse.v7i2.7061

Article

Fabrication and property analysis of treated and untreated bagasse powder-reinforced epoxy resin composites

A. Nayeem Faruqui[*], **Md. Samiur Rahman Tarafdar, Anindya Das Jayanta, Md. Rezaul Karim Sheikh**

Department of Applied Chemistry and Chemical Engineering, University of Rajshahi, Rajshahi 6205, Bangladesh
*** Corresponding author:** A. Nayeem Faruqui, nayeemfaruqui@yahoo.com

CITATION

Faruqui AN, Tarafdar MSR, Jayanta AD, Sheikh MRK. Fabrication and property analysis of treated and untreated bagasse powder-reinforced epoxy resin composites. Journal of Polymer Science and Engineering. 2024; 7(2): 7061. https://doi.org/10.24294/jpse.v7i2.7061

ARTICLE INFO

Received: 11 June 2024
Accepted: 2 July 2024
Available online: 19 July 2024

Abstract: Bagasse fiber from sugarcane waste is used with epoxy resin to make natural composites. The raw fibers are treated chemically to improve compatibility and adherence with the epoxy polymer. It's anticipated that epoxy resin matrix composites reinforced with bagasse particles would work as a trustworthy replacement for conventional materials utilized in the building and automobile sectors. The amount and distribution of reinforcing particles inside the matrix are two factors that impact the composite's strength. Furthermore, the precise proportion of reinforcing elements—roughly 20–30 weight percent—into the matrix plays a critical role in providing a noticeable boost in improving the properties of the composites. This research investigates the impact of reinforcing alkali-treated bagasse and untreated bagasse powder into an epoxy matrix on aspects of mechanical and morphological characteristics. The hand layup technique is used to create alkali-treated bagasse and untreated bagasse powder-reinforced epoxy composites. Composites are designed with six levels of reinforcement weight percentages (5%, 10%, 15%, 20%, 25%, and 30%). Microstructural analysis was performed using SEM and optical microscopes to assess the cohesion and dispersion of the reinforcing particles throughout the hybrid composites' matrix phase. With reinforcement loading up to 20 wt%, the tensile strength, impact strength, and toughness of epoxy-alkali-treated bagasse and untreated bagasse powder-reinforced composites increased. In contrast, treated bagasse epoxy composites were superior to untreated epoxy composites in terms of efficacy. The results indicate that 20 wt% alkali bagasse powder provides better mechanical properties than other combinations.

Keywords: bagasse powder; epoxy; microstructure; mechanical properties; eco-friendly

1. Introduction

The studies on composite materials constitute a significant proportion of the designed materials that promote various applications ranging from everyday products to advanced technologies. Composites consist of a continuous phase combined with one or more discontinuous phases. The discontinuous phase is typically more rigid and durable than the continuous phase, and it is referred to as the "reinforcement or reinforcing material", whereas the continuous phase is referred to as the 'matrix'. Composites can be categorized as reinforced composites with natural fibers (bamboo, jute, flax, sisal, hemp, etc.) or synthetic fibers (graphite, Kevlar, carbon, boron, glass, etc.). The characteristics of the constituent materials, their distribution, and their interactions with one another all have a significant influence on the properties of composites. Although composites have already demonstrated their value as materials that reduce weight, the current challenge is to make them cheaper and more sustainable [1,2].

Several scholars have been researching the benefits of employing natural powders as load-bearing elements in composite materials in recent years. The usage of such materials in composites is increasing over synthetic powders due to their relatively low cost, ability to recycle, and ability to compete well in terms of strength to weight of material [3,4]. Natural powders come in a variety of forms, including bagasse powder, coir powder, banana powder, jute powder, and hemp powder. Bagasse powders are utilized as a reinforcing material in the manufacture of new forms of composites because of their low fabrication costs and high-quality green final material. Bagasse, a by-product of sugarcane, is used in paper, electricity, and factories as raw materials. However, its low heating value makes burning it as fuel inefficient. Currently, 85% of bagasse is burned, leaving excess waste. Ethanol production uses only 9% of bagasse, but its efficiency is low [5]. Boosting bagasse's economic value is crucial. Sugarcane is widely available due to its cultivation in Bangladesh and around the world. As a result, the supply of bagasse remains constant and stable day after day. Bagasse-based composites are applicable for building and construction materials. Bagasse is also sustainable because it is biodegradable, recyclable, and reused [6,7].

This research is being conducted in order to make a large volume of waste bagasse powders usable as reinforcement in polymer matrixes such as epoxy. Epoxy resin is a well-known thermoset polymer matrix due to its great mechanical strength [8], strong erosion and corrosion resistance, high thermal stability, minimal shrinkage, excellent adherence to a variety of surfaces, and ease of workability [9,10]. It is amorphous and extensively cross-linked, resulting in high tensile strength and modulus, high hardness, simple manufacturing, good thermal and chemical resistance, and dimensional stability [11]. Bagasse improves mechanical qualities such as tensile strength, flexural strength, hardness, and impact strength when modified and fabricated [12]. It is readily modified with chemicals and mixes effectively with other composite materials.

Bagasse powder is hydrophilic and extremely polar, whereas polymer matrixes are predominantly non-polar and hydrophobic. As a result, both bagasse fiber and epoxy matrix surfaces are intrinsically incompatible, restricting stress transfer at the interface. Because the hydrophilic natural fibers and the hydrophobic polymer matrix are incompatible, there is poor interfacial adhesion, resulting in a composite material with poor physical and mechanical properties [13]. To overcome these drawbacks, many methods for surface modification of natural fibers have been used, including alkaline treatment [14], esterification [15,16], etherification [17,18], graft copolymerization [19,20], permanganate, benzoyl, anhydride treatment, silylation [21], or a combination of these methods [22]. Among these methods, the alkaline treatment method is used in this literature for bagasse fiber. Several formulations of bagasse powder and thermosetting in both virgin and impregnated form are proposed, and the composite samples are made using the hand layup technique. These composites are tested to justify their material performance. For microstructural study, optical microscopes (OM) and scanning electron microscopes (SEM) are utilized, and mechanical properties are analysed with a universal testing machine (UTM) and an impact tester. In consideration of the importance of chemical modification and the development of research on bagasse-polymer composites, this research presents an overall review of the manufacturing, morphological behavior, mechanical performance, and application of alkali-treated bagasse powder-reinforced epoxy resin composites.

2. Materials and methods

2.1. Materials

The matrix used was Araldite AW 106, a thermoset epoxy resin, and the hardener used was HV 953 IN. Those were collected from Nasim Plastic, Dhaka, Bangladesh. The molecular weight of epoxy resin was 393 Da, the viscosity was 9–14 Pas, the density was 1160 kg/m^{-3} and the flash point was > 150 °C. The molecular weight of the hardener was 305 Da, its viscosity was 0.45 Pas, its density was 900 kg/m^{-3} and its flash point was 129 °C. The reinforcing material, sugarcane bagasse fibers, was brought from Rajshahi Sugar Mills Ltd., Bangladesh. Sodium hydroxide pellets (NaOH) were collected from MERCK, Mumbai, India. The purity was 97.16%.

2.2. Chemical treatment

The bagasse fibers were washed with distilled water. The bagasse fiber was then treated with a 5% NaOH solution at room temperature for 60 minutes while maintaining a liquid-to-fiber ratio of 15:1. After alkali treatment, the fibers were thoroughly rinsed with distilled water until a neutral pH was achieved. A hot air oven set to 105 °C is used to remove moisture from treated fibers. After alkaline treatment, bagasse fibers were taken to a mixer grinder (model MX-AC400) to be ground into powder. The powders were subjected to passing into screens with sieves no. 70 and openings 210 microns. The untreated bagasse fibers were washed with distilled water and dried in a hot air oven at 105 °C.

The untreated fibers were ground into powder using a mixer grinder (model MX-AC400) and then passed through screens with sieve no. 70 and 210 micron openings.

2.3. Composite preparation method

Epoxy resin creates a three-dimensional structure when it combines with the hardener or curing agent. The characteristics of epoxy resin can be changed by utilizing various epoxy oligomers and curing processes. Epoxy resin is mixed with hardener in a ratio of 10:1 by weight. Then alkali-treated bagasse powder with different weight percentages (5, 10, 15, 20, 25, and 30) was mixed by hand mixer for uniform distribution of epoxy resin, hardener, and reinforcement. To prepare one type of composite, a 200-gram mixture of matrix and reinforcement was used. A mold of dimension (3 × 10 × 80) mm^3 was used for casting the composite sheet. A coat of oil was applied to the inner side of the mold because of the quick and easy removal of the composite. The usual hand lay-up technique was used to manufacture the composite of 6 mm thickness at room temperature for 24 h (**Figure 1**).

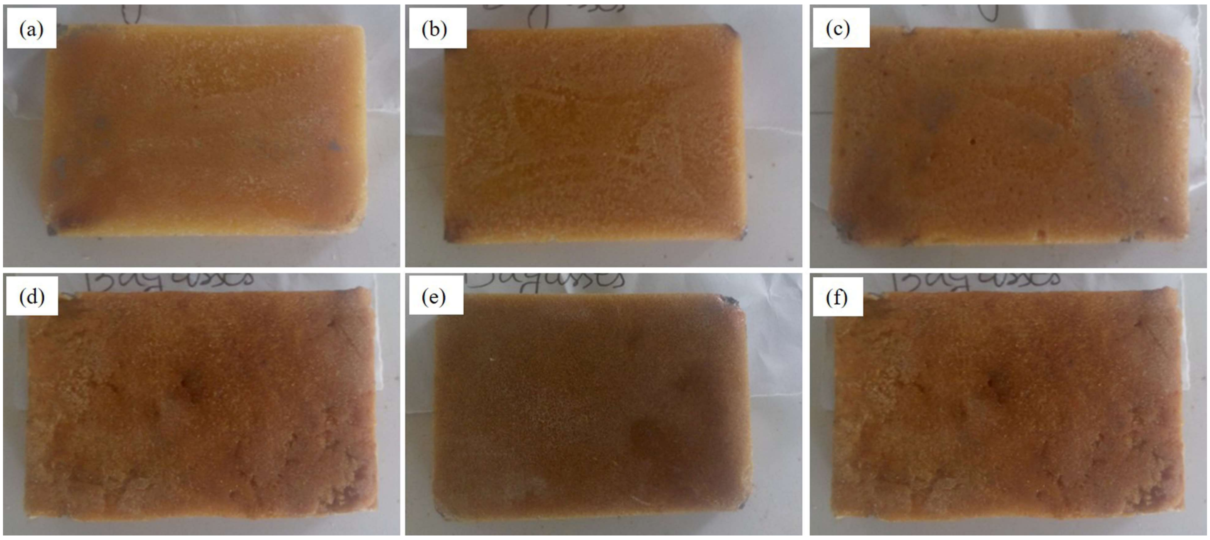

Figure 1. Images of composites having: **(a)** 95–5 wt% epoxy-alkali treated bagasse powder; **(b)** 90–10 wt% epoxy-alkali treated bagasse powder; **(c)** 85–15 wt% epoxy-alkali treated bagasse powder; **(d)** 80–20 wt% epoxy-alkali treated bagasse powder; **(e)** 75–25 wt% epoxy-alkali treated bagasse powder; **(f)** 70–30 wt% epoxy-alkali treated bagasse powder.

The same hand-lay procedure was used to create composites from untreated bagasse powder (**Figure 2**). Untreated bagasse powder with different weight percentages (5, 10, 15, 20, 25, and 30) was mixed with epoxy by hand mixer.

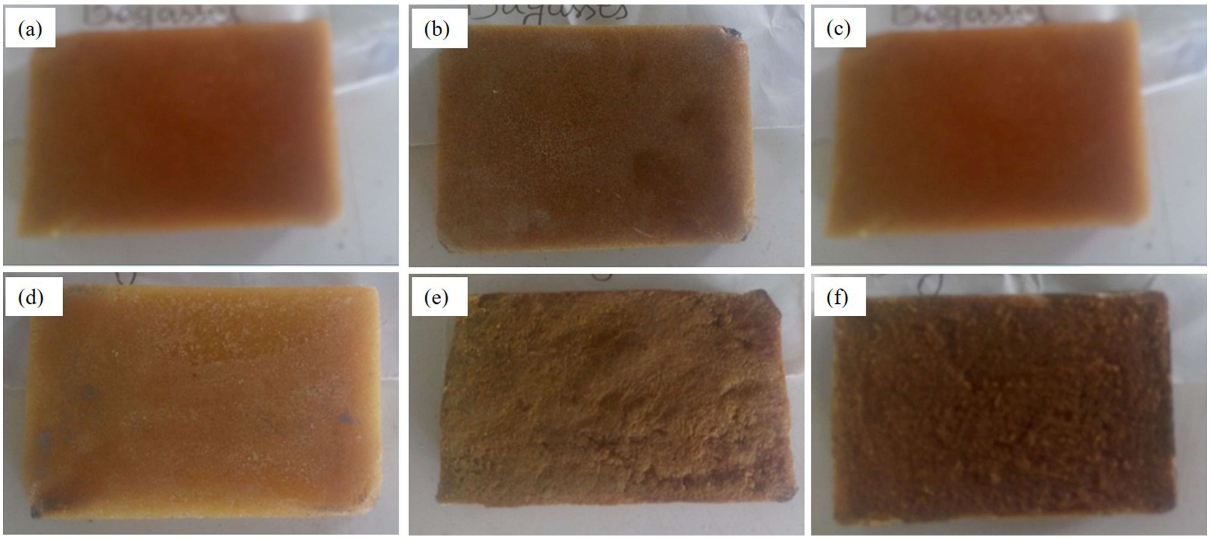

Figure 2. Images of composites having **(a)** 95–5 wt% epoxy-untreated bagasse powder; **(b)** 90–10 wt% epoxy-untreated bagasse powder; **(c)** 85–15 wt% epoxy-untreated bagasse powder; **(d)** 80–20 wt% epoxy-untreated bagasse powder; **(e)** 75–25 wt% epoxy-untreated bagasse powder; **(f)** 70–30 wt% epoxy-untreated bagasse powder.

2.4. Microstructural analysis

Optical microscopy (OM) (ML-803, Taiwan) and a scanning electron microscope (SEM) (JSM-7600 F) provided by JEOL Company Limited, Japan, were used to investigate the interfacial bonding between the reinforcement and epoxy matrix in the produced composites. Prior to morphological investigation under a scanning electron microscope, composite samples were coated with gold.

2.5. Mechanical testing

The materials underwent tensile, charpy impact, and toughness testing. For every test and composite type, five species were examined, and the average values were recorded. Following ASTM D 638-01, tensile tests were performed at a crosshead speed of 10 mm·min^{-1} using a Universal Testing Machine (UTM) (Model: MSC-5/500, Agawn Seiki Company Limited, Japan). Using a Universal Impact Testing Machine (Model: 7408, Hung Ta, Taiwan), dynamic Charpy impact tests and toughness tests were conducted on notched composite specimens in accordance with ASTM D 6110–9724 and ASTM E23.

3. Results and discussion

3.1. Morphological observation

The microstructure of the prepared composite samples was observed using an optical microscope (OM) at various magnifications (10 X, 40 X, and 60 X) to find out the presence or absence of clusters, cracks, voids, particle distribution, particle aggregation, and morphology of the composites [23,24].

In **Figure 3**, uniform dispersion of bagasse powder is clearly seen throughout the matrix phase. Each particle is also surrounded by a matrix phase, which prevents bagasse powder aggregation in the composite. In other words, the uniformity of reinforcement in the matrix phase is nearly reached, increasing the load-bearing capability of composites. The interfaces are sharp, with no big voids or reaction substances, and the integrities are intact [25].

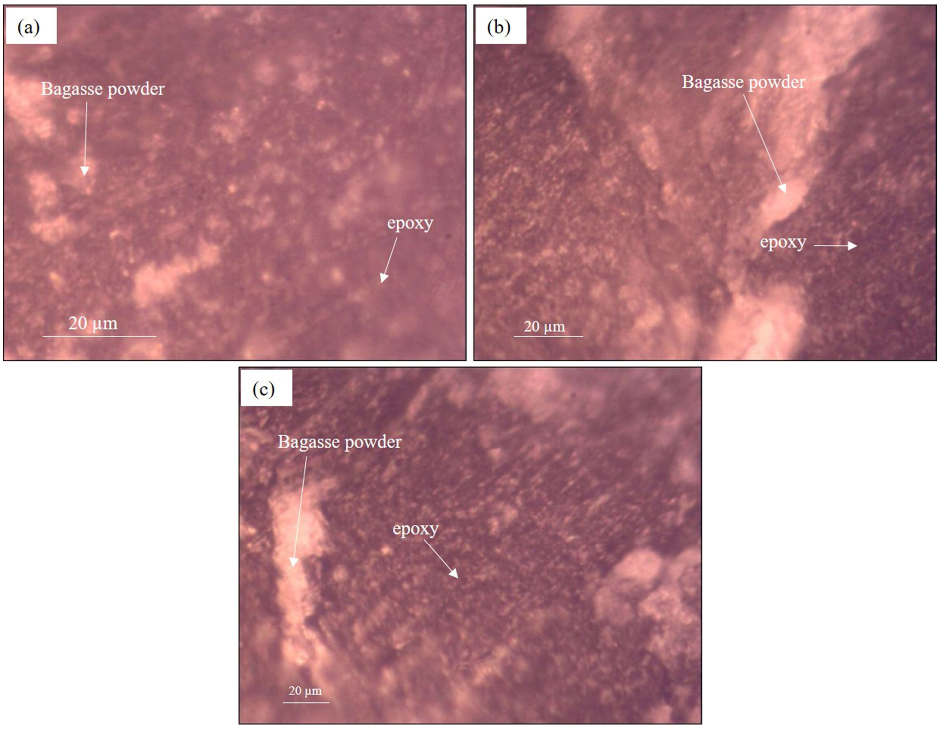

Figure 3. Optical micrograph of cross-section of composites at **(a)** 10 X; **(b)** 40 X; **(c)** 60 X; magnification for 20 wt% of epoxy-alkali-treated bagasse powder composite.

SEM (scanning electron microscope) observation of the cross-section of the composites can reveal information about the sample, such as the exterior morphology (texture), chemical composition, interfacial adhesion, crystalline structure, and orientation of the materials that make up the sample. In this research, SEM (scanning electron microscope) was used to observe the uniformity of reinforcement at the micro level [26].

Figure 4 shows the morphology of a 20 wt% epoxy-alkali-treated bagasse powder composite. A uniform distribution of reinforcement throughout the matrix phase is observed, which is evidence of good interfacial bonding [27]. Here, a very good mixing of alkali-treated bagasse powder and epoxy is noticed. The lack of pores, cavities, or voids is also observed in this SEM micrograph. The findings reveal that in a composite, the intermediate load-bearing components are the major working factor of the matrix. Although the primary function of reinforcement is to retain the load and thereby maximize the strength of composites, since there are no voids or cracks present in the composites, they should display better mechanical properties.

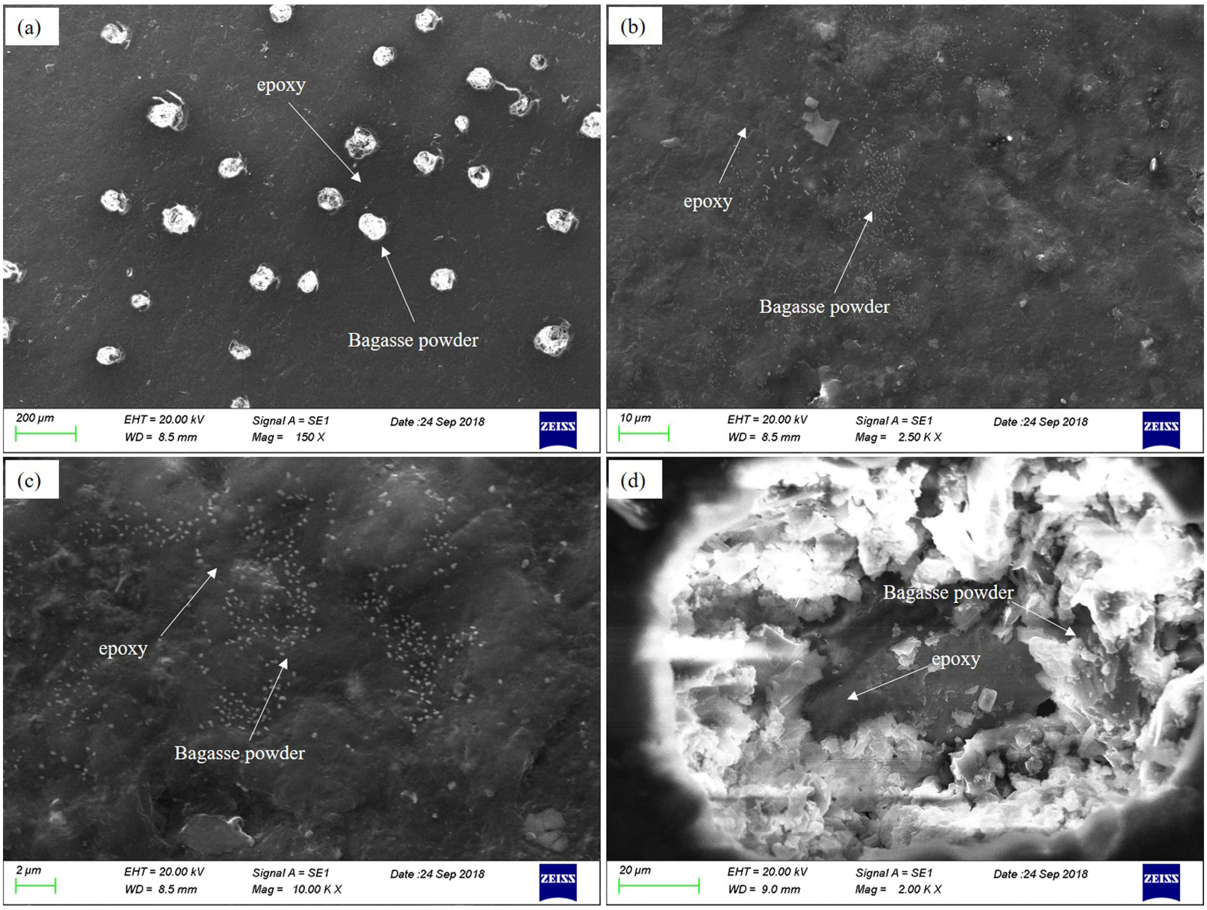

Figure 4. SEM micrograph of cross-section of composites at **(a)** 150 X; **(b)** 2.5 KX; **(c)** 10 KX; **(d)** 2 KX; magnification for 20 wt% of epoxy-alkali-treated bagasse powder composite.

Although the form of the powder remained largely unchanged, it is evident that it underwent a definite separation of its structure following treatment with a 5% NaOH solution (**Figure 4**). This allegedly occurred as a result of some lignin components dissolving upon the addition of the base. Morphological alterations in bagasse after NaOH modification. Intermolecular hydrogen bonds on the carboxylic group connecting the fibers into a break are thought to be the mechanism separating them from one another. This occurs because adding NaOH causes the Na atom in the carboxylic group to replace the H atom [28].

3.2. Mechanical properties

3.2.1. Tensile properties

Tensile tests are used to measure the strength of polymer composites by applying a constant tensile load along the material's axis. The Universal Testing Machine (UTM) (H5OKS, Hounsfield, USA) is suitable for these tests, measuring tensile properties at a speed of 100 mm·min^{-1}.

Figure 5 shows that the tensile strength is increasing with an increase in the weight percentage of powder up to 20 wt% reinforcement. The maximum value of tensile strength is 14.042 MPa for epoxy-untreated bagasse powder composites and 15.839 MPa for epoxy-alkali-treated bagasse powder composites at a 20 wt% powder-to-matrix ratio. Further increase in powder ratio, decrease in tensile strength. The improved load-carrying capacity of powder over matrix increases the tensile strength of up to 20 wt% powder ratio. Tensile strength decreased as reinforcement was loaded farther because of inadequate interfacial adhesion between powder and matrix. In addition, microspace formation in composites increased [29]. Additionally, as compared to virgin epoxy matrix, the treated and untreated composites show superior tensile strength (**Figures 5a**,**b**).

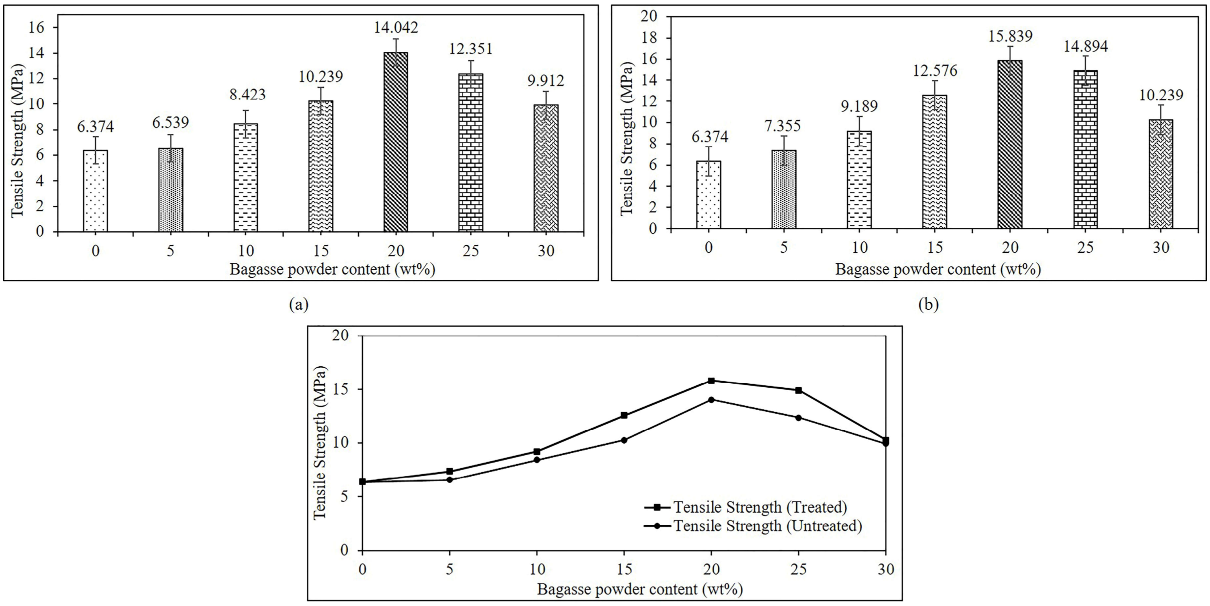

(a) (b)

(c)

Figure 5. Tensile strength of **(a)** epoxy-untreated bagasse powder composites; **(b)** epoxy-alkali-treated bagasse powder composites; **(c)** a comparison graph of tensile strength between treated and untreated powder composites.

The tensile strength curve of the epoxy-alkali-treated bagasse powder composite is slightly higher than that of the epoxy-untreated bagasse powder composite, as shown in **Figure 5c**. Alkaline treatment of bagasse powders increases the powder's load-bearing capability by eliminating a smaller fraction of lignin, pectin, waxes, and contaminants. Furthermore, alkali treatment increases particle strength, giving the powder relatively excellent mechanical qualities. In addition, this resulted in a rough powder surface, which tends to provide better adherence to the matrix. The alkaline treatment method also resulted in a swollen structure due to changes in structure, morphological, mechanical, and dimension properties [30]. Alkaline treatment breaks the alkaline-sensitive hydroxyl groups (–O–H bond structure) found in natural powder molecules. It then reacted with water, phenols, or alcohol molecule groups (H–O–H bond structure) and migrated in or out of the powder structure depending on the powder's characteristics toward the alkaline reaction. Thus, the remaining reactive molecules indirectly produced the powder cell of the –O–Na bond structure between the cellulose molecular chain [31,32].

3.2.2. Impact strength and toughness

Figure 6 depicts the impact characteristics increasing with powder loading of the epoxy-untreated bagasse powder composite and the epoxy-alkali-treated bagasse powder composite. They indicate a distinct trend from those for tensile strength. Furthermore, **Figure 6a**,**b** show that both the treated and untreated composites have better impact energy-absorbing capacity than virgin epoxy matrix. This is because powder absorbs more energy than matrix [33]. **Figure 6c** further shows that treated composites have superior impact properties compared to untreated composites.

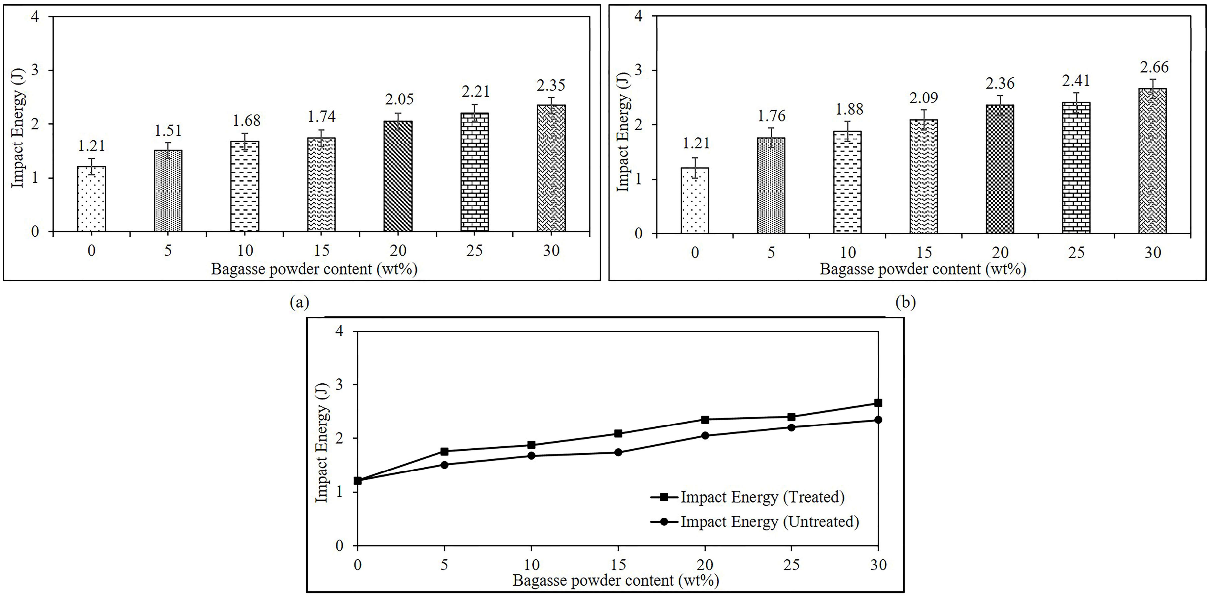

(a) (b)

(c)

Figure 6. Impact energy of **(a)** epoxy-untreated bagasse powder composites; **(b)** epoxy-alkali-treated bagasse powder composites; **(c)** comparison graph of impact energy between treated and untreated powder composites.

Similarly, the toughness of composites improves as the powder content increases. Toughness is the capacity of a material to tolerate stress and deformation without rupturing, as measured by the amount of energy absorbed per unit volume before fracture. Ductility is a measurement of the plastic deformation of a material before rupture. High ductility does not ensure high toughness; it can be obtained by combining strength and ductility. Brittle materials with poor ductility, such as ceramics, are not tough, whereas ductile materials with low strength do not have high toughness ratings. A small specimen was used to measure toughness [34].

Figure 7 reveals the toughness parameters of epoxy-alkali-untreated and epoxy-alkali-treated bagasse powder-reinforced polymer composites. Toughness steadily rises as the powder content increases. In addition, **Figure 7c** demonstrated that treated composites had better toughness characteristics than untreated composites. Because lignin, pectin, oil, wax, and other impurities are removed from the cell wall surfaces of the fibers, the alkaline treatment increases the bonding between natural fiber and polymers, strengthening the structure of natural fiber with composites. This increases the surface roughness of the fiber, exposing short-length crystallites and improving its mechanical properties [35].

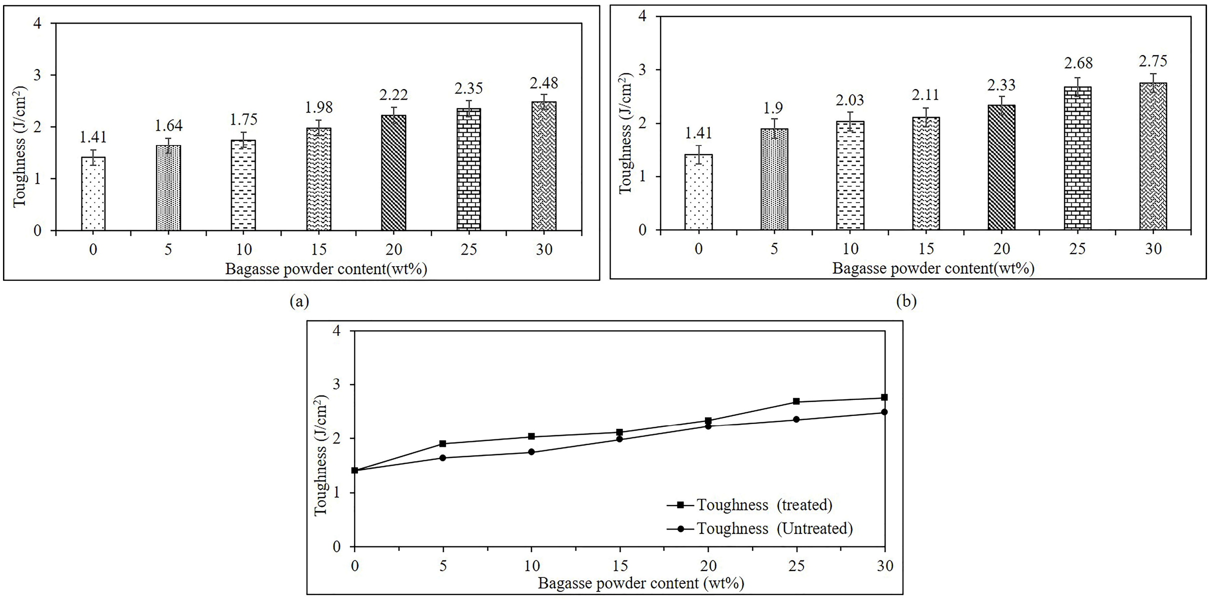

(a) (b)

(c)

Figure 7. Toughness properties of **(a)** epoxy-untreated bagasse powder composites; **(b)** epoxy-alkali-treated bagasse powder composites; **(c)** a comparison graph of toughness between treated and untreated powder composites.

The reinforcement particles act as an adhesive by filling up pores in the polymer matrix, resulting in a stronger link between the matrix and the reinforcement. As a result, when the matrix and particles develop a stronger link, the mechanical characteristics of the composites are improved.

4. Conclusion

Natural fibers are available in nature and can be easily made into reinforcement materials. In this study, treated and untreated bagasse powder is combined with epoxy resin through a hand-lay process to produce composites with the desired properties. According to the optical microscope (OM) and screening electron microscope (SEM) analyses, no large voids, cavities, or reaction products are found in the composites, and a uniform distribution of reinforcement is also observed. The mechanical characteristics of the composite improve as the weight of bagasse powder increases. Tensile strength is maximum at 20 wt% reinforcement, whereas impact energy and toughness are maximum at 30 wt% reinforcement. Alkaline treatment is significant because it increases the powder's load-bearing capability by eliminating a small percentage of lignin, pectin, waxes, and impurities. Bagasse powder-reinforced epoxy composite has several technical applications due to its environmental acceptability, technological feasibility, and economic viability. One of the major applications of bagasse-based composites is the fabrication of tiles for construction industries [36]; it is also used in the automotive industry, the aerospace industry [37], the building industry, the furniture industry [38], etc.

Author contributions: Conceptualization, ANF; methodology, ANF and MSRT; software, ANF and ADJ; validation, ANF, MSRT, ADJ and MRKS; formal analysis, ANF and MSRT; investigation, ANF and MSRT; resources, ANF, MSRT and MRKS; data curation, ANF, MSRT and ADJ; writing-original draft preparation, ANF, MSRT and ADJ; writing-review and editing, ANF and ADJ; visualization, ANF; supervision, ANF; project administration, ANF and MSRT; funding acquisition, ANF. All authors have read and agreed to the published version of the manuscript.

Acknowledgments: The authors are thankful to the University of Rajshahi under the department of Applied Chemistry and Chemical Engineering for their support.

Conflict of interest: The authors declare no conflict of interest.

References

1. Devadiga DG, Bhat KS, Mahesha G. Sugarcane bagasse fiber reinforced composites: Recent advances and applications. Cogent Engineering. 2020; 7(1): 1823159. doi: 10.1080/23311916.2020.1823159
2. Gholampour A, Ozbakkaloglu T. A review of natural fiber composites: properties, modification and processing techniques, characterization, applications. Journal of Materials Science. 2019; 55(3): 829-892. doi: 10.1007/s10853-019-03990-y
3. Karimah A, Ridho MR, Munawar SS, et al. A review on natural fibers for development of eco-friendly bio-composite: characteristics, and utilizations. Journal of Materials Research and Technology. 2021; 13: 2442-2458. doi: 10.1016/j.jmrt.2021.06.014
4. Elanchezhian C, Ramnath BV, Ramakrishnan G, et al. Review on mechanical properties of natural fiber composites. Materials Today: Proceedings. 2018; 5(1): 1785-1790. doi: 10.1016/j.matpr.2017.11.276
5. Timung R, Naik Deshavath N, Goud VV, et al. Effect of Subsequent Dilute Acid and Enzymatic Hydrolysis on Reducing Sugar Production from Sugarcane Bagasse and Spent Citronella Biomass. Journal of Energy. 2016; 2016: 1-12. doi: 10.1155/2016/8506214
6. Guna V, Ilangovan M, Hu C, et al. Valorization of sugarcane bagasse by developing completely biodegradable composites for industrial applications. Industrial Crops and Products. 2019; 131: 25-31. doi: 10.1016/j.indcrop.2019.01.011
7. Cao Y, Shibata S, Fukumoto I. Mechanical properties of biodegradable composites reinforced with bagasse fiber before and after alkali treatments. Composites Part A: Applied Science and Manufacturing. 2006; 37(3): 423-429. doi: 10.1016/j.compositesa.2005.05.045
8. Singla M, Chawla V. Mechanical Properties of Epoxy Resin-Fly Ash Composite. Journal of Minerals and Materials Characterization and Engineering. 2010; 09(03): 199-210. doi: 10.4236/jmmce.2010.93017
9. Liu Y, Zhang J, Chen R, et al. Ethylene vinyl acetate copolymer modified epoxy asphalt binders: Phase separation evolution and mechanical properties. Construction and Building Materials. 2017; 137: 55-65. doi: 10.1016/j.conbuildmat.2017.01.081
10. Jiang J, Lu Z, Niu Y, et al. Investigation of the properties of high-porosity cement foams containing epoxy resin. Construction and Building Materials. 2017; 154: 115-122. doi: 10.1016/j.conbuildmat.2017.06.178
11. Balguri PK, Samuel DGH, Thumu U. A review on mechanical properties of epoxy nanocomposites. Materials Today: Proceedings. 2021; 44: 346-355. doi: 10.1016/j.matpr.2020.09.742
12. Mohan PA. Critical Review: The Modification, Properties, and Applications of Epoxy Resins. Polymer-Plastics Technology and Engineering. 2013; 52(2): 107-125. doi: 10.1080/03602559.2012.727057
13. Gwon JG, Lee SY, Chun SJ, et al. Effects of chemical treatments of hybrid fillers on the physical and thermal properties of wood plastic composites. Composites Part A: Applied Science and Manufacturing. 2010; 41(10): 1491-1497. doi:

10.1016/j.compositesa.2010.06.011

14. Setswalo K, Molaletsa N, Oladijo OP, et al. The Influence of Fiber Processing and Alkaline Treatment on the Properties of Natural Fiber-reinforced Composites: A Review. Applied Science and Engineering Progress. 2021; 14(4): 632-650 doi: 10.14416/j.asep.2021.08.005
15. Naik JB, Mishra S. Esterification effect of maleic anhydride on swelling properties of natural fiber/high density polyethylene composites. Journal of Applied Polymer Science. 2007; 106(4): 2571-2574. doi: 10.1002/app.25329
16. Naik JB, Mishra S. Esterification Effect of Maleic Anhydride on Surface and Volume Resistivity of Natural Fiber/Polystyrene Composites. Polymer-Plastics Technology and Engineering. 2007; 46(5): 537-540. doi: 10.1080/03602550701298630
17. Li G, Shang Y, Wang Y, et al. Reaction Mechanism of Etherification of Rice Straw with Epichlorohydrin in Alkaline Medium. Scientific Reports. 2019; 9(1). doi: 10.1038/s41598-019-50860-3
18. Islam MN, Khatton A, Sarker J, et al. Modification of Jute Fiber by Etherification Method for Diverse Textile Uses. Saudi Journal of Engineering and Technology. 2022; 7(2): 107-111. doi: 10.36348/sjet.2022.v07i02.007
19. Thakur VK, Thakur MK, Gupta RK. Graft copolymers of natural fibers for green composites. Carbohydrate Polymers. 2014; 104: 87-93. doi: 10.1016/j.carbpol.2014.01.016
20. Thakur VK, Thakur MK, Gupta RK. Rapid synthesis of graft copolymers from natural cellulose fibers. Carbohydrate Polymers. 2013; 98(1): 820-828. doi: 10.1016/j.carbpol.2013.06.072
21. Xie Y, Hill CAS, Xiao Z, et al. Silane coupling agents used for natural fiber/polymer composites: A review. Composites Part A: Applied Science and Manufacturing. 2010; 41(7): 806-819. doi: 10.1016/j.compositesa.2010.03.005
22. La Mantia FP, Morreale M. Green composites: A brief review. Composites Part A: Applied Science and Manufacturing. 2011; 42(6): 579-588. doi: 10.1016/j.compositesa.2011.01.017
23. Singh T, Tejyan S, Patnaik A, et al. Fabrication of waste bagasse fiber-reinforced epoxy composites: Study of physical, mechanical, and erosion properties. Polymer Composites. 2019; 40(9): 3777-3786. doi: 10.1002/pc.25239
24. Saini G, Narula AK, Choudhary V, et al. Effect of Particle Size and Alkali Treatment of Sugarcane Bagasse on Thermal, Mechanical, and Morphological Properties of PVC-Bagasse Composites. Journal of Reinforced Plastics and Composites. 2009; 29(5): 731-740. doi: 10.1177/0731684408100693
25. Manikandan P, Nayeem Faruqui A, Raghukandan K, et al. Underwater shock consolidation of Mg-SiC composites. Journal of Materials Science. 2010; 45(16): 4518-4523. doi: 10.1007/s10853-010-4547-8
26. Dixit M, Srivastava R. The effect of copper granules on interfacial bonding and properties of the copper-graphite composite prepared by flake powder metallurgy. Advanced Powder Technology. 2019; 30(12): 3067-3078. doi: 10.1016/j.apt.2019.09.013
27. Prasad L, Kumar S, Patel RV, et al. Physical and Mechanical Behavior of Sugarcane Bagasse Fiber-Reinforced Epoxy Bio-Composites. Materials. 2020; 13(23): 5387. doi: 10.3390/ma13235387
28. Sunarsih S, Andaka G, Wahyuningtyas D. Characterization of morphological changes on modified sugarcane bagasse with potassium hydroxide. Journal of Physics: Conference Series. 2020; 1511(1): 012067. doi: 10.1088/1742-6596/1511/1/012067
29. Bakri MKB, Jayamani E, Hamdan S. Processing and Characterization of Banana Fiber/Epoxy Composites: Effect of Alkaline Treatment. Materials Today: Proceedings. 2017; 4(2): 2871-2878. doi: 10.1016/j.matpr.2017.02.167
30. Bartos A, Anggono J, Farkas ÁE, et al. Alkali treatment of lignocellulosic fibers extracted from sugarcane bagasse: Composition, structure, properties. Polymer Testing. 2020; 88: 106549. doi: 10.1016/j.polymertesting.2020.106549
31. Ogah AO, Afiukwa JN. Characterization and comparison of mechanical behavior of agro fiber-filled high-density polyethylene bio-composites. Journal of Reinforced Plastics and Composites. 2013; 33(1): 37-46. doi: 10.1177/0731684413509425
32. Agarwal K, Kuchipudi SK, Girard B, et al. Mechanical properties of fiber reinforced polymer composites: A comparative study of conventional and additive manufacturing methods. Journal of Composite Materials. 2018; 52(23): 3173-3181. doi: 10.1177/0021998318762297
33. Kosedag E, Ekici R. Low-velocity impact performance of B4C particle-reinforced Al 6061 metal matrix composites. Materials Research Express. 2019; 6(12): 126556. doi: 10.1088/2053-1591/ab5815
34. Dogra V, Kishore C, Verma A, et al. Fabrication and Experimental Testing of Hybrid Composite Material Having Biodegradable Bagasse Fiber in a Modified Epoxy Resin: Evaluation of Mechanical and Morphological Behavior. Applied

Science and Engineering Progress. 2021; 14(4): 661-667. doi: 10.14416/j.asep.2021.06.002

35. Adeniyi AG, Onifade DV, Ighalo JO, et al. A review of coir fiber reinforced polymer composites. Composites Part B: Engineering. 2019; 176: 107305. doi: 10.1016/j.compositesb.2019.107305
36. Marichelvam MK, Manimaran P, Verma A, et al. A novel palm sheath and sugarcane bagasse fiber based hybrid composites for automotive applications: An experimental approach. Polymer Composites. 2020; 42(1): 512-521. doi: 10.1002/pc.25843
37. Asim M, Saba N, Jawaid M, et al. Potential of natural fiber/biomass filler-reinforced polymer composites in aerospace applications. Sustainable Composites for Aerospace Applications. 2018; 253-268. doi: 10.1016/b978-0-08-102131-6.00012-8
38. Oliveira SL, Mendes RF, Mendes LM, et al. Particleboard Panels Made from Sugarcane Bagasse: Characterization for Use in the Furniture Industry. Materials Research. 2016; 19(4): 914-922. doi: 10.1590/1980-5373-mr-2015-0211

Journal of Polymer Science and Engineering 2024, 7(2), 6758.
https://doi.org/10.24294/jpse.v7i2.6758

Article

Waterproofing materials by incorporating as grown carbon nanotubes into paint

Iara Alves Martins de Souza[1], **Evandro Augusto de Morais**[2], **Viviany Geraldo**[1,*]

[1] Instituto de Engenharias Integradas (IEI), Universidade Federal de Itajubá (UNIFEI)—Campus Itabira, Rua Irmã Ivone Drummond 200 Distrito Industrial II, Itabira 35903-087, Minas Gerais, Brazil
[2] Instituto de Ciências Puras e Aplicadas (ICPA), Universidade Federal de Itajubá (UNIFEI)—Campus Itabira, Rua Irmã Ivone Drummond 200 Distrito Industrial II, Itabira 35903-087, Minas Gerais, Brazil
*** Corresponding author:** Viviany Geraldo, vivianygm@unifei.edu.br

CITATION

Souza IAMd, Morais EAd, Geraldo V. Waterproofing materials by incorporating as grown carbon nanotubes into paint. Journal of Polymer Science and Engineering. 2024; 7(2): 6758. https://doi.org/10.24294/jpse.v7i2.6758

ARTICLE INFO

Received: 30 May 2024
Accepted: 5 July 2024
Available online: 1 August 2024

Abstract: We report a method for effectively and homogeneously incorporating carbon nanotubes (CNTs) in the form of double-wall (DWCNTs) and multi-wall (MWCNTs) structures into commercial paints without the use of additives, surfactants, or chemical processes. The process involves the physical mixing of the nanotubes and polymers using the cavitation energy of an ultrasonic bath. It is a simple, fast method that allows for uniform distribution of carbon nanotube bundles within the polymer for direct application. Due to the hydrophobic properties of the carbon nanotubes as grown, we used paint samples containing 0.3% by mass of both types of CNTs and observed an improvement in waterproofing through wettability and water absorption through immersion tests on the samples. Different solvents such as water, formaldehyde, and glycerin were used, and the results showed an increase in paint impermeability of 30% and 25% with the introduction of DWCNTs and MWCNTs, respectively. This indicates a promising, economically viable, and revolutionary method for applying nanotechnology in the polymer industry.

Keywords: paint; carbon nanotubes; dispersion method; impermeability; nanotechnology

1. Introduction

Nanoparticles, also known as particles with nanoscale dimensions, have been incorporated into polymeric matrices to produce materials with different chemical and physical properties [1–4]. Several industries worldwide are using these composites in various applications to reduce the weight of certain components and improve the mechanical and chemical properties of materials. In paints, the use of carbon nanotubes (CNTs) is widely employed to enhance properties such as porosity, corrosion resistance, thermal resistance, and impermeability. Typically, these nanoparticle incorporation processes involve surfactants, additives, and functionalization, making them small-scale and expensive [5].

Carbon nanotubes are known for their excellent properties [6,7] such as mechanical strength and electrical and thermal conductivity. For example, a CNT's Young's modulus of 1.28 ± 0.5 TPa [8] is five times larger than that of commercial steel. There are several papers involving CNTs that report studies and applications in various areas, from theoretical modeling to experimental analysis and a combination of both, such as beam, plate, and sheel structures [9–14].

However, when dispersed in polymers, due to their high aspect ratio and hydrophobicity, they tend to agglomerate over time, potentially leading to a deterioration in the properties of the polymer composite. CNTs as grown are naturally hydrophobic materials, and their uniform dispersion within the polymer matrix has traditionally required surfactants/additives or sophisticated chemical processes involving some form of chemical modification [7,8,15–20]. CNTs show real promise in the processing of polymer composites to provide mechanical reinforcement as well as enhance thermal and electrical conductivity, thereby enabling the development of lighter materials.

Thus, several studies have been carried out on composites, primarily cementitious matrices, using the "in situ" methodology, where CNTs are grown directly on other materials and their dispersion in the matrix occurs naturally, without chemical processes [21–25]. However, due to the chemical reactivity of polymers and the synthesis temperature of CNTs, the direct growth of carbon nanotubes on polymers has not yet been reported. Furthermore, when dispersed in polymer without chemical treatment, in addition to the cost, the material retains its hydrophobicity within the polymer matrix, contributing to the impermeability of the composite [5].

In this work, we report a simple, additive-free, and non-sophisticated chemical process for incorporating CNTs into polymeric matrices, such as commercial paints. This new incorporation method is based on the physical mixing of these materials (carbon nanotubes) into polymers using an ultrasonic bath. The synthesis of CNTs is carried out by chemical vapor deposition (CVD) using ethylene as the carbon source. Two types of CNTs were used: double-wall (DWCNTs) and multi-wall (MWCNTs) carbon nanotubes, and they were dispersed in commercial paint.

Wettability tests were conducted on mortar samples painted with both reference paint and nanostructured paint in order to analyze whether the incorporation of carbon nanotubes would positively influence the impermeability of the polymer (paint). It was observed that the effect of these nanomaterials on the wettability of the samples, using three types of solvents (water, formaldehyde, and glycerin), rendered the polymer more impermeable in all cases, highlighting the efficiency of the dispersion method. Thus, this work presents new perspectives for the practical application of nanostructured polymers in industry, improving the impermeability property of paints in a simple and cost-effective manner.

2. Materials and methods

2.1. Catalyst preparation and carbon nanotube synthesis

For the preparation of multi-walled carbon nanotubes (MWCNTs), a catalyst based on iron and cobalt supported on magnesium oxide (MgO) was developed [23–25]. The ionic solution of Fe and Co salts is impregnated into MgO by dry impregnation and then calcined at 500 ℃ for 2 h in an oxidizing atmosphere. The catalyst used for the synthesis of DWCNTs was prepared similarly using iron and cobalt, but now supported by aluminum oxide (Al_2O_3), as previously described [26]. The synthesis of the CNTs was performed by Chemical Vapor Deposition (CVD) using argon as the carrier gas (500 sccm) and ethylene as the carbon source (300 sccm). Both catalysts were used in the synthesis, resulting in a yield increase of 2300% for MWCNTs and approximately 800% for DWCNTs.

2.2. Dispersion CNT in commercial paint

The process of obtaining nanostructured paint described herein is achieved in a simple manner, free from additives, surfactants, and chemical processes such as functionalization for the incorporation of carbon nanotubes into polymeric matrices. The novel incorporation method involves the use of bath ultrasonics, utilizing cavitation energy at room temperature. **Figure 1** shows optical photos of the methodology and dispersion used.

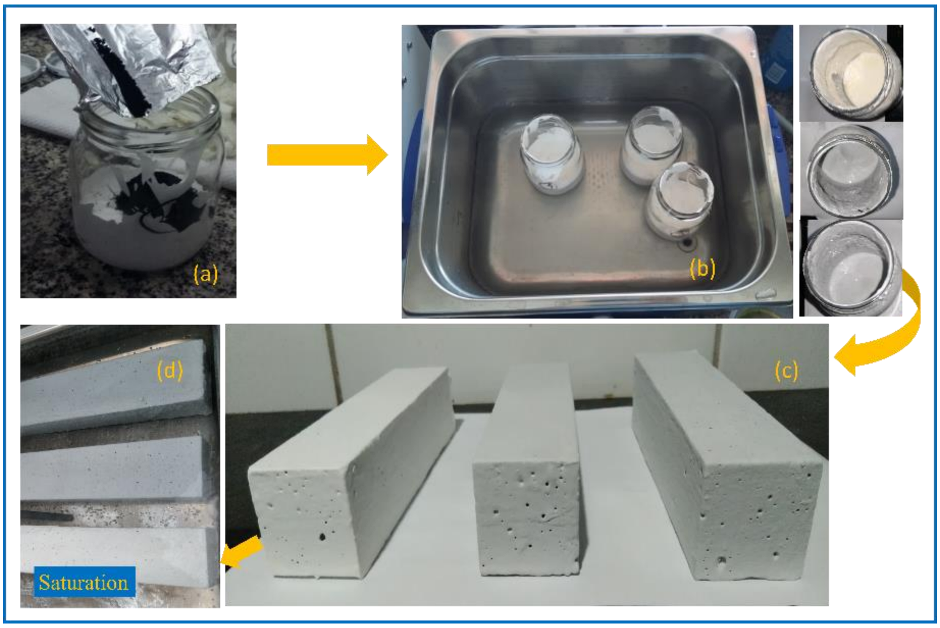

Figure 1. (a) Optical photos showing CNTs and paint mixture; **(b)** nanostructured paints at 0.3% of CNT and dispersion of the material with US; **(c)** appearance of mortar painted with nanostructured paints; **(d)** the samples of the mortar into water at 90 ℃ to saturation and impermeability measurements.

The as-grown DWCNTs and MWCNTs are incorporated into the polymer paint at 0.3% by weight (**Figure 1a**) by physical mixing and subjected to ultrasonic (US) treatment at a frequency of 40 Hz for 30 min using cavitation energy (**Figure 1b**). Cavitation occurs when millions of tiny, microscopic bubbles (cavities) collide in a liquid. Thus, cavitation occurs when there is an alternation of high- and low-pressure areas that diffuse through the liquid. The entire process takes place at room temperature. The same ultrasonic bath treatment is applied to the reference paint to expose it to the same cavitation energy. Subsequently, nanostructured paints suitable for direct application on mortar are obtained (**Figure 1c**).

Using standardized measurements (NBR 9978), the paint-coated mortar specimens are immersed in water at room temperature, and the volume of the specimen is periodically measured, then heated to saturation at 90 ℃ (**Figure 1d**) for impermeability measurements. In addition, the nanostructured paint samples are applied to glass slides (with a 0.38 mm spacer) for wettability measurements. In these experiments, 3 mL of fluids of different polarities and densities, namely water, glycerin, and formaldehyde, are added. Photographs of the bubbles formed on each surface are taken for contact angle measurements.

2.3. Procedures and equipment

The following procedures and equipment were used for the characterization of the materials and the paint samples:

Morphological analyses by Scanning Electron Microscopy (SEM) were performed using a Vega3-TESCAN microscope. Voltage ranges of 2–5 kV and magnifications ranging from 5000 X to 100,000 X were employed.

Transmission electron microscopy (TEM) was carried out at CNT using a FEI-Tecnai G2-20 SuperTwin microscope operating at a voltage of 200 kV.

Measurements of the impermeability are performed by NBR 9978 using samples of the mortar and absorption by immersion.

3. Results and discussion

3.1. Carbon nanotube types

Figure 2 shows SEM images (**Figure 2a**) and TEM images (**Figure 2b**) of the MWCNTs produced, revealing the presence of slender CNTs with an outer diameter of about 12–20 nm and lengths of several microns, along with the absence of amorphous carbon. In **Figure 2c** and **Figure 2d**, similar analyses are performed on DWCNT. The main difference between the two types, apart from the number of walls, is the length of the tubes. DWCNTs are arranged in bundles with lengths of about 300 μm, whereas MWCNTs have lengths on the order of 50 μm.

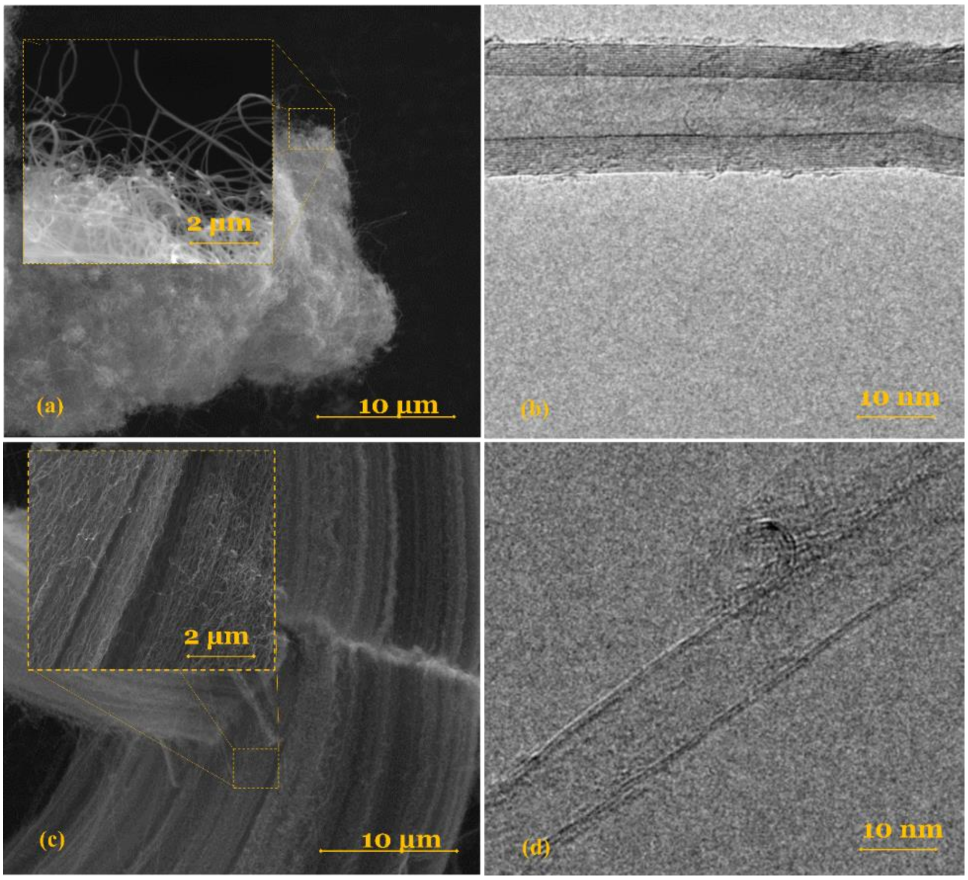

Figure 2. (a) and **(c)** SEM imagens and TEM images; **(b)** and **(d)** at types of the Carbon Nanotubes synthesized, MWCNTs and DWCNTs.

3.2. Nanostructured paint

To characterize the nanostructured paints, initial UV-vis absorbance measurements were performed on reference paste paints (without CNTs) and those with 0.3% DWCNTs and MWCNTs. UV-vis spectroscopy is a technique commonly used to evaluate the dispersion of CNTs in polymers. [20]. During UV-vis experiments, CNTs are activated and show characteristic bands. However, CNT aggregates are hardly sensitized even when analyzed in the UV-vis region between 200 and 800 nm, probably due to charge transfer between the individual nanotubes, which minimizes translational, rotational, and vibrational effects. Nevertheless, it is possible to establish a relationship between the individually dispersed nanotubes in solution and the corresponding absorption spectrum intensity. In this way, UV-vis spectroscopy can be used to monitor the dynamics of the CNT dispersion process.

The results shown in **Figure 3a** demonstrate the presence of CNTs, indicated by changes in the curve behavior and peaks in the region around 255 nm, associated with dispersion. In the case of the DWCNTs sample, the change in signal is more pronounced, probably due to the length of the CNTs bundles (approximately 300 μm), while for MWCNTs, the bundles are four times shorter.

To further demonstrate the temporal stability effect of cavitation dispersion of CNTs, the inset of **Figure 3b** shows an optical photograph of the paints dispersed in 1 L of water after ultrasonic dispersion with only mechanical agitation and a new UV-Vis spectroscopy measurement on diluted paints. In the spectrum in **Figure 3b**, peaks at 235 nm (not marquet) and 350 nm were observed for nanostructured paints. The absorption can be attributed to the π–π^* transition of aromatic C=C bonds and the n–π^* transition of surface functional groups of the polymers, such as C = O [27]. The higher intensity and peak shift from 350 nm to 375 nm in the pure paint indicate a variation in the optical path length traveled by the beam in the UV-vis spectrometry analyses due to the presence of dispersed CNTs.

The spectrum exhibits higher absorbance intensity in the nanostructured paints (indicating good dispersion), along with specific CNT bands.

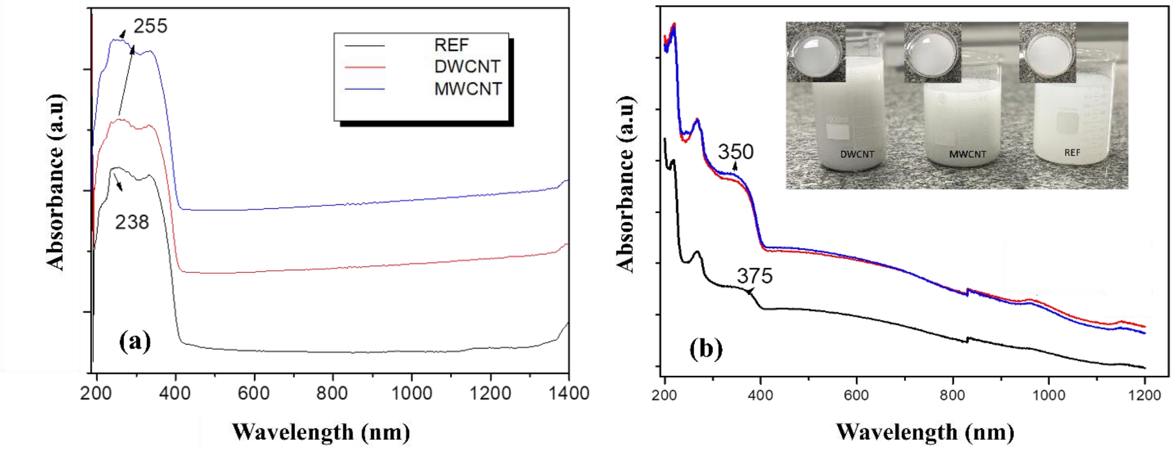

Figure 3. (a) Absorbance in UV-vis (200–1200 nm) for paints after US; **(b)** after dilution in water.

3.3. Impermeability by immersion

After preparing the paints, three mortar test specimens were painted with standardized thickness. The comparative results of all the prepared samples are shown in **Figure 4**. A significant difference in color can be observed between the reference sample (without nanotubes) and the samples with nanostructured paint containing DWCNTs and MWCNTs. **Table 1** shows the dry density data of the painted mortar samples before the water immersion experiment.

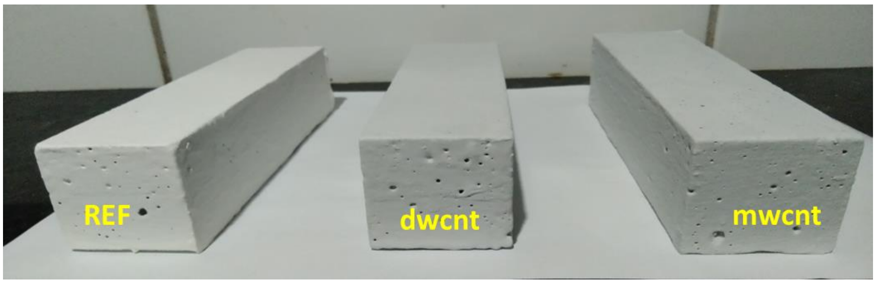

Figure 4. Optical photograph of mortar test specimens painted with paint without CNTs and nanostructured paint.

Table 1. Data of the density of the mortar test specimens painted with the prepared paints.

Samples	**Dry mass (g)**	**Volume (cm^3)**	**Dry density (g/cm^3)**
REF	551.91	224.64	2.46
DWCNT	566.65	230.40	2.46
MWCNT	582.61	237.12	2.46

After painting the three mortar test specimens, and due to the hydrophobic nature of carbon nanotubes as they grow, an expected result would be an improvement in paint impermeability with the introduction of CNTs. According to NBR9978 for mortar, the samples must be immersed in water for a minimum of 24 h to assess water absorption by immersion. Subsequently, the samples are boiled and saturated, and the absorption and impermeability are calculated. **Figure 5a** presents the data obtained for water absorption by immersion before boiling over 48 h, showing that the nanostructured samples exhibit lower water absorption throughout the analyzed period, with the sample containing DWCNT having even lower absorption than the one with MWCNT, mainly due to the significantly greater length of the CNTs.

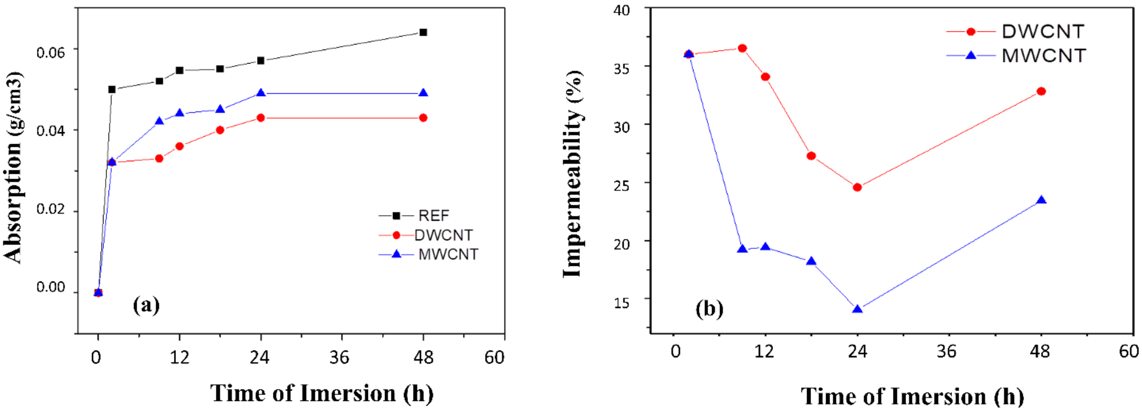

Figure 5. (a) Absorption by immersion in water by 48 h; **(b)** impermeability analyses after boiling at 5 h in relation to reference sample.

Following the boiling (at 90 °C) for 5 h and complete saturation of the samples, **Figure 5b** confirms the previous data regarding lower absorption, or, as shown, higher impermeability (compared to the reference sample), with the sample with nanostructured paint containing DWCNTs being up to 30% more impermeable and with MWCNTs being approximately 25% more impermeable, compared to the reference paint without carbon nanotubes after 48 h. And **Figure 6** shows the absorption and impermeability measurements after saturation for all samples, confirming the results.

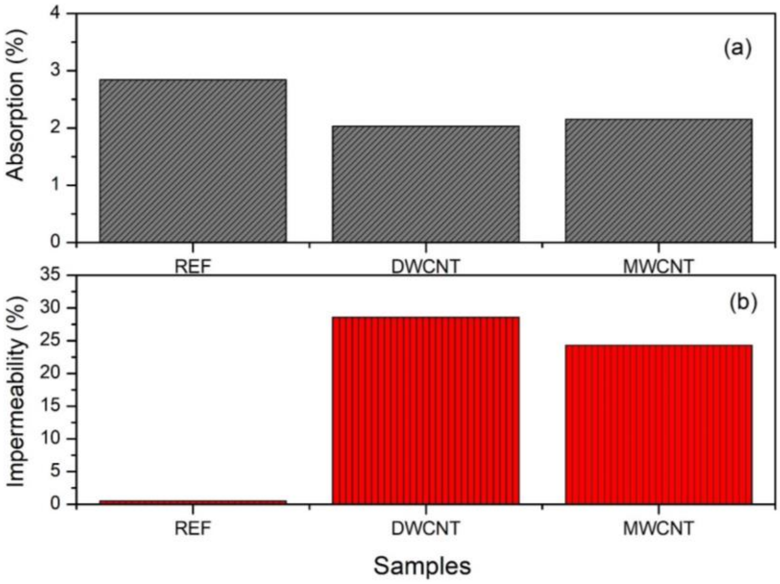

Figure 6. Absorption and impermeability at samples after saturation for 48 h.

These results demonstrate the effective dispersion of as-grown CNTs in paints and maintain the hydrophobic properties of the CNTs (dispersed without external treatment), thereby improving the impermeability of the polymer.

3.4. Wettability

With the introduction and dispersion of CNTs in the paints, there has been an increase in the impermeability of the test specimens, as CNTs are known to be hydrophobic. The interaction between a surface and a particular liquid can be studied by measuring the so-called contact angle (θ) [28]. This is defined as the angle between a plane tangent to a drop of liquid and the plane containing the surface on which the liquid is deposited. The nanostructured paint samples are applied to glass slides, and the determination of the angle was made from images taken with a CCD camera. The experiment was conducted in an unrefrigerated environment, and different reagents (water, formaldehyde, and glycerin) were used. The results obtained for the three coatings analyzed, REF, DWCNT, and MWCNT, are shown in **Figure 7**, and the wettability (or gain in impermeability) is summarized in **Table 2**.

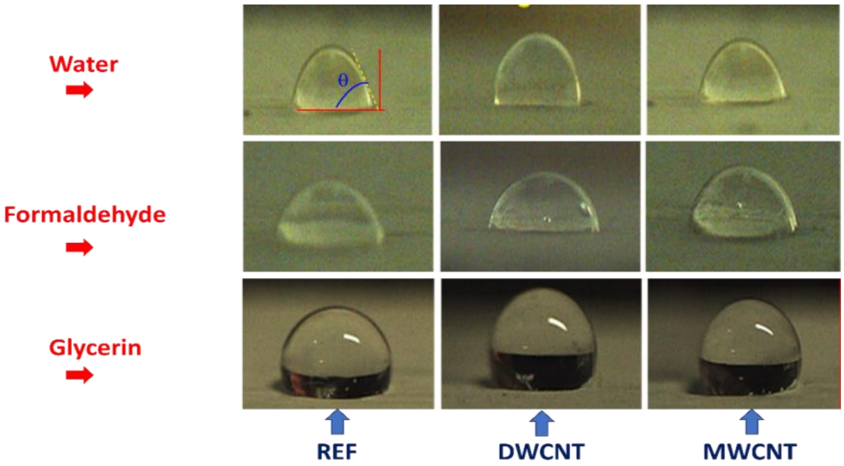

Figure 7. Photos obtained in the wettability experiment with different solvents for the REF, DWCNT, and MWCNT paints analyzed, showing the contact angle.

Table 2. Wettability data at contact angle of REF paints, with 0.3% DWCNT and with 0.3% MWCNT, in addition to the gain compared to the reference (in red).

Solvent	**Reference**	**DWCNT**	**MWCNT**
Water	60.0°	78.4° (+31%)	69.1° (+15%)
Formaldehyde	54.4°	66.6° (+22%)	61.9° (+14%)
Glycerin	99.0°	138.4° (+40%)	120.4° (+22%)

From **Table 2,** it can be observed that the presence of CNTs, as they are produced in the paints, promotes a lower gain in impermeability or wettability, regardless of the solvent polarity. Furthermore, this imperviousness effect is greater for the sample with DWCNTs than with MWCNTs, probably due to the way the CNT bundles are dispersed, where DWCNTs are four times longer.

4. Conclusion

This work presents prospects for the direct application of carbon nanotubes as produced in polymers, indicating a path towards an economically viable and environmentally sustainable application (without chemical functionalization processes) of nanotechnology in polymer composites. The main contributions are:

1) The method of dispersing CNT bundles in paint by Us-Bath is simple, effective, and demonstrates temporal stability with no additional cost to CNT synthesis.
2) Impermeability and wettability measurements showed that 0.3% of grown CNTs can improve the waterproof layer of exterior paint by up to 30%.

Author contributions: Conceptualization, VG; methodology, VG and IAMdS; formal analysis, EAdM; investigation, VG, IAMdS and EAdM; writing—original draft preparation, VG; writing—review and editing, VG, IAMdS and EAdM; visualization, EAdM; supervision, VG; project administration, VG. All authors have read and agreed to the published version of the manuscript.

Funding: The authors would like to thank Minas Gerais Research Support Foundation (FAPEMIG- APQ-01836-22) and Federal University of Itajubá (UNIFEI), for the financial support. And to thanks also profa. Edelma Eleto da Silva for discussions.

Conflict of interest: The authors declare no conflict of interest.

References

1. Omanović-Mikličanin E, Badnjević A, Kazlagić A, et al. Nanocomposites: a brief review. Health and Technology. 2019; 10(1): 51-59. doi: 10.1007/s12553-019-00380-x
2. Öztürk MC, Kaya Aktaş D. Structural characterization, bandgap energy, and mechanic deformation studies of polyacrylamide (PAAm) nanocomposite hydrogels doped with homogeneously-distributed multiwalled carbon nanotubes (MWCNTs). Journal of Polymer Research. 2023; 30(9). doi: 10.1007/s10965-023-03752-0
3. Pączkowski P, Sigareva NV, Gorelov BM, et al. The Influence of Carbon Nanotubes on the Physical and Chemical Properties of Nanocomposites Based on Unsaturated Polyester Resin. Nanomaterials. 2023; 13(23): 2981. doi: 10.3390/nano13232981
4. Shubhadarshinee L, Mohapatra P, Behera S, et al. Synergistic effect of gold nanoparticles decorated functionalized carbon nanotubes nanohybrids on the thermal, dielectric, and sensing properties of polyaniline ternary nanocomposites. Journal of Applied Polymer Science. 2024. doi: 10.1002/app.55611
5. Oliveira CEM, da Silva EE, de Morais EA, Geraldo V. Carbon Nanotube Research Developments: Published Scientific Documents and Patents, Synthesis, and Production. In: Handbook of Carbon Nanotubes. Springer International Publishing, Cham; 2021. pp. 1-38. doi: 10.1007/978-3-319-70614-6_49-1
6. Ansón-Casaos A, Mis-Fernández R, López-Alled CM, et al. Transparent conducting films made of different carbon nanotubes, processed carbon nanotubes, and graphene nanoribbons. Chemical Engineering Science. 2015; 138: 566-574. doi: 10.1016/j.ces.2015.09.002
7. Jang SH, Park YL. Carbon nanotube-reinforced smart composites for sensing freezing temperature and deicing by self-heating. Nanomaterials and Nanotechnology. 2018; 8: 184798041877647. doi: 10.1177/1847980418776473
8. Shen P, Jiang Z, Viktorova J, et al. Conductive and Self-Healing Carbon Nanotube-Polymer Composites for Mechanically Strong Smart Materials. ACS Appl Nano Mater. 2023; 6: 986-994. doi: 10.1021/acsanm.2c04370
9. Gawah Q, Bourada F, Al-Osta MA, et al. An Improved First-Order Shear Deformation Theory for Wave Propagation Analysis in FG-CNTRC Beams Resting on a Viscoelastic Substrate. International Journal of Structural Stability and Dynamics. 2024. doi: 10.1142/S0219455425500105
10. Alsubaie A, Alfaqih I, Al-Osta M, et al. Tahir, Porosity-dependent vibration investigation of functionally graded carbon nanotube-reinforced composite beam. Computers and Concrete. 2023; 32: 75-85. doi: 10.12989/cac.2023.32.1.075
11. Zhang YW, Ding HX, She GL, Tounsi A. Wave propagation of CNTRC beams resting on elastic foundation based on various higher-order beam theories. Geomechanics and Engineering. 2023; 33. doi: 10.12989/gae.2023.33.4.381
12. Huang Y, Karami B, Shahsavari D, Tounsi A. Static stability analysis of carbon nanotube reinforced polymeric composite doubly curved micro-shell panels. Archives of Civil and Mechanical Engineering. 2021; 21: 139. doi: 10.1007/s43452-021-00291-7
13. Heidari F, Taheri K, Sheybani M, et al. On the mechanics of nanocomposites reinforced by wavy/defected/aggregated nanotubes. Steel and Composite Structures. 2021; 38: 533-545. doi: 10.12989/scs.2021.38.5.533
14. Mangalasseri AS, Mahesh V, Mahesh V, et al. Vibration based energy harvesting performance of magneto- electro-elastic beams reinforced with carbon nanotubes. Advances in Nano Research. 2023; 14(1): 27-43. doi: 10.12989/anr.2023.14.1.027
15. Yum SG, Yin H, Jang SH. Toward Multi-Functional Road Surface Design with the Nanocomposite Coating of Carbon Nanotube Modified Polyurethane: Lab-Scale Experiments. Nanomaterials. 2020; 10: 1905. doi:10.3390/nano10101905
16. Feng P, Kong Y, Liu M, et al. Dispersion strategies for low-dimensional nanomaterials and their application in biopolymer implants. Mater Today Nano. 2021; 15: 100127. doi: 10.1016/j.mtnano.2021.100127
17. Huang YY, Ahir SV, Terentjev EM. Dispersion rheology of carbon nanotubes in a polymer matrix. Phys Rev B. 2006; 73: 125422. doi: 10.1103/PhysRevB.73.125422
18. Gojny F, Wichmann M, Fiedler B, Schulte K. Influence of different carbon nanotubes on the mechanical properties of epoxy matrix composites—A comparative study. Composites Science Technology. 2005; 65: 2300-2313. doi: 10.1016/j.compscitech.2005.04.021
19. Hu L, Yu X, Hao J, Xu L. pH- and near-infrared light-responsive, biomimetic hydrogels from aqueous dispersions of carbon

nanotubes. Nano Research. 2014; 17; 3120-3129. doi: 10.1007/s12274-023-6034-y

20. Sanli A, Cinfer ŞP, Yoruç Hazar AB. Effects of different types of surfactant treatments on the electromechanical properties of multiwalled carbon nanotubes decorated electrospun nanofibers. Tekstil ve Konfeksiyon. 2022.
21. Li S, Yan J, Zhang Y, et al. Comparative investigation of carbon nanotubes dispersion using surfactants: A molecular dynamics simulation and experimental study. Journal of Molecular Liquids. 2023; 377: 121569. doi: 10.1016/j.molliq.2023.121569
22. Zerbini Costal G, da Silva Calderón-Morales BR, do Carmo Lima Carvalho J, et al. CNT grown in situ from iron ore tailings: simple dispersion and environmental sustainability. Journal of Nanoparticle Research. 2023; 25: 199. doi: 10.1007/s11051-023-05846-8
23. do Carmo Lima Carvalho J, Zerbini Costal G, de Morais EA, et al. Synthesis and application of carbon nanotubes grown directly on pozzolanic clay. Journal of Nanoparticle Research. 2023; 25: 186. doi: 10.1007/s11051-023-05822-2
24. Geraldo V, de Oliveira S, da Silva EE, et al. Synthesis of carbon nanotubes on sand grains for mortar reinforcement, Construction and Building Materials. 2020; 252: 119044. doi: 10.1016/j.conbuildmat.2020.119044
25. Costal GZ, Oliveira CEM, de Morais EA, et al. High-yield synthesis of carbon nanotubes in-situ on iron ore tailing. Carbon Trends. 2021; 5: 100098. doi: 10.1016/j.cartre.2021.100098
26. da Cunha THR, de Oliveira S, Martins IL, et al. High-yield synthesis of bundles of double- and triple-walled carbon nanotubes on aluminum flakes. Carbon. 2018; 133: 53-61. doi: 10.1016/j.carbon.2018.03.014
27. Yuan T, Meng T, He P, et al. Carbon quantum dots: an emerging material for optoelectronic applications. Journal of Materials Chemistry C. 2019; 7: 6820-6835. doi:10.1039/C9TC01730E
28. Hodgson G, Passmore M, Skarysz M, et al. Contact angle measurements for automotive exterior water management. Exp Fluids. 2021; 62: 119. doi: 10.1007/s00348-021-03219-2

Journal of Polymer Science and Engineering 2024, 7(2), 6263.
https://doi.org/10.24294/jpse.v7i2.6263

Article

Study of the impact of polymeric solution preparation parameters on the production of nanofibers based on PAN and PVA

Luiz Fernando Pimenta Gonçalves, Ariandy Botezini, Erika Peterson Gonçalves*

Vale do Paraíba University, São José dos Campos, São Paulo 12244-000, Brazil
*** Corresponding author:** Erika Peterson Gonçalves, erika@univap.br

CITATION

Pimenta Gonçalves LF, Botezini A, Gonçalves EP. Study of the impact of polymeric solution preparation parameters on the production of nanofibers based on PAN and PVA. Journal of Polymer Science and Engineering. 2024; 7(2): 6263. https://doi.org/10.24294/jpse.v7i2.6263

ARTICLE INFO

Received: 7 May 2024
Accepted: 7 August 2024
Available online: 11 September 2024

Abstract: The search for the development of nanostructured materials has led to the study of the properties of their precursors. For the production of nanofibers by the electrospinning process, it is necessary to determine the rheological parameters of the precursor solutions. Since these properties can be influenced by the processing variables and chemical composition of the polymer, this study aims to elucidate the effect of the addition of vinyl monomers in the formulation of nanofibers based on polyacrylonitrile and to determine the optimal parameters for the production of the precursor polymer solution. The effects of temperature and addition of vinyl monomers were evaluated by rheometry, from the analysis of the variation of the viscosity of the solutions, and by microscopy, the morphology of the nanofibers produced. It was observed that the increase in the temperature used to produce the solutions improves the fibers' properties. Still, there is a relationship between the time of exposure of the polymeric solution to the temperature and the homogeneity of the fibers, which cannot exceed 45 min. The addition of vinyl monomers, to produce PAN-PVA co-polymeric fibers, increases the conductivity and reduces the viscosity of the solutions, resulting in more refined and homogeneous fibers.

Keywords: nanofiber; copolymer; PAN; PVA; electrospinning; rheometry

1. Introduction

The Fourth Industrial Revolution is unlike anything humanity has ever experienced. New technologies allow the fusion of the physical, digital, and biological worlds to create promising solutions to old problems. Materials engineering greatly influences this process since it studies technologies that enable the execution of such fusions. Although there are various nanostructured materials like nanoparticles, nanodots, nanoleaves, nanorods, nanoflowers, etc. [1–3].

At the forefront of the development of nanostructured materials is the production of polymeric nanofibers, which, with their unique characteristics, manufacturing methods, and adjustable properties, have become a much-explored area for application in the most diversified areas such as aeronautics and automobiles [4], sensors [5], tissue engineering [1], catalysis [6], energy devices [7], environment [8], pharmaceutical [9], food [10], filtration [11], distillation [2], etc.

There has been a growing interest in developing nanostructured composites from inserting reinforcement fibers produced by electrospinning techniques. However, the market interest in these fibers goes beyond the already-known structural applications [4,10–12]. PAN and PVA-based copolymer nanofibers are promising for biomedical applications due to the biocompatible and biodegradable character of the monomers [13–16].

Electrospinning can produce these, where nanofibers are obtained from precursor polymer solutions. Electrospinning is one of the most promising methods for producing nanofibers. This versatile technique allows process adaptations that enable the production of fibers with optimal morphological characteristics for the desired application.

Electrospinning is an easy and versatile method to prepare nanofibers (NFs) using natural and synthetic polymers and a high-voltage power supply [17–19]. First reported in the 30's by Formhals [20], electrospinning presented itself as a versatile, multifunctional, and relatively simple method [21] since, for the production of nanofibers, it is only necessary to have a spinneret with a metal needle, a syringe pump, a high voltage power supply, and a grounded collector to mount the electrospinning apparatus [22,23].

The primary mechanism of this technique involves a complicated electrophysical relationship between the polymeric solution and the electrostatic force [24] to produce ultra-thin polymeric fibers with micro to nanometer diameters [25,26]. Electrospinning generates a high-voltage electric field between the injection needle and the collecting apparatus [27]. During the controlled injection process, a drop of polymeric solution is formed in the region of the needle tip [28]. The Taylor cone is formed from this droplet, which is the result of the conical stretching of the polymer droplet with an increase in the surface charge on the polymer droplet over time, increasing the voltage [29]. A polymer jet begins to form shortly after it exceeds the surface charge of the polymer droplet. As the solvent in the polymer jet evaporates, the surface charge of the jet increases, which causes its instability [30]. To compensate for this instability, the polymer jet splits geometrically, initially into two jets and eventually into many jets. This division is caused by the electrostatic force acting on the polymer droplets in constant fragmentation, resulting in the characteristic pattern of nanofibers.

Determining the electrospinning parameters and the rheological and electrical properties of the solution allows the control of the shape and morphology of the fibers. The solution behavior of these materials results from the intermolecular interactions of solubilized oligomers and solvent molecules and the physicochemical properties of the components. They are commonly reported as "unstructured" materials, but many polymers have interactions that are responsible for organizing polymer chains in solutions. These interactions can generate the alignment of the chains, the formation of micelles, weak intermolecular bonds between the chain and the solvent, and the formation of clusters, which directly influence the electrospinning process, impacting the physical and morphological characteristics of the fibers obtained [31].

The composition, average molecular weight, and tactics of the polymers strongly influence the behavior of the polymeric precursor solution of electrospun nanofibers. The viscosity, electrical conductivity, and surface tension of polymeric solutions influence the morphology and geometry of the nanofibers produced [32].

To obtain uniform nanofibers, the viscoelasticity of the solution must be minimal, and this parameter is directly proportional to the diameter of the fibers obtained. The low viscoelasticity of polymeric solutions is achieved with the low concentration of chains in the solution; However, this low concentration results in capillary instability in the electrospinning jet, generating an electrostatic scattering causing the deposition of polymeric granules in the middle of the nanofibers [7].

Controlling the solution's surface tension can mitigate bead formation in the process. Taylor cone formation occurs when the applied potential exceeds the surface tension of the polymer solution, and the lower the solution's surface tension values, the lower the probability of bead formation.

The average diameter of the fibers produced depends on the electrical conductivity of the polymeric solution because, with the application of the external electric field, the charges are oriented, allowing the droplet to undergo a greater elongation, resulting in less thick segments and reducing the diameter of the fibers. Other factors influencing nanofibers' cross-geometry and morphology are ambient temperature, humidity, and air composition. The chemical nature of the polymer, combined with the presence of moisture in the electrospinning environment, can alter the diameter of the nanofibers. Moisture can generate porosity in the nanofibers produced in hydrophilic polymers [31].

Some parameters can be controlled and determined to obtain fibers with the desired morphologies. Among them, it is possible to list the rate of evaporation of the solvent, the difference in polarity between the components of the solution, electrical conductivity, surface tension, and viscoelasticity of the polymeric solution, in addition to synthetic characteristics such as average molar mass and degree of polymer entanglement and environmental parameters such as temperature and humidity [4].

This work is the first to compare the morphology of homopolymeric PAN nanofibers and copolymeric PAN-PVA nanofibers obtained using different parameters of solution preparation and electrospinning.

2. Methods

Polymeric solutions with 10% W Polyacrylonitrile (PAN) (Quimlab) and Polyacrylonitrile-co-Vinyl Acetate (PAN-PVA) (Quimlab) in N,N-dimethylformamide (Neon) were prepared by varying temperature and solubilization time, as shown in **Table 1**.

Table 1. Preparation parameters of polymeric solutions.

Sample code		Temperature (°C)	Prepare Time (min)
PAN	I	50	60
	II	80	15
	III	80	30
	IV	80	45
	V	80	60
PAN/PVA	I	50	60
	II	80	15
	III	80	30
	IV	80	45
	V	80	60

The solubilization of the polymeric mass is carried out in the previously heated solvent under magnetic agitation. To verify the influence of the solution's homogenization time on the morphological characteristics of the nanofibers, the stirring time of the solutions prepared at 80 °C was varied, as shown in **Table 1**. Stabilization of polymeric solutions is carried out at rest under refrigeration (4–5 °C) overnight [33].

Electrospinning was performed in an environment with a temperature of 25 °C and air humidity below 30%. The setup consisted of a high-voltage power supply, an electrically conductive spinneret (hypodermic needle), a syringe pump, and a conductive collector plate. A schematic of the setup was created at biorender.com and shown in **Figure 1**.

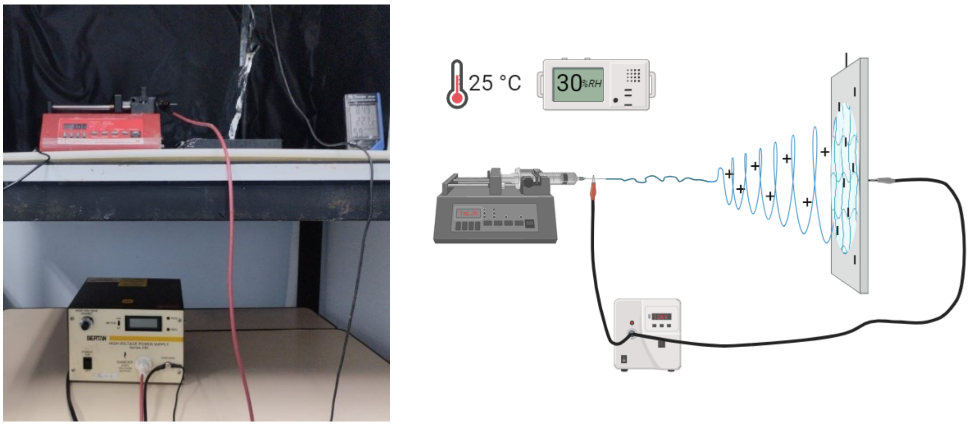

(a) **(b)**

Figure 1. (a) Picture of the experimental equipment under working conditions; **(b)** Schematic of the assembly of the experimental apparatus for electrospinning.

The nanofibers were deposited on a stationary copper plate covered in aluminum foil. The needle selected for extruding the polymer solution had an inner diameter of 0.2 mm. The electrospinning parameters were constant throughout the experiment, having a needle tip-to-collector distance of 10 cm, applied voltage of 12 kV, and solution flow rate of 1.0 mL/h [34].

The polymeric solutions studied were analyzed using a rotational test on a rheometer (Thermo Scientific HAAKE MARS rheometer). Viscosity was determined from shear stress versus strain rate curves at 25 °C, using a cylindrical rotor; 100 complete cycles with 300 s were applied. The electrical conductivity of the solutions was determined using a conductivity meter (Láctea, model mCA 150, Brazil), with measurements performed at room temperature (25 ± 2 °C). The viscosity and conductivity determinations of the samples were performed in triplicate, and the means were compared by Tukey's test for a significance level of 5%, using analysis of variance (ANOVA) in the Origin 8.5 software. The nanofibers' morphology was evaluated by scanning electron microscopy (SEM) in a Zeiss microscope model EVO MA10.

3. Results and discussions

Rheological analyses performed on polymeric solutions indicated the Newtonian behavior of the polymer/solvent system, expressed for Pearson correlation coefficient (R) in **Figure 2**. Therefore, considering the effect of the power phenomena described by Ostwald de Waale, the rheological parameters need not be analyzed [35].

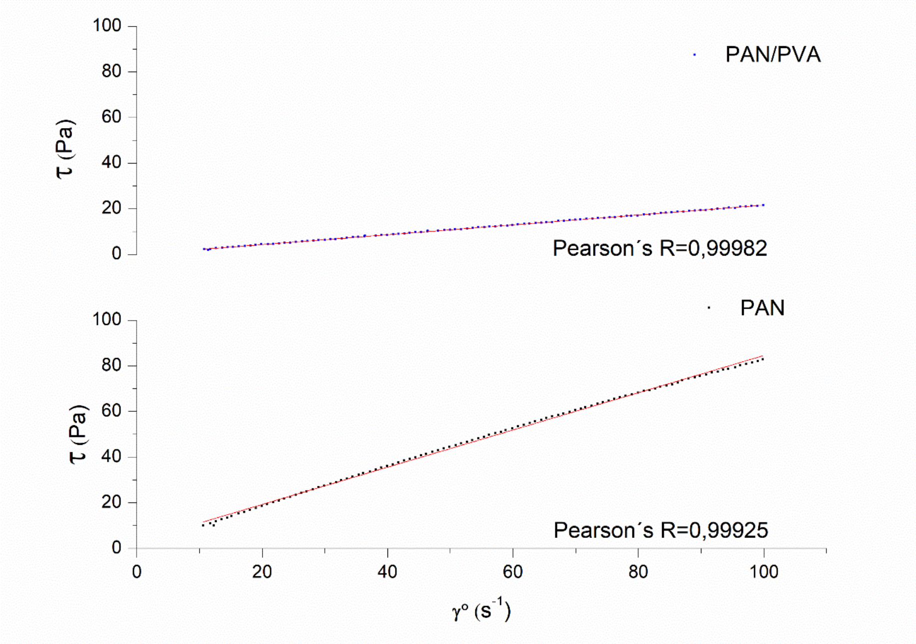

Figure 2. Rheological results of the behavior of the fluid studied.

Polymer-solvent interactions are of great importance in the electrospinning process and, consequently, in the diameter and morphology of the resulting fibers. The initial step of the electrospinning process involves preparing the polymer solution by dissolving the solid precursors in a solvent. Ideally, stable solutions should be obtained which do not undergo significant changes in viscosity over time [31]. Polymer solubilization is a slow process that involves two steps; obtaining an accurate solution is preceded by the gel swelling step. In this first stage, the solid tends to swell when it meets the solvent, which penetrates the polymeric mass's interior through the diffusion of the molecules. As the diffusional process of the solvent continues, the swelling gel disintegrates, with the consequent formation of a true solution [36].

Solubility is related to the cohesive energy of polymers and solvents. Cohesive energy is required to remove a molecule from its environment and from its neighbors. Thus, cohesive energy is associated with evaporation for solvents, while cohesive energy is associated with solubilization for polymeric solids. It is a measure of the level of intensity of secondary forces [36].

Among the basic rules of polymer solubilization is the importance of chemical and structural similarity between the polymer and the solvent and the directly proportional relationship between the solubility and the preparation temperature of the solution for a given polymer/solvent pair [37,38].

One way to quantify this energy is through generalized solubilization parameters (δ), which are calculated from the relative contributions to dispersion forces, hydrogen bonds, and dipole-dipole interactions. For solubilization to occur, the modulus difference between the solubility parameter of the polymer and the solvent must be as slight as possible, i.e., they must have chemical and structural similarities. **Table 2** shows the values of the theoretical solubilization parameters for the homopolymers and solvents studied in this work [36].

Table 2. Values of the theoretical solubilization parameters for materials used.

Compound	δ (g·cm^{-3})
DMF	12.14
PAN	15.42
PVA	9.43

In materials science, a general rule of mixtures is a weighted mean used to predict various properties of a material. It provides a theoretical approximation of final properties. Thus, with the addition of vinyl monomers in the formulation of the PAN/PVA copolymer, the solubilization parameters are expected to be reduced, approaching the value presented by the solvent.

Figure 3 shows the lower viscosity of the copolymeric solution when compared to the homopolymer solution, which is explained by the higher affinity between the solvent and the solute that reduced the viscosity of the prepared PAN/PVA solutions, regardless of the preparation conditions.

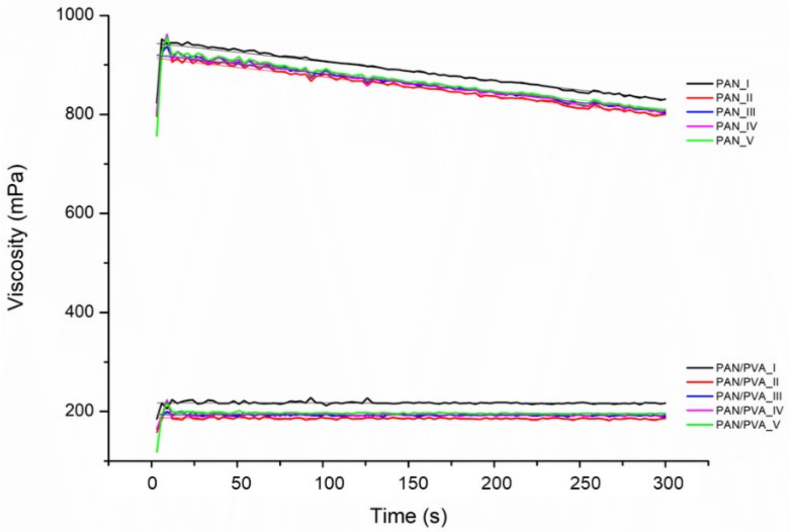

Figure 3. Viscosity behavior over shear time.

Viscoelasticity is a time-dependent phenomenon that occurs in polymer systems. When it comes to dilute solutions, such as those studied in this work, it is possible to verify that at rest, the solute molecules assume a coiled/coiled conformation and random configuration, a condition of equilibrium with lower energy. Once the solution is sheared, these molecules move away from equilibrium. This effect occurs even if, initially, each molecule assumes a particular orientation under the stress; with the maintenance of the shear effort, the molecules will align with the neighboring molecules, reducing the randomness of the distribution and giving rise to viscoelastic behavior [39].

Figure 4 schematically shows the behavior of the polymeric molecules under agitation, which directly influences the viscosity of the studied solutions as a function of time. The analytical results obtained by rheometry indicate that the solutions prepared with the PAN/PVA copolymer presented the lowest viscosities and lowest time dependencies. In addition to the generalized solubilization parameters (δ)

optimized, this comportment can be elucidated too due to the greater chemical and structural similarity between the polymer/solvent pair presented by the copolymer that with the mixture, even if in a low proportion, inserts to the polymeric structure double bonds with oxygen to the polymeric molecule, resembling it even more closely with the n,n-dimethylformamide molecule, **Figure 5**.

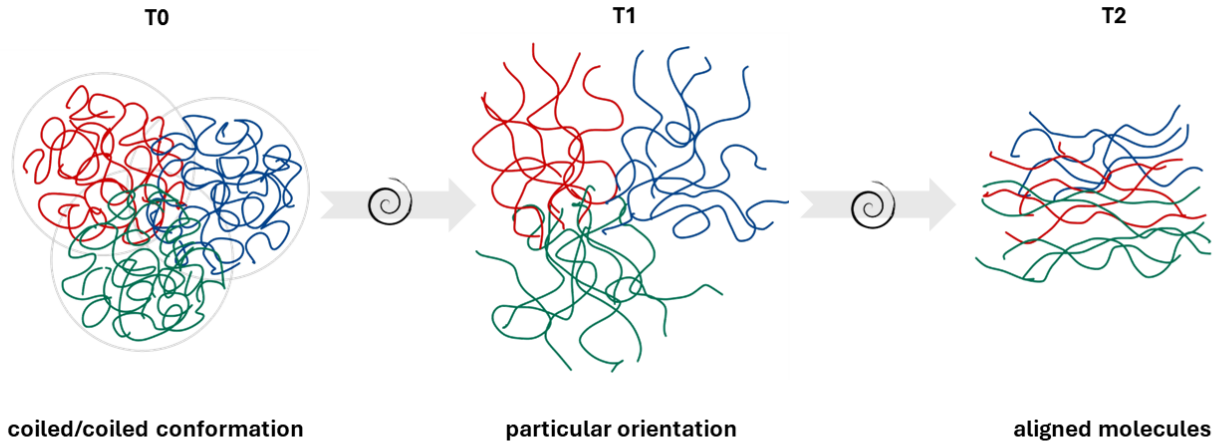

NOTE:
* Consider homopolymer. The different colors aim to facilitate visualization of the alignment stages under shear.
* shear time : T2>T1>T0
* ◎ : solution shear

Figure 4. Illustrative scheme of the behavior of molecules in solution when subjected to shearing over time.

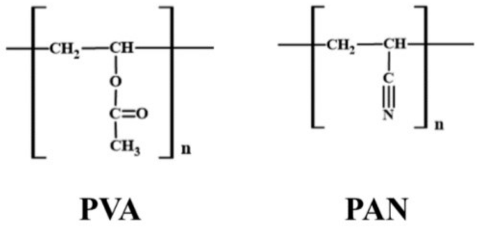

$$-\left[CH_2-CH(O-C(=O)-CH_3)\right]_n- \qquad -\left[CH_2-CH(C\equiv N)\right]_n-$$

Figure 5. The structural formula of mere PVA and PAN.

In the results presented in **Figures 6** and **7**, it is observed that the increase in the temperature of the preparation of the solutions implies a reduction in the viscosity found. In both cases studied, homopolymeric (PAN_I and PAN_V) or copolymeric (PAN/PVA_I and PAN/PVA_V) solutions, there was an approximate 10% drop in the measured viscosity, **Figure 8**, this occurs since for a polymer/solvent pair the solubility is increased with the increase in temperature, providing greater mobility between the chains.

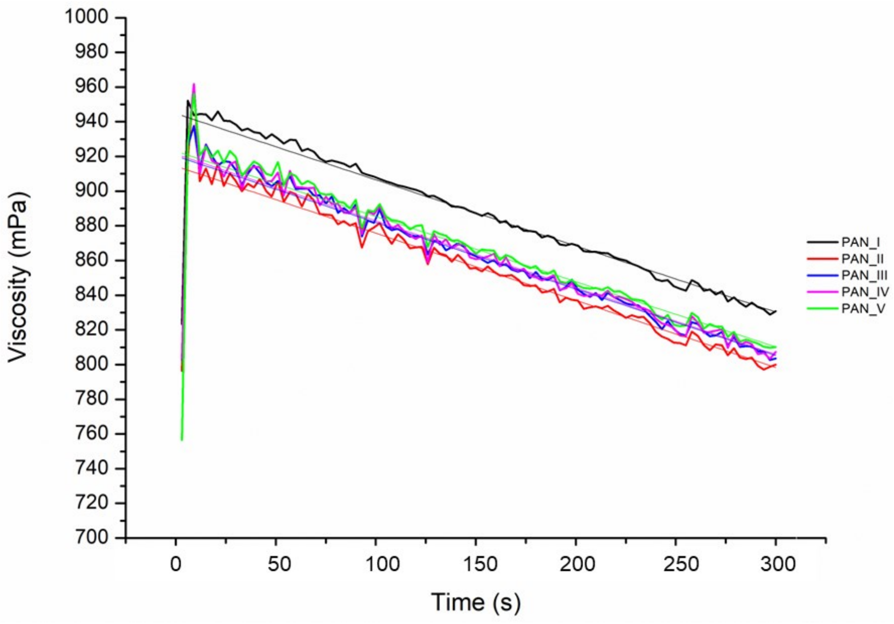

Figure 6. Rheological behavior of PAN solutions at different preparation temperatures.

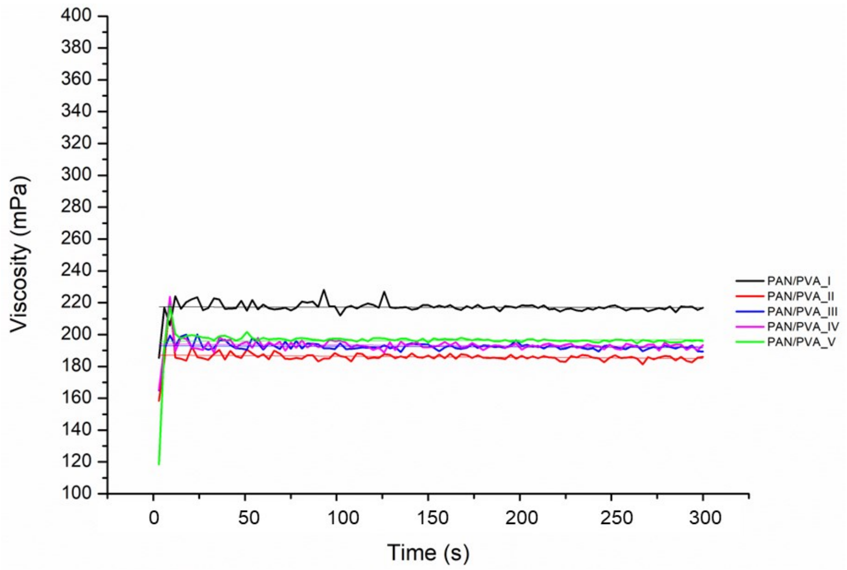

Figure 7. Rheological behavior of PAN/PVA solutions at different preparation temperatures.

When comparing the preparation times of the solutions at 80 ℃, **Figure 8**, it is observed that, in both cases, as the preparation time is increased, the viscosity increases, possibly because the second stage of polymer solubilization has been reached, where homogeneity is achieved in the distribution of the polymeric chains in the organic solution.

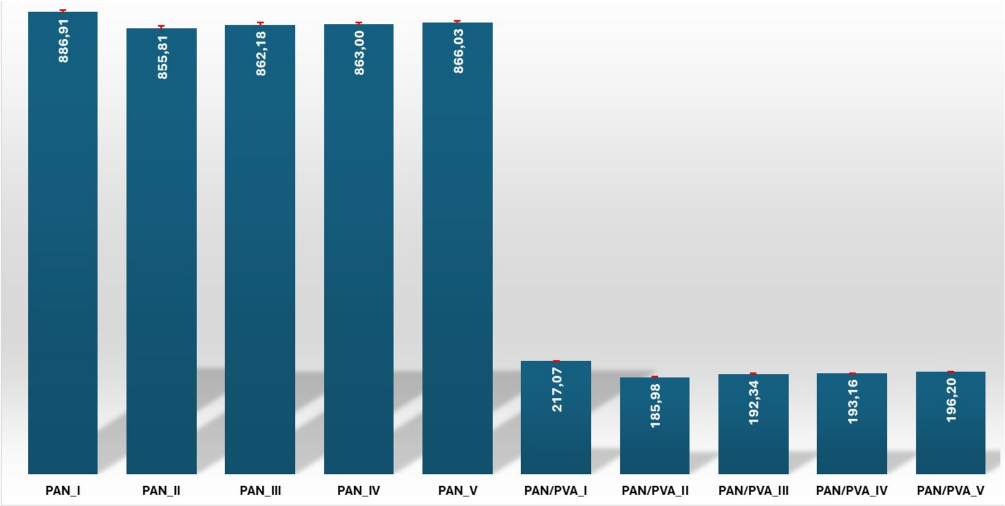

Figure 8. Comparative of the average viscosity of the solutions studied.

The viscosity of the polymeric solution influences the morphology of the electrospun nanofibers since the fibers' homogeneity is obtained from forming a continuous jet without rupture from the tip of the capillary to the collector [38]. A lower viscosity generally favors the formation of finer and more homogeneous fibers. However, if the viscosity is too low, the entanglement of the polymer chains is insufficient for the formation or maintenance of the jet since the interactions between the polymer chains are too weak to overcome the Rayleigh instability. In this case, there will be a greater tendency to spray, producing fibers with defects in the form of beads, which are polymeric agglomerates. As the concentration increases, the jet will no longer break, and the shape of the beads will change from spherical to spindle-like, eventually forming uniform fibers due to increased chain entanglement and viscosity. If the viscosity is too high, it becomes difficult to eject the solution from the spinneret, and polymeric clusters may form in the collector, resembling beads [32].

The polymer concentration effect is quite interesting. It can be noted that the viscoelastic properties of concentrated solutions say those in the range of 15%−20%, are quite typical for viscoelastic solutions. Thus, in the solutions studied, with a concentration of 10%w, the storage module is independent of the frequency, with no implications in the results due to variations in the injection rates during the electrospinning process [40].

On the other hand, the change in the formulation, with the addition of vinyl monomers, resulted in a change in the conductivity of the solutions studied, which influences the morphology of the fibers produced. As the liquid's electrical conductivity increases, the operational flow rates decrease, and the jet becomes thinner and shorter. The higher electrical conductivity of the solution allows the droplet to undergo greater elongation with the application of the electric field, resulting in fibers with a smaller average diameter [41]. The jet is short and the at high conductivities, resulting in refined fibers.

This behavior was observed in the fibers produced in this study since the electrical conductivity measured for the homopolymer was 30.74 µS/cm, and for the copolymer, 52.29 µS/cm. The most refined fibers were those obtained from the electrospinning of copolymer solutions. **Figure 9** shows the micrographs of the fibers obtained from the solutions and preparation conditions studied.

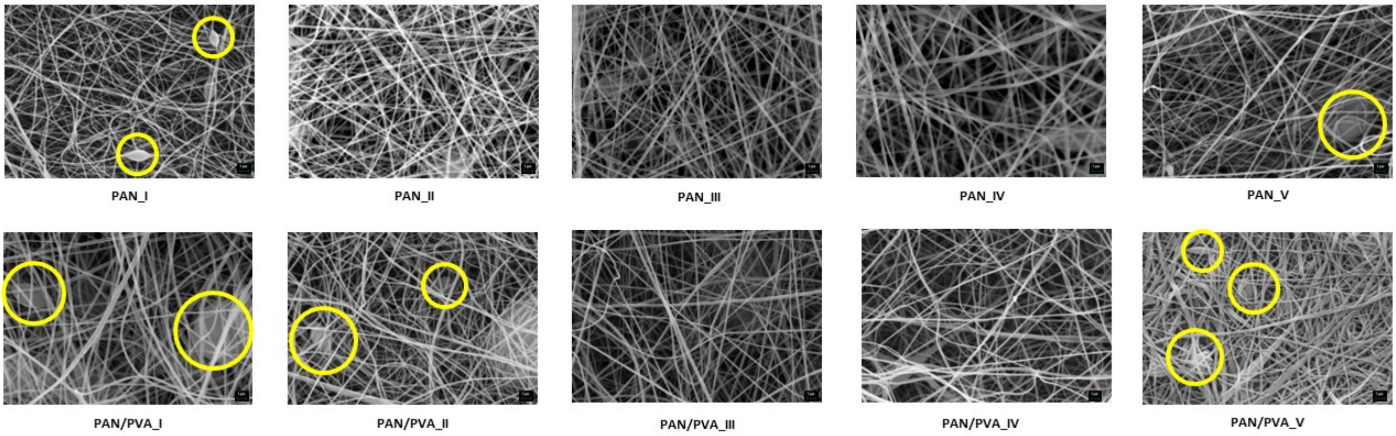

PAN_I PAN_II PAN_III PAN_IV PAN_V

PAN/PVA_I PAN/PVA_II PAN/PVA_III PAN/PVA_IV PAN/PVA_V

Figure 9. Micrographs of the nanofibers were obtained by electrospinning the solutions studied.

It is observed that the fibers obtained from solutions prepared at 50 °C presented nanofibers with bead formation because of the higher viscosities of these solutions. In addition, the copolymeric nanofibers showed irregularity in their diameters, presenting a wide distribution of fiber diameter.

Since the reduction of the viscosity of the solutions was observed with the increase of the temperature of preparation of the solutions, the systematic study of different preparation times showed that this factor also influences the viscosity of the solutions and, consequently, the morphology of the fibers. It was noted that with the increase in exposure to temperature and shear, there was an increase in the viscosities presented, so it is expected that the fibers obtained from the solutions prepared for shorter times will present a more homogeneous morphology and free of beads. This was true for the homopolymer fibers since it is observed that the diameter of the fibers tends to increase with the increase of the solution preparation time, culminating in the formation of beads in the samples obtained after 60 min of heating and shearing (**Figure 9** PAN_II, PAN_III, PAN_IV, and PAN_V). The formation of beads in this situation may be related to the higher viscosity value. This behavior was not observed in the copolymer nanofibers since even in the lowest exposure time (**Figure 9** PAN/PVA_II), which presented the lowest viscosity, the presence of beads intertwined with the nanofibers was noted; this can be explained by greater difficulty in achieving the stability of the solution due to the different radical groups present in the copolymer. In this case, the nanofibers produced with the solutions prepared for 30 and 45 min (**Figure 9** PAN/PVA_III, PAN/PVA_IV) presented the best morphologies, while due to the higher viscosity, the nanofibers obtained from the solutions prepared for 60 min (**Figure 9** PAN/PVA_V) showed thickening of the diameters and the presence of beads intertwined with the fibers.

4. Conclusions

Based on the above, the addition of vinyl monomers in the formulation of the polymeric solution directly influenced the morphology of the fibers since, with this addition, the viscosity was considerably reduced, and the electrical conductivity of the solution increased, resulting in thinner and more homogeneous fibers. The increase in the preparation temperature by 30 °C in the preparation of the solutions resulted in a reduction of approximately 10% in the final viscosity, implying the production of more homogeneous fibers without forming beads. The exposure time at a temperature of 80 °C showed that times longer than 45 min can lead to the formation of beads, and it is appropriate to apply times between 30 and 45 min of agitation under heating to make the optimal solution for the electrospinning of nanofibers based on PAN.

Author contributions: Conceptualization, methodology, LFPG, AB and EPG; validation, formal analysis, LFPG; investigation, resources, AB; data curation, LFPG and AB; writing—original draft preparation, writing—review and editing, supervision, project administration, EPG. All authors have read and agreed to the published version of the manuscript.

Funding: This research was funded by the Financier of Studies and Projects-FINEP, projects n° 01.13.0275.00 and 01.18.0053.00.

Conflict of interest: The authors declare no conflict of interest.

References

1. Rahmati M, Mills DK, Urbanska AM, et al. Electrospinning for tissue engineering applications. Progress in Materials Science. 2021; 117: 100721. doi: 10.1016/j.pmatsci.2020.100721
2. Yalcinkaya F. A review on advanced nanofiber technology for membrane distillation. Journal of Engineered Fibers and Fabrics. 2019; 14: 155892501882490. doi: 10.1177/1558925018824901
3. Liu Y, Hao M, Chen Z, et al. A review on recent advances in application of electrospun nanofiber materials as biosensors. Current Opinion in Biomedical Engineering. 2020; 13: 174-189. doi: 10.1016/j.cobme.2020.02.001
4. Uslu E, Gavgali M, Erdal MO, et al. Determination of mechanical properties of polymer matrix composites reinforced with electrospinning N66, PAN, PVA and PVC nanofibers: A comparative study. Materials Today Communications. 2021; 26: 101939. doi: 10.1016/j.mtcomm.2020.101939
5. Gusmão AP, Rosenberger AG, Muniz EC, et al. Characterization of Microfibers of Carbon Nanotubes Obtained by Electrospinning for Use in Electrochemical Sensor. Journal of Polymers and the Environment. 2020; 29(5): 1551-1565. doi: 10.1007/s10924-020-01964-9
6. Wang BB, Zhong XX, Zhu J, et al. Single-step synthesis of TiO2/WO3-hybrid nanomaterials in ethanoic acid: Structure and photoluminescence properties. Applied Surface Science. 2021; 562: 150180. doi: 10.1016/j.apsusc.2021.150180
7. Maduraiveeran G, Jin W. Carbon nanomaterials: Synthesis, properties and applications in electrochemical sensors and energy conversion systems. Materials Science and Engineering: B. 2021; 272: 115341. doi: 10.1016/j.mseb.2021.115341
8. Baji A, Agarwal K, Oopath SV. Emerging Developments in the Use of Electrospun Fibers and Membranes for Protective Clothing Applications. Polymers. 2020; 12(2): 492. doi: 10.3390/polym12020492
9. Filiz BC. Application of Electrospun Materials in Catalysis. WILEYonline Library. 2020: 113-130. doi: 10.1002/9781119655039.ch4
10. Kazemianrad F, Koocheki A, Ghorani B. Encapsulation of caffeine in sandwich structured Alyssum homolocarpum seed gum/PVA/gelatin nanofibers using electrospinning technique. Food Hydrocolloids. 2023; 140: 108604. doi: 10.1016/j.foodhyd.2023.108604
11. Burts KS, Plisko TV, Bildyukevich AV, et al. Development of dynamic PVA/PAN membranes for pervaporation: Correlation between kinetics of gel layer formation, preparation conditions, and separation performance. Chemical Engineering Research and Design. 2022; 182: 544-557. doi: 10.1016/j.cherd.2022.04.016
12. Zhan F, Yan X, Li J, et al. Encapsulation of tangeretin in PVA/PAA crosslinking electrospun fibers by emulsion-electrospinning: Morphology characterization, slow-release, and antioxidant activity assessment. Food Chemistry. 2021; 337: 127763. doi: 10.1016/j.foodchem.2020.127763

13. Nasibi S, Nargesi khoramabadi H, Arefian M, et al. A review of Polyvinyl alcohol/Carboxiy methyl cellulose (PVA/CMC) composites for various applications. Journal of Composites and Compounds. 2020; 2(3): 68-75. doi: 10.29252/jcc.2.2.2
14. Rodríguez-Rodríguez R, Espinosa-Andrews H, Velasquillo-Martínez C, et al. Composite hydrogels based on gelatin, chitosan and polyvinyl alcohol to biomedical applications: a review. International Journal of Polymeric Materials and Polymeric Biomaterials. 2019; 69(1): 1-20. doi: 10.1080/00914037.2019.1581780
15. Khan R, Haider S, Khan MUA, et al. Fabrication of amine-functionalized and multi-layered PAN-(TiO2)-gelatin nanofibrous wound dressing: In-vitro evaluation. International Journal of Biological Macromolecules. 2023; 253: 127169. doi: 10.1016/j.ijbiomac.2023.127169
16. Luo C, Guo A, Zhao Y, et al. A high strength, low friction, and biocompatible hydrogel from PVA, chitosan and sodium alginate for articular cartilage. Carbohydrate Polymers. 2022; 286: 119268. doi: 10.1016/j.carbpol.2022.119268
17. Afshar S, Rashedi S, Nazockdast H, et al. Preparation and characterization of electrospun poly(lactic acid)-chitosan core-shell nanofibers with a new solvent system. International Journal of Biological Macromolecules. 2019; 138: 1130-1137. doi: 10.1016/j.ijbiomac.2019.07.053
18. Hong Thien DV. Electrospun chitosan/pva nanofibers for drug delivery. Vietnam Journal of Science and Technology. 2018; 54(4B): 185. doi: 10.15625/2525-2518/54/4b/12040
19. Van-Pham DT, Thi Bich Quyen T, Van Toan P, et al. Temperature effects on electrospun chitosan nanofibers. Green Processing and Synthesis. 2020; 9(1): 488-495. doi: 10.1515/gps-2020-0050
20. Anton F. Method and apparatus for spinning. Google Patents; 1944.
21. Sasipriya K, Suriyaprabha R, Prabu P, et al. Synthesis and characterisation of polymeric nanofibers poly (vinyl alcohol) and poly (vinyl alcohol)/silica using indigenous electrospinning set up. Materials Research. 2013; 16(4): 824-830. doi: 10.1590/s1516-14392013005000050
22. Zhengming H, Yanzhong Z, Masaya K, et al. A review on polymer nanofibers by electrospinning and their applications in nanocomposites. Compos Sci Technol 2003; 63: 2223-2253. doi: 10.1016/S0266-3538(03)00178-7
23. Wang H, Feng Y, Fang Z, et al. Fabrication and characterization of electrospun gelatin-heparin nanofibers as vascular tissue engineering. Macromolecular Research. 2013; 21(8): 860-869. doi: 10.1007/s13233-013-1105-7
24. Faridi MR, Naderi N, Koochaki JA. Needleless electrospinning apparatus. Google Patents; 2016.
25. Chronakis IS. Micro-/Nano-Fibers by Electrospinning Technology. Micro-Manufacturing Engineering and Technology. William Andrew Publishing; 2010. pp. 264-286. doi: 10.1016/b978-0-8155-1545-6.00016-8
26. Ghorbani F, Nojehdehyan H, Zamanian A, et al. Synthesis, Physico-chemical Characteristics and Cellular Behavior of Poly (lactic-co-glycolic Acid)/Gelatin Nanofibrous Scaffolds for Engineering Soft Connective Tissues. Advanced Materials Letters. 2016; 7(2): 163-169. doi: 10.5185/amlett.2016.6003
27. Andrady AL, Ensor DS, Walker TA, Prabhu P. Nanofiber mats and production methods thereof. Google Patents; 2009.
28. Liu W, Thomopoulos S, Xia Y. Electrospun Nanofibers for Regenerative Medicine. Advanced Healthcare Materials. 2011; 1(1): 10-25. doi: 10.1002/adhm.201100021
29. Garg K, Bowlin GL. Electrospinning jets and nanofibrous structures. Biomicrofluidics. 2011; 5(1). doi: 10.1063/1.3567097
30. Liu Y, Wang C. Advanced Nanofibrous Materials Manufacture Technology Based on Electrospinning. Routledge; 2019. doi: 10.1201/9780429085765
31. Mercante L, Andre R, Macedo J, et al. Electrospun nanofibers and their applications: advances in the last decade (Portuguese). Química Nova; 2021. doi: 10.21577/0100-4042.20170721
32. Xue J, Wu T, Dai Y, et al. Electrospinning and Electrospun Nanofibers: Methods, Materials, and Applications. Chemical Reviews. 2019; 119(8): 5298-5415. doi: 10.1021/acs.chemrev.8b00593
33. Gonçalves LFP, Botezini A, Wittcinski CO, et al. Study of the influence of the parameters of preparation of polymeric solutions obtaining nanofibers by electrospinning. The Journal of Engineering and Exact Sciences. 2022; 8(8): 14838-01e. doi: 10.18540/jcecvl8iss8pp14838-01e
34. Hulsey S, Absar S, Choi H. Comparative Study of Polymer Dissolution Techniques for Electrospinning. Procedia Manufacturing. 2017; 10: 652-661. doi: 10.1016/j.promfg.2017.07.010
35. Rodrigo GFC, Juliano EO, Gustavo EP, et al. Electrospinning polymers in solution (Portuguese). Polímeros. 2012. 22(2): 170-177. doi: 10.1590/S0104-1428201200500002
36. Sebastião VCJ. Polymer Science: A basic text for technologists and engineers (Portuguese). São Paulo: Artliber; 2002.
37. Haider A, Haider S, Kang IK. A comprehensive review summarizing the effect of electrospinning parameters and potential

applications of nanofibers in biomedical and biotechnology. Arabian Journal of Chemistry. 2018; 11(8): 1165-1188. doi: 10.1016/j.arabjc.2015.11.015

38. Mishra RK, Mishra P, Verma K, et al. Electrospinning production of nanofibrous membranes. Environmental Chemistry Letters. 2018; 17(2): 767-800. doi: 10.1007/s10311-018-00838-w
39. Rômulo FN. Fundamentals of Polymer Rheology (Portuguese). Caxias do Sul, Educ; 1997.
40. Malkin A, Ilyin S, Roumyantseva T, et al. Rheological Evidence of Gel Formation in Dilute Poly(acrylonitrile) Solutions. Macromolecules. 2012; 46(1): 257-266. doi: 10.1021/ma301423u
41. Rosell-Llompart J, Grifoll J, Loscertales IG. Electrosprays in the cone-jet mode: From Taylor cone formation to spray development. Journal of Aerosol Science. 2018; 125: 2-31. doi: 10.1016/j.jaerosci.2018.04.008

Journal of Polymer Science and Engineering 2024, 7(2), 7394.
https://doi.org/10.24294/jipd7394

Article

Coir powder-reinforced epoxy resin composites: Fabrication and characteristics analysis

A. Nayeem Faruqui[*], **Mst. Tamanna Akter, Ria Biswas, Md. Rezaul Karim Sheikh**

Department of Applied Chemistry and Chemical Engineering, University of Rajshahi, Rajshahi 6205, Bangladesh
*** Corresponding author:** A. Nayeem Faruqui, nayeemfaruqui@yahoo.com

CITATION

Faruqui AN, Akter MT, Biswas R, Sheikh MRK. (2024). Coir powder-reinforced epoxy resin composites: Fabrication and characteristics analysis. Journal of Polymer Science and Engineering. 7(2): 7394. https://doi.org/10.24294/jipd7394

ARTICLE INFO

Received: 27 June 2024
Accepted: 9 October 2024
Available online: 19 November 2024

Abstract: In order to replace conventional materials in the existing composite world, there has been a focus on adopting coir fibres, which are lightweight, adaptable, efficient, and have great mechanical qualities. This study describes the creation of environmentally responsible bio-composites with good mechanical characteristics that employ coir powder as a reinforcement, which has good interfacial integrity with an epoxy matrix. And these epoxy-coir composites supplemented with coir particles are predicted to function as a reliable substitute for traditional materials used in industrial applications. Here, untreated and alkali-treated coir fibres powder were employed as reinforcement, with epoxy resin serving as a matrix. An experimental investigation has been carried out to study the effect of coir powder reinforcement at different weight percentages (5 wt%, 10 wt%, 15 wt%, 20 wt%, 25 wt%, and 30 wt%). The morphological study, followed by a scanning electron microscope (SEM) and an optical microscope (OM), demonstrated that the powder and matrix had the strongest adhesion at 20 wt% coir powder-reinforced composite, with no voids, bubbles, or cracks. Based on the entire investigation, the polymer composite with 20 wt% reinforcement exhibited better mechanical qualities than the other combinations.

Keywords: composite; coir powder; epoxy resin; mechanical properties; SEM

1. Introduction

Over the last several years, a number of scholars have been researching the use of natural fibres as load-bearing elements in composite materials. Composite material is a multi-phase system composed of matrix and reinforcing materials. The matrix specifies the volume of the composite material, combines the reinforcing agent, and uniformly distributes the applied load to reinforcements, giving strength and stiffness for structural loads.

Polymer matrix composites (PMCs) are powder-reinforced polymers in which a thermoset or thermoplastic polymer serves as the matrix. Polymer matrix composites (PMCs) are often used in a variety of sectors, including vehicles, ships, and structural applications, due to their high strength-to-weight ratio, simplicity of manufacture, and low cost [1,2]. Polymeric composites can be reinforced with synthetic fibres such as glass, carbon, boron, graphite, or natural fibres including sisal, hemp, flax, bamboo, coir, and jute. Natural fibre composites are suitable for building [3,4], packing [5–7], car interiors [8,9], and storage equipment due to their low density, environmental benefits, and cost-effectiveness [10].

After the flesh of the coconut and sap are removed, leftover shells are used to create coir fibres, a common natural fibre [11]. Brushes, carpets, and other everyday items were traditionally made from the majority of coir fibres [12,13]. The application of coir fibres as reinforcing fibres in composite materials has been the subject of increased investigation in recent years [14]. Therefore, using coir fibres is not only a good technique to repurpose coconut waste but also a means to lessen the environmental problems produced by the buildup and burning of waste coconut shells. Not only do coir fibres increase the toughness of epoxy resin, but they also have good mechanical qualities, with the best elongation of any known natural fibre. It can be utilised as a reinforced material because it is non-toxic, inexpensive to manufacture, high in lignin content, and strong [15]. Coir fibre includes 45.84% lignin, 43.44% cellulose, and 0.25% hemicellulose [16]. The water that has been adsorbed into the hydrophilic coir fibre’s lignocellulosic surface hinders efficient adhesion to the hydrophobic polymer matrix, affecting the mechanical efficacy of polymer composites for any fibre volume fraction. However, there are potential ways to reverse this decreasing mechanical property condition. Here, the scholar relied on an alkali process for treating the surface of the coir fibre. A strong alkali treatment boosts coir fibre adherence to the polyester matrix, elevating composite strength by around 50% for a 30% coir fibre volume fraction [17].

In this research, coir powder-reinforced polymer composites contain both untreated and alkali-treated coir powder. Alkali treatment raises strength, lowers impurities, and improves the interfacial bonding ability by removing some non-cellulosic substances from the fibres and increasing the surface roughness of the fibres, which brings benefits such as lightweight, high strength, simple manufacture, and superior insulation [18–20]. The efficacy of coir powder-reinforced composites is assessed by alkali treatment. After the experiment, alkali-treated composites would show greater mechanical qualities [21].

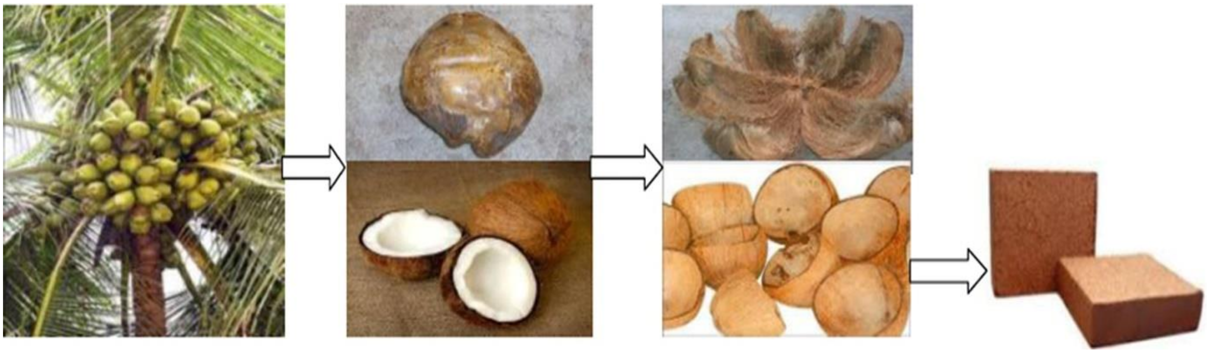

Figure 1. Formation of coconut fibre bio-composite material [22].

In this study, epoxy resin is utilized as a composite matrix due to its great strength and adhesiveness. It is comprised of amorphous, highly cross-linked polymers, which provide these materials with excellent features such as high tensile strength and modulus, ease of manufacturing, strong thermal and chemical resistance, and dimensional stability. However, it results in low hardness and poor fracture resistance [23]. Epoxy resins are used in a variety of applications, including general-purpose adhesives [24], binder in cements and mortars [25], the production of hard foams [26], industrial paints and coatings [25,27], and more [28].

The mechanical characteristics of a natural fibre powder-reinforced composite are influenced by powder particle size, modulus, and distribution. A robust powder-matrix interface connection is vital to maximizing the composite's strength and optimum stress transfer from the matrix to the reinforcement powder [29]. This study analyzes several combinations of untreated and treated coir fibre power with thermoset epoxy resin composites (**Figure 1**). The fabrication of the composite samples is done by hand-layup process. The distribution of reinforcement in matrix resin is investigated through an optical microscope (OM) and a scanning electron microscope (SEM). The mechanical properties were also measured using a universal testing machine (UTM). We applied a different treatment to the coir fibres because there are several methods for handling natural fibres. In order to improve the interfacial bonding capabilities of coir-fiber-reinforced epoxy resin composites, we also made coir fibre to particle and compared different test results to find a more suitable procedure that enhanced the compatibility between coir powder and the matrix.

2. Materials and methods

2.1. Materials

A thermoset epoxy resin was employed as the matrix, along with a hardener. Those were gathered from Nasim Plastic in Dhaka, Bangladesh. Epoxy resin has a molecular weight of 393 Da, a viscosity of 9–14 Pa·s, a density of 1160 kgm^{-3}, and a flash point above >150 ℃. The hardener had a molecular weight of 305 Da, a viscosity of 0.45 Pa·s, a density of 900 kgm^{-3}, and a flash point of 129 ℃. Coir fibre was collected as waste material for coconut from local sources. Pellets of sodium hydroxide (NaOH) were obtained from MERCK in Mumbai, India. It had a purity level of 97.16%.

2.2. Chemical modification of coir fibre

Alkali treatment

Initially, coir fibre was split into little pieces of around 2 inches. The fibres were washed using distilled water. Then the fibres were treated with a 5% NaOH solution at room temperature for 60 min, keeping the liquid to fibres ratio at 15:1. After 1 h, the fibres were carefully cleaned with distilled water three times. The cleaned fibre was then dried in the sun and air. Following that, moisture was removed from treated fibres using a hot air oven set at 105 ℃. The alkali-treated coir fibres were ground into powder using a Panasonic mixer grinder (model MX-AC400). The particles were passed through filters with sieve no. 70 and apertures of 210 microns (**Figure 2**).

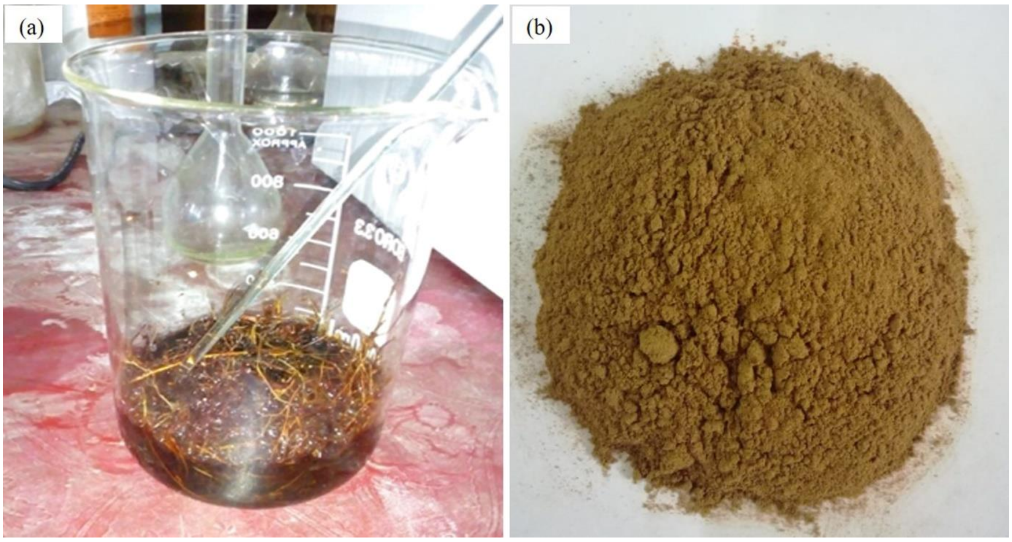

Figure 2. (a) Alkali treatment of coir fibre; **(b)** Alkali treated coir fibre powder.

2.3. Untreated of coir fibre

The untreated coir fibres were ground into powder using a Panasonic mixer grinder (Model MX-AC400). The powders were passed through filters with sieve no. 70 and apertures of 210 microns (**Figure 3**).

Figure 3. Untreated Coir fibre powder.

2.4. Composite preparation method

Epoxy resin, an example of an epoxy oligomer, creates a three-dimensional structure when complemented with a hardener or curing agent. Epoxy resin characteristics may be changed by using different epoxy oligomers and curing processes. The weight ratio between epoxy resin and hardener was 10:1. At first resin and hardener mixed well with super hand mixer (Model: HE-133, Scarlett, England). After that the alkali-treated coir powder at various weight percentages (5 wt%, 10 wt%, 15 wt%, 20 wt%, 25 wt%, and 30 wt%) was blended with epoxy resin utilizing super hand mixer. To manufacture one type of composite at a time, a 100-gram matrix and reinforcement combination were utilized. The matrix, containing 95 gm epoxy resin, and 5 gm coir fibre powder, was blended and stirred for 5 min to generate 5 wt% of reinforcement. Again, for 10 wt%, 15 wt%, 20 wt%, 25 wt%, and 30 wt%, the taken weight of matrix was 90 gm, 85 gm, 80 gm, 75 gm, and 70 gm epoxy resin, respectively. The composite was cast using a mould with dimensions of 3mm × 10mm × 80 mm. The mould was waxed with a releasing agent before being filled with a resin-powder mixer. The releasing agents utilized serve to prevent the sample from sticking or becoming lodged inside the mould, as well as allowing for simple removal of the sample. The samples were stored in the mould for 24 h before testing (**Figure 4**).

The same hand-lay technique was used to make composites from untreated coir fibre powder. Mix untreated coir fibre powder with epoxy at various weight percentages (5 wt%, 10 wt%, 15 wt%, 20 wt%, 25 wt%, and 30 wt%) using a super hand mixer. After that, the mixer was poured into the mould for making untreated coir powder-epoxy composites. It was also stored for 24 h for solidification.

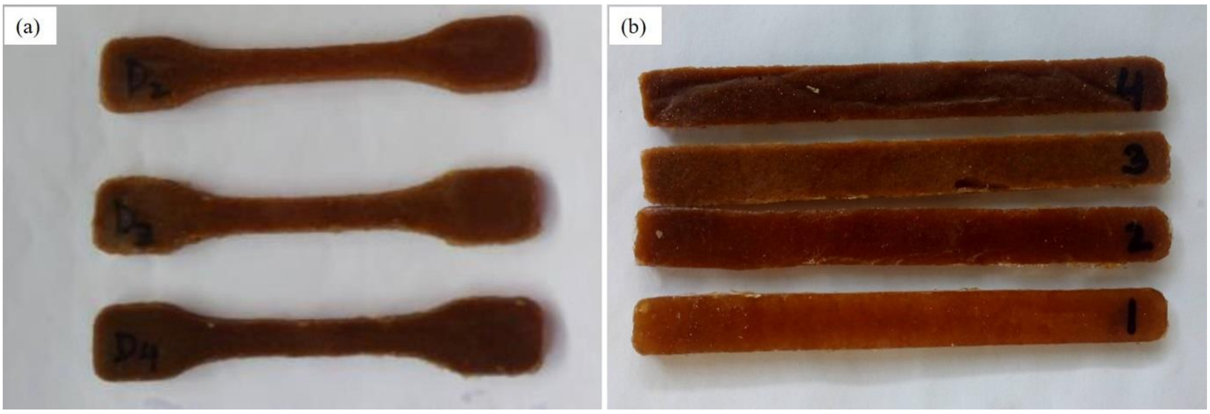

Figure 4. Images of prepared coir powder reinforced epoxy resin composite.

2.5. Microstructural analysis

The interfacial bonding between the reinforcement and epoxy matrix in the created composites was examined using optical microscopy (OM) (ML-803), Taiwan, and a scanning electron microscope (SEM) (JSM-7600 F), supplied by JEOL Company Limited, Japan. Composite samples were coated in gold before morphological analysis was done using a scanning electron microscope.

2.6. Mechanical testing

Tensile, Charpy impact, and toughness tests were performed on the materials. Five species were analyzed, and the average results were noted for each test and composite type. Tensile testing was conducted using a Universal Testing Machine (UTM) (Model: MSC-5/500, Agawn Seiki Company Limited, Japan) in accordance with ASTM D 638-01, at a crosshead speed of 10 $\text{mm}\cdot\text{min}^{-1}$. In compliance with ASTM D 6110–9724 and ASTM E23, dynamic Charpy impact tests and toughness tests were performed on notched composite specimens using a Universal Impact Testing Machine (Model: 7408, Hung Ta, Taiwan).

3. Results and discussion

3.1. Morphological observation

The microstructure of the developed composite samples was studied using an optical microscope (OM) with different magnifications (such as 10x, 40x, and 60x). The optical microstructural observations of the epoxy-alkali-treated coir powder-reinforced composite were primarily made to examine the distribution of coir particles in the polymer matrix, the presence or absence of particle clusters and agglomeration, and the presence of any inclusions and voids.

In **Figure 5**, we can see the microstructure of an 80 wt%–20 wt% epoxy-alkali-treated coir powder composite. Here, a uniform distribution of coir powder on the epoxy resin surface was observed, and no significant void, crack, or cluster was found.

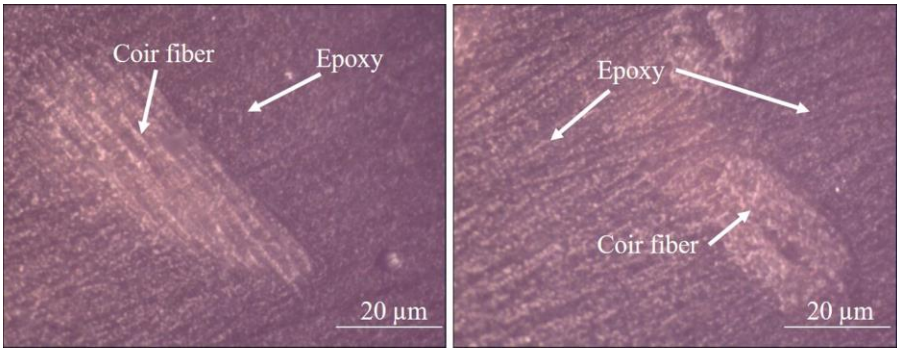

Figure 5. Optical micrographs of composite surfaces: 80–20 wt% epoxy-alkali-treated coir powder.

Scanning electron microscope (SEM) surface inspection offers substantial insights into composite samples, such as outer morphology (texture), chemical composition, interfacial adhesion, crystalline structure, and material orientation, presenting beneficial details about the specimen. This research employs SEM (scanning electron microscope) in order to generate images with high resolution along with extensive surface information from the specimen.

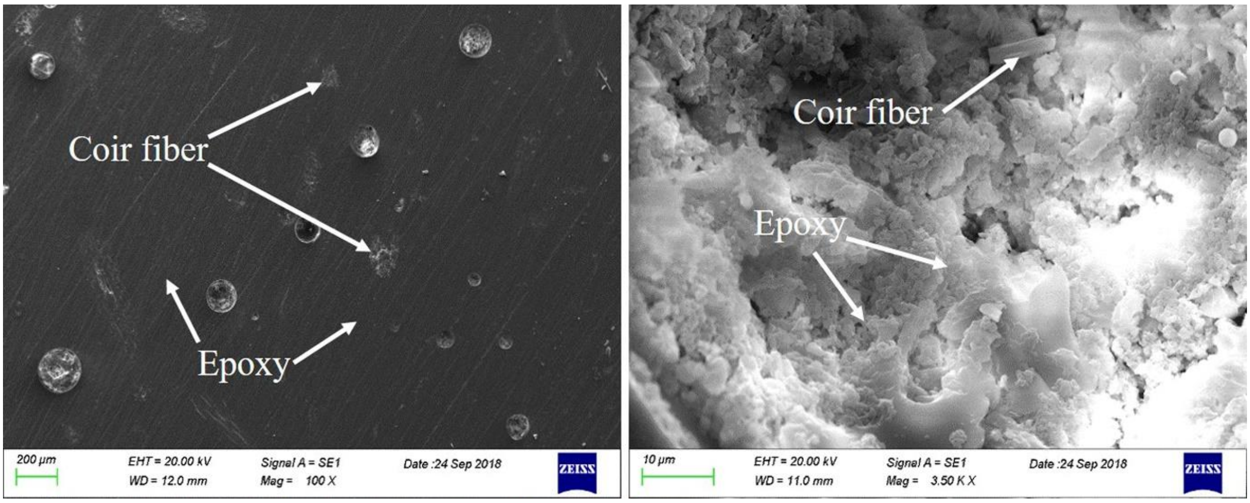

Figure 6. SEM micrographs of composite surfaces: 80 wt%–20 wt% epoxy-alkali-treated coir powder.

Figure 6 demonstrates that coir powders were embedded in a matrix with no gaps, and their surfaces were treated with polymer, which suggests strong interface bonding. Strong adhesion at the interface between the particle and polymer matrix has been observed, resulting in more effective mechanical characteristics. Coir powders were arranged on top of each other in the matrix and the particle size are around ~ 200 µm was revealed. There were no gaps, cavities, or voids, and the coir fibre and polymer were very well blended. It looks like the matrix and reinforcement composites are well bound up, and they are on track toward exhibiting considerable basic features and multifunctional textures. Based on research, the matrix in a composite is the intermediary load-bearing ingredient, while the reinforcement serves to cover the matrix and maximize its strength. A well-bonded interaction facilitates the efficient transfer and spreading of loads from the matrix to the reinforcement [30].

3.2. Mechanical properties

3.2.1. Tensile properties

Tensile strength is the maximum strain that a material tolerates without fracturing when stretched, divided by its initially formed cross-sectional area. When doing mechanical testing on polymer composites, the Universal Testing Machine (UTM) bends the sample while applying increasing tension along the material's axis. Tensile characteristics are examined at 100 $\text{mm}\cdot\text{min}^{-1}$ and the specimen was expanded using a moving crosshead.

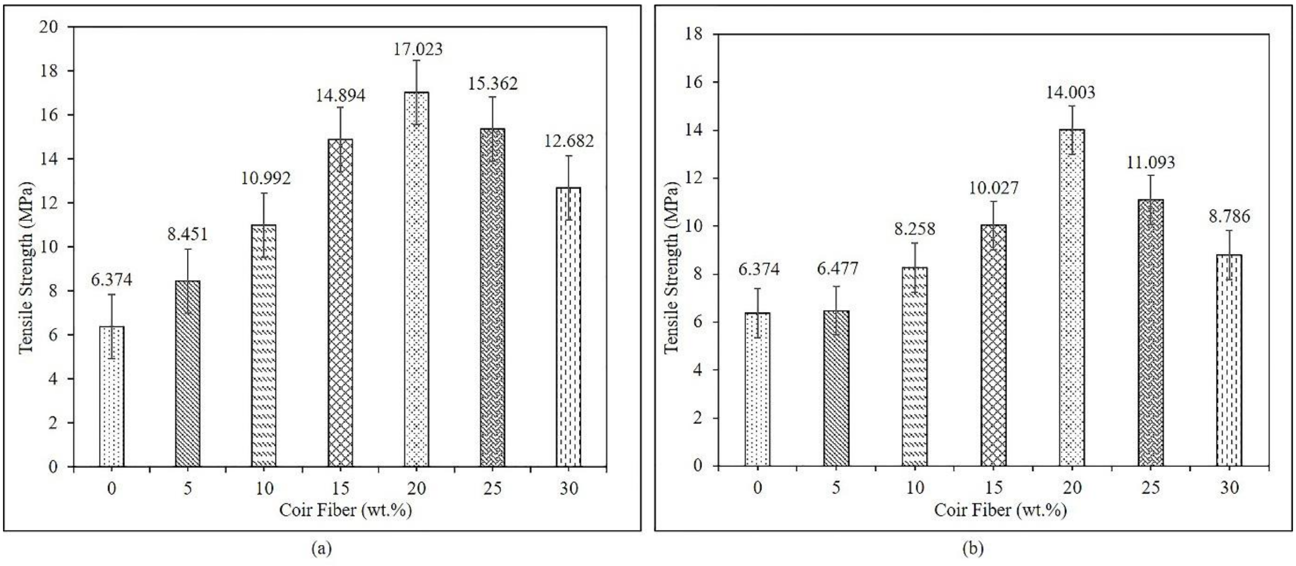

Figure 7. Tensile strength of **(a)** epoxy-alkali-treated coir powder composites; **(b)** epoxy-untreated coir powder composites.

According to **Figure 7**, enhancing the weight percentages of the powder increases the tensile strength of a composite material by up to 20 wt%. The highest recorded tensile strength of epoxy-untreated coir powder composites is 14.003 MPa, while epoxy-alkali-treated coir composites at a 20 wt% powder-to-matrix ratio possess a tensile strength of 17.023 MPa. A further increase in powder loading decreases the tensile strength. Tensile strength improves by up to 20 wt% with the loading of powder due to the powders higher load-bearing capability over the matrix. Tensile strength reduces under greater loading due to poor interfacial adhesion between powder and matrix, as well as a rise in microspace formation in composites because excessive powder generates a gap between the matrix material [31]. In addition, below 20 wt% loading may not be satisfactory for increasing the matrix's strength, and insufficient stress transfer may have resulted in a reduced strength [32].

3.2.2. Impact strength and toughness

The composite's strength, hardness, and impact energy are significantly impacted by the coconut shell particles [33]. When materials undergo an impact load, their ability to withstand fracture is gauged by their impact strength. The component material nature, the fiber/matrix interface, the composite's structure and shape, and the test circumstances all have a significant impact on the characteristics of composites that are impactful. Impact strength is correlated with the composite's higher elasticity, which in turn improved matrix deformability. As a stress-transferring medium and a means of interacting with the crack development, natural fibers often play a major part in the impact resistance of fiber-reinforced composites [34].

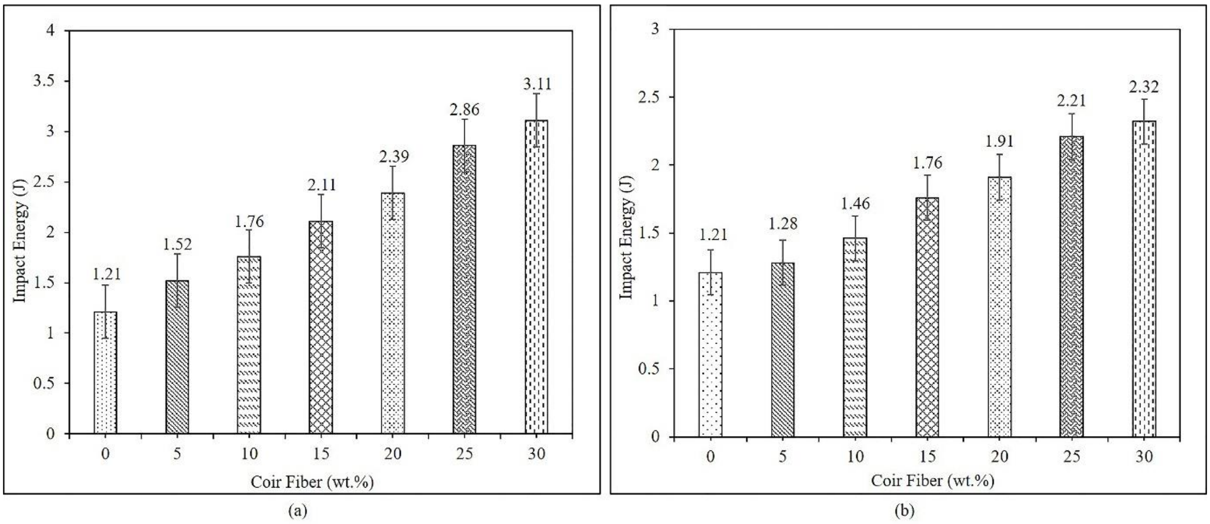

Figure 8. Impact energy of **(a)** epoxy-alkali-treated coir powder composites; **(b)** epoxy-untreated coir powder composites.

Figure 8 shows the impact characteristics of the epoxy-untreated coir powder composite compared to the alkali-treated coir powder composite. Impact energy increases with the higher loading of powder, and it reaches up to 3.11 J for epoxy-treated coir powder composites, whereas epoxy-untreated coir composites at 30 wt% percentages revealed 2.32 J. The impact energy increases with higher powder concentrations due to the larger energy absorption capacity of powders compared to matrix. This phenomenon might also be due to the good interfacial bonding of matrix to powder, which results in better energy absorption during impact [35].

Toughness is the property of the material that enables it to withstand shock and deformation without rupturing. High toughness can be achieved by a good combination of strength and ductility.

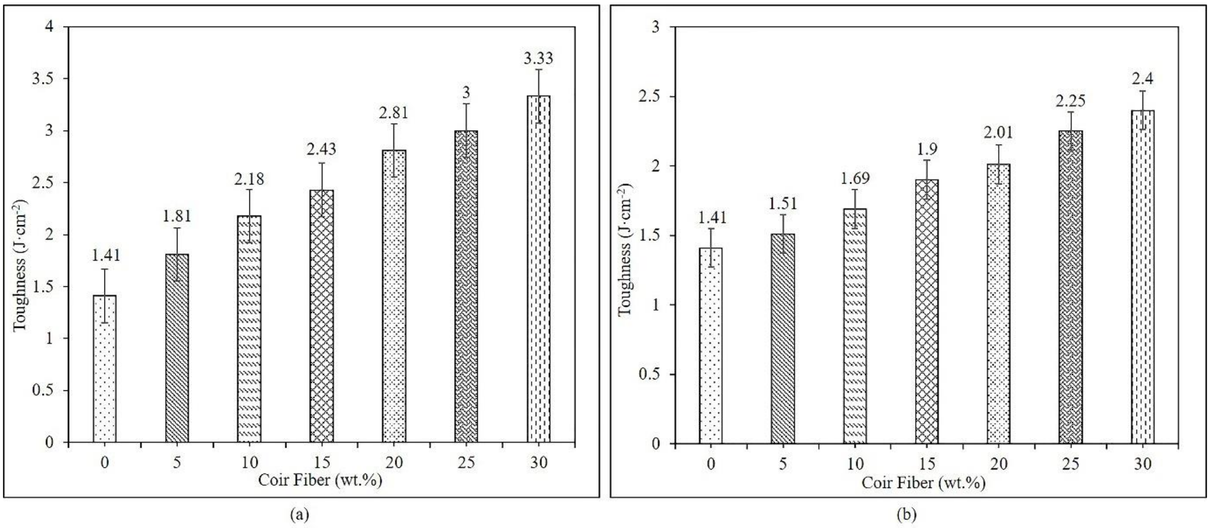

Figure 9. Toughness properties of **(a)** epoxy-alkali-treated coir powder composites; **(b)** epoxy-untreated coir powder composites.

Findings from **Figure 9** show the toughness of the epoxy-untreated coir powder composite compared to the epoxy-alkali-treated coir powder composite. The toughness of composites increases with an increase in powder concentration. However, analyzing toughness between epoxy-alkali-treated and untreated coir powder reinforcement composites shows that the improvement in toughness of epoxy-alkali-treated composites is a little more than that of epoxy-untreated coir powder-reinforced composites. At 30 wt% reinforcement composites, epoxy-alkali-treated composites exhibit 3.33 J·cm^{-2} and epoxy-untreated coir powder-reinforced composites exhibit 2.4 J·cm^{-2}. This is because alkaline treatment increases natural fibre and polymer bonding, which builds a robust structure of natural fibre with composites because of the elimination of lignin, pectin, oil, wax, and impurities on the cell wall surfaces of the fibres, which leads to the exposure of short-length crystallites and a rise in surface roughness on the fiber, which results in improved mechanical properties [36]. The alkaline-sensitive hydroxyl groups (-O-H bond structure) present in natural powder molecules are broken down by alkaline treatment. Following that, it interacted with groups of alcohol molecules, phenols, or water (H-O-H bond structure), migrating either within or outside of the powder structure in response to the alkaline reaction, depending on the properties of the powder. The cellulose molecular chain's powder cell of the -O-Na bond structure was therefore indirectly created by the residual reactive molecules, allowing the increment of mechanical properties [37].

The function of reinforcement in a composite is to contain the matrix and so improve the composites' strength, whereas the matrix's primary functioning elements are the intermediate load-bearing parts. Distribution and transmission of load from the matrix to the reinforcement are made easier by a well-bonded interface. In contrast, weak bonds restrict the amount of strengthening since they reduce load transmission. Improvements in mechanical characteristics are thus the consequence of a stronger interfacial connection [38]. In the case of the coir fibre-reinforced epoxy resin composites considered in this study, fine coir particles dispersed homogeneously on the resin matrix play an important role for good bonding of the composite. In addition, the uniformly distributed coir particles obtained by mixer grinder contribute to attaining a good compact. As shown in **Figures 5** and **6**, the interface between the matrix and the reinforcement exhibits a good interfacial integrity. Thus, it can be concluded that coir powder mixing with matrix with optimized matrix-reinforcement ratio can be very effective in improving the properties of the composite.

4. Conclusion

Composite materials are gaining popularity for their lightweight, outstanding mechanical characteristics, clarity of manufacture, and low pricing. Due to their high specific strength and modulus, powder-reinforced polymer composites, especially ones with coir fibre powder, have been frequently used. Coir fibre, an affordable and widely accessible natural fibre, can be utilized as a byproduct in coconut production for making a beneficial and useful coir powder-reinforced polymer composite. The objective of this research is to develop and explain innovative composites with untreated and alkali-treated coir fibres powder as reinforcement and epoxy resin as a matrix through a hand-lay process. The morphological observation inquiries indicate that epoxy-coir powder composites have a consistent reinforce distribution with no voids, cavities, or pores, as observed according to the Optical Microscope (OM) and Scanning Electron Microscope (SEM). The weight percentages of coir powder have significant effects on the mechanical properties of epoxy-coir-reinforced composites, such as tensile strength, impact energy, and toughness. Tensile qualities enhance along with 20 wt% coir powder loading, while impact energy and toughness increase with 30 wt% coir powder loading due to the powder's higher load-bearing capacity. Coir fibre composites treated with alkali (NaOH) have superior mechanical characteristics than untreated fibre composites. This procedure eliminates contaminants and harsher fibre surfaces, increasing the coir powder's adhesive ability in the composite matrix and resulting in improved mechanical qualities. Epoxy-Coir fibre reinforced composites have a possibility for application in low-cost housing [39], furniture [40], fencing, flooring [41,42], sports equipment [43], aerospace [44], and industrial applications [42]. These composites have a greater prospect for future development.

Author contributions: Conceptualization, ANF and MRKS; methodology, ANF, MRKS and MTA; software, ANF, MTA and RB; validation, ANF, MTA, RB and MRKS; formal analysis, ANF, MRKS, MTA and RB; investigation, ANF, MRKS and MTA; resources, ANF, MTA and MRKS; data curation, ANF, MTA, RB and MRKS; writing-original draft preparation, ANF, MTA and RB; writing-review and editing, ANF and RB; visualization, ANF and MRKS; supervision, ANF and MRKS; project administration, ANF, MRKS and MTA; funding acquisition, ANF, MTA and MRKS. All authors have read and agreed to the published version of the manuscript.

Acknowledgments: The authors are thankful to the University of Rajshahi under the department of Applied Chemistry and Chemical Engineering for their support.

Conflict of interest: The authors declare no conflict of interest.

References

1. Kangishwar S, Radhika N, Sheik AA, et al. A comprehensive review on polymer matrix composites: material selection, fabrication, and application. Polymer Bulletin. 2022; 80(1): 47–87. doi: 10.1007/s00289-022-04087-4
2. Rajak D, Pagar D, Menezes P, et al. Fiber-Reinforced Polymer Composites: Manufacturing, Properties, and Applications. Polymers. 2019; 11(10): 1667. doi: 10.3390/polym11101667
3. Al-Azad N, Asril MFM, Shah MKM. A Review on Development of Natural Fibre Composites for Construction Applications. Journal of Materials Science and Chemical Engineering. 2021; 09(07): 1–9. doi: 10.4236/msce.2021.97001
4. Lau K tak, Hung P yan, Zhu MH, et al. Properties of natural fibre composites for structural engineering applications. Composites Part B: Engineering. 2018; 136: 222–233. doi: 10.1016/j.compositesb.2017.10.038
5. Pulikkalparambil H, Varghese SA, Chonhenchob V, et al. Recent Advances in Natural Fibre-Based Materials for Food Packaging Applications. Polymers. 2023; 15(6): 1393. doi: 10.3390/polym15061393
6. Majeed K, Jawaid M, Hassan A, et al. Potential materials for food packaging from nanoclay/natural fibres filled hybrid composites. Materials & Design (1980–2015). 2013; 46: 391–410. doi: 10.1016/j.matdes.2012.10.044
7. Ali HT, Alghtani AH, Felemban BF, et al. Multivariable analysis for selection of natural fibers as fillers for a sustainable food packaging industry. Materials Research Express. 2021; 8(9): 095504. doi: 10.1088/2053-1591/ac17a9
8. Naik V, Kumar M, Kaup V. A Review on Natural Fiber Composite Material in Automotive Applications. Engineered Science. 2022; 18: 1–10. doi: 10.30919/es8d589
9. Huda MS, Drzal LT, Ray D, et al. Natural-fibre composites in the automotive sector. In: Pickering KL (editor). Properties and Performance of Natural-Fibre Composites, Woodhead Publishing Series in Composites Science and Engineering; 2008. pp. 221–268.
10. Verma D, Gope PC, Shandilya A, et al. Coir fibre reinforcement and application in polymer composites. Journal of Materials and Environmental Science. 2013; 4(2): 263–276.
11. Freitas BR, Braga JO, Orlandi MP, et al. Characterization of coir fiber powder (cocos nucifera L.) as an environmentally friendly inhibitor pigment for organic coatings. Journal of Materials Research and Technology. 2022; 19: 1332–1342. doi: 10.1016/j.jmrt.2022.05.098
12. Rencoret J, Ralph J, Marques G, et al. Structural Characterization of Lignin Isolated from Coconut (Cocos nucifera) Coir Fibers. Journal of Agricultural and Food Chemistry. 2013; 61(10): 2434–2445. doi: 10.1021/jf304686x
13. Alharbi MAH, Hirai S, Tuan HA, et al. Effects of chemical composition, mild alkaline pretreatment and particle size on mechanical, thermal, and structural properties of binderless lignocellulosic biopolymers prepared by hot-pressing raw microfibrillated Phoenix dactylifera and Cocos nucifera fibers and leaves. Polymer Testing. 2020; 84: 106384. doi: 10.1016/j.polymertesting.2020.106384
14. Bensalah H, Raji M, Abdellaoui H, et al. Thermo-mechanical properties of low-cost “green” phenolic resin composites reinforced with surface modified coir fiber. The International Journal of Advanced Manufacturing Technology. 2021; 112(7–8): 1917–1930. doi: 10.1007/s00170-020-06535-9
15. Arrakhiz FZ, El Achaby M, Kakou AC, et al. Mechanical properties of high density polyethylene reinforced with chemically modified coir fibers: Impact of chemical treatments. Materials & Design. 2012; 37: 379–383. doi: 10.1016/j.matdes.2012.01.020
16. Mir SS, Hasan SMN, Hossain MdJ, et al. Chemical Modification Effect on the Mechanical Properties of Coir Fiber. Engineering Journal. 2012; 16(2): 73–84. doi: 10.4186/ej.2012.16.2.73
17. Biswas S, Kindo S, Patnaik A. Effect of fiber length on mechanical behavior of coir fiber reinforced epoxy composites. Fibers and Polymers. 2011; 12(1): 73–78. doi: 10.1007/s12221-011-0073-9
18. Saha P, Manna S, Chowdhury SR, et al. Enhancement of tensile strength of lignocellulosic jute fibers by alkali-steam treatment. Bioresource Technology. 2010; 101(9): 3182–3187. doi: 10.1016/j.biortech.2009.12.010
19. Shibata S, Cao Y, Fukumoto I. Flexural modulus of the unidirectional and random composites made from biodegradable resin and bamboo and kenaf fibres. Composites Part A: Applied Science and Manufacturing. 2008; 39(4): 640–646. doi: 10.1016/j.compositesa.2007.10.021
20. Valášek P, D’Amato R, Müller M, et al. Mechanical properties and abrasive wear of white/brown coir epoxy composites. Composites Part B: Engineering. 2018; 146: 88–97. doi: 10.1016/j.compositesb.2018.04.003
21. Dixit S, Goel R, Dubey A, et al. Natural Fibre Reinforced Polymer Composite Materials—A Review. Polymers from

Renewable Resources. 2017; 8(2): 71–78. doi: 10.1177/204124791700800203

22. Udhayasankar R, Karthikeyan B. A review on coconut shell reinforced composites. International Journal of Chemtech Research. 2015; 8(11): 624–637.
23. Sapuan SM, Harimi M, Maleque M. Mechanical properties of epoxy/coconut shell filler particle composites. Arabian Journal for Science and Engineering. 2003; 28(2): 171–182.
24. Frihart CR. Epoxy adhesives from natural materials. In: Dunky M, Mittal KL (editors). Biobased Adhesives: Sources, Characteristics and Applications. Scrivener Publishing LLC; 2023. pp. 367–393.
25. Rahman MdM, Akhtarul Islam M. Application of epoxy resins in building materials: progress and prospects. Polymer Bulletin. 2021; 79(3): 1949–1975. doi: 10.1007/s00289-021-03577-1
26. Auad ML, Zhao L, Shen H, et al. Flammability properties and mechanical performance of epoxy modified phenolic foams. Journal of Applied Polymer Science. 2007; 104(3): 1399–1407. doi: 10.1002/app.24405
27. Verma C, Olasunkanmi LO, Akpan ED, et al. Epoxy resins as anticorrosive polymeric materials: A review. Reactive and Functional Polymers. 2020; 156: 104741. doi: 10.1016/j.reactfunctpolym.2020.104741
28. Saba N, Jawaid M, Alothman OY, et al. Recent advances in epoxy resin, natural fiber-reinforced epoxy composites and their applications. Journal of Reinforced Plastics and Composites. 2015; 35(6): 447–470. doi: 10.1177/0731684415618459
29. Karnani R, Krishnan M, Narayan R. Biofiber—reinforced polypropylene composites. Polymer Engineering & Science. 1997; 37(2): 476–483. doi: 10.1002/pen.11691
30. Faruqui AN, Manikandan P, Sato T, et al. Mechanical milling and synthesis of Mg-SiC composites using underwater shock consolidation. Metals and Materials International. 2012; 18(1): 157–163. doi: 10.1007/s12540-012-0019-9
31. Adhikari RK, Gowda BSK. Exploration of mechanical properties of banana/jute hybrid polyester composite. Materials Today: Proceedings. 2017; 4(8): 7171–7176. doi: 10.1016/j.matpr.2017.07.043
32. Colom X, Carrasco F, Pagès P, et al. Effects of different treatments on the interface of HDPE/lignocellulosic fibre composites. Composites Science and Technology. 2003; 63(2): 161–169. doi: 10.1016/S0266-3538(02)00248-8
33. Olumuyiwa AJ, Isaac TS, Samuel SO. Study of Mechanical Behaviour of Coconut Shell Reinforced Polymer Matrix Composite. Journal of Minerals and Materials Characterization and Engineering. 2012; 11(08): 774–779. doi: 10.4236/jmmce.2012.118065
34. Jawaid M, Khalil HA, Bakar AA, et al. Effect of jute fibre loading on the mechanical and thermal properties of oil palm–epoxy composites. Journal of Composite Materials. 2012; 47(13): 1633–1641. doi: 10.1177/0021998312450305
35. Salleh Z, Hyie KM, Yunus S, et al. Tensile and Impact Strength of Coir Fibre Reinforced Polypropylene Composites: Effect of Different Temperature Conditions. Applied Mechanics and Materials. 2015; 763: 25–29. doi: 10.4028/www.scientific.net/amm.763.25
36. Adeniyi AG, Onifade DV, Ighalo JO, et al. A review of coir fiber reinforced polymer composites. Composites Part B: Engineering. 2019; 176: 107305. doi: 10.1016/j.compositesb.2019.107305
37. Ng YR, Shahid SNAM, Nordin NIAA. The effect of alkali treatment on tensile properties of coir/polypropylene biocomposite. IOP Conference Series: Materials Science and Engineering. 2018; 368: 012048. doi: 10.1088/1757-899x/368/1/012048
38. Tham LM, Gupta M, Cheng L. Effect of limited matrix—reinforcement interfacial reaction on enhancing the mechanical properties of aluminium–silicon carbide composites. Acta Materialia. 2001; 49(16): 3243–3253. doi: 10.1016/S1359-6454(01)00221-X
39. Saba N, Jawaid M. Epoxy resin based hybrid polymer composites. In: Thakur VK, Thakur MK, Pappu A (editors). Hybrid Polymer Composite Materials Properties and Characterisation. Woodhead Publishing; 2017. pp. 57–82.
40. Sadeq NS, Mohammadsalih ZG, Mohammed RH. Effect of grain size on the structure and properties of coir epoxy composites. SN Applied Sciences. 2020; 2(7). doi: 10.1007/s42452-020-2991-x
41. Chaudari P, Gajare K, Kulkarni MDS. Epoxy resin based egg shell powder and coconut coir fibre composites. Journal of Adhesion Science and Technology. 2022; 9(6): 3296–3301.
42. Mittal M, Chaudhary R. Experimental investigation on the mechanical properties and water absorption behavior of randomly oriented short pineapple/coir fiber-reinforced hybrid epoxy composites. Materials Research Express. 2018; 6(1): 015313. doi: 10.1088/2053-1591/aae944
43. Singh Y, Singh J, Sharma S, et al. Fabrication and characterization of coir/carbon-fiber reinforced epoxy based hybrid composite for helmet shells and sports-good applications: influence of fiber surface modifications on the mechanical, thermal

and morphological properties. Journal of Materials Research and Technology. 2020; 9(6): 15593–15603. doi: 10.1016/j.jmrt.2020.11.023

44. Virk GS, Singh B, Singh Y, et al. Abrasive water jet machining of coir fibre reinforced epoxy composites: a review. Functional Composites and Structures. 2022; 4(1): 014001. doi: 10.1088/2631-6331/ac586c

Journal of Polymer Science and Engineering 2024, 7(2), 8724.
https://doi.org/10.24294/jpse8724

Article

Study on the painting methods, amount and thermal properties of waterborne acrylic paint on bamboo-laminated lumber for furniture

Jie Chen[1,2], **Shaofei Yuan**[1], **Jian Zhang**[1], **Hongyan Wang**[1,*]

[1] Key Laboratory of Bamboo Research of Zhejiang Province, Zhejiang Academy of Forestry, Hangzhou 310023, China
[2] Zhejiang Agriculture and Forestry University, Hangzhou 311300, China
*** Corresponding authors:** Hongyan Wang, 15990054143@163.com

CITATION

Chen J, Yuan S, Zhang J, Wang H. Study on the painting methods, amount and thermal properties of waterborne acrylic paint on bamboo-laminated lumber for furniture. Journal of Polymer Science and Engineering. 2024; 7(2): 8724. https://doi.org/10.24294/jpse8724

ARTICLE INFO

Received: 22 August 2024
Accepted: 13 November 2024
Available online: 27 November 2024

Abstract: In order to understand the finishing effect of Waterborne Acrylic Paint under different painting methods and amount, bamboo-laminated lumber for furniture was coated with waterborne acrylic paint, then the effects of different painting methods and amount on the drying rate, smoothness, hardness, adhesion and wear resistance of the paint film were investigated. Further, the mechanism of film formation was described by thermal property analysis using thermogravimetry and differential scanning calorimeter. The results show that different painting methods have little effect on film properties, the drying time of primer and topcoat are not affected by them, which is 8/8.5 min for primer surface/solid and 6.5/7 min for topcoats. The film surface hardness and adhesion can reach B and 0 grade, the best wear resistance of the film is 51.24 mg·100 r^{-1} when using one-layer primer one-layer topcoat. Different coating amount has great influence on film properties, the drying speed of the film increases with the increase of the painting amount. The film properties reach the best when the painting amount is 80 g/m^2, while too little painting amount leads to the decrease of hardness, and too much leads to the wear resistance weaken. Thermal analysis of the primer and topcoat show that water decomposition occurs at 100 ℃ and thermal decomposition of organic components occur at 350 ℃. Topcoats have better thermal stability than primers higher than that of topcoat, the topcoat displayed better thermal stability than the primer.

Keywords: waterborne acrylic paint; painting method; painting amount; film properties bamboo-laminated lumber

1. Introduction

Waterborne paints (WBPs) use water as a solvent or dispersion medium which have the advantages of non-toxic, safe, environmental friendly compared with traditional paints [1–3].

In recent years, as awareness of people regarding environmental protection national environmental protection policies increases, the proportion of WBPs used in furniture, interior decoration, construction and other industries is increasing year by year, and WBPs will gradually replace traditional organic paints. With the continuous development of WBPs industry, it plays an increasingly important role in the development of bamboo. At present, bamboo and wood furniture is still mainly painted with organic solvents. In the future, WBPs will be more and more widely used in bamboo furniture [4–6]. “Three parts paint and seven parts painting process” [7–10] highlights the significance of the painting process (including the method and amount) to the film properties. Some scholars have studied the painting process and adhesion mechanism of water-based paint [11,12], But in generally speaking, at present, some scholars have done some research on the painting method and amount of water-based paint, but they mainly focus on wood painting [13–15], there is little research on the painting of bamboo waterborne paint.

In this paper, bamboo-laminated lumber for furniture was coated with waterborne acrylic paint. The effects of different painting methods (one-layer primer one-layer topcoat, one-layer primer two-layer topcoat, two-layer primer one-layer topcoat and two-layer primer two-layer topcoat) and amount (60, 80, 100, 120 g/m^2) on the drying rate, smoothness, hardness, adhesion and wear resistance of the paint film were investigated. Further, the thermal properties of the paint were analysed using thermogravimetry and differential scanning calorimeter to study on the mechanism of film formation. It can provide the theoretical basis for the painting of bamboo, moreover, these can be used as a reference for waterborne painting of bamboo in furniture production.

2. Materials and methods

2.1. Materials

Bamboo-laminated lumber with the density about 0.8 g/cm^3, consisting of side-pressured carbonised Moso bamboo (*Phyllostachys edulis*) sheets, was cut into (100 × 100 × 10) mm^3 in size, the number of the samples was about 30. The bamboo-laminated lumber surface remained uncoated, and the moisture content was controlled under 10%.

Waterborne acrylic paints were bought from Zhejiang Feida new material Co., Ltd which consist of primer (D) and topcoat (M). Main parameters of the paints are showed in **Table 1**.

Additional materials used in this paper include gauze strips, absorbent cotton, a high-grade drawing pencil from a Chinese brand, qualitative filter paper and scotch tape.

Table 1. Main performance parameters of waterborne acrylic paints.

Paints	pH value	Clour	Particle size(nm)	Viscosity (mPa·s)	Polymer dispersity index	Solid content (/%)
Primer (D)	7	Light yellow	221.8	15.7	1.000	29
Topcoat (M)	7	Milky white	925.2	30.8	1.000	38

2.2. Major equipment

Painting equipments: special wool brush for WPBs, sandpapers (240 #, 320 # and 400 #) and electronic scales.

Analytical equipment: Paint film drying time tester (type QGS, produced by Zhongya Cangzhou Zhongya Test Instrument Co., Ltd), pencil hardness tester (type QHQ-A, produce by Zhejiang Airuipu Test Instrument Co., Ltd), wear-resisting instrument (type JM-IV, produced by Pushen Testing Instrument (shanghai) Co., Ltd), super-depth-of-field microscope (type PA53, produced by Shenzhen Huaxian Optical Instrument Co., Ltd), thermalgravimetric analyser (TG for short, type DSC 214 Polyma, produced by NETZSCH-Gerätebau GmbH) and differential scanning calorimeter (DSC for short, type 209F1, produced by NETZSCH-Gerätebau GmbH).

2.3. Preparation of paint films

2.3.1. Different painting methods

In this section, a single-factor experimental method was used. Bamboo-laminated lumber was painted using four different painting method (including one-layer primer one-layer topcoat, one-layer primer two-layer topcoat, two-layer primer one-layer topcoat and two-layer primer two-layer topcoat) at room temperature, as shown in **Figure 1**. Moreover, amount of paint used to the primer and topcoat was maintained at (80 ± 5) g/m^2. Before the primer painting, the bamboo-laminated lumber was sanded with 240 # sandpaper until the surface became smooth (usually, the roughness is less than 10 μm). Before the topcoat coating, the surface was sanded with 320 # sandpaper until the surface was smooth (usually, the roughness is less than 5 μm). After painting, the samples were immediately dried in a temperature and humidity chamber, with conditions set at 50 °C, 20% relative humidity and 0 m/s wind speed. Once the paint film was completely dried, bamboo-laminated lumber was left in an indoor environment for a week to acclimate with the drying time and the paint film performance before testing.

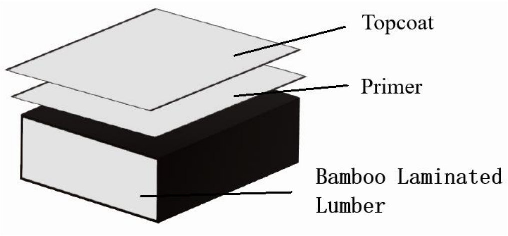

Figure 1. Painting process.

2.3.2. Different amounts of applied paint

In this section, the single-factor experimental method based on the result of the different painting methods and the optimal painting techniques was chosen, then four different amounts of paint (60 g/m^2, 80 g/m^2, 100 g/m^{2}and 120 g/m^2) were applied to primer and topcoat for further examination.

2.4. Testing and Characterisation

The drying rate (including surface drying time and solid drying time) of the paint film were tested according to GB/T 1728-2020, the hardness of the paint film was tested according to GB/T 6739-2006(pencil scratches of different hardness6B-6H were used), the wear resistance (the Loss of film weight) and adhesion (the method of grid) were according to the GB/T 4893.8-2013standard [16,17]. Five parallel samples were tested, and the average was the final result.

Before testing, the completely dried paint film was needed to balance in a natural environment for one week. Each test was conducted at room temperature. Each experiment needs to be repeated five times and the experimental error was observed to below 10.0%.

The super-depth-of-field microscope was used to analyse the surface smoothness of the paint films.

The thermal properties of the liquid primer, topcoat and solid films were analysed using TG and DSC. The temperature range was 30–600 °C, with a heating rate of 10 °C/min.

3. Results and discussion

3.1. Effect of the painting method on the performance of paint films

3.1.1. Effect of the painting method on the drying rate of paint films

Table 2. Surface and solid drying time of the paint films with different painting methods.

Painting Methods	**First Primer**		**Second Primer**		**First Topcoat**		**Second Topcoat**	
	Surface Drying Time (min)	**Solid Drying Time (min)**	**Surface Drying Time (min)**	**Solid Drying Time (min)**	**Surface Drying Time (min)**	**Solid Drying Time (min)**	**Surface Drying Time (min)**	**Solid Drying Time (min)**
one-layer primer one-layer topcoat	8 (0.5)	8.5 (0.41)	/	/	6.5 (0.5)	7 (0.38)	/	/
one-layer primer two-layer topcoat	8 (0.5)	8.5 (0.41)	/	/	6.5 (0.5)	7 (0.38)	6.5 (0.58)	7 (0.51)
two-layer primer one-layer topcoat	8 (0.5)	8.5 (0.41)	6 (0.36)	6.5 (0.53)	6.5 (0.43)	7 (0.46)	/	/
two-layer primer two-layer topcoat	8 (0.5)	8.5 (0.41)	6 (0.36)	6.5 (0.53)	6.5 (0.43)	7 (0.46)	6.5 (0.41)	7 (0.42)

Note: standard deviations are provided in the brackets.

The drying time of paint film can be divided into surface drying and solid drying. Surface drying time refers to the paint surface has been dry, but it still contains water or volatile materials, solid drying refers to the moisture and the volatile materials of the paint have been completely dried.

Table 2 shows the paint films' surface and solid drying time under different painting methods. As shown, the four different painting methods had minimal effect on the film's drying time; the surface drying times for the primers (first and second) were 8 and 6 min, respectively, and the solid drying time were 8.5 and 6.5 min, respectively. Alternatively, the surface drying times of topcoats were 6.5 and 6.5 min, which the solid drying time of primers were 7 and 7 min. Notably, the effect of painting techniques on the drying time of the primer is greater than that of the topcoat. This could be because the first primer layer is in direct contact with the bamboo surface, resulting in the primer permeating into the bamboo surface and requiring a longer period for water evaporation. In contrast, when applying the second primer layer, moisture evaporated directly without permeating the surface. Additionally, a chemical reaction between the first primer and the bamboo surface could lead to a longer surface and solid drying time.

3.1.2. Effect of painting method on the mechanical properties of paint films

The mechanical properties of paint films, including hardness, adhesion and wear resistance, for the four different painting methods are shown in **Table 3**. The hardness of the films obtained using all these four painting methods was grade B and the adhesion was grade 0, indicating that the painting method has little effect on the hardness and adhesion of the film. In this experiment, the four-painting method's quality loss were 51.24, 71.27, 69.68 and 83.65 $\text{mg}\cdot 100\text{r}^{-1}$, respectively. The highest wear resistance was achieved with the one-layer primer one-layer topcoat method, whereas the lowest was observed with the two-layer primer two-layer topcoat method. This may be because the thickness of the film increased with an increase in the paint layers, leading to poor wear resistance. Furthermore, large painting thickness might result in the film's pinhole and hanging, reducing its wear resistance.

Table 3. Mechanical properties of paint films in different painting methods.

Painting methods	**Hardness (grade)**	**Adhesion (grade)**	**Loss of film quality (mg·100r^{-1})**
one-layer primer one-layer topcoat	B	0	51.24 (2.06)
one-layer primer two-layer topcoat	B	0	71.27 (8.29)
two-layer primer one-layer topcoat	B	0	69.68 (10.46)
two-layer primer two-layer topcoat	B	0	83.65 (9.06)

Note: standard deviations are provided in the brackets.

3.1.3. Effect of painting method on the surface smoothness of paint films

The analysis of super-depth-of-field optical microscope is one of the key methods for surface characterization of composite materials. Its advantage lies in the non-destructive optical detection, and the super depth of field, which can observe the micro-area more clearly. The smoothness of the material surface can be directly seen through the super-depth-of-field optical microscope image.

Figure 2 shows a three-dimensional (3D) view of the surface of the paint films painted using the four different painting methods, which measured by the super-depth-of-field optical microscope.

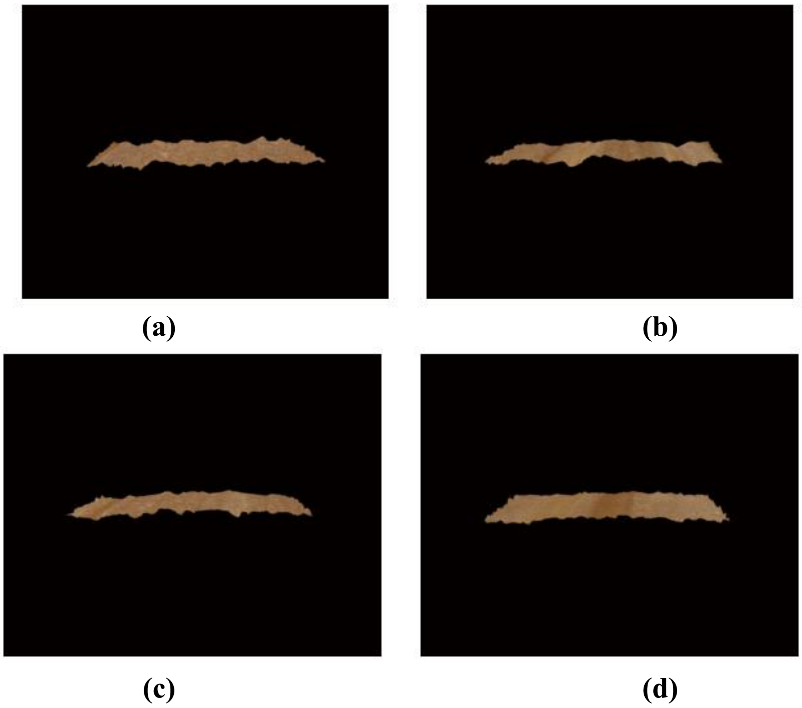

Figure 2. Surface smoothness of films in four painting methods was analysed using super-depth-of-field microscope. **(a)** one-layer primer one-layer topcoat; **(b)** one-layer primer two-layer topcoat; **(c)** two-layer primer one-layer topcoat; **(d)** two-layer primer two-layer topcoat.

The surface smoothness of the paint film increased with increasing paint layers. Hence, among the different painting techniques, two-layer primer two-layer topcoat had the best film surface smoothness. This is probably because the primer serves to fill gaps on the bamboo surface, while the topcoat fills gaps on the primer layer. As the number of paint layers increases, the remaining pores are filled, resulting in a smoother surface.

3.2. Effect of the different paint amount on the performance of paint films

3.2.1. Effect of different paint amount on the drying rate of paint films

The results of the mechanical properties of paint films for the four different painting methods show that the film with one-layer primer one-layer topcoat has the best mechanical performance. Consequently, in this section, bamboo-laminated lumber was painted using a one-layer primer one-layer topcoat with different amount of paint, and the surface and solid drying times of the paints are shown in **Table 4**.

Table 4. Surface and solid drying times of the paint films after applying different amounts of paint.

Amount of paint (g/m^2)	**Primer**		**Topcoat**	
	Surface Drying time (min)	**Solid Drying Time (min)**	**Surface Drying time (min)**	**Solid Drying Time (min)**
60	7 (0.39)	7.5 (0.43)	6 (0.31)	7 (0.34)
80	8 (0.5)	8.5 (0.41)	6.5 (0.5)	7.5 (0.38)
100	9 (0.64)	10 (0.58)	8 (0.52)	9 (0.36)
120	10 (0.34)	10.5 (0.29)	9 (0.63)	9.5 (0.56)

Note: standard deviations are provided in the brackets.

Table 4 shows that the shortest drying time occurs when the amount of paint applied is 60 g/m^2 and that the drying time is longest when the amount of paint applied is 120 g/m^2. The drying time for surface or solid drying were different among the four different painting amounts, showing the following trend: the drying time increases as the amount of paint applied increases. The thickness of the paint increases with the amount of paint, and thus the heat required for water evaporation also increases, which results in a slower drying rate. Additionally, as the amount of paint applied increases, internal molecular motion is relatively difficult, which leads to a slower drying rate. However, a smaller amount of applied paint is not necessarily better as too little paint can weaken the bond between the paint film and the substrate, leading to insufficient adhesion. When the amount of painting reaches a certain degree, the performance of the paint film can meet the requirement.

Figure 3 shows the moisture curves of the primer and topcoat painting tinplate at different paint amounts. As seen in **Figure 3**, the moisture volatilisation rate, which represents the drying rate of the paint film, increases first and then decreases rapidly and then tends to zero, at approximately 2 min, the water volatilisation rate reaches its highest value, furthermore, the drying rate decreases gradually with an increase in the amount of paint. The moisture volatilisation reaches the saturation point fastest, so that the drying time of the film is the shortest. The results in **Figure 3** are consistent with those in **Table 4**. The smaller the amount, the thinner will be the painting, and faster will be the surface water evaporation rate in comparison to the paint film's curing speed. When the paint thickness increases, the curing layer on the film's surface affects water evaporation. The drying speed of the paint film is affected by the coordination of moisture volatilisation and curing speed of the paint film, a high number of film-forming substances in the paint reduces the rate of water leaving the film's surface, which results in a decrease in the drying rate.

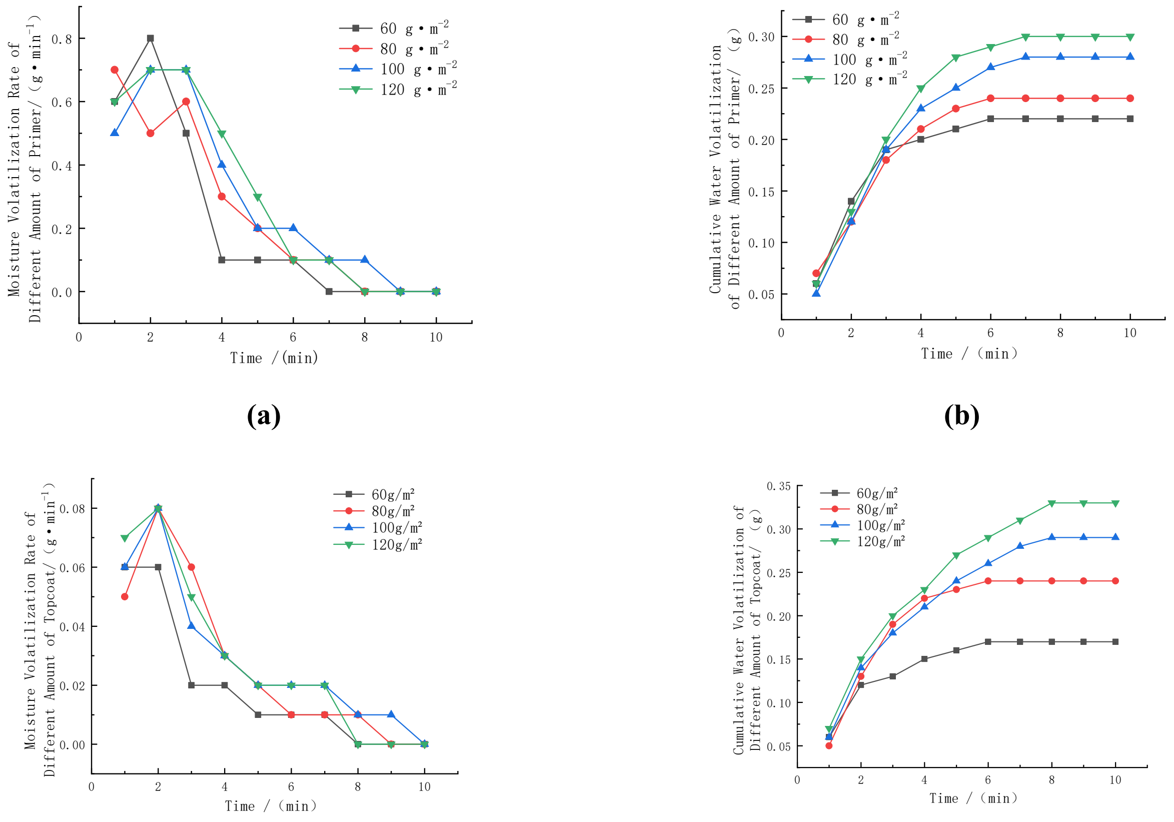

(a) **(b)**

(c) **(d)**

Figure 3. Moisture curves of primer and topcoat painting tinplate in different paint amounts. **(a)** the water volatilisation of primer; **(b)** the cummlative water volatilisation of primer; **(c)** the water volatilisation of topcoat; **(d)** the cummlative water volatilisation of topcoat.

3.2.2. Effect of amount of paint on the mechanical properties of paint films

Table 5. Mechanical properties of the paint films when different amount of paint is applied.

Painting amount (g/m^2)	Hardness (grade)	Adhesion (grade)	Loss of film quality (mg·100r^{-1})
60	2B	0	75.41 (6.77)
80	B	0	51.24 (2.06)
100	B	0	83.16 (6.71)
120	B	0	89.65 (3.68)

Note: standard deviations are provided in the brackets.

Table 5 shows the hardness, adhesion and wear resistance of paint films for four different painting amounts. It can be observed that when the amount of paint applied is 60 g/m^2, the paint film's hardness is lowest, with a grade of 2B, indicating that the amount of paint affects the hardness of the film. As the paint amount increases, the hardness of the film will be improved. However, once the hardness reaches a certain level, the amount of applied paint no longer affects the film's hardness. Here, the paint film's hardness was B grade for the other three painting amounts. The adhesion of the paint films was grade 0. During painting, a large one-time paint amount can lead to film uniformity issues, and painting becomes difficult due to paint hanging as a result of a large amount. The highest wear resistance for the paint film was observed when the amount of paint applied was 80 g/m^2, whereas the lowest wear resistance was found at 120 g/m^2. The reason could be that when using a large amount of paint, part of the paint cannot penetrate the substrate and accumulate on its surface, making it more susceptible to wear. However, if the amount of paint is too small, it cannot form enough paint nails between the paint and bamboo, reducing the effect of the force and making it easy to wear. Therefore, the amount of applied paint 80 g/m^2 is appropriate for wear resistance.

3.2.3. Effect of amount of applied paint on the surface smoothness of paint films

Figure 4 shows the 3D view of the paint film surfaces when applying four different paint amounts. As can be seen from the figure, the flatness of the paint film surface gradually increases with an increase in the amount of applied paint. This may be because, when the paint amount is small, the paint cannot completely cover the pores existing on the surface. Therefore, an increase in the coating amount can effectively fill the pores, hence, the surface smoothness of the film is highest when the paint amount was 120 g/m^2.

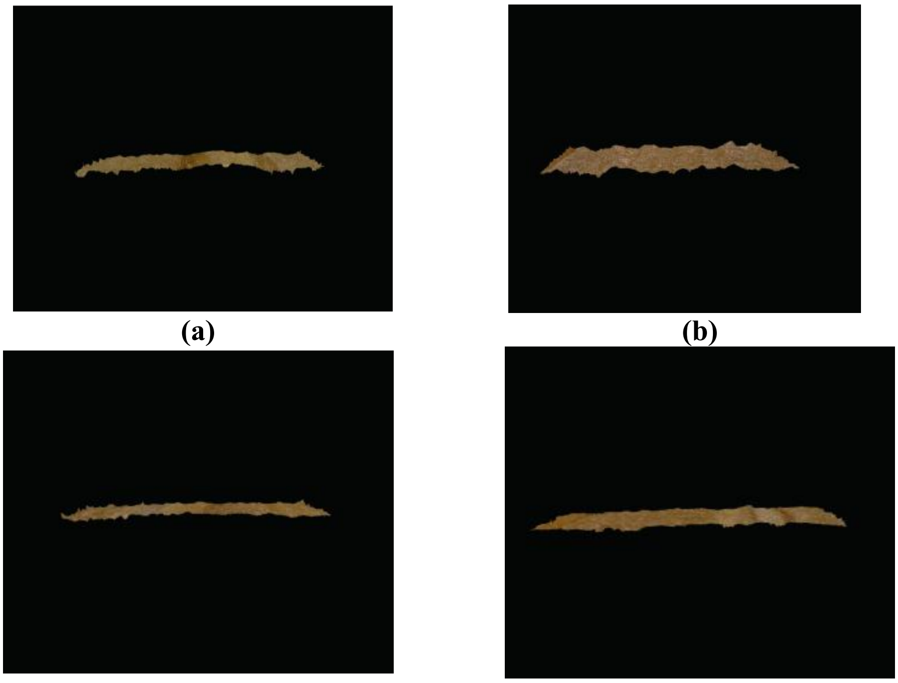

(a) **(b)**

(c) **(d)**

Figure 4. Super-depth-of-field microscope analysed the surface smoothness of the films in the four painting methods (**(a)**, **(b)**, **(c)**, **(d)** are the amount of applied paint 60 g/m^2,80 g/m^2 ,100 g/m^2 and 120 g/m^2).

3.3. Thermal properties analyses of the paints and paint films

3.3.1. Analyses of TG and DTG

TG analysis is a thermal analysis method which can show the relationship between the mass of a substance and temperature or time at a programmed temperature. By analyzing the thermogravimetric curves, the thermal stability, thermal decomposition and the intermediate products can be known.

Figure 5 shows the TG curves of the paints and films. The thermal decomposition processes of primer and topcoat are the same (**Figure 5**), which can be divided into two steps. Firstly, thermal decomposition occurred when the temperature reaches 100 °C, mainly due to water evaporation. Furthermore, the quality of the paints decreases rapidly, and at around 140 °C, the water has completely evaporated, transforming the liquid paints into solids, then the teds to be stabilised. Secondly, thermal decomposition occurred when the temperature reaches 350 °C, which corresponds to the thermal decomposition of polymers (organic components) in the solid paints, the quality of the paints decreases rapidly again, and thermal decomposition of the polymers was completed at approximately 400 °C [18]. The rate of paint weightlessness was 98%. Like liquid paints, the thermal decomposition process of primer and topcoat films can be divided into two steps. First is the evaporation of residual water and other additives in films, then, the rate of film weightlessness was not more than 25%. Second is the thermal decomposition of polymers in the films when the temperature reaches 340 °C. In these steps, the quality of the paints decreases rapidly, and the rate of weight loss is consistent with that of liquid paints, which is finally at 98% [19,20].

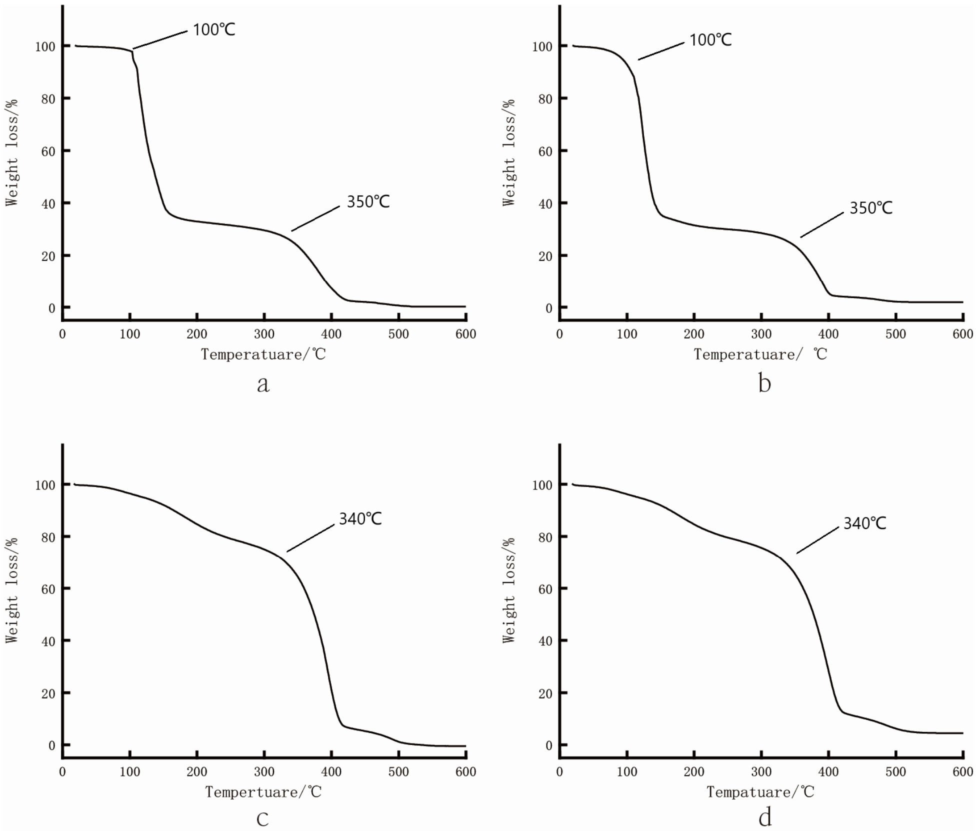

Figure 5. TG curves of paints and films. **(a)** the primer; **(b)** the topcoat; **(c)** the primer film; **(d)** the topcoat film.

DTG is the first derivative of a TG curve to temperature or time. In the DTG curve, the vertical coordinate is the rate of mass change, the horizontal coordinate is the temperature or time.

Figure 6 shows the DTG curves of the paints and films. DTG indicates the weight loss rate. As seen in **Figure 6**, the first peak of the DTG curves for the primer occurred at approximately 110 °C, whereas it appeared at about 130 °C for the topcoat. Similarly, in the DTG curves of the films, the temperature of the peak of the primer film was 400 °C, which is lower than that of the topcoat film. Simultaneously, the thermal loss rate of the primer was higher than that of the topcoat, and all of these results show that the thermal stability of the topcoat was better.

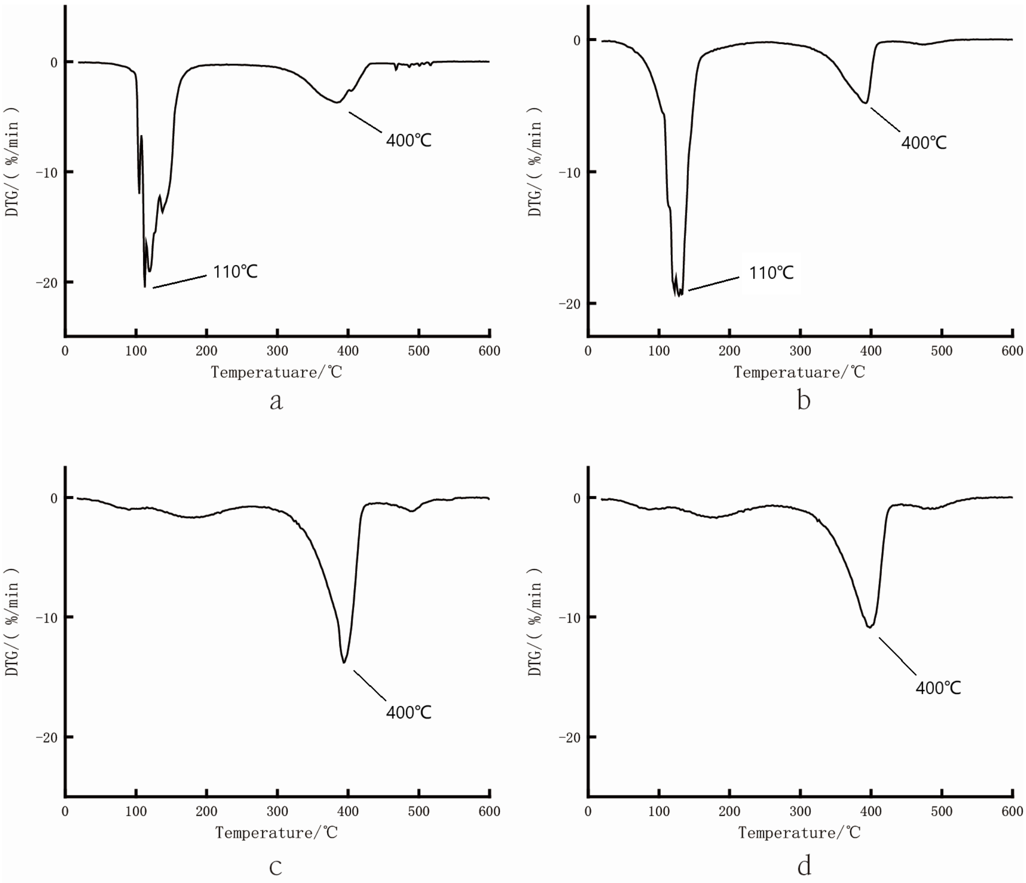

Figure 6. DTG curves of paints and films. **(a)** the primer; **(b)** the topcoat; **(c)** the primer film; **(d)** the topcoat film.

3.3.2. Analysis of DSC

Figure 7 shows the DSC curves of the paints and films. DSC curves are consistent with the results of TG, the DSC curves of primer and topcoat. Firstly, it is mainly the thermal decomposition of water and additives at 100–200 °C. Secondly, it is mainly the thermal decomposition of polymers (organic components) in the paints at 350–550°C. In the DSC curves of films, there is no peak between 100–200 °C as there is no water decomposition, besides, there are two peaks between 400–500 °C, at about 410 °C and 450 °C, respectively.

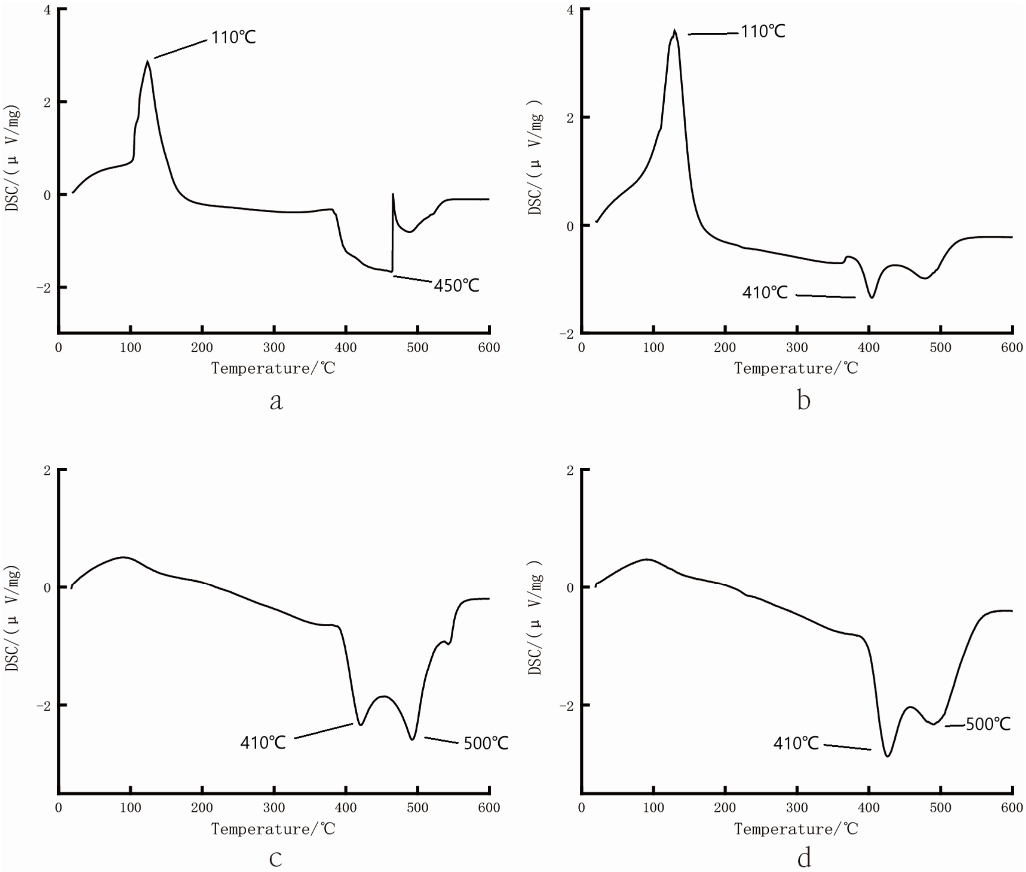

Figure 7. DSC curves of paints and films. **(a)** the primer; **(b)** the topcoat; **(c)** the primer film; **(d)** the topcoat film.

3.3.3. Analysis of the film-forming mechanism

In the thermal analysis results of paints, regardless of primer or topcoat, the first step is the decomposition of water and additives. Hence, the film forming of paint on the bamboo-laminated lumber can be divided into the following stages, as seen in **Figure 8**. First, particles are dispersed in the emulsion paint, then in stage I, water evaporates, and particles pack tightly. In stage II, particle mix together, and finally in state III, the mixed particles form the film [21].

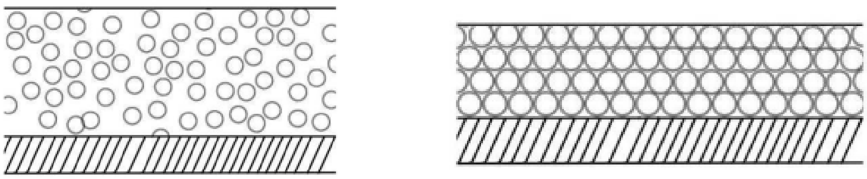

(a) Emulsion paint **(b)** Stage I

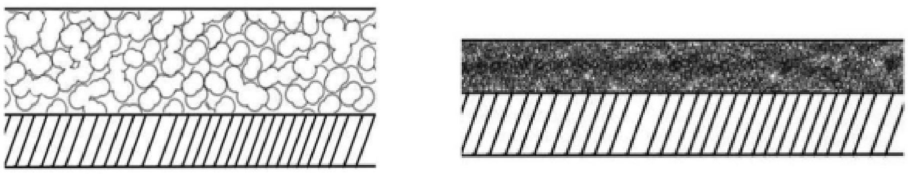

(c) Stage II **(d)** Stage III

Figure 8. Diagram of film formation. **(a)** Emulsion paint: Particles are dispersed; **(b)** Stage I: Water evaporates and particles pack tightly; **(c)** Stage II: Particles mix together; **(d)** Stage III: Film formation.

We know that waterborne acrylic paint is one of the water-soluble paints, so the particles of the paint are dispersed uniformly (emulsion paint). The water in the pants evaporates when painting on the bamboo-laminated lumber (stage I). With the further evaporation of water, the average contact number and contact area of latex particles increase, and the irreversible interaction between particles from disordered state at contact interface deforms, and the density of arrangement increases, the local and the whole reaches the most compact accumulation state, at this stage the force further causes the latex particles to fuse and deform (stage II). Then, the force or surface tension produced by the shrinking surface plays a leading role, and the molecular chains at the polymer interface diffuse, infiltrate and entangle each other, and the boundary of the particles is fully fused, macroscopically, it can form continuous paint film with certain mechanical properties (stage III).

4. Conclusions

In this study, bamboo-laminated lumber for furniture was coated with waterborne acrylic paints and the effects of four different painting methods and amount on the drying rate, smoothness, hardness, adhesion and wear resistance of the paint film were investigated. These results can be used as a reference for waterborne bamboo painting in furniture production. The conclusions are as follows.

(1) The painting method has little effect on the drying time, flatness, hardness and adhesion of the paint film; however, it had a certain influence on wear resistance. In this paper, the flatness of the films is relatively similar when using different painting methods. The drying times of the surface and solid of the primer are 8 and 8.5 min, respectively, whereas those of the topcoat are 6.5 and 7 min, respectively. The hardness and adhesion of the paint films are grade B and grade 0, respectively. The paint film exhibits the best wear resistance (51.24 mg·100 r^{-1}) when painted with one-layer primer one-layer topcoat.

(2) The amount of applied paint remarkably influenced the drying time and flatness of the paint film. As the amount increased, the surface/solid drying time of the paints also increased, and the flatness of the paint film increase first and then decrease. When the amount of applied paint is 80 g/m^2, the film's adhesion, hardness and wear resistance were the best at grade 0, grade B and 51.24 mg·100 r^{-1}, respectively.

(3) The thermal analysis results of the primer and topcoat show that water decompose at 100 °C, while the thermal decomposition of organic components occurs at 350 °C. The weight loss of the primer and topcoat are the same, but the thermal loss rate of primer is higher than that of topcoat. This indicates that the thermal stability of topcoat was better.

Author contributions: Conceptualization, HW and SY; methodology, HW; formal analysis, JZ and JC; writing—original draft preparation, JC; writing—review and editing, HW.

Funding: The authors gratefully thank the financial support from Zhejiang Provincial Cooperative Forestry Science and Technology Project (No.2023SY05) and Zhejiang Provincial Science and Technology Project (No.2024F1065-2).

Conflict of interest: The authors declare no conflict of interest.

References

1. Yao H, Li L, Li W, et al. Application of nanomaterials in waterborne coatings: A review. Resources Chemicals and Materials. 2022; 1(2): 184–200. doi: 10.1016/j.recm.2022.06.004
2. Si Z, Zhang M, Su X, et al. Research status and development trend of environmental friendly waterborne coatings. Coating and Protection. 2021; 42: 24–29, 46.
3. García-Pacios V, Costa V, Colera M, et al. Waterborne polyurethane dispersions obtained with polycarbonate of hexanediol intended for use as coatings. Progress in Organic Coatings. 2011; 71(2): 136–146. doi: 10.1016/j.porgcoat.2011.01.006
4. Wu Y, Zhang H, Yang L, et al. Understanding the effect of extractives on the mechanical properties of the waterborne coating on wood surface by nanoindentation 3D mapping. Journal of Materials Science. 2020; 56(2): 1401–1412. doi: 10.1007/s10853-020-05347-2
5. Wu Y, Sun Y, Yang F, et al. The Implication of Benzene–Ethanol Extractive on Mechanical Properties of Waterborne Coating and Wood Cell Wall by Nanoindentation. Coatings. 2019; 9(7): 449. doi: 10.3390/coatings9070449
6. Yi YF. Synthesis, characterization and properties of waterborne polyurethane acrylic hybrid emulsions. Taiyuan University of Technology; 2017.
7. Yang F, Wu Y, Zhang S, et al. Mechanical and Thermal Properties of Waterborne Polyurethane Coating Modified through One-Step Cellulose Nanocrystals/Graphene Materials Sols Method. Coatings. 2020; 10(1): 40. doi: 10.3390/coatings10010040
8. Yusuf M, Farooqi AS, Alam MA, et al. Response surface optimization of syngas production from greenhouse gases via DRM over high performance Ni–W catalyst. International Journal of Hydrogen Energy. 2022; 47(72): 31058–31071. doi: 10.1016/j.ijhydene.2021.05.153
9. Zhou H, Wang H, Zhu XB, et al. Synthesis and characterization of acrylate/waterborne polyurethane three layers shell-core hybrid latexes. Chemical Research. 2016; 27: 369–373.
10. Wang S, Li W, Han D, et al. Preparation and application of a waterborne acrylic copolymer-siloxane composite: improvement on the corrosion resistance of zinc-coated NdFeB magnets. RSC Advances. 2015; 5(99): 81759–81767. doi: 10.1039/c5ra10851a
11. Li G. Application of Waterborne Acrylic Resin in Home Improvement. China Plastics Industry, 2017; 45(06): 5-6.
12. Chen H, Zhang Y, Yang X, et al. A comparative study of the microstructure and water permeability between flattened bamboo and bamboo culm. Journal of Wood Science. 2019; 65(1). doi: 10.1186/s10086-019-1842-0
13. Hazir E, Koc KH. Evaluation of wood surface coating performance using water based, solvent based and powder coating. Maderas Ciencia y tecnología. 2019; 21(4). doi: 10.4067/s0718-221x2019005000404
14. Gibbons MJ, Nikafshar S, Saravi T, et al. Analysis of a Wide Range of Commercial Exterior Wood Coatings. Coatings. 2020; 10(11): 1013. doi: 10.3390/coatings10111013
15. Darmawan W, Nandika D, Noviyanti E, et al. Wettability and bonding quality of exterior coatings on jabon and sengon wood surfaces. Journal of Coatings Technology and Research. 2017; 15(1): 95–104. doi: 10.1007/s11998-017-9954-1
16. Zhang J, Xu K, Yuan S, et al. Study on drying rate and film properties of waterborne polyurethane coatings. Journal of Central South University of Forestry & Technology. 2019; 39(1):134–140.
17. Lin X, Zhang Q, Huang Y, et al. Painting technology and adhesion mechanism of waterborne paint based on bamboo laminated lumber. Journal of Beijing Forestry University. 2022; 44(9): 158–164.
18. Zhang G, Yue L, Ye J, et al. Pyrolysis characteristics and kinetics behavior analysis of bamboo powder using TG-FTIR. Journal of Light Industry. 2021; 36(02):74–82.
19. Guo Y, Cui H, Song S, et al. Curing Behavior of Poly (silicon alkyne imide) Resin. Journal of Functional polymers. 2021; 34(06): 506–511.
20. Zhou D, Zhao J, Wu J, et al. Application of TG-DSC in the Analysis and Evaluation of Six Fireproof Coatings. Contemporrry Chemical Industry. 2021; 50(10): 2283–2286.
21. Dillon RE, Bradford EB, Andrews RD. Plasticizing a Synthetic Latex. Industrial & Engineering Chemistry. 1953; 45(4): 728–735. doi: 10.1021/ie50520a024

Journal of Polymer Science and Engineering 2024, 7(2), 8606.
https://doi.org/10.24294/jpse8606

Article

Studies of the structure and properties of polymer dispersed liquid crystal films to create a polarizer

Mukhtor Egamov[1,2]

[1] Khudjand Scientific Center, National Academy of Sciences of Tajikistan, Khujand 735714, Tajikistan; egamov62@mail.ru
[2] Mining and Metallurgical Institute of Tajikistan, Buston 735730, Tajikistan

CITATION

Egamov M. Studies of the structure and properties of polymer dispersed liquid crystal films to create a polarizer. Journal of Polymer Science and Engineering. 2024; 7(2):8606. https://doi.org/10.24294/jpse8606

ARTICLE INFO

Received: 15 August 2024
Accepted: 25 October 2024
Available online: 26 November 2024

Abstract: A novel composite material based on polymers (polyvinyl alcohol, polyvinyl butyral) and liquid crystal (4-n-pentyl-4’-cyanobiphenyl) has been developed and studied. Configuration transformations of point defects in nematic droplets under the influence of an electric field, caused by localized changes in the concentration of NLC within the polymer matrix, have been discovered and analyzed. The boundary conditions necessary for achieving a nematic structure with homogeneous alignment of the director both within the droplet and at its surface have been established, optimizing the anisotropy of light transmission in polymer-dispersed liquid crystal (PDLC) films. Additionally, polarization effects inside nematic droplets under the application of an electric field have been identified.

Keywords: polyvinyl alcohol; polyvinyl butyral; polarizers; liquid crystal; surfactant; refractive index; matrix; planar and homeotropic alignments; interfacial anchoring; droplets; textures

1. Introduction

Film polarizers (polaroids) based on polymer films are widely used across various industries, ranging from instrumentation and industrial electronics to consumer and medical equipment. Most polarizers are designed for the visible spectrum and are commonly used in liquid crystal display devices, such as LC indicators and LC displays. Additionally, film polarizers serve as light filters in numerous optical and optoelectronic devices. They are indispensable in specialized fields such as polarization microscopy, magnetometry, spectrophotometry, ellipsometry, and electrical signal measurement [1–3]. Recently, the application of film polarizers has expanded to include devices for detecting hidden images, providing robust protection against forgery for trademarks, securities, and confidential documents. In all these applications, the primary function of film polarizers is to convert incident light into polarized light.

For polaroids, dichroism is due to the introduction of special additives into the polymer matrix or the anisotropy of the intrinsic electronic absorption bands of the macromolecules of the polymer used. However, in laser and optical technologies, polaroid films are applicable only in the case of low radiation intensity, since light absorption can lead to heating and subsequent thermal destruction of the polymer matrix.

Polymer compounds, primarily polyvinyl alcohol (PVA), serve as the main matrix (substrate) material in polarizer films [4]. The PVA polarizer film is a uniaxially oriented polymer containing a dichroic agent. The uniaxial stretching of the film contributes to the orientation of the PVA macromolecules in a specific direction, which ultimately produced a dichroic agent. In this case, the electrical energy is converted into thermal energy. The component of the light radiation polarized orthogonally to the iodine chains usually passes through the PVA polarizer [4]. PVA films are easily subjected to uniaxial orientation, after which they become optically anisotropic and partially polarize the transmitted light radiation. To maximize light transmission, the study [5] investigated the reorientation process of cholesteric liquid crystal, induced by electric-controlled ionic modification of surface anchoring. It was established that in the initial state, the homeotropic orientation of the director was realized in the liquid crystal cell, and when exposed to a constant electric field, a twisted home planar structure of the cholesteric was formed.

In the transformation of the director configuration was investigated when the boundary conditions were changed from planar to homeotropic for bipolar nematic droplets dispersed in a polymer matrix [6]. The authors presented characteristic texture patterns for droplets with different concentrations of homeotropic surfactants and determined their orientational structure. They demonstrated that by using a computational method for minimizing the elastic deformation energy of the director within the droplet and introducing non-uniform boundary conditions, it is possible to obtain orientational structures necessary for maximizing light transmission. However, the main drawback of most traditional and new methods for producing polarizers is the inability to achieve high concentrations of fillers in the final solutions, as well as the complexity of implementation and the use of aggressive substances [7]. Moreover, many methods for producing a new class of polarizers require thorough and labor-intensive purification of the resulting product.

Therefore, in the present work, a new polymer composite material, called PDLC, is proposed, based on the nematic liquid crystal 5CB and polymer matrices (PVA and PVB), which eliminates this drawback.

The use of uniaxially stretched films dispersed with polymer-dispersed liquid crystals (PDLC) that exhibit anisotropic light scattering as polarizing elements allows for a significant increase in the maximum luminous flux power [8]. PDLC films effectively polarize radiation across the entire transparency range of their components (visible and near-infrared), whereas traditional polaroids operate only within the dichroic absorption band of the material or its impurities. Furthermore, the anisotropy of light transmission in LC films can be controlled by applying an electric field. PDLC films are especially promising for use in laser devices, as the collimated nature of the radiation allows for easy removal of scattered light with a diaphragm. Doping the liquid crystal with a suitable surfactant, followed by uniaxial stretching of the composite film, offers a promising approach to overcoming this challenge, enabling the selection of optimal technological conditions for producing highly efficient film polarizers based on the anisotropy of light scattering.

2. Research objects and experimental methods

The nematic liquid crystal (NLC) 4-n-pentyl-4’-cyanobiphenyl (5CB), from the alkyl biphenyl series, was used to prepare and investigate polymer-dispersed liquid crystal (PDLC) films, a type of composite material. Two thermoplastic polymers were utilized as the matrix: polyvinyl alcohol (PVA) and polyvinyl butyral (PVB).

These polymers, after dissolution in appropriate solvents and subsequent drying, do not undergo chemical transformations.

The components of the studied materials were in the proportional ratios of 1:33.03:1.04:0.003 for NLC 5CB:PVA:Gly:CTAB and 1:33.2:1.17 for NLC 5CB:PVB:CTAB, respectively. For PVB, there was no need to add glycerin to provide elasticity, as NLC 5CB simultaneously acts as a plasticizer. The physical parameters and coefficients required for studying light transmission, contrast, and texture characterization of nematic droplets are presented in **Table 1**.

Table 1. Physical parameters of the research objects.

Materials	**The temperature of enlightenment, °C**	**Refractive index coefficient**		**Wavelength, µm**
NLC 5CB	34	1.717	1.531	0.633
PVA	22	1.52		0.633
PVB	22	1.488		0.633

Polymer matrices (PVA, PVB) have one refractive index equal to n_p 1.52. The liquid crystal 5CB, due to optical anisotropy, has two refractive indices: n parallel and n perpendicular. In the initial state, i.e., before the start of the study of the PDLC films, the refractive indices of the polymer ($n_p = 1.52$) and the parallel component of the refractive index of LC 5CB ($n_{II} = 1.531$) are equal to each other, but, conversely, the refractive indices of the polymer ($n_p = 1.52$) and the perpendicular component of the refractive index of LC 5CB are very different ($n_{\perp} = 1.717$). This fact is better known as optical anisotropy, based on the phenomenon of double refraction. In order for the equality conditions ($n_{\perp} = n_p$) to be fulfilled, we needed to apply an electric field to the LC cell. Then the LC 5CB molecules are reoriented along the direction of the electric field strength and the above equation is fulfilled. This equality contributes to the maximum light transmission of PDLC films.

As shown by the numerical values in **Table 1**, the condition ($n_{\perp} = n_p$) is well satisfied for both PVA and 5CB. For pure PVB, the refractive index is approximately 0.04 lower than the $n_{\perp}$ value of 5CB. However, during phase separation in the encapsulation process, a portion of the liquid crystal remains dissolved in the polyvinyl butyral matrix, leading to an increase in the absolute refractive index (n_p) of the polymer, aligning it more closely with the refractive index of the nematic [9]. Both polymers set the planar (tangential) orientation of the LC 5CB molecules. To modify the boundary conditions on the surface of the polymer matrix from tangential to homeotropic, two homeotropic surfactants were selected [10]: cetyltrimethylammonium bromide (CTAB) $C_{19}H_{42}NBr$, belonging to the cationic type, and phosphatidylcholine (lecithin). Their concentration relative to the nematic varied in the range of 0%–7% by weight.

Samples of PDLC films were produced by emulsifying NLC in an aqueous polymer solution for composition with polyvinyl alcohol and using the SIPS (solvent induced phase separation) method using PVB [11]. Glycerin was added to the composition to reduce the hardness of the PVA. The resulting films had a thickness of 25–85 µm with sufficiently evenly distributed nematic droplets of varying size in the volume and on the surface of the polymer matrix.

The orientation structures in the liquid crystal droplets and their optical textures were studied using the polarizing optical method with a POLAR-2 microscope, in the geometry of crossed polarizers, as well as with the analyzer turned off. This technique enables a reliable determination of the director configuration both within the volume of the droplet and at its boundary with the polymer.

The study of the electro-optical orientation effect feature was carried out on a typical configuration, illustrated in **Figure 1**. Laser light from a He-Ne laser (Linos) with an occurrence of $\lambda = 633$ nm was applied as a power cause. The light transmission coefficient of the PDLC films was measured using a light-sensor photodetector. The signal from the photodetector was recorded by a digital multimeter. The radiation scattered on the studied samples was slowed by a diaphragm with, which made it possible to register only directly transmitted light. An fluctuate potential with a periodicity of 1 kHz was applied to the PDLC cell from the signal generator.

The morphology of the samples and the visual textures of the nematic droplets were investigated using a polarizing optical microscope POLAR-2 equipped with a MyScope 500 M digital video camera (Webbers), which made it possible to photograph and videotape the ongoing processes (**Figure 1**). The studies were carried out in the geometry of crossed polarizers and with the analyzer turned off [12]. For microscopic analyzed of the droplet answer to an electrical field, samples with a spacer thickness of 30 µm and an average droplet size of 7.2 µm were made. At the concluding phase of the preparatory process, the sample was cooled to 23 ℃ for 60 minutes. It should be noted that for this purpose, the composite film samples must be made so that the liquid crystal droplets in the field of view do not overlap each other and are sufficiently large [13].

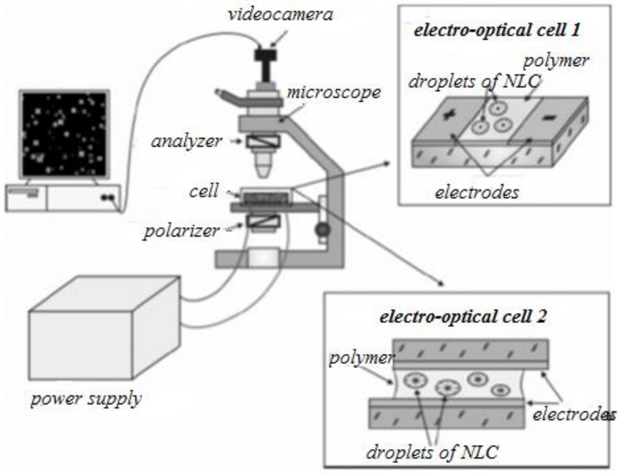

Figure 1. Schematic diagram of the setup for visual observation and image recording of the optical textures of nematic droplets and their transformations under the influence of an electric field. In electro-optical cell 1, the field is directed parallel to the substrate plane, while in cell 2, the field is directed perpendicular to the substrates.

The design of one of the electro-optical cells made it possible to observe changes in optical textures for the example when the electric applied is directed aligned to the area of the cell (electro-optical cell 1 in **Figure 1**). Such geometry allows to determine with a sufficient degree of accuracy the boundary conditions formed as a consequence of the exposure of the electric field [14].

The distance between the electrode strips ranged from 100 to 300 µm. To observe optical textures and their transformations under the influence of an external factors directed perpendicular to the cell surface; an electro-optical cell 2 was used. In this case; the distance between the electrodes was 70 µm. The cells were supplied with a constant voltage from a direct current electrical supply B5-49 with a voltage of up to 100 V. The pulse duration depended on the experimental conditions and varied from 1 sec to tens of secs [7,15]. To obtain higher voltages; a rectangular pulse signal source with a duration of 1 second and a variable amplitude of up to 1000 V was used.

To determine the angle of reorientation (α) of the LC molecules inside the droplet; a schematic image of the PDLC film was used (**Figure 2**). Here the plane of the Cartesian system (*xoy*) coincides with the plane of the PDLC film. The drip directors are oriented mainly along the *ox* axis. The angles φ and θ determine the deviation of the director relative to the axis *ox*; respectively; in the *xoy* and *xoz* planes. The schematic distribution of the droplet directors at the angles of maximum reorientation (φ_{max} and θ_{max}) is shown in **Figure 3**.

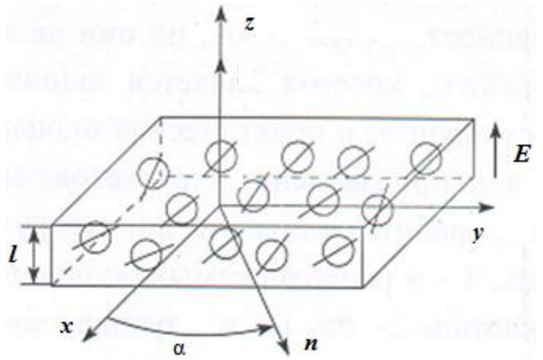

Figure 2. Schematic representation of the PDLC films in the microscope lens: *E* is the electric field strength vector, α is the angle of rotation (reorientation) of the nematic molecule inside the droplet, *l* is the film thickness, *n* is the preferred orientation (director) of the LC molecules.

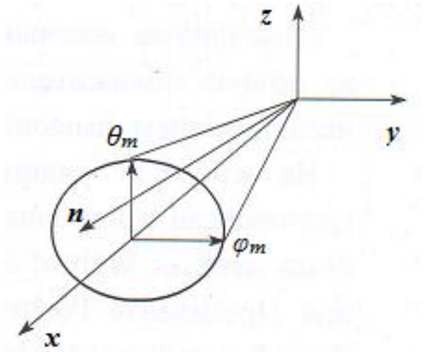

Figure 3. Orientation of the LC droplet directors: *n* corresponds to the orientation of the director of a single droplet, *φm* and *θm* are the maximum deflection angles of the droplet director, respectively, in the *xoy* and *xoz* planes.

3. Experiment

According to [16] PVB defines homeotropic barrier determines for both the nematic mixture E7 and the cholesteric blend based on the nematic amalgam EN18 [17]. In the PDLC cells based on NLC 5CB and PVB studied by us, the droplet textures (**Figure 4**) vary considerably from those characteristic of both homeotropic anchoring: (radial, axial, flowing radial structures) and planar anchoring: (bipolar, twist-bipolar, toroidal configurations).

Figure 5 presents the droplet textures (**Figure 4a**) at small angles of rotation of the specimen relative to the polarizers. Four topological particularities split the circumference of the droplet into four equal arcs are investigated in the absence of an analyzer (**Figure 5a**, below).

The inherent scheme for an orientation configurates with two boojums (black semicircles) and defects in the annular surface are sensible in the right part of **Figure 5** under the symbol (d). The bipolar axis is oriented horizontally, as in the case for **Figure 5a**. In the schematic representation, the symbol α indicates the angle the slope between the local orientation of the director and the normal to the surface. In all observed patterns, the droplet size is 10 μm.

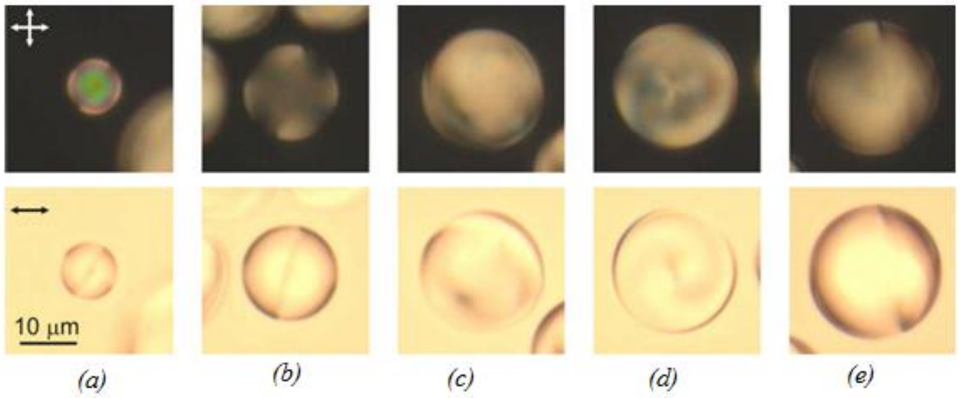

Figure 4. Pictures of specifically droplet optical textures **(a)–(e)** investigated in 5CB and PVB in stricken polarizers (upper range) and without an analyzer (lower range).

It can be seen that a dark line called the straight quenching branches, the positions of which do not change in the vertical and horizontal planes, connects the upper and lower defects. Under the action of an electric field in the nematic droplets, the textures change: a solid quenching disk occupying the boundary areas of the droplet projection replaces the quenching cross. This evidences that the molecules LC is oriented mainly parallel to the polarizer. A perpendicular thin attenuation band connecting the upper and lower defects at the boundary, and a horizontal attenuation band combining two other defects are also visible in crossed polarizers (**Figure 5a**, upper row). Furthermore, four attenuation districts appear, located close to each other in a circle in the drop and located approximately the same distance from the perpendicular and horizontal lines.

Rotating the cell by 45° clockwise relative to the polarizers completely qualitative transformation the optical texture observed both in stricken polarizers and without an analyzer (**Figure 5c**). An interference color configuration appears in crossed polarizers in the absence of a fade band. Four identical sections are also visible along the border of the drop without an analyzer. When moving the droplet clockwise, maximum darkening is observed in the characteristic sections. Then the image clearness of the brink slowly decreases to the next image.

The optical structure shown in **Figure 5a** is similar to the picture obtained without an analyzer (**Figure 5c**). Consequently, when the analyzer is turned off, the boundaries of the droplet lose their clarity. When comparing the extinction band (**Figure 5**, upper row), taking into account the predominant orientation of the director at the boundary of the drop (**Figure 5**, lower row), it is possible to determine the angle of inclination α between the n director and the N perpendicular to the plane (**Figure 5d**). The predominant direction of nematic molecules can be parallel to any horizontal or vertical polarizer in the attenuation region located at the bottom left (**Figure 5a**, top row).

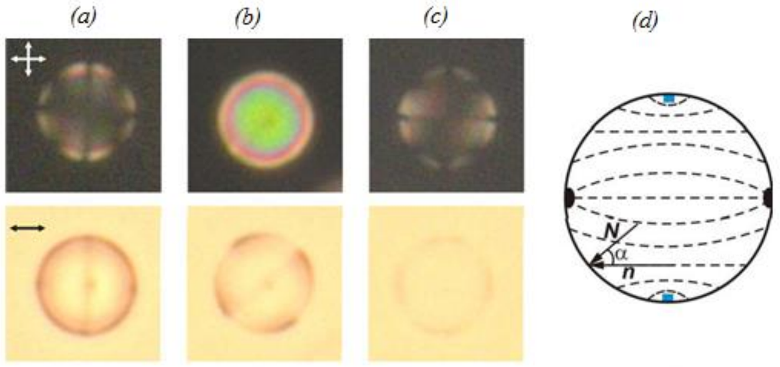

Figure 5. Images of nematic droplets under crossed polarizers (upper row) and without an analyzer (lower row). In **(a)**; the lines connecting diametrically opposite defects at the boundary are aligned with the polarizers. The cell is rotated clockwise by 45° relative to the polarizers in **(b)** and by 90° in **(c)**. The configuration of the director **(d)** corresponding to the textures **(a–c)**: the dashed lines inside the droplets show the local direction of the director.

Nevertheless, observation of the droplet absent an analyzer showed that the priority direction here is oriented almost horizontally (**Figure 5d**). The angle determined in this way at various points of the interface, with the exception of the surroundings of the objects, is $\alpha = 40^o \pm 4^o$.

The invariance of the angle α along the droplet's circumference allows for a schematic illustration of the orientation structure in the most significant region of the droplet on the plane of the film (**Figure 5d**). This pattern of the director field distribution corresponds to a structure with two point topological defects—boojums—and an annular topological defect, which has been previously observed in polymer matrices [18–20]. The segment of the annular defect on the film surface appears as two attractions at the droplet boundary. The bipolar axis connecting the boojums serves as the symmetry axis for the droplet's orientation structure.

In the PDLC samples studied, the optical textures demonstrate in **Figure 5** were discovered only inside droplets of 10 µm in size and smaller. A similar structure with two boojums and an annular defect on the surface was found in larger droplets

(**Figure 4b**), however, attenuation bands in the central part of the droplet are absent at any orientation of the bipolar axis relative to stricken polarizers. This is typical for a twisted orientation structure inside a droplet. The angle of rotation, defined as the azimuthal angle α between the orientation of the bipolar axis and the orientation of the director at the interface of the droplet surface in the equatorial surface, was determined by the method presented in detail in [21].

When the refractive indices of the polymer and liquid crystal are equal, the light passing through the droplet under crossed polarizers will scatter synchronously if the following conditions are met:

1) the bipolar axis of the droplet is oriented perpendicular to the direction of observation;
2) the polarizer is aligned either perpendicular or parallel to the projection of the director on the lower surface of the droplet;
3) the analyzer is aligned either parallel or perpendicular to the projection of the director on the upper surface of the droplet.

The angle of rotation at which the orientation of the director in the central segment of the drop is parallel to the bipolar axis consider be selected from two practicable ones. For such droplets with two boojums and an annular defect, this means that the bipolar axis must be in the plane of the cell and the surface of the annular defect must be normal to the plane of the film. The twist angle measured using this manner (**Figure 6**) for different droplets arranging the above positions depends on the size of the droplet. In this figure, the bipolar axis of the droplet is normal to the polarizer, and the angle between the polarizer and the analyzer is 90° (a). In the second case, the bipolar axis is rotated 20° counterclockwise correlative to the polarizer, and the angle between the polarizer and the analyzer is 130° (b).

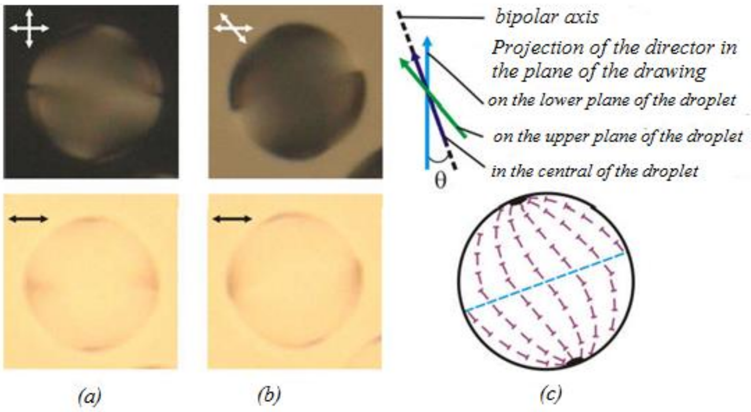

Figure 6. Images of nematic droplets in crossed polarizers when the angle between the polarizer and the analyzer is 90°. **(a)** turned counterclockwise by 20° relative to the polarizer; **(b)** calculated configuration of the LC director; **(c)** double arrows show the orientation of the polarizers.

The **Figure 6** shows in a separate view on the right a diagram of the considerable orientation of the bipolar axis of the drop, the planning of the director on the image planes along the lower and upper edges (top), as well as the director's field above the upper surface of the drop (bottom) (c). For all the paintings we observed and the micrographs depicted in **Figure 6**, the drop size was 17 μm. Thus, a comparative analysis of the obtained microscopic images suggests that for droplets with a diameter less than 10 μm, the twist angle is $\theta = 12^o \pm 3^o$, and for droplets with a diameter greater than 21 μm, $\theta = 27^o \pm 3^o$.

In addition to the above-described droplet textures, other types of paintings based on micrography are also observed, illustrated in **Figure 6c**. The rotation of the sample correlative to the polarizers leads to a complex transformation in the texture of droplets both in crossed polarizers and without an analyzer. These results are shown in **Figure 7** For all observed patterns, the drop size is 21 μm.

When the microscope stage is at a rotation angle of 0° (**Figure 7a**), the droplet boundaries appear less distinct without the analyzer, and a single point defect can be observed. As the sample is rotated, the droplet boundary becomes progressively sharper (**Figure 7b, c**). The sharpest boundaries are visible at a 90° rotation angle (**Figure 7d**). By lowering the microscope stage, a single point defect (**Figure 8a**), an annular defect (**Figure 8b**), and a second point defect (**Figure 8c**) can be clearly observed.

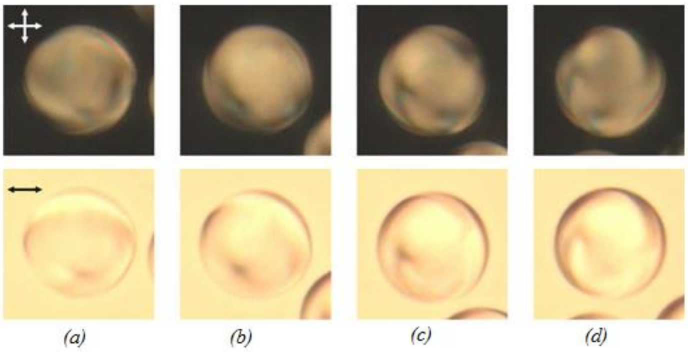

Figure 7. Images of a liquid crystal droplet under crossed polarizers (upper row) and without an analyzer (lower row) at microscope stage rotation angles of. **(a)** 0^o; **(b)** 30^o; **(c)** 60^o; **(d)** 90^o.

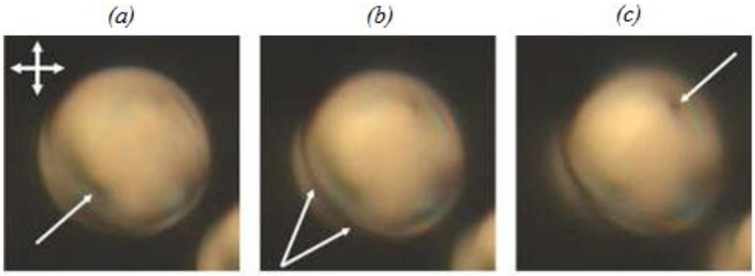

Figure 8. POM-images of a liquid crystal droplet shown in **Figure 5c** in stricken polarizers. The lens focuses on the lower defect-boojum **(a)** the annular defect; **(b)** the upper defect boojum; **(c)** single arrows indicate the location of the defects.

Compounding the obtained optical texture, it can be stated that the droplet has an orientation structure with two boojums, an annular defect and a bipolar axis inclined to the plane of the cell. The missing of attenuation bands indicates the presence of torsion deformation, as in the case of **Figure 4b** and **Figure 6**. The angle between the bipolar axis and the cell plane can vary from 0° (**Figure 4a**, **b**) to approximately 90° (**Figure 4d**) in the ensemble of droplets. If the bipolar axis is perpendicular to the cell plane, the optical texture does not depend on the rotation of the microscope stand (platform).

Let’s return to the drop shown in **Figure 4e**, where there are also two boojums and a ring defect. **Figure 9** shows figures of this droplet at different angles of orientation of the bipolar axis relative to the polarizer. It should be noted that the plane of the annular defect extends from the center of the drop to one of the boojums. At the same time, torsion deformation occurs inside the droplet. Such structures are usually investigated inside large droplets (more than 15 µm). The substitution of the annular defect may be different within different droplets.

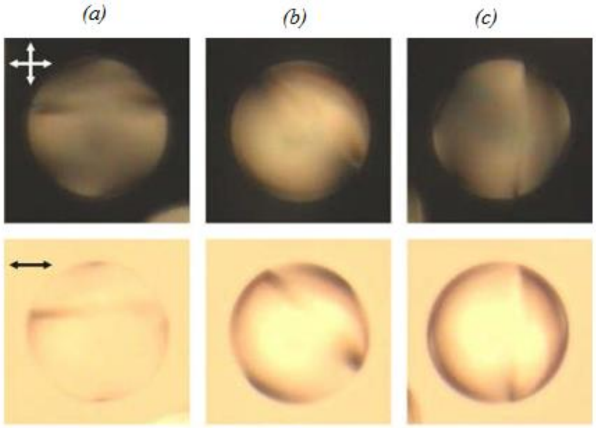

Figure 9. Pictures in stricken polarizers (upper range) and absent analyzer (lower range). **(a)** The bipolar axis is perpendicular to the polarizer; **(b)** the sample is rotated 45° clockwise relative to the polarizer; **(c)** the sample is rotated 90° clockwise.

For the scientific interpretation of the obtained textures, we determined the surface adhesion forces. In samples with inclined boundary positions, the strength of surface adhesion is established by the free field manner, which makes it possible to analyze the Bloch or Neel domain walls formed in the LC layer of the schlieren texture [22].

A schlieren texture [22] with point and linear defects, the so-called Bloch domain walls, is formed in a cell manufactured by us to conclude the surface adhesion durability for an LC film and a polymer film based on PVB (75%) + NLC 5CB (25%). If the plane of the domain wall contains optical anisotropy, then the reorientation of the director in the domains will be parallel to the wall. In this case, the LC molecules inside the droplet rotates in the plane of the wall, changing their direction to the opposite. The strength of the surface adhesion W_S to the polar surface can be determined by measuring the layer *d* of the Bloch walls [23,24]:

$$W_S\left(1-\frac{sin\,4\,\alpha}{2(\pi-2\alpha)}\right)=\frac{h}{d^2}x\frac{K_{22}}{2}x(\pi-2\alpha)^2 \tag{1}$$

where α is the angle between the preferential orientation of nematic molecules and the normal to the interface, h is the layer of the cell, K_{22} is the elastic torsion strain constant. We measured the thickness of the cell h = 13 μm and the thickness of the Bloch wall d = 3.0 μm. The angle α = 40° was taken from dimensions in liquid crystal droplets internal the polymer matrix (**Figure 3**) and $K_{22}\sim10^{-12}$ (H) [23]. Using these data, the surface anchoring force to the polar surface was determined, which was equal to $W_S = 2.4\times10^6 \times K_{22}\sim10^{-6}$ (J m^{-2}).

4. Conclusions

In nematic droplets of spheroidal and ellipsoidal shape, with homogeneous anchoring transition, an inhomogeneous director field with topological point defects is always realized. Such orientation structures of NLC 5CB droplets are not optimal, especially due to the residual scattering of the orthogonal component of the incident radiation in the area of lateral defects. In order to obtain the maximum possible anisotropy of the light transmission of PDLC films, it is necessary to form nematic droplets with a uniform distribution of the director in the droplet volume. This option is possible only if inhomogeneous boundary conditions are realized, which vary in the meridian direction from tangential in the equatorial region to homeotropic near the poles of the drop of NLC 5CB. It was found that the nematic droplets have an orientation structure with two boojums and an annular topological defect. Such orientation structures are formed with uniform inclined coupling. Similar structures have previously been observed only inside liquid crystal droplets dispersed in their own isotropic phase [14], or in a liquid matrix doped with a homeotropic surfactant [11].

It is shown that the bipolar axis internal the droplets is oriented at different angles relative to the surface of the film, since the LC droplets inside the LC look like a flattened ellipsoid. This shape results in the orientation of the symmetrical axis of the bipolar droplets along the cell surface, while the symmetrical axis in the axial droplets inclines to be oriented orthogonal to the cell surface along the little axis of the ellipsoid.

It has been proved that the configuration with inclined coupling studied by us has attribute of either a bipolar structure (the central spindle-shaped part of the droplets close to the bipolar axis) and an axial one (the insignificant region of the droplets). Possibly, this feature of the orientation structure support a small difference in the energy of the LC at different orientations of the bipolar axis relative to the cell surface.

It has been established that PDLC cells with inclined boundary positions have an orientation structure combining appears of both bipolar and axial configurations [15]. Such accentuate open up opportunities for the use of these materials in the production of electro-optical devices with memory effect and low control voltage.

Conflict of interest: The author declares no conflict of interest.

References

1. Gunning W.J.; Foschaar J. Improvement in the transmission of iodine-polyvinyl alcohol polarizers //Applied Optics. – 1983. –V.22. – № 20. – P. 3229-3231.

2. Zwick M.M. The blue complexes of iodine in polyvinyl alcohol //J. Polymer Science. – Pt. A-1. 1966. – Vol4. – P.1642-1644.
3. Nagy A.W.; Trapani G.B. Polarizer lamination /pat. US 40256889 (A); IPC1-7; B32B15/08; Go2B5/30; Go2BF1/1335 //Applicant Polaroid Corporation. – Appl. Number US 19750634635; appl. 19751124; publ.19770524
4. Hecht E. Optics. //– 2nd ed. – MA: Addison Wesley. – 1990. – Chapter 8.
5. Sutormin V.S; Timofeev I.V.; Krakhalev M.N.; Prishchepa O.O.; Zyryanov V.Ya. Transformation of orientation structures and optical textures of cholesteric induced electrically controlled ion modification anchoring transition //Izvestia RAN. Physics series. 2017. V. 81. No. 5. – p. 649-652
6. Gunyakov V.A.; Krakhalev M.N.; Zyryanov V.Ya.; Shabanov V.F.; Loiko V.A. Modulation of defect modes intensity by controlled light scattering in photonic crystal with liquid crystal domain structure // Journal of Quantitative Spectroscopy and Radiative Transfer. 2016. No. 178. – p. 263-268
7. Egamov M.H. Anisotropy of light scattering of polymer-liquid crystal composite systems under uniaxial tension //Fundamental problems of modern materials science. 2012. – No.1-2. – pp. 675-680.
8. Egamov M.Kh.; Maksudov B.I.; Faizulloev I.Kh. Optical hysteresis in composites based on polymer-nematic liquid crystal under uniaxial deformation //Russian Physics Journal; 2022; Vol. 65; №3. –p.488-492
9. Zyryanov V.Ya.; Smorgon S.L.; Shabanov V.F. Elongated films of polymer dispersed liquid crystals as scattering polarizers // Molecular Engineering. – 1992. – Vol. 1. – №4. –P. 305–310.
10. Zyryanov V.Ya. Uniaxially Oriented Films of Polymer Dispersed Liquid Crystals: Textures; Optical Properties and Applications // Mol. Cryst. Liq. Cryst. – 2005. Vol. 438. – No. 1. – P. 163/[1727]-173[1737].
11. Drzaic P.S. Liquid crystal dispersions // Singapore: World Scientific. – 1995. – 428 p.
12. Egamov M.Kh. Rotations of the plane of polarization of light radiation in nematic liquid crystals //Fundamental problems of modern materials science. 2024. Vol. 21; No.2. – pp. 199-204
13. Kitzerov H.S. Polymer dispersed liquid crystals. From the nematic curvilinear aligned phase to ferroelectric films //Liq. Cryst. – 1994. –Vol.16. – No. 1. – P.1-31.
14. Rakhimova U.J. The effect of light scattering of polymer-liquid crystal composites with spontaneous self-organization of the structure //Izvestiya NAS Tajikistan. - 2022. – No. 3. – pp. 78-84.
15. Kovalchuk A.V.; Kurik M.V.; Lavrentovich O.D.; Sergan V.V. Structural transformations in nematic droplets in an external electric field. //JETPh- 1988. – vol. 94. – No. 5. – pp. 350-364.
16. Xie; A.; Higgings D.A. Electric-field-induced dynamics in radial liquid crystal droplets studied by multiphoton-excited fluorescence microscopy //Appl. Phys. Lett. – 2004. – Vol. 84 – P. 4014–4016.
17. Loiko V.A.; Konkolovich A.V.; Miskevich A.A.; Zyryanov V.Ya. Light transmission of polymer-dispersed liquid crystal layer composed of droplets with inhomogeneous surface anchoring //J. Quant. Spectr.; Radiat. Transf. – 2016. – Vol. 178. – P. 243-152.
18. Rakhimova U.J.; Egamov M.H. Structural modifications of polymer-liquid crystal composites with spontaneous self-organization of the structure //Reports of the National Academy of Sciences of Tajikistan. - 2021. – Volume 64. – No. 11-12. – pp. 682-686.
19. Madhusudana N.V.; Sumathy K.R. Nematic droplets with a new structure // Mol. Cryst. Liq. Cryst. – 1983. – Vol. 92 (Letters). – P. 179–185.
20. Kim Y.K.; Shiyanovskii S.V.; Lavrentovich O.D. Morphogenesis of defects and tactoids during isotropic-nematic phase transition in self-assembled lyotropic chromonic liquid crystals //J. Phys. Condens. Matter. – 2013. – Vol. 25 – P. 404202.
21. Drzaic P.S. A case of mistaken identity: spontaneous formation of twisted bipolar droplets from achiral nematic materials //Liq. Cryst. – 1999. – № 26. – P. 623–627.
22. Ryschenkow G.; Kleman M. Surface defects and structural transitions in very low anchoring energy nematic thin films //J. Chem. Phys. – 1976. – Vol. 64. – P. 404–412.
23. Petrov V.I.; Spivak G.V.; Pavlyuchenko O.P. Electron microscopy of the magnetic structure of thin films //UFN; 1972; Volume 106; Issue 2. – p. 229-278.
24. Bloch F. Zur theorie des austausch problems und remanenzersccheinung der ferromagnetika //Ztschr. Phys. 1932. Bd. 74; No. 5/6. – p. 295-335

Journal of Polymer Science and Engineering 2024, 7(2), 4220.
https://doi.org/10.24294/jpse.v7i2.4220

Review

A review of electrochemical cells and liquid metal battery (LMB) parameter development

Simon Ejededawe Igberaese

Department of Electrical/Electronic Engineering, Federal Polytechnic, P.M.B. 13, Auchi, Edo State, Nigeria; igberaesesimon@gmail.com

CITATION

Igberaese SE. A review of electrochemical cells and liquid metal battery (LMB) parameter development. Journal of Polymer Science and Engineering. 2024; 7(2): 4220.
https://doi.org/10.24294/jpse.v7i2.4220

ARTICLE INFO

Received: 21 November 2023
Accepted: 18 December 2023
Available online: 4 February 2024

Abstract: Liquid Metal Battery (LMB) technology is a new research area born from a different economic and political climate that has the ability to address the deficiencies of a society where electrical energy storage alternatives are lacking. The United States government has begun to fund scholarly research work at its top industrial and national laboratories. This was to develop Liquid Metal Battery cells for energy storage solutions. This research was encouraged during the Cold War battle for scientific superiority. Intensive research then drifted towards high-energy rechargeable batteries, which work better for automobiles and other applications. Intensive research has been carried out on the development of electrochemical rechargeable all-liquid energy storage batteries. The recent request for green energy transfer and storage for various applications, ranging from small-scale to large-scale power storage, has increased energy storage advancements and explorations. The criteria of high energy density, low cost, and extensive energy storage provision have been met through lithium-ion batteries, sodium-ion batteries, and Liquid Metal Battery development. The objective of this research is to establish that Liquid Metal Battery technology could provide research concepts that give projections of the probable electrode metals that could be harnessed for LMB development. Thus, at the end of this research, it was discovered that the parameter estimation of the Li//Cd-Sb combination is most viable for LMB production when compared with Li//Cd-Bi, Li-Bi, and Li-Cd constituents. This unique constituent of the LMB parameter estimation would yield a better outcome for LMB development.

Keywords: LMB; SOC; terminal voltage; resistance; capacitance; time; charge; open circuit voltage

1. Introduction

Liquid Metal Batteries (LMBs) have the ability to store energy coming from generating, transmitting, and distribution stations. The storage capability dynamics of the LMBs would greatly enhance their efficiency and reliability, particularly when intermittent renewable energy technologies (such as wind and solar) are incorporated [1]. For a long time, batteries have been considered a strong alternative remedy owing to their advantages of easy handling, simplicity in maintenance, and flexibility in sitting [2]. The twenty-first century technological advancement has shown the feasibility of developing high-capacity energy storage devices out of many liquid combinations of alkali or alkaline-earth metals as well as metalloids [2]. Though the major challenge to widespread acceptance of battery technology is its high cost of production. Hence, the description of a Lithium-Antimony-Cadmium (Li//Sb-Cd) liquid metal battery could meet the performance requirements for stationary energy storage [2,3]. The LMB comprises liquid lithium as the negative electrode, a molten salt electrolyte, lithium chloride-lithium fluoride-lithium iodide (LiCl-LiF-LiI) fusion, and an antimony-cadmium alloy as the positive electrode, which would separate on its own accord by density into three distinct layers. This is due to the immiscibility property of the electrolyte and the electrodes interphase. The liquid characteristics of the constituents of the LMB bring to mind the merits of high current density and prolong cycle life or life span over conventional battery technology [2,4].

2. Brief review on liquid metal battery (LMB)

The advancement of LMB innovation has been revisited by a group of research pathfinders since 2006 at the Massachusetts Institute of Technology (MIT), United States of America. The recent MIT investigations were conducted as a result of the work carried out at Argonne National Laboratory in the 1960s. The study began with Sodium Bismuth (Na-Bi), but after a short while, attention quickly shifted towards Magnesium Antimony (Mg-Sb) and Lithium Lead Antimony (Li-Pb-Sb) candidates [2]. For alkali and alkaline-earth liquid metal electrodes, their solubility in their halides increases with the halide atomic number in the order of Fluoride < Chloride < Bromide < Iodide (F < Cl < Br < I). Hence, the alkali and alkaline-earth liquid metals and sodium-based systems have the main challenge of their high solubility in liquid electrolytes [5]. The electronic conductivity of the sodium system is high, and it experiences a high self-discharge current. The improvement on sodium-based systems would necessarily require the development of an electrolyte that would minimize sodium's solubility challenge [5]. The United States government began to fund scholarly research work at its top industrial and national laboratories. This was to develop an all-liquid cell for energy storage solutions. This research was encouraged during the Cold War battle for scientific superiority. Intensive research then drifted towards high-energy rechargeable batteries, which are better suited for automobiles and other applications [7]. The motivation was due to the incessant power outages around the globe at that time. For liquid metal battery applications, an elevated operating temperature is detrimental because of its tendency to corrode, mostly for alkaline or alkaline earth metals. The major drawback of the Mg-Sb candidate is that it has a low cell voltage of 0.21 V. This made the Mg-Sb system impracticable. In Mg-Sb collaborations, NaCl-KCl-MgCl2 electrolyte was examined at a very high temperature, producing a high charge efficiency, a deceased voltage efficiency, and a fairly low electrolyte conductivity of 0.8 S cm^{-1} [4]. The cell performance characteristics of the Li-Sb LMB were a 1.9 Ah theoretical capacity cell built-in with a Li electrode, a Sb-Pb electrode, and a LiF-LiCl-LiI electrolyte [7]. A potential of 1.2 V was measured for Li-Sb LMB, which is relatively low, and a self-discharge current of 0.6 mAcm^{-2} was significantly lower than 20 mAcm^{-2} [8]. Intensive research has been conducted on the development of electrochemical rechargeable all-liquid energy storage batteries. The recent request for green energy transfer and storage for various applications, ranging from small-scale to large-scale power stations, has increased energy storage advancements and explorations. The criteria of high energy densities, low cost, and extensive energy storage provision have been met through lithium-ion batteries, sodium-ion batteries, and LMBs [6].

3. Description of a liquid metal battery (LMB)

An LMB cell is made up of two metal electrodes that are in their liquid states splitted by an electrolyte that separate it into three layers based upon their density and immiscibility property is shown in **Figure 1**:

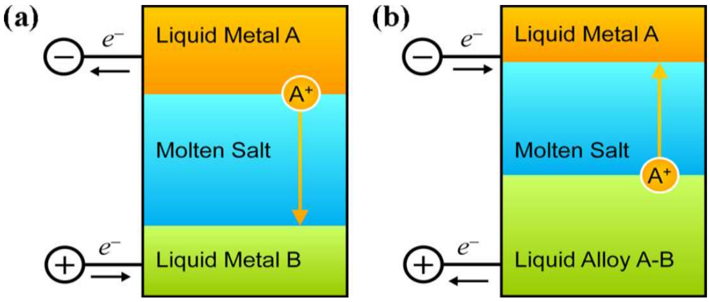

Figure 1. Schematic diagram of a Liquid Metal Battery (L.M.B.) upon **(a)** discharging and **(b)** charging [2].

Table 1. Proposed developmental parameters of the LMB cell.

Design parameters	Li//Cd-Sb	Li//Cd-Bi	Li-Bi	Li-Cd
Electrode composition in moles	47-36-17 48-36-16 49-35-16 50-34-16	42-38-20 47-33-20 45-35-20 44-32-24	45-55 40-60 50-50 48-52	70-30 60-40 50-50 65-35
Operating temperature in O °C	450–500	400–500	350–400	300–400
Electrode area in cm^2	1.30–2.50	1.00–1.50	1.00–2.00	1.50–2.00
Inter-electrode distance in cm	1.00–1.50	1.00–2.00	1.50–2.00	1.50–2.00
Charge–discharge current, A	0.34–0.55	0.34–0.55	0.34–0.55	0.34–0.55
Coulombic efficiency in %	80–99	80–99	80–99	80–99
Voltage efficiency in %	65–80	65–80	65–80	65–80
Average discharge voltage in volts	0.65–0.75	0.65–0.75	0.65–0.75	0.65–0.75
Theoretical capacity in Ah	0.75–0.90	0.75–0.90	0.75–0.90	0.75–0.90
Discharge capacity in Ah	0.55–0.80	0.55–0.80	0.55–0.80	0.55–0.80
Voltage input in volts	12.0 12.1 12.3 11.9	12.5 12.6 11.8 12.0	11.6 11.7 11.9 12.1	11.5 11.6 11.8 11.7
Voltage output in volts	220 215 225 235	225 220 230 230	230 225 235 225	235 230 240 220

4. Material preparation and procedure

1) All samples would be carried out in a controlled glove box environment through the melting of lithium (Li) and alloys of antimony (Sb) and cadmium (Cd). When the alloys are completely fluid, a tungsten wire would be inserted and the alloys would be allowed to cool, ensuring intimate contact between the electrode material and the tungsten wire.
2) The electrolyte would be prepared in the controlled atmosphere by the combinat

ion of lithium chloride (LiCl), lithium iodide (LiI), lithium bromide (LiBr), and lithium fluoride (LiF) in a vessel. The vessel would be positioned in the test vessel and dried under vacuum for some hours, and then the temperature could be increased to a higher temperature in the heater.

3) The container containing the electrolyte would be passed through argon gas before the temperature would be increased to a higher temperature for some hours in order to remove traces of residues from it. On cooling, the electrolyte would be removed from the vessel in the glove box and stored until use.
4) Electrochemical measurements could be carried out in a test vessel sealed against the outer environment.
5) The samples of the induction-melted electrodes prepared initially in No 1 above would be located in an alumina vessel with the pre-melted electrolyte. The assembling of the LMB would be done in the controlled glove box.
6) The charge tester would be used to measure the charge and discharge characteristics of the battery.

5. Battery model with variable parameter equations

Table 2 presents an estimation of the variable parameters in terms of efficiency, standard error, statistics, and probability. The different values in terms of efficiency, standard error, statistics, and probability give a mathematical value that defines the variable parameters used and their outputs for LMB estimation.

Table 2. A table of the battery model with variable parameters in terms of efficiency, standard error, statistics and probability of estimation.

Variable parameters	Efficiency	Standard error	Statistics	Probability
OCV	0.000347	0.007368	0.047076	0.9626
R	0.067178	0.054790	1.226096	0.2233
I	–0.003409	0.002345	–1.453833	0.1494
CP	–0.000164	0.000293	–0.560209	0.5767
T	0.000396	0.000356	1.113499	0.2684
TV	–0.001823	0.008424	–0.216355	0.8292
CHG	0.000597	0.001011	0.590636	0.5562
C	0.647579	0.128301	5.047355	0.0000

Estimation command:

$$\text{LSM, SOC, OCV, R, I, CP, T,TV, CHG} \tag{1}$$

Estimated model equation:

$$SOC = C(1) \times OCV + C(2) \times R + C(3) \times I + C(4) \times CP + C(5) \times T + C(6) \times TV + C(7) \times CHG + C(8) \tag{2}$$

Substituted coefficients:

$$\begin{gathered} SOC = 0.000346863777113 \times OCV + 0.0671776941118 \times R - 0.00340942723159 \times I - 1.63965521212 \times 10^{-6} \times \\ CP + 0.000395913781329 \times T - 0.00182250310982 \times TV + 0.000597393328656 \times CHG + 0.6475785799 \end{gathered} \tag{3}$$

Estimation command abbreviations:

Least Square Method (LSM), State of Charge (SOC), Open Circuit Voltage (OCV), Resistance (R), Current (I), Capacitance (CP), Temperature (T). Terminal Voltage (TV) Charge (CHG). (4)

6. Discussion of results of the simulated parameters for LMB development

The parameters of all sections of the LMB are based on the initial selection of the structural element combinations previously stated above. All the relevant parameters were simulated at varying ranges of values for all input and output parameters.

Figure 2 explains that at the various levels where the SOC parameters are dynamic or vigorous. At the various SOC terminals on the horizontal side, the SOC values are fairly vigorous, but at certain values, the SOC parameter values begin to display a high dynamic, particularly at 33, 45, 54, 57, 79, and 85. Hence, to conclude, the highest SOC for the LMB battery would be set at 85%, which is absolutely a good SOC value fit for the battery production.

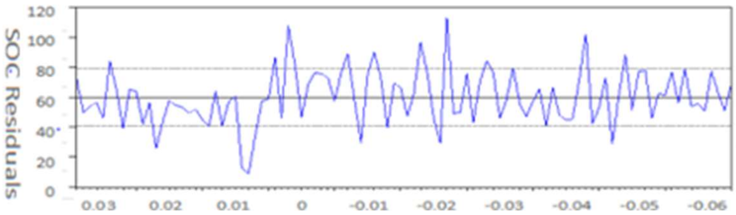

Figure 2. State of charge (SOC) residual parameters.

From **Figure 3**, an analysis was examined between the residual, actual, and fitted battery SOC parameters. It was observed that the graph of the residual and actual values of the battery SOC value looks the same. It is only that the fitted display has better steady-state values of SOC.

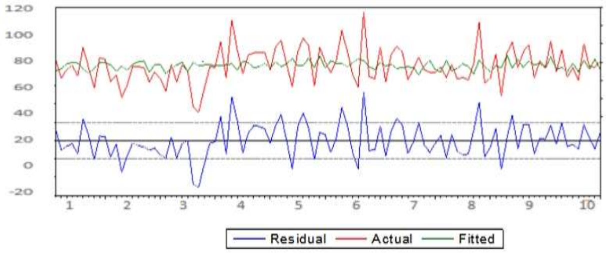

Figure 3. Comparison of the residual, actual and the fitted battery state of charge (SOC).

From **Figure 4**, the battery's standardized residuals for both the positive and the negative value are stable. On the positive side of the graph, the residuals are in regular patterns, showing that the state of charge is implementable.

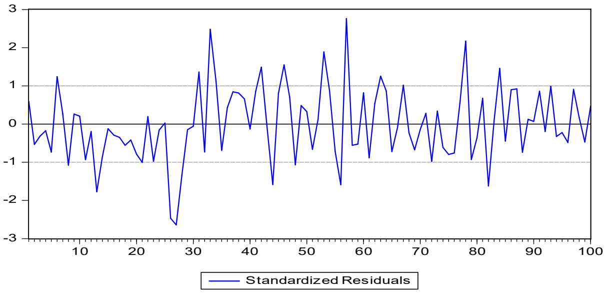

Figure 4. Simulation of standardized residuals for the battery's state of charge.

From **Figure 5**, the Open Circuit Voltage (OCV) must be within the permissible operational voltage of a battery. The Open Circuit Voltage (OCV) for the LMB as stated in the graph is 12.19 V.

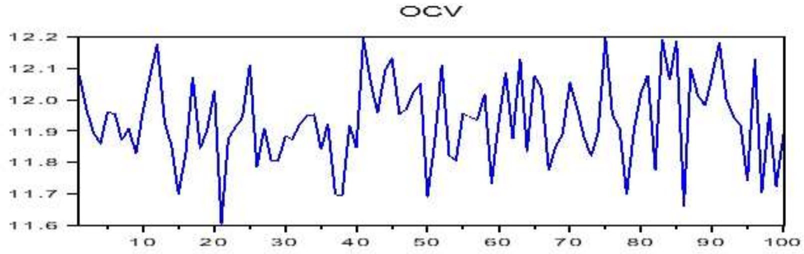

Figure 5. Simulation of Open Circuit Voltage (OCV) for the LMB.

From **Figure 6**, the SOC and resistance parameters were plotted. The graphical signal output of the SOC parameter shows that the SOC signal is stable at various points until the peak point, where the value is highest at 0.876, which depicts 87.6%.

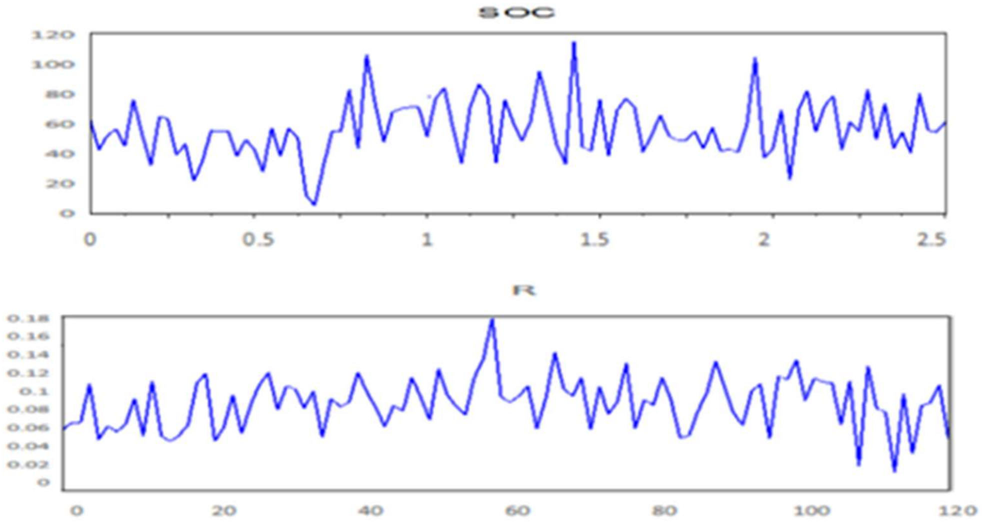

Figures 6. Simulation of actual State of Charge (SOC) and Resistance (R) respectively.

For **Figure 7**, the resistance parameter, there was an unsteady state display of the resistance value at different points until the point where the steady state peak value for output resistance at 0.09 Ω was measured at exactly 50.

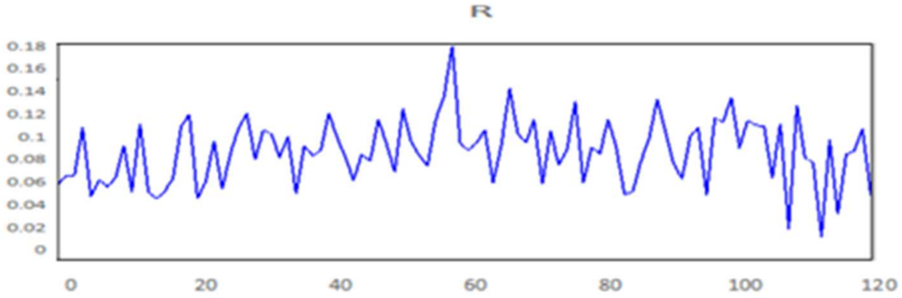

Figure 7. Simulation of output resistance (R) of the battery.

From **Figure 8**, the current at the peak point was 4.0 A, and other values for current fluctuation span between 3.0 A and 3.8 A. Meaning that the current is within a pre-determined range. Taking the average of the different values of current at 3 A and at 3.8 A is equal to 3.4 A, which is the estimated actual current of the LMB.

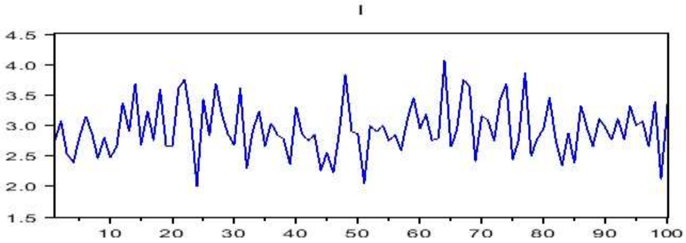

Figure 8. Simulation of the input current (I) of the battery.

The actual time in **Figure 9** as stated in the above graphical representation is 34 minutes.

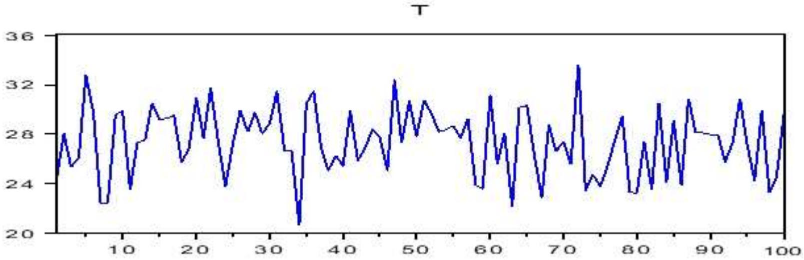

Figure 9. Simulation of the actual time (T) of the battery.

From **Figure 10**, the charge has varying values between 0 and 100. But the actual charge that is displayed at the graphical representation is at 98 coulombs (C).

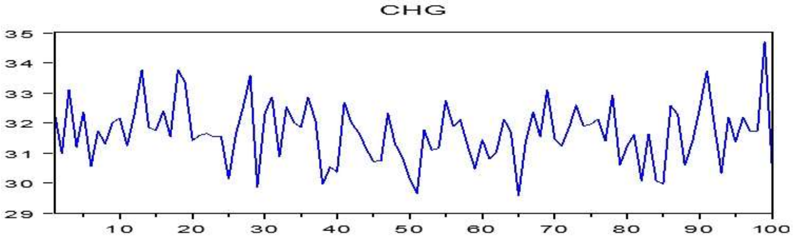

Figure 10. Simulation of the charge (CHG) of the battery.

The simulated graph at **Figure 11** for the terminal voltage (TV) of the battery is captured at point 12.1 V.

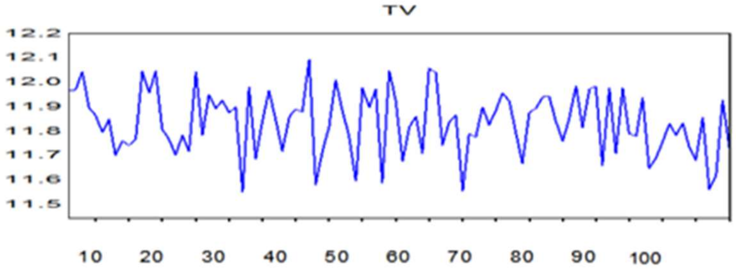

Figure 11. Simulation of the terminal voltage (TV) of the battery.

From **Figure 12**, the capacitance displayed at the graphical representation is at 3.6 × 103 Farads (3.6 KF).

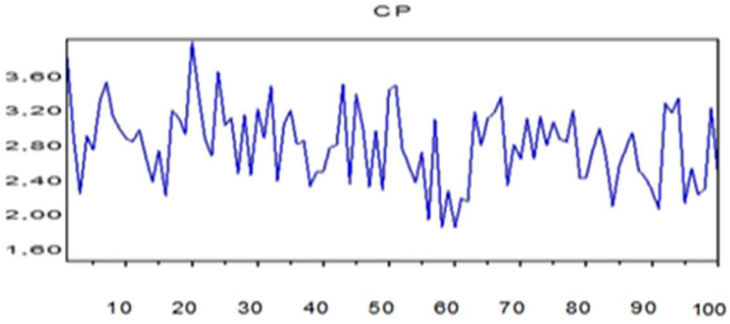

Figure 12. Simulation of the capacitance (CP) of the battery.

7. Conclusion

Liquid Metal Batteries (LMBs) have some dynamic characteristics in parameter estimation during various charge and discharge periods. Due to parameter estimation through the comparative analysis of the simulated chemical constituents of varying metals and electrolytes, the Li//Cd-Sb combination is most viable for LMB production when compared with Li//Cd-Bi, Li-Bi, and Li-Cd constituents. The values for Open Circuit Voltage (OCV), Terminal Voltage (TV), Charge (CHG), Time (T), Current (I), Resistance (R), Capacitance (CP), and State of Charge (SOC) are determined for the preferred LMB combination for battery development. This would make the operation of the LMB highly practicable for both domestic and small industrial uses.

Acknowledgments: I want to use this awesome opportunity to thank God for His infinite mercy upon me to carry out this research work. There was no funding sources or sponsorship for this research.

Conflict of interest: The author declares no conflict of interest.

References

1. Barnhart CJ, Benson SM. On the importance of reducing the energetic and material demands of electrical energy storage. Energy & Environmental Science. 2013; 6(4): 1083. doi: 10.1039/c3ee24040a
2. Kim H, Boysen DA, Newhouse JM, et al. Liquid Metal Batteries: Past, Present, and Future. Chemical Reviews. 2012; 113(3): 2075-2099. doi: 10.1021/cr300205k
3. Yang Z, Zhang J, Kintner-Meyer MCW, et al. Electrochemical Energy Storage for Green Grid. Chemical Reviews. 2011; 111(5): 3577-3613. doi: 10.1021/cr100290v
4. Bradwell DJ, Kim H, Sirk AHC, et al. Magnesium–Antimony Liquid Metal Battery for Stationary Energy Storage. Journal of the American Chemical Society. 2012; 134(4): 1895-1897. doi: 10.1021/ja209759s
5. Dunn B, Kamath H, Tarascon JM. Electrical Energy Storage for the Grid: A Battery of Choices. Science. 2011; 334(6058): 928-935. doi: 10.1126/science.1212741
6. Liu Z, Song T, Paik U. Sb-based electrode materials for rechargeable batteries. Journal of Materials Chemistry A. 2018; 6(18): 8159-8193. doi: 10.1039/c8ta01782d
7. Soloveichik GL. Battery Technologies for Large-Scale Stationary Energy Storage. Annual Review of Chemical and Biomolecular Engineering. 2011; 2(1): 503-527. doi: 10.1146/annurev-chembioeng-061010-114116
8. Wang K, Jiang K, Chung B, et al. Lithium–antimony–lead liquid metal battery for grid-level energy storage. Nature. 2014; 514(7522): 348-350. doi: 10.1038/nature13700

Journal of Polymer Science and Engineering 2024, 7(2), 6518.
https://doi.org/10.24294/jpse.v7i2.6518

Review

Fabrication of polymer-based bone scaffolds—Conventional vs. advanced methods

Feven Mattews Michael, Mohan Raj Krishnan*, Edreese Housni Alsharaeh*

College of Science and General Studies, AlFaisal University, Riyadh 11533, Saudi Arabia
*** Corresponding authors:** Mohan Raj Krishnan, mkrishnan@alfaisal.edu; Edreese Housni Alsharaeh, ealsharaeh@alfaisal.edu

CITATION

Michael FM, Krishnan MR, Alsharaeh EH. Fabrication of polymer-based bone scaffolds—Conventional vs. advanced methods. Journal of Polymer Science and Engineering. 2024; 7(2): 6518. https://doi.org/10.24294/jpse.v7i2.6518

ARTICLE INFO

Received: 20 May 2024
Accepted: 19 June 2024
Available online: 12 July 2024

Abstract: This review comprehensively summarizes various preparatory methods of polymeric bone scaffolds using conventional and modern advanced methods. Compilations of the various fabrication techniques, specific composition, and the corresponding properties obtained under clearly identified conditions are presented in the commercial formulations of bone scaffolds in current orthopedic use. The gaps and unresolved questions in the existing database, efforts that should be made to address these issues, and research directions are also covered. Polymers are unique synthetic materials primarily used for bone and scaffold applications. Bone scaffolds based on acrylic polymers have been widely used in orthopedic surgery for years. Polymethyl methacrylate (PMMA) is especially known for its widespread applications in bone repair and dental fields. In addition, the PMMA polymers are suitable for carrying antibiotics and for their sustainable release at the site of infection.

Keywords: bone scaffold; polymer; polymethyl methacrylate; tissue engineering; orthopedic surgery

1. Introduction

Bones are dense connective tissues with a solid, calcified outer layer (cortical bone) that comprises more than three-fourths of the bone's mass. Cortical bone has a relatively low porosity, ranging from 5% to 10%. The soft inner spaces of bone (usually described as cancellous or trabecular bone) form the remaining one-fourth of the bone mass. Cancellous bone has a high porosity, ranging from 60% to 90%, and contains the bone marrow, which consists of blood stem cells, adipose cells, osteoblasts, and osteocytes. From these, the osteoblasts are essential for the deposition and mineralization of the extracellular matrix of new bone, while osteocytes are the supporters of bone matrix calcification. In addition, specific growth factors and proteins, mainly residing in the extracellular matrix of bone, regulate cellular activity and stimulate the intracellular environment.

Bone possesses a high compressive strength of 170 MPa but a low tensile strength of 104–121 MPa and a very low shear stress strength of 51.6 MPa [1,2]. This means that bone can be fractured given that torsion force is exerted. In other words, bone is more sensitive to pulling or torsion than pushing. Though bones are naturally brittle (80% of CaP), a significant degree of elasticity is shown due to collagen. However, the likelihood of human bones failing due to mechanical problems, injuries, diseases, infections, and tumors increases with age. This means that wrong movement of the body or diseases like osteoporosis [3–5], scoliosis [6–8], and osteomyelitis [9–11] can cause the bones to fracture or deteriorate.

Naturally, bones can regenerate in case of minor injury and continuously remodel throughout adulthood [12–14]. These bone injuries heal without forming scar tissue while regenerating the bone with its pre-existing properties. In addition, the regenerated bone is indistinguishable from the uninjured bone. However, significant injuries involving the load-bearing bone require orthopedic surgery to place a bone graft over the defective bone site to encourage new bone growth while preventing other tissues from interfering with osteogenesis. During osteogenesis, the osteoblasts (cells with single nuclei that form the bone) originating from the bone graft enhance the growth of new bone. This is conducted through osteoinduction and osteoconduction processes. Osteoinduction is the recruitment of immature cells and stimulation of these cells to develop into bones [15–17]. Osteoconduction is when bone grows on a surface—a phenomenon seen in the case of bone implants [18]. Polymers are unique synthetic materials [19–43] that are extensively used in various industrial applications [44–50]. Likewise, it is primarily used for bone and scaffold applications. This paper provides various fabrication techniques and their potential use in orthopedic surgery.

2. Tissue engineering

Tissue engineering combines cells, materials, engineering methods, and suitable biochemical and physic-chemical factors to improve or replace biological functions [52,53]. The main goal of tissue engineering is to regenerate and replace the structural and functional of the injured bone beyond its natural healing capacity [53]. For this to happen, external regenerative materials such as scaffolds, cell growth factors, or a combination of either are required [54]. Tissue engineering uses undifferentiated cells seeded within the scaffold, which defines the geometry of the replacement tissues and provides environmental indications to promote the development of new tissues, as demonstrated in **Figure 1** [55]. However, the interaction between the cell and the material used to develop the scaffold plays a vital role in tissue engineering. This is because the developed scaffold must mimic the properties of the injured bone structurally and bio-functionally. Therefore, it is essential to understand the requirements and properties of the injured bone before designing the scaffold [56–58].

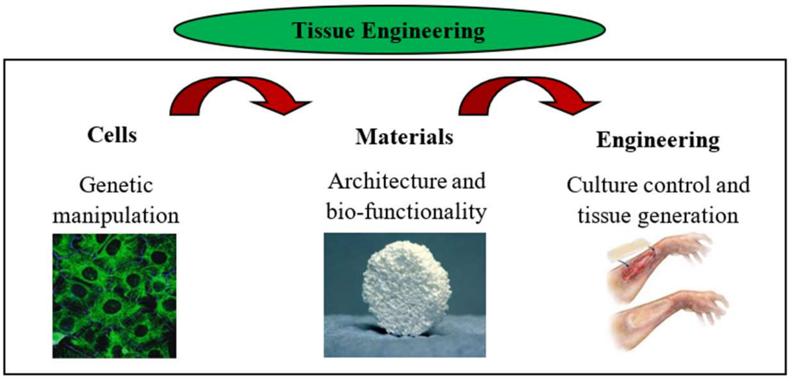

Figure 1. Schematic illustration of tissue engineering process.

3. Bone scaffolds and their requirements

Scaffolds are materials developed to perform in the body as devices able to support and possibly induce a complex pattern of events whose final goals are tissue repair and tissue function recovery [59–61]. Generally, the application of scaffolds can be summarized as:

- Allow cell attachment and migration.
- Deliver and retain cells and biochemical factors.
- Enable diffusion of vital cell nutrients and expressed products.
- Exert specific mechanical and biological influences to modify the behavior of the cell phase.

However, to achieve the goal of tissue engineering and bone regeneration, scaffolds must meet some specific requirements [62,63]. The scaffold should be biocompatible to integrate well within the tissue host without provoking any immune reaction and biodegradable into carbon dioxide and water forms. In addition, scaffolds should possess an open pore and be fully interconnected with highly porous structures [64,65]. These are the fundamental characteristics for providing space for cells to migrate and vascularize the tissue. In other words, the pore size of the scaffold is used to regulate cell survival, growth, and differentiation. Hence, the minimum pore size required is considered to be 100 µm due to the cell size, migration conditions, and transport [66,67]. However, pore sizes bigger than 300 µm are recommended to improve the new bone formation and to develop a net of capillaries. More on the effects of pore size on tissue regeneration is summarised in **Table 1**. Furthermore, the larger the surface area to volume ratio available, the more cell interactions will occur [68]. Scaffolds should also have the mechanical strength to retain their structure after implantation, mainly for the load-bearing tissues, as depicted in **Table 2**. Moreover, the scaffolds should be osteoinductive to recruit and stimulate the differentiation pathway of the stem and develop osteoblast cells to the defective bone [69].

Table 1. Effect of pore size on tissue regeneration [2].

Tissue formation/cell growth	Required pore size (µm)
Neovascularization	5
Fibroblas ingrowth	5–15
Regeneration of adult mammalian skin	20–115
Regeneration of bone	100–350
Osteoid ingrowth	40–100
Hepatocytes ingrowth	20
Fibrovascular tissue	500

Table 2. Mechanical properties of human tissues.

	Tensile strength (MPa)	Compressive strength (MPa)	Young’s modulus (GPa)	Fracture toughness (MPa.m$^{1/2}$)
Cancellous bone	-	4–12	0.02–0.5	-
Cortical bone	60–160	130–180	3–30	2–12
Cartilage	3.7–10.5	-	0.7–15.3 (MPa)	-
Ligament	13–46	-	0.065–0.541	-
Tendon	24–112	-	0.143–2.31	-

In summary, a scaffold is required to match bone properties closely. However, achieving all these properties in one material is a complex challenge due to the lack of strength associated with porosity. Therefore, to make it possible, the scaffold materials must be optimized from the atomic level through the macroscale to the nanoscale structure with respect to the cellular response [70].

4. Bone scaffold preparation techniques—Conventional methods

Conventional, non-designed manufacturing techniques are used to fabricate an interconnected porous structured scaffold [71]. Some methods include solvent casting/particulate leaching, freeze-drying, phase inversion, and electrospinning. However, they lack precision when controlling the pore size, geometry interconnectivity, and spatial distribution of pores [72,73].

4.1. Solvent casting and particulate leaching

Solvent casting on its own is an attractive method in the polymer field due to its ability to obtain films with high quality [74,75]. Aside from being a relatively simple technique, the film's thickness, uniformity, and distribution can easily be controlled [76]. However, solvent-casting techniques can fabricate a scaffold in combination with particulate leaching. In this technique, the first stage involves dissolving the polymer into chloroform and casting it in a petri dish filled with porogen (sodium chloride, ammonium bicarbonate, or glucose). The composite is then placed in a dust-free environment to evaporate the solvent and washed with distilled water to remove the porogen. Here, the properties of the developed scaffold, such as porosity and pore size, can be controlled by the amount of salt added and salt crystals, respectively [77]. However, homogenous distribution of the salt into the polymer is difficult to attain because the density of the polymer and salt is different. Other factors, such as casting temperature and drying conditions, can also affect the properties of the scaffold. To overcome this limitation, researchers have suggested adding a centrifugation stage to improve the pore uniformity and interconnectivity of the scaffold, as shown in **Figure 2** [78]. In these studies, the polymer solution mixed with salt was centrifuged and dried (air-dried and vacuum-dried), followed by salt leaching in distilled water, resulting in the fabrication of an interconnected porous scaffold with porosity >90% [79].

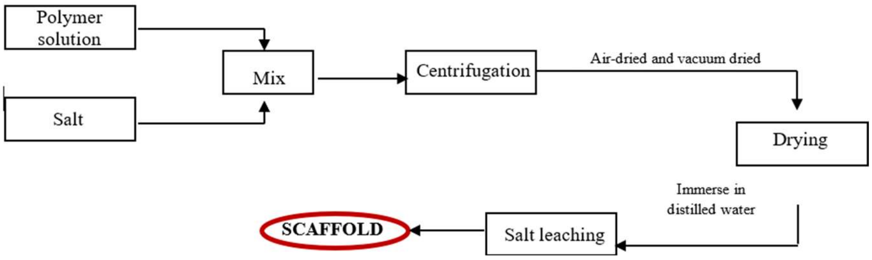

Figure 2. Schematic diagram for fabrication of scaffold using solvent casting and particulate leaching in addition to centrifugation stage.

4.2. Freeze-drying

In this technique, the polymer solution is mixed homogeneously with an acid (acetic acid) before the sublimation of ice using freeze drying, causing the formation of ice crystals, as shown in **Figure 3** [80–82]. The freezing temperature and rate can control the pore size properties of the developed scaffold. For instance, a scaffold freeze-dried pore size at −20 °C and −196 °C was 200–250 µm and 80–100 µm, respectively [45,46,83–88]. However, in another research, the addition of an annealing stage after freeze-drying (low temperature) has been shown to increase the pore size from 96–150 µm to 85–325 µm (~40% increase). This is due to the rise in temperature of the frozen suspension, which increased the ice crystal growth rate [89].

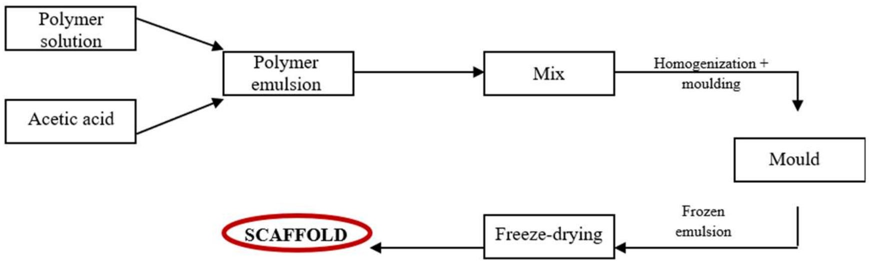

Figure 3. Schematic diagram for fabrication of scaffold using freeze-drying.

4.3. Phase inversion

Phase inversion is an effective technique for developing porous scaffolds by combining mass transfer and liquid phase separation, as depicted in **Figure 4** [61,90–93]. Initially, the mixed solution of polymer dissolved in a solvent and ethanol (non-solvent) would be cast or molded. Then, the dried casted gel will be induced to phase separation by immersing it into the non-solvent used [94]. After the extraction of the remaining solvent, the developed scaffold will be dried in a controllable environment. However, the drying stages can be avoided using supercritical fluid [95], such as carbon dioxide [96], which is biocompatible (non-toxic, non-corrosive, and non-flammable) and affordable [97]. The polymer solution is poured into a container and placed inside a heated high-pressure vessel. The supercritical fluid is pumped into the vessel with a high-pressure pistol. The fabrication of the scaffold was completed once the phase separation took place. A porous structure can be developed without any remaining solvent in this process. Nonetheless, the overall properties of the developed scaffold depend on the solubility and diffusivity of the supercritical fluid in the polymer. The phase separation technique has produced micro-patterned nanofibrous sheets (50–500 nm) with properties comparable to those obtained by electrospinning. The pore interconnectivity can increase when the phase inversion technique is combined with the particulate porogen leaching method, which can further be used for bone tissue regeneration applications [98].

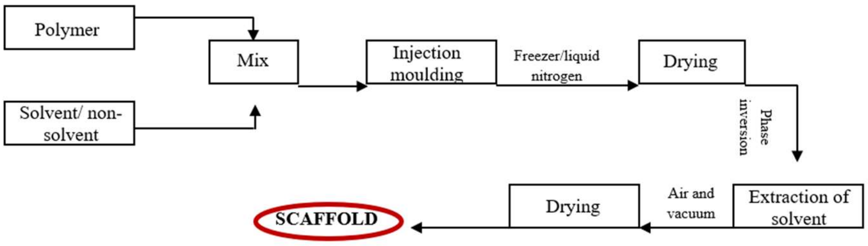

Figure 4. Schematic diagram for fabrication of scaffold using thermally induced phase inversion.

4.4. Electrospinning

Electrospinning, though not a new technique, has recently become significant in developing nanostructures in the form of fibers that can be used for scaffolds [99–105]. The basic tools required to fabricate this scaffold via the electrospinning technique include three components: a syringe, high voltage, and a collector plate, as shown in **Figure 5**. The polymer or composite solution prepared is poured into the syringe at a slow flow rate. Then, the tip of the needle is connected to the positive electrode of the high voltage, whereas the negative electrode is connected to the collecting plate. Finally, the polymer/composite is ejected from the syringe to the collecting plate as non-woven fibrous structures. These non-woven fibrous structures have unique characterization with a high surface area to volume ratio, flexible surface functionality, and mechanical properties superior to large fibers [105,106]. In addition, the pore size can be manipulated using either the properties of the polymer or composite solution prepared, the voltage applied, the processing temperature, or the distance between the collecting plate and the syringe [107–109]. However, the maximum pore size obtained through this technique is 10 μm, which is relevant to applications related to hindering cell infiltration [110]. The porosity can be increased by either removing one of the composite components used or using phase separation technology during electrospinning [111].

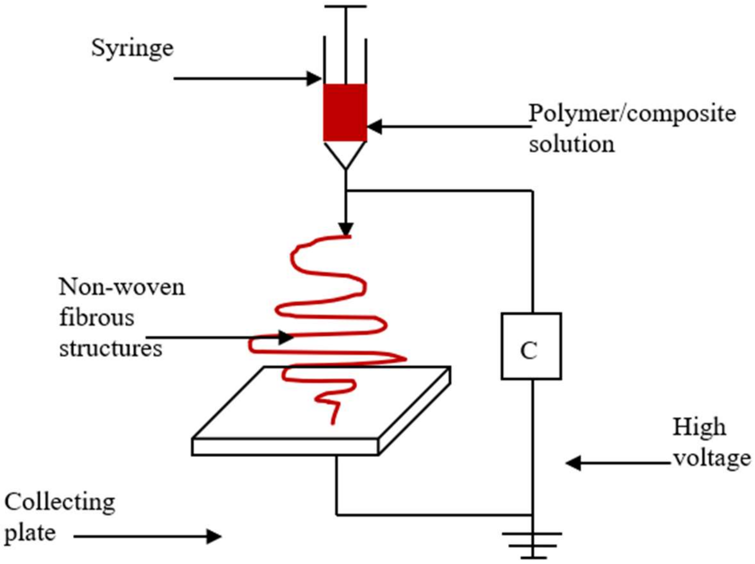

Figure 5. Schematic diagram for fabrication of scaffold using electrospinning.

5. Bone scaffold preparation techniques—Advanced methods

5.1. Computer-aided tissue engineering (CATE)

Advanced techniques, also known as designed manufacturing techniques in cooperation with computer-aided tissue engineering (CATE), have been known for a while [112–116]. This technique integrates advanced imaging technologies such as computer tomography (CT), magnetic resonance imaging (MRI), computer-aided design (CAD) technology, and rapid prototyping (RP) with tissue engineering applications, as shown in **Figure 6** [117–119]. Generally, CATE consists of two major processes: 1) non-invasive imaging data acquisition, where an image or scan of 3D tissue structural view is produced using CT or MRI, and 2) 3D reconstruction, where the physical model of the image is fabricated using CAD followed by RP and finally used for tissue implementation [120,121].

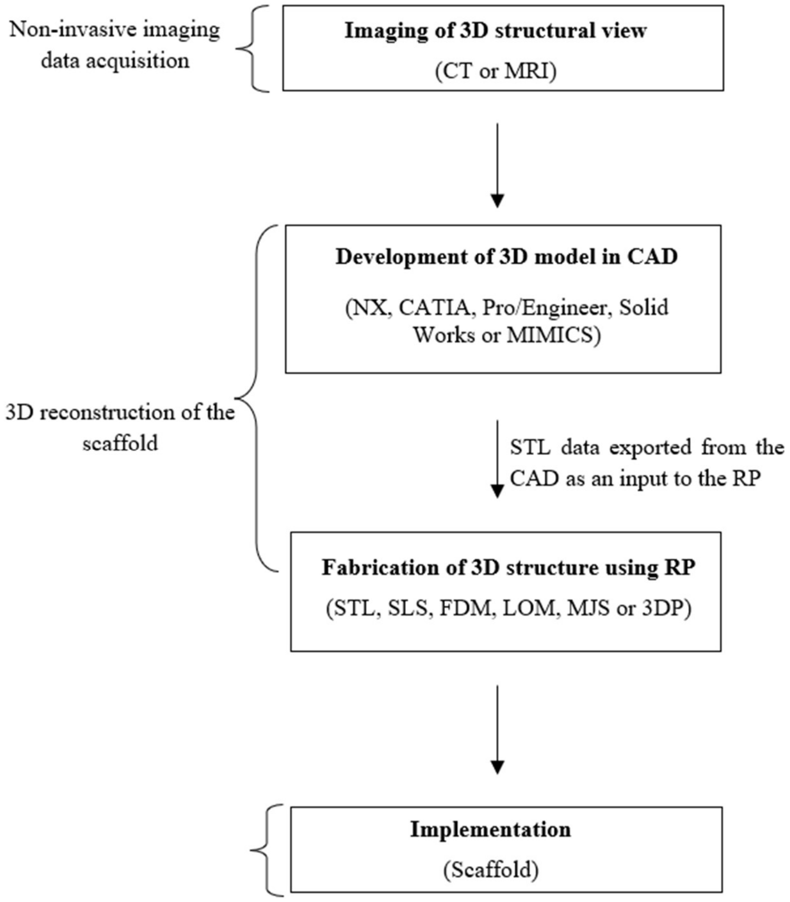

Figure 6. Schematic diagram for fabrication of scaffold using CATE.

5.2. Computed tomography (CT)

Computed tomography (CT) is one of the techniques employed to construct a 2D or 3D image of any tissue inside the body using special X-ray equipment with computer programs [122–126]. CT scanning has been used for many studies, including bone mass and morphology, growth and development analysis, mechanical loading and unloading, and evaluation of fracture healing [127]. The most crucial step in this technique is image acquisition, involving the preparation and positioning of the sample, the selection of scanning medium, the determination of the X-ray energy required, the voxel size and image resolution needed, and the recognition of the area of interest for the study [128]. Then, the image obtained is filtered to reduce signal noise while maintaining its resolution. Furthermore, the mineralized and non-mineralized structures in the image are separated using a segmentation process for analysis [129].

There are main advantages to using CT: 1) allows direct 3-D measurement of any morphology; 2) compared to the 2D image, a larger volume is studied; 3) it is faster than histologic analysis; and 4) the evaluation is non-destructive; hence can be used for other studies [130]. On the other hand, CT uses X-rays in the form of ionizing radiation, which can be harmful. However, compared to the naturally occurring radiation everyone is exposed to daily, a 1-time low dose of CT radiation exposure is equivalent to 6 months of natural radiation. That being said, there are still three ways to reduce the overall exposure to radiation doses: 1) reduce the number of CT scans prescribed; 2) reduce the CT dose used in a person; and 3) whenever practical, replace CT use with MRI, such as for imaging the liver. As a result, the most recent CT machines, known as multi-slice CT or multi-detector CT scanners, take the image in a spiral manner rather than individual parts of the body, making it faster, producing better 3D images with fewer CT scans, and detecting minor irregularities.

5.3. Magnetic resonance imaging (MRI)

Magnetic resonance imaging (MRI) is the other technique besides CT used to scan part of the body using a magnetic field and radio waves [131–133]. Due to its non-invasive and non-radiant nature and high resolution, MRI is preferred for in vivo assessments [134–136]. Unlike CT, MRI produces a magnetic field that temporarily releases hydrogen atoms into the body. That being said, the movement limiting its applications can easily affect MRI scanners. Furthermore, the images might suffer geometric distortions caused by variations in the magnetic field strength [137,138].

5.4. Computer-aided design (CAD)

Computer-aided design (CAD) is widely used to design an approach that provides a powerful tool to model 3D scaffold geometries [139–143]. CAD designs the model using constructive solid geometry (CSG) or boundary representation (B-Rep). CSG models are designed using boolean operations, whereas B-Rep uses software like NX (Siemens PLM Software), CATIA (Dassault Systemes), Pro/Engineer (PTC), SolidWorks (Dassault Systemes), and MIMICS (Materialize Gmbh) to design the model [144]. Developing a CAD scaffold is well-suited when combined with rapid prototyping techniques to fabricate the physical scaffolds [145].

5.5. Rapid prototyping (RP)/Solid freeform fabrication (SFF)

Rapid prototyping (RP), also known as the solid freeform fabrication (SFF) technique, is a controllable 3D structure designed layer by layer [146–149]. Designing a scaffold using this technique allows excellent reproducibility and the possibility of designing a structure that mimics the natural bone structure to be replaced [150]. Some of the RP techniques employed include stereolithography (STL), selective laser sintering (SLS), fused deposited modeling (FDM), laminated object manufacturing (LOM), multiphase jet solidification (MJS), and three-dimensional printing (3DP) [59,151,152].

6. Summary and future direction

This review comprehensively summarized various fabrication techniques of bone scaffold preparation techniques and their potential use in orthopedic surgery. Polymethylmethacrylate remains one of the most enduring materials in orthopedic surgery. It has a central role in the success of total joint replacement and is also used in newer techniques such as percutaneous vertebroplasty and kyphoplasty. The use of bone scaffolds is nowadays an important aid in the orthopedic field, both in situations in which it is necessary to fix a fracture in patients with severe osteoporosis (“augmentation”) and in cases where it must ensure greater stability in the system of the prosthetic hip, knee, and shoulder. In cases of prosthetic infection, joint antibiotic-loaded spacers are used, and PMMA has gained favor as a vehicle for the delivery of antibiotics. Antibiotic-loaded acrylic cement in joint replacement provides short- to medium-term protection against prosthetic infection. It aims to overlap with and replace the prophylaxis provided by peri-operative intravenous antibiotics. Recently, new materials such as bioglass and porous cement have been developed, which seem to provide good results in clinical trials. These materials exploit their potential biological value, allowing the bone to integrate within the acrylic cement structure and favoring the mechanical and biological stability of the bone cement system. For future development of these materials (PMMA, antibiotic-loaded cement, glass, and porous cement), the aim is to improve osseointegration to promote better mechanical stability and better biological integration on the interface of bone cement.

Bone scaffold research focuses on better mechanical quality and biocompatibility. Biomaterials, such as calcium phosphates and hydroxyapatite, more efficiently induce bone growth. Advances in the biocompatibility of PMMA bone scaffolds might be achieved by introducing osteogenic agents, such as bone morphogenic proteins or transforming growth factors, to scaffold surfaces that contact the surrounding bone. PMMA for vertebroplasty has greater stiffness than vertebral cancellous bone, causing higher incidences of fracture of neighboring vertebral bodies.

Author contributions: Original manuscript writing and editing, FMM and MRK; supervised the project, EHA. All authors have read and agreed to the published version of the manuscript.

Data availability statement: No experimental to disclose.

Funding: This research was funded by Alfaisal University grant number 726174. The authors gratefully acknowledge Alfaisal University and its Office of Research & Innovation for their continuous support throughout this study.

Conflict of interest: The authors declare no conflict of interest.

References

1. Turner CH, Wang T, Burr DB. Shear Strength and Fatigue Properties of Human Cortical Bone Determined from Pure Shear Tests. Calcified Tissue International. 2001; 69(6): 373-378. doi: 10.1007/s00223-001-1006-1
2. Lee H, Liao JD, Guo YS, et al. Biomimetic Design for a Dual Concentric Porous Titanium Scaffold with Appropriate Compressive Strength and Cells Affinity. Materials. 2020; 13(15): 3316. doi: 10.3390/ma13153316
3. Lin JT, Lane JM. Osteoporosis. Clinical Orthopaedics and Related Research. 2004; 425: 126-134. doi: 10.1097/01.blo.0000132404.30139.f2
4. Marcus R, Dempster DW, Cauley JA, Feldman D. Osteoporosis. Academic Press; 2013.
5. Rachner TD, Khosla S, Hofbauer LC. Osteoporosis: now and the future. The Lancet. 2011; 377: 1276-1287. doi: 10.1016/S0140-6736(10)62349-5
6. Brooks H, Azen S, Gerberg E, et al. Scoliosis. The Journal of Bone & Joint Surgery. 1975; 57(7): 968-972. doi: 10.2106/00004623-197557070-00015

7. MacLennan A. Scoliosis. The British Medical Journal. 1922; 2(3227): 864-866.
8. Rogala EJ, Drummond DS, Gurr J. Scoliosis. The Journal of Bone & Joint Surgery. 1978; 60(2): 173-176. doi: 10.2106/00004623-197860020-00005
9. Calhoun JH, Manring MM. Adult Osteomyelitis. Infectious Disease Clinics of North America. 2005; 19(4): 765-786. doi: 10.1016/j.idc.2005.07.009
10. Lew DP, Waldvogel FA. Osteomyelitis. New England Journal of Medicine. 1997; 336(14): 999-1007. doi: 10.1056/nejm199704033361406
11. Waldvogel FA, Vasey H. Osteomyelitis: The Past Decade. New England Journal of Medicine. 1980; 303(7): 360-370. doi: 10.1056/nejm198008143030703
12. Ramesh N, Moratti SC, Dias GJ. Hydroxyapatite–polymer biocomposites for bone regeneration: A review of current trends. Journal of Biomedical Materials Research Part B: Applied Biomaterials. 2017; 106(5): 2046-2057. doi: 10.1002/jbm.b.33950
13. Dimitriou R, Jones E, McGonagle D, et al. Bone regeneration: current concepts and future directions. BMC Medicine. 2011; 9(1). doi: 10.1186/1741-7015-9-66
14. Soucacos PN, Johnson EO, Babis G. An update on recent advances in bone regeneration. Injury. 2008; 39: S1-S4. doi: 10.1016/S0020-1383(08)70009-3
15. Cornell CN, Lane JM. Current Understanding of Osteoconduction in Bone Regeneration. Clinical Orthopaedics and Related Research. 1998; 355S: S267-S273. doi: 10.1097/00003086-199810001-00027
16. Albrektsson T, Johansson C. Osteoinduction, osteoconduction and osseointegration. European Spine Journal. 2001; 10(0): S96-S101. doi: 10.1007/s005860100282
17. Kuzyk PRT, Schemitsch EH. The basic science of peri-implant bone healing. Indian Journal of Orthopaedics. 2011; 45(2): 108-115. doi: 10.4103/0019-5413.77129
18. Chang BS, Hong KS, Youn HJ, et al. Osteoconduction at porous hydroxyapatite with various pore configurations. Biomaterials. 2000; 21: 1291-1298. doi: 10.1016/S0142-9612(00)00030-2
19. Krishnan MR, Alsharaeh E. Potential removal of benzene-toluene-xylene toxic vapors by nanoporous poly(styrene-r-methylmethacrylate) copolymer composites. Environmental Nanotechnology, Monitoring & Management. 2023; 20: 100860. doi: 10.1016/j.enmm.2023.100860
20. Krishnan MR, Alsharaeh EH. Polymer gel amended sandy soil with enhanced water storage and extended release capabilities for sustainable desert agriculture. Journal of Polymer Science and Engineering. 2023; 6(1): 2892. doi: 10.24294/jpse.v6i1.2892
21. Krishnan MR, Alsharaeh EH. Facile fabrication of thermo-mechanically reinforced polystyrene-graphene nanocomposite aerogel for produced water treatment. Journal of Porous Materials. 2024; 31: 1363-1373. doi: 10.1007/s10934-024-01602-y
22. Krishnan MR, Alsharaeh EH. High-performance functional materials based on polymer nanocomposites—A review. Journal of Polymer Science and Engineering. 2023; 6(1): 3292. doi: 10.24294/jpse.v6i1.3292
23. Krishnan MR, Rajendran V. Sulfonated mesoporous polystyrene-1D multiwall carbon nanotube nanocomposite as potential adsorbent for efficient removal of xylene isomers from aqueous solution. Characterization and Application of Nanomaterials. 2023; 6(2): 3516. doi: 10.24294/can.v6i2.3516
24. Krishnan M, Michal F, Alsoughayer S, et al. Thermodynamic and Kinetic Investigation of Water Absorption by PAM Composite Hydrogel. In: Proceedings of the SPE Kuwait Oil & Gas Show and Conference; 13-16 October 2019; Mishref, Kuwait. doi: 10.2118/198033-ms
25. Krishnan MR, Aldawsari YF, Alsharaeh EH. Three-dimensionally cross-linked styrene-methyl methacrylate-divinyl benzene terpolymer networks for organic solvents and crude oil absorption. Journal of Applied Polymer Science. 2020; 138(9). doi: 10.1002/app.49942
26. Krishnan MR, Aldawsari Y, Michael FM, et al. 3D-Polystyrene-polymethyl methacrylate/divinyl benzene networks-Epoxy-Graphene nanocomposites dual-coated sand as high strength proppants for hydraulic fracture operations. Journal of Natural Gas Science and Engineering. 2021; 88: 103790. doi: 10.1016/j.jngse.2020.103790
27. Krishnan MR, Aldawsari Y, Michael FM, et al. Mechanically reinforced polystyrene-polymethyl methacrylate copolymer-graphene and Epoxy-Graphene composites dual-coated sand proppants for hydraulic fracture operations. Journal of Petroleum Science and Engineering. 2021; 196: 107744. doi: 10.1016/j.petrol.2020.107744
28. Krishnan M, Chen HY, Ho RM. Switchable structural colors from mesoporous polystyrene films. In: Proceedings of the ACS 252nd. National Meeting; 18-26 August 2016; Philadelphia, Pennsylvania, USA.

29. Krishnan MR, Almohsin A, Alsharaeh EH. Syntheses and fabrication of mesoporous styrene-co-methyl methacrylate-graphene composites for oil removal. Diamond and Related Materials. 2022; 130: 109494. doi: 10.1016/j.diamond.2022.109494
30. Krishnan MR, Omar H, Yazeed Y, et al. Insight into Thermo-Mechanical Enhancement of Polymer Nanocomposites Coated Microsand Proppants for Hydraulic Fracturing. SSRN Electronic Journal. 2022. doi: 10.2139/ssrn.4243574
31. Krishnan MR, Rajendran V, Alsharaeh E. Anti-reflective and high-transmittance optical films based on nanoporous silicon dioxide fabricated from templated synthesis. Journal of Non-Crystalline Solids. 2023; 606: 122198. doi: 10.1016/j.jnoncrysol.2023.122198
32. Krishnan MR, Li W, Alsharaeh EH. Ultra-lightweight Nanosand/Polymer Nanocomposite Materials for Hydraulic Fracturing Operations. SSRN Electronic Journal. 2022. doi: 10.2139/ssrn.4233321
33. Krishnan MR, Omar H, Almohsin A, et al. An overview on nanosilica–polymer composites as high-performance functional materials in oil fields. Polymer Bulletin. 2023; 81(5): 3883-3933. doi: 10.1007/s00289-023-04934-y
34. Krishnan MR, Li W, Alsharaeh EH. Cross-linked polymer nanocomposite networks coated nano sand light-weight proppants for hydraulic fracturing applications. Characterization and Application of Nanomaterials. 2023; 6(2): 3314. doi: 10.24294/can.v6i2.3314
35. Krishnan MR, Almohsin A, Alsharaeh EH. Thermo-Mechanically Reinforced Mesoporous Styrene-Co-Methyl Methacrylate-Graphene Composites for Produced Water Treatment. SSRN Electronic Journal. 2022.
36. Aldosari MA, Alsaud KBB, Othman A, et al. Microwave Irradiation Synthesis and Characterization of Reduced-(Graphene Oxide-(Polystyrene-Polymethyl Methacrylate))/Silver Nanoparticle Nanocomposites and Their Anti-Microbial Activity. Polymers. 2020; 12(5): 1155. doi: 10.3390/polym12051155
37. Krishnan MR, Almohsin A, Alsharaeh EH. Mechanically robust and thermally enhanced sand-polyacrylamide-2D nanofiller composite hydrogels for water shutoff applications. Journal of Applied Polymer Science. 2023; 141(7). doi: 10.1002/app.54953
38. Almohsin A, Michal F, Alsharaeh E, et al. Self-Healing PAM Composite Hydrogel for Water Shutoff at High Temperatures: Thermal and Rheological Investigations. In: Proceedings of the SPE Gas & Oil Technology Showcase and Conference; 21-23 October 2019; Dubai, United Arab Emirates. doi: 10.2118/198664-ms
39. Almohsin A, Alsharaeh E, Michael FM, Krishnan MR. Polymer-Nanofiller Hydrogels. US Patent, US11828116B2, 31 October 2023.
40. Almohsin A, Alsharaeh E, Krishnan MR. Polymer-Sand Nanocomposite Lost Circulation Material. US Patent, US11828116B2, 28 November 2023.
41. Almohsin A, Alsharaeh E, Krishnan MR, Alghazali M. Coated Nanosand as Relative Permeability Modifier. US Patent, US11827852B2, 28 November 2023.
42. Almohsin A, Krishnan MR, Alsharaeh E, et al. Preparation and Properties Investigation on Sand-Polyacrylamide Composites with Engineered Interfaces for Water Shutoff Applications. In: Proceedings of the Middle East Oil, Gas and Geosciences Show; 19-21 February 2023; Manama, Bahrain. doi: 10.2118/213481-ms
43. Keishnan MR, Michael FM, Almohsin AM, et al. Thermal and Rheological Investigations on N,N'-Methylenebis Acrylamide Cross-Linked Polyacrylamide Nanocomposite Hydrogels for Water Shutoff Applications. In: Proceedings of the Offshore Technology Conference Asia; 2-6 November 2020; Kuala Lumpur, Malaysia. doi: 10.4043/30123-ms
44. Krishnan MR, Aldawsari YF, Alsharaeh EH. 3D-poly(styrene-methyl methacrylate)/divinyl benzene-2D-nanosheet composite networks for organic solvents and crude oil spill cleanup. Polymer Bulletin. 2021; 79(6): 3779-3802. doi: 10.1007/s00289-021-03565-5
45. Krishnan MR, Lu K, Chiu W, et al. Directed Self-Assembly of Star-Block Copolymers by Topographic Nanopatterns through Nucleation and Growth Mechanism. Small. 2018; 14(16). doi: 10.1002/smll.201704005
46. Ho RM, Krishnan MR, Siddique SK, Chien YC. Method for Fabricating Nanoporous Polymer Thin Film and Corresponding Method for Fabricating Nanoporous Thin Film. US Patent, US11059205B2, 13 July 2021.
47. Alsharaeh EH, Krishnan MR. Method of Making Mutlilayer Soil with Property for Extended Release Water for Desert Agriculture. US Patent, US10772265B1, 15 September 2020.
48. Tasleem S, Bongu CS, Krishnan MR, et al. Navigating the hydrogen prospect: A comprehensive review of sustainable source-based production technologies, transport solutions, advanced storage mechanisms, and CCUS integration. Journal of Energy Chemistry. 2024; 97: 166-215. doi: 10.1016/j.jechem.2024.05.022

49. Michael FM, Krishnan MR, Fathima A, et al. Zirconia/graphene nanocomposites effect on the enhancement of thermo-mechanical stability of polymer hydrogels. Materials Today Communications. 2019; 21: 100701. doi: 10.1016/j.mtcomm.2019.100701
50. Michael FM, Krishnan MR, AlSoughayer S, et al. Thermo-elastic and self-healing polyacrylamide -2D nanofiller composite hydrogels for water shutoff treatment. Journal of Petroleum Science and Engineering. 2020; 193: 107391. doi: 10.1016/j.petrol.2020.107391
51. Vacanti CA. The history of tissue engineering. Journal of Cellular and Molecular Medicine. 2006; 10(3): 569-576. doi: 10.1111/j.1582-4934.2006.tb00421.x
52. Chapekar MS. Tissue engineering: challenges and opportunities. Journal of Biomedical Materials Research. 2000; 53: 617-620. doi: 10.1002/1097-4636(2000)53:6<617::AID-JBM1>3.0.CO;2-C
53. Atala A, Lanza R. Methods of Tissue Engineering. Gulf Professional Publishing; 2001.
54. Stock UA, Vacanti JP. Tissue Engineering: Current State and Prospects. Annual Review of Medicine. 2001; 52(1): 443-451. doi: 10.1146/annurev.med.52.1.443
55. Black CRM, Goriainov V, Gibbs D, et al. Bone Tissue Engineering. Current Molecular Biology Reports. 2015; 1(3): 132-140. doi: 10.1007/s40610-015-0022-2
56. Shafiee A, Atala A. Tissue Engineering: Toward a New Era of Medicine. Annual Review of Medicine. 2017; 68(1): 29-40. doi: 10.1146/annurev-med-102715-092331
57. Patrick CW, Mikos AG, McIntire LV. Prospectus of Tissue Engineering. In: Patrick CW, Mikos AG, McIntire LV, Langer RS (editors). Frontiers in Tissue Engineering, 1st ed. Pergamon; 1998. pp. 3-11. doi: 10.1016/b978-008042689-1/50003-0
58. Ikada Y. Tissue Engineering: Fundamentals and Applications. Elsevier; 2011.
59. Abdelaziz AG, Nageh H, Abdo SM, et al. A Review of 3D Polymeric Scaffolds for Bone Tissue Engineering: Principles, Fabrication Techniques, Immunomodulatory Roles, and Challenges. Bioengineering. 2023; 10(2): 204. doi: 10.3390/bioengineering10020204
60. Hutmacher DW. Scaffolds in tissue engineering bone and cartilage. Biomaterials. 2000; 21: 2529-2543. doi: 10.1016/S0142-9612(00)00121-6
61. Guarino V, Causa F, Netti PA, et al. The role of hydroxyapatite as solid signal on performance of PCL porous scaffolds for bone tissue regeneration. Journal of Biomedical Materials Research Part B: Applied Biomaterials. 2008; 86B(2): 548-557. doi: 10.1002/jbm.b.31055
62. Gómez S, Vlad MD, López J, et al. Design and properties of 3D scaffolds for bone tissue engineering. Acta Biomaterialia. 2016; 42: 341-350. doi: 10.1016/j.actbio.2016.06.032
63. Mirkhalaf M, Men Y, Wang R, et al. Personalized 3D printed bone scaffolds: A review. Acta Biomaterialia. 2023; 156: 110-124. doi: 10.1016/j.actbio.2022.04.014
64. Wu S, Liu X, Yeung KWK, et al. Biomimetic porous scaffolds for bone tissue engineering. Materials Science and Engineering: R: Reports. 2014; 80: 1-36. doi: 10.1016/j.mser.2014.04.001
65. Qu H, Fu H, Han Z, et al. Biomaterials for bone tissue engineering scaffolds: a review. RSC Advances. 2019; 9(45): 26252-26262. doi: 10.1039/c9ra05214c
66. Lichte P, Pape HC, Pufe T, et al. Scaffolds for bone healing: Concepts, materials and evidence. Injury. 2011; 42(6): 569-573. doi: 10.1016/j.injury.2011.03.033
67. Chocholata P, Kulda V, Babuska V. Fabrication of Scaffolds for Bone-Tissue Regeneration. Materials. 2019; 12(4): 568. doi: 10.3390/ma12040568
68. Wang C, Huang W, Zhou Y, et al. 3D printing of bone tissue engineering scaffolds. Bioactive Materials. 2020; 5(1): 82-91. doi: 10.1016/j.bioactmat.2020.01.004
69. Alonzo M, Alvarez Primo F, Anil Kumar S, et al. Bone tissue engineering techniques, advances, and scaffolds for treatment of bone defects. Current Opinion in Biomedical Engineering. 2021; 17: 100248. doi: 10.1016/j.cobme.2020.100248
70. Polo-Corrales L, Latorre-Esteves M, Ramirez-Vick JE. Scaffold Design for Bone Regeneration. Journal of Nanoscience and Nanotechnology. 2014; 14(1): 15-56. doi: 10.1166/jnn.2014.9127
71. Cao S, Zhao Y, Hu Y, et al. New perspectives: In-situ tissue engineering for bone repair scaffold. Composites Part B: Engineering. 2020; 202: 108445. doi: 10.1016/j.compositesb.2020.108445
72. Collins MN, Ren G, Young K, et al. Scaffold Fabrication Technologies and Structure/Function Properties in Bone Tissue Engineering. Advanced Functional Materials. 2021; 31(21). doi: 10.1002/adfm.202010609

73. Roseti L, Parisi V, Petretta M, et al. Scaffolds for Bone Tissue Engineering: State of the art and new perspectives. Materials Science and Engineering: C. 2017; 78: 1246-1262. doi: 10.1016/j.msec.2017.05.017
74. Thadavirul N, Pavasant P, Supaphol P. Development of polycaprolactone porous scaffolds by combining solvent casting, particulate leaching, and polymer leaching techniques for bone tissue engineering. Journal of Biomedical Materials Research Part A. 2013; 102(10): 3379-3392. doi: 10.1002/jbm.a.35010
75. Sola A, Bertacchini J, D'Avella D, et al. Development of solvent-casting particulate leaching (SCPL) polymer scaffolds as improved three-dimensional supports to mimic the bone marrow niche. Materials Science and Engineering: C. 2019; 96: 153-165. doi: 10.1016/j.msec.2018.10.086
76. Prasad A, Sankar MR, Katiyar V. State of Art on Solvent Casting Particulate Leaching Method for Orthopedic ScaffoldsFabrication. Materials Today: Proceedings. 2017; 4(2): 898-907. doi: 10.1016/j.matpr.2017.01.101
77. Koyyada A, Orsu P. Recent Advancements and Associated Challenges of Scaffold Fabrication Techniques in Tissue Engineering Applications. Regenerative Engineering and Translational Medicine. 2020; 7(2): 147-159. doi: 10.1007/s40883-020-00166-y
78. Zhang Z, Feng Y, Wang L, et al. A review of preparation methods of porous skin tissue engineering scaffolds. Materials Today Communications. 2022; 32: 104109. doi: 10.1016/j.mtcomm.2022.104109
79. Suamte L, Tirkey A, Barman J, et al. Various manufacturing methods and ideal properties of scaffolds for tissue engineering applications. Smart Materials in Manufacturing. 2023; 1: 100011. doi: 10.1016/j.smmf.2022.100011
80. Fereshteh Z. Freeze-drying technologies for 3D scaffold engineering. In: Deng Y, Kuipe J (editors). Functional 3D Tissue Engineering Scaffolds. Elsevier; 2018. pp. 151-174. doi: 10.1016/b978-0-08-100979-6.00007-0
81. Kazimierczak P, Benko A, Palka K, et al. Novel synthesis method combining a foaming agent with freeze-drying to obtain hybrid highly macroporous bone scaffolds. Journal of Materials Science & Technology. 2020; 43: 52-63. doi: 10.1016/j.jmst.2020.01.006
82. Putra DFA, Aji BB, Ningsih HS, et al. Preparation and Characterization of Freeze-Dried β-Tricalcium Phosphate/Barium Titanate/Collagen Composite Scaffolds for Bone Tissue Engineering in Orthopedic Applications. Ceramics. 2023; 6(4): 2148-2161. doi: 10.3390/ceramics6040132
83. Samitsu S, Zhang R, Peng X, et al. Flash freezing route to mesoporous polymer nanofibre networks. Nature Communications. 2013; 4(1). doi: 10.1038/ncomms3653
84. Krishnan MR, Samitsu S, Fujii Y, et al. Hydrophilic polymer nanofibre networks for rapid removal of aromatic compounds from water. Chem Commun. 2014; 50(66): 9393-9396. doi: 10.1039/c4cc01786b
85. Krishnan MR, Chien YC, Cheng CF, et al. Fabrication of Mesoporous Polystyrene Films with Controlled Porosity and Pore Size by Solvent Annealing for Templated Syntheses. Langmuir. 2017; 33(34): 8428-8435. doi: 10.1021/acs.langmuir.7b02195
86. Cheng CF, Chen YM, Zou F, et al. Li-Ion Capacitor Integrated with Nano-network-Structured Ni/NiO/C Anode and Nitrogen-Doped Carbonized Metal–Organic Framework Cathode with High Power and Long Cyclability. ACS Applied Materials & Interfaces. 2019; 11(34): 30694-30702. doi: 10.1021/acsami.9b06354
87. Chien YC, Huang LY, Yang KC, et al. Fabrication of metallic nanonetworks via templated electroless plating as hydrogenation catalyst. Emergent Materials. 2020; 4(2): 493-501. doi: 10.1007/s42247-020-00108-y
88. Lo TY, Krishnan MR, Lu KY, et al. Silicon-containing block copolymers for lithographic applications. Progress in Polymer Science. 2018; 77: 19-68. doi: 10.1016/j.progpolymsci.2017.10.002
89. Mi A, Guo L, Guo S, et al. Freeze-casting in synthetic porous materials: Principles, different dimensional building units and recent applications. Sustainable Materials and Technologies. 2024; 39: e00830. doi: 10.1016/j.susmat.2024.e00830
90. Hajihasani Biouki M, Mobedi H, Karkhaneh A, et al. Development of a simvastatin loaded injectable porous scaffold in situ formed by phase inversion method for bone tissue regeneration. The International Journal of Artificial Organs. 2018; 42(2): 72-79. doi: 10.1177/0391398818806161
91. Duarte ARC, Mano JF, Reis RL. Dexamethasone-loaded scaffolds prepared by supercritical-assisted phase inversion. Acta Biomaterialia. 2009; 5(6): 2054-2062. doi: 10.1016/j.actbio.2009.01.047
92. Duarte ARC, Mano JF, Reis RL. Supercritical phase inversion of starch-poly(ε-caprolactone) for tissue engineering applications. Journal of Materials Science: Materials in Medicine. 2009; 21(2): 533-540. doi: 10.1007/s10856-009-3909-8
93. Duarte ARC, Mano JF, Reis RL. The role of organic solvent on the preparation of chitosan scaffolds by supercritical assisted phase inversion. The Journal of Supercritical Fluids. 2012; 72: 326-332. doi: 10.1016/j.supflu.2010.12.004

94. Seyed Hakim R, Maghsoud Z, Halabian R. Fabrication and evaluation of polycaprolactone/olive oil scaffolds by phase inversion for tissue engineering. European Polymer Journal. 2021; 150: 110394. doi: 10.1016/j.eurpolymj.2021.110394
95. Duarte ARC, Mano JF, Reis RL. Supercritical fluids in biomedical and tissue engineering applications: a review. International Materials Reviews. 2009; 54(4): 214-222. doi: 10.1179/174328009x411181
96. Yang DZ, Chen AZ, Wang SB, et al. Preparation of poly(L-lactic acid) nanofiber scaffolds with a rough surface by phase inversion using supercritical carbon dioxide. Biomedical Materials. 2015; 10(3): 035015. doi: 10.1088/1748-6041/10/3/035015
97. Duarte ARC, Mano JF, Reis RL. Preparation of starch-based scaffolds for tissue engineering by supercritical immersion precipitation. The Journal of Supercritical Fluids. 2009; 49(2): 279-285. doi: 10.1016/j.supflu.2008.12.008
98. Papenburg BJ, Bolhuis-Versteeg LAM, Grijpma DW, et al. A facile method to fabricate poly(l-lactide) nano-fibrous morphologies by phase inversion. Acta Biomaterialia. 2010; 6(7): 2477-2483. doi: 10.1016/j.actbio.2009.12.051
99. Yoshimoto H, Shin Y, Terai H, Vacanti J. A biodegradable nanofiber scaffold by electrospinning and its potential for bone tissue engineering. Biomaterials. 2003; 24: 2077-2082. doi: 10.1016/S0142-9612(02)00635-X
100. Yu Y, Hua S, Yang M, et al. Fabrication and characterization of electrospinning/3D printing bone tissue engineering scaffold. RSC Advances. 2016; 6(112): 110557-110565. doi: 10.1039/c6ra17718b
101. Prabhakaran MP, Venugopal J, Ramakrishna S. Electrospun nanostructured scaffolds for bone tissue engineering. Acta Biomaterialia. 2009; 5(8): 2884-2893. doi: 10.1016/j.actbio.2009.05.007
102. Wang Z, Wang Y, Yan J, et al. Pharmaceutical electrospinning and 3D printing scaffold design for bone regeneration. Advanced Drug Delivery Reviews. 2021; 174: 504-534. doi: 10.1016/j.addr.2021.05.007
103. Maji K, Pramanik K. Electrospun scaffold for bone regeneration. International Journal of Polymeric Materials and Polymeric Biomaterials. 2021; 71(11): 842-857. doi: 10.1080/00914037.2021.1915784
104. Lin W, Chen M, Qu T, et al. Three-dimensional electrospun nanofibrous scaffolds for bone tissue engineering. Journal of Biomedical Materials Research Part B: Applied Biomaterials. 2019; 108(4): 1311-1321. doi: 10.1002/jbm.b.34479
105. Qi Y, Lv H, Huang Q, et al. The Synergetic Effect of 3D Printing and Electrospinning Techniques in the Fabrication of Bone Scaffolds. Annals of Biomedical Engineering. 2024; 52(6): 1518-1533. doi: 10.1007/s10439-024-03500-5
106. Khajavi R, Abbasipour M, Bahador A. Electrospun biodegradable nanofibers scaffolds for bone tissue engineering. Journal of Applied Polymer Science. 2015; 133(3). doi: 10.1002/app.42883
107. Andric T, Wright LD, Taylor BL, et al. Fabrication and characterization of three-dimensional electrospun scaffolds for bone tissue engineering. Journal of Biomedical Materials Research Part A. 2012; 100A(8): 2097-2105. doi: 10.1002/jbm.a.34045
108. Jang JH, Castano O, Kim HW. Electrospun materials as potential platforms for bone tissue engineering. Advanced Drug Delivery Reviews. 2009; 61(12): 1065-1083. doi: 10.1016/j.addr.2009.07.008
109. Yang C, Shao Q, Han Y, et al. Fibers by Electrospinning and Their Emerging Applications in Bone Tissue Engineering. Applied Sciences. 2021; 11(19): 9082. doi: 10.3390/app11199082
110. Bhattarai DP, Aguilar LE, Park CH, et al. A Review on Properties of Natural and Synthetic Based Electrospun Fibrous Materials for Bone Tissue Engineering. Membranes. 2018; 8(3): 62. doi: 10.3390/membranes8030062
111. Li W, Laurencin CT, Caterson EJ, et al. Electrospun nanofibrous structure: A novel scaffold for tissue engineering. Journal of Biomedical Materials Research. 2002; 60(4): 613-621. doi: 10.1002/jbm.10167
112. Sun W, Darling A, Starly B, et al. Computer-aided tissue engineering: overview, scope and challenges. Biotechnology and Applied Biochemistry. 2004; 39(1): 29-47. doi: 10.1042/ba20030108
113. Sun W, Lal P. Recent development on computer aided tissue engineering-a review. Computer Methods and Programs in Biomedicine. 2002; 67: 85-103. doi: 10.1016/S0169-2607(01)00116-X
114. Giannitelli SM, Accoto D, Trombetta M, et al. Current trends in the design of scaffolds for computer-aided tissue engineering. Acta Biomaterialia. 2014; 10(2): 580-594. doi: 10.1016/j.actbio.2013.10.024
115. Top N, Şahin İ, Gökçe H, et al. Computer-aided design and additive manufacturing of bone scaffolds for tissue engineering: state of the art. Journal of Materials Research. 2021; 36(19): 3725-3745. doi: 10.1557/s43578-021-00156-y
116. Di Gravina GM, Loi G, Auricchio F, et al. Computer-aided engineering and additive manufacturing for bioreactors in tissue engineering: State of the art and perspectives. Biophysics Reviews. 2023; 4(3). doi: 10.1063/5.0156704
117. Zenobi E, Merco M, Mochi F, et al. Tailoring the Microarchitectures of 3D Printed Bone-like Scaffolds for Tissue Engineering Applications. Bioengineering. 2023; 10(5): 567. doi: 10.3390/bioengineering10050567

118. Bardini R, Di Carlo S. Computational Methods for Biofabrication in Tissue Engineering and Regenerative Medicine - a literature review. Computational and Structural Biotechnology Journal. 2024; 23: 601-616. doi: 10.1101/2023.03.03.530995
119. Bermejillo Barrera MD, Franco-Martínez F, Díaz Lantada A. Artificial Intelligence Aided Design of Tissue Engineering Scaffolds Employing Virtual Tomography and 3D Convolutional Neural Networks. Materials. 2021; 14(18): 5278. doi: 10.3390/ma14185278
120. Foresti R, Rossi S, Pinelli S, et al. Highly-defined bioprinting of long-term vascularized scaffolds with Bio-Trap: Complex geometry functionalization and process parameters with computer aided tissue engineering. Materialia. 2020; 9: 100560. doi: 10.1016/j.mtla.2019.100560
121. Sahai N, Gogoi M. Computer aided designing and finite element analysis for development of porous 3D tissue scaffold - a review. International Journal of Biomedical Engineering and Technology. 2020; 33(2): 174. doi: 10.1504/ijbet.2020.107712
122. Fernández MP, Witte F, Tozzi G. Applications of X-ray computed tomography for the evaluation of biomaterial-mediated bone regeneration in critical-sized defects. Journal of Microscopy. 2019; 277(3): 179-196. doi: 10.1111/jmi.12844
123. Noroozi R, Tatar F, Zolfagharian A, et al. Additively Manufactured Multi-Morphology Bone-like Porous Scaffolds: Experiments and Micro-Computed Tomography-Based Finite Element Modeling Approaches. International Journal of Bioprinting. 2022; 8(3): 556. doi: 10.18063/ijb.v8i3.556
124. Liu Y, Xie D, Zhou R, et al. 3D X-ray micro-computed tomography imaging for the microarchitecture evaluation of porous metallic implants and scaffolds. Micron. 2021; 142: 102994. doi: 10.1016/j.micron.2020.102994
125. Dixit K, Gupta P, Kamle S, et al. Structural analysis of porous bioactive glass scaffolds using micro-computed tomographic images. Journal of Materials Science. 2020; 55(27): 12705-12724. doi: 10.1007/s10853-020-04850-w
126. Rawson SD, Maksimcuka J, Withers PJ, et al. X-ray computed tomography in life sciences. BMC Biology. 2020; 18(1). doi: 10.1186/s12915-020-0753-2
127. Olăreț E, Stancu IC, Iovu H, et al. Computed Tomography as a Characterization Tool for Engineered Scaffolds with Biomedical Applications. Materials. 2021; 14(22): 6763. doi: 10.3390/ma14226763
128. Farina E, Gastaldi D, Baino F, et al. Micro computed tomography based finite element models for elastic and strength properties of 3D printed glass scaffolds. Acta Mechanica Sinica. 2021; 37(2): 292-306. doi: 10.1007/s10409-021-01065-3
129. Verykokou S, Ioannidis C, Soile S, et al. The Role of Cone Beam Computed Tomography in Periodontology: From 3D Models of Periodontal Defects to 3D-Printed Scaffolds. Journal of Personalized Medicine. 2024; 14(2): 207. doi: 10.3390/jpm14020207
130. Vanlenthe G, Hagenmuller H, Bohner M, et al. Nondestructive micro-computed tomography for biological imaging and quantification of scaffold–bone interaction in vivo. Biomaterials. 2007; 28(15): 2479-2490. doi: 10.1016/j.biomaterials.2007.01.017
131. Yang A, Wang Y, Feng Q, et al. Integrating Fluorescence and Magnetic Resonance Imaging in Biocompatible Scaffold for Real-Time Bone Repair Monitoring and Assessment. Advanced Healthcare Materials. 2023; 13(6). doi: 10.1002/adhm.202302687
132. Washburn NR, Weir M, Anderson P, et al. Bone formation in polymeric scaffolds evaluated by proton magnetic resonance microscopy and X-ray microtomography. Journal of Biomedical Materials Research Part A. 2004; 69A(4): 738-747. doi: 10.1002/jbm.a.30054
133. Zhao M, Li X, Fu F, et al. Magnetic resonance imaging-three-dimensional printing technology fabricates customized scaffolds for brain tissue engineering. Neural Regeneration Research. 2017; 12(4): 614. doi: 10.4103/1673-5374.205101
134. van der Zande M, Sitharaman B, Walboomers XF, et al. In Vivo Magnetic Resonance Imaging of the Distribution Pattern of Gadonanotubes Released from a Degrading Poly(Lactic-Co-Glycolic Acid) Scaffold. Tissue Engineering Part C: Methods. 2011; 17(1): 19-26. doi: 10.1089/ten.tec.2010.0089
135. Sajesh KM, Ashokan A, Gowd GS, et al. Magnetic 3D scaffold: A theranostic tool for tissue regeneration and non-invasive imaging in vivo. Nanomedicine: Nanotechnology, Biology and Medicine. 2019; 18: 179-188. doi: 10.1016/j.nano.2019.02.022
136. Huang J, Lv Z, Wang Y, et al. In Vivo MRI and X-Ray Bifunctional Imaging of Polymeric Composite Supplemented with GdPO4·H2O Nanobundles for Tracing Bone Implant and Bone Regeneration. Advanced Healthcare Materials. 2016; 5(17): 2182-2190. doi: 10.1002/adhm.201600249

137. Stuckey DJ, Ishii H, Chen QZ, et al. Magnetic Resonance Imaging Evaluation of Remodeling by Cardiac Elastomeric Tissue Scaffold Biomaterials in a Rat Model of Myocardial Infarction. Tissue Engineering Part A. 2010; 16(11): 3395-3402. doi: 10.1089/ten.tea.2010.0213
138. Chesnick IE, Fowler CB, Mason JT, et al. Novel mineral contrast agent for magnetic resonance studies of bone implants grown on a chick chorioallantoic membrane. Magnetic Resonance Imaging. 2011; 29(9): 1244-1254. doi: 10.1016/j.mri.2011.07.022
139. Heljak MK, Kurzydlowski KJ, Swieszkowski W. Computer aided design of architecture of degradable tissue engineering scaffolds. Computer Methods in Biomechanics and Biomedical Engineering. 2017; 20(15): 1623-1632. doi: 10.1080/10255842.2017.1399263
140. Lacroix D, Planell JA, Prendergast PJ. Computer-aided design and finite-element modelling of biomaterial scaffolds for bone tissue engineering. Philosophical Transactions of the Royal Society A: Mathematical, Physical and Engineering Sciences. 2009; 367(1895): 1993-2009. doi: 10.1098/rsta.2009.0024
141. Fang Z, Starly B, Sun W. Computer-aided characterization for effective mechanical properties of porous tissue scaffolds. Computer-Aided Design. 2005; 37(1): 65-72. doi: 10.1016/j.cad.2004.04.002
142. Sun W, Starly B, Darling A, et al. Computer-aided tissue engineering: application to biomimetic modelling and design of tissue scaffolds. Biotechnology and Applied Biochemistry. 2004; 39(1): 49-58. doi: 10.1042/ba20030109
143. Ramin E, Harris RA. Advanced computer-aided design for bone tissue-engineering scaffolds. Proceedings of the Institution of Mechanical Engineers, Part H: Journal of Engineering in Medicine. 2009; 223(3): 289-301. doi: 10.1243/09544119jeim452
144. Sahai N, Saxena KK, Gogoi M. Modelling and simulation for fabrication of 3D printed polymeric porous tissue scaffolds. Advances in Materials and Processing Technologies. 2020; 6(3): 530-539. doi: 10.1080/2374068x.2020.1728643
145. Naing MW, Chua CK, Leong KF, et al. Fabrication of customised scaffolds using computer-aided design and rapid prototyping techniques. Rapid Prototyping Journal. 2005; 11(4): 249-259. doi: 10.1108/13552540510612938
146. Quadrani P, Pasini A, Mattioli-Belmonte M, et al. High-resolution 3D scaffold model for engineered tissue fabrication using a rapid prototyping technique. Medical & Biological Engineering & Computing. 2005; 43(2): 196-199. doi: 10.1007/bf02345954
147. Chua CK, Leong KF, An J. Introduction to rapid prototyping of biomaterials. Rapid Prototyping of Biomaterials. Published online 2020: 1-15. doi: 10.1016/b978-0-08-102663-2.00001-0
148. Sing SL, Tey CF, Tan JHK, et al. 3D printing of metals in rapid prototyping of biomaterials: Techniques in additive manufacturing. In: Rapid Prototyping of Biomaterials. Elsevier. 2020: 17-40. doi: 10.1016/b978-0-08-102663-2.00002-2
149. Ansari AI, Sheikh NA. Bone Tissue Regeneration: Rapid Prototyping Technology in Scaffold Design. Journal of The Institution of Engineers (India): Series C. 2022; 103(5): 1303-1324. doi: 10.1007/s40032-022-00872-2
150. Sun F, Wang T, Yang Y. Hydroxyapatite composite scaffold for bone regeneration via rapid prototyping technique: a review. Rapid Prototyping Journal. 2021; 28(3): 585-605. doi: 10.1108/rpj-09-2020-0224
151. Sharma P, Joshi D, Dhanopia A, et al. A review of rapid prototyping and its applications. SKIT Research Journal. 2020; 10(1): 89. doi: 10.47904/ijskit.10.1.2020.89-97
152. Leong K, Cheah C, Chua C. Solid freeform fabrication of three-dimensional scaffolds for engineering replacement tissues and organs. Biomaterials. 2003; 24: 2363-2378. doi: 10.1016/S0142-9612(03)00030-9

Journal of Polymer Science and Engineering 2024, 7(2), 6671.
https://doi.org/10.24294/jpse.v7i2.6671

Review

Shallow penetration conformance sealants (SPCS) based on organically cross-linked polymer and particle gels—An overview

Mohan Raj Krishnan[*], **Edreese Housni Alsharaeh**[*]

College of Science and General Studies, AlFaisal University, Riyadh 11533, Saudi Arabia
*** Corresponding authors:** Mohan Raj Krishnan, mkrishnan@alfaisal.edu; Edreese Housni Alsharaeh, ealsharaeh@alfaisal.edu

CITATION

Krishnan MR, Alsharaeh EH. Shallow penetration conformance sealants (SPCS) based on organically cross-linked polymer and particle gels—An overview. Journal of Polymer Science and Engineering. 2024; 7(2): 6671. https://doi.org/10.24294/jpse.v7i2.6671

ARTICLE INFO

Received: 27 May 2024
Accepted: 4 July 2024
Available online: 2 August 2024

Abstract: This review summarizes some of the recent advances related to shallow penetration conformance sealants (SPCS) based on cross-linked polymer nanocomposite gels. The cross-linked polymer nanocomposite gels formed a three-dimensional (3D) gel structure upon contact with either water or oil when placed at the downhole. Therefore, the cross-linked polymer nanocomposite gels offer a total or partial water shutoff. Numerous polymeric gels and their nanocomposites prepared using various techniques have been explored to address the conformance problems. Nevertheless, their instability at high temperature, high pressure, and high salinity down-hole conditions (HT-HP-HS) often makes the treatments unsuccessful. Incorporating inert particles into the cross-linked polymer nanocomposite gel matrices improves stability under harsh down-hole conditions. This review discusses potential polymeric nanocomposite gels and their successful application in conformance control.

Keywords: shallow penetration conformance sealants; water shutoff; cross-linked polymer gels; silica nanoparticles; particle gels; conformance control

1. Introduction

Hydrocarbon extraction from reservoirs is always accompanied by excessive water production, which is one of the most severe issues in the industry to date [1–6]. Such water production significantly impacts the oil wells' economic life and causes other potential problems of sand production, scaling, and corrosion of the pipelines [7,8]. The problems include leaks in the casing, water coning, and direct communication from the injector to the producer through fractures [9–15]. Numerous techniques have been exploited to address the water production issue successfully, and each of the methods has its own merits and drawbacks [16–19]. One such method was to squeeze cement into the formation and shut off the water production of the wellbore. Squeezing the cement operation was an efficient treatment in many cases, but there were significant limitations, too. One such drawback was that it required complete drilling out of the cement left in the wellbore, and this process could be time-consuming and costly [20]. Also, the cement in the formations can be damaged during the drilling-out process; hence, the seal over the offending zones is conceded, allowing the water to continue flowing into the wellbore [21,22].

The other treatment type involves using polymer gel sealants to plug the offending zone [23–25]. During the last two decades, polymer gel systems have been the most effective tools to control excessive water production. During the last decade, organically cross-linked polymer (OCP) gel and their nanocomposite systems were among the most successful treatment systems for water shutoff [8,26–29]. These potential sealant systems offer various advantages, including easy pumping into the wellbore and the rock matrix. After the squeeze of the formulation into the formation, the fluid becomes a 3D gel that plugs the treated zone [30]. More importantly, the sealant system can be used effectively for several years, but the only drawback is that the treated zone should be isolated from the productive zones [31,32]. Also, if the sealants enter the production zone, it could potentially damage either the permeability or completely shut off the hydrocarbon zone [33]. Therefore, it is essential to use the isolation technique, which sometimes is not feasible because of the configuration of the wellbore or can be costly [34]. Nevertheless, it is crucial to control excessive water production, and this should be achieved by any means. Polymers and their nanocomposites are found to be promising candidates for various industrial applications [6,10–12,35–68]. This review paper discusses a method that uses polymer gel sealants with fluid-loss control additives and non-cement particulates that can limit leakage into the formation [69]. A typical sealant is composed of (1) an organically cross-linked polymer, (2) a fluid-loss control polymer, and (3) non-cement inert particulates to provide leak-off control. Once the filtrate, the porosity fill-sealant, is inside the rock matrix, the system is thermally activated, forming a 3D gel structure that efficiently seals the targeted formation [70–72]. After the sealant formulation is squeezed, the bore-well conditions activate the polymeric formulations to crosslink. **Figure 1** shows the cased hole and perforated wellbore producing at high water cut from multiple zones [8]. Once the SPCS system arrives at perforations, a squeeze pressure is applied so that the sealing polymer filtrate leaks off into the matrix with a controlled, shallow penetration. After the system is set up, the excess SPCS system in the wellbore is washed/jetted out.

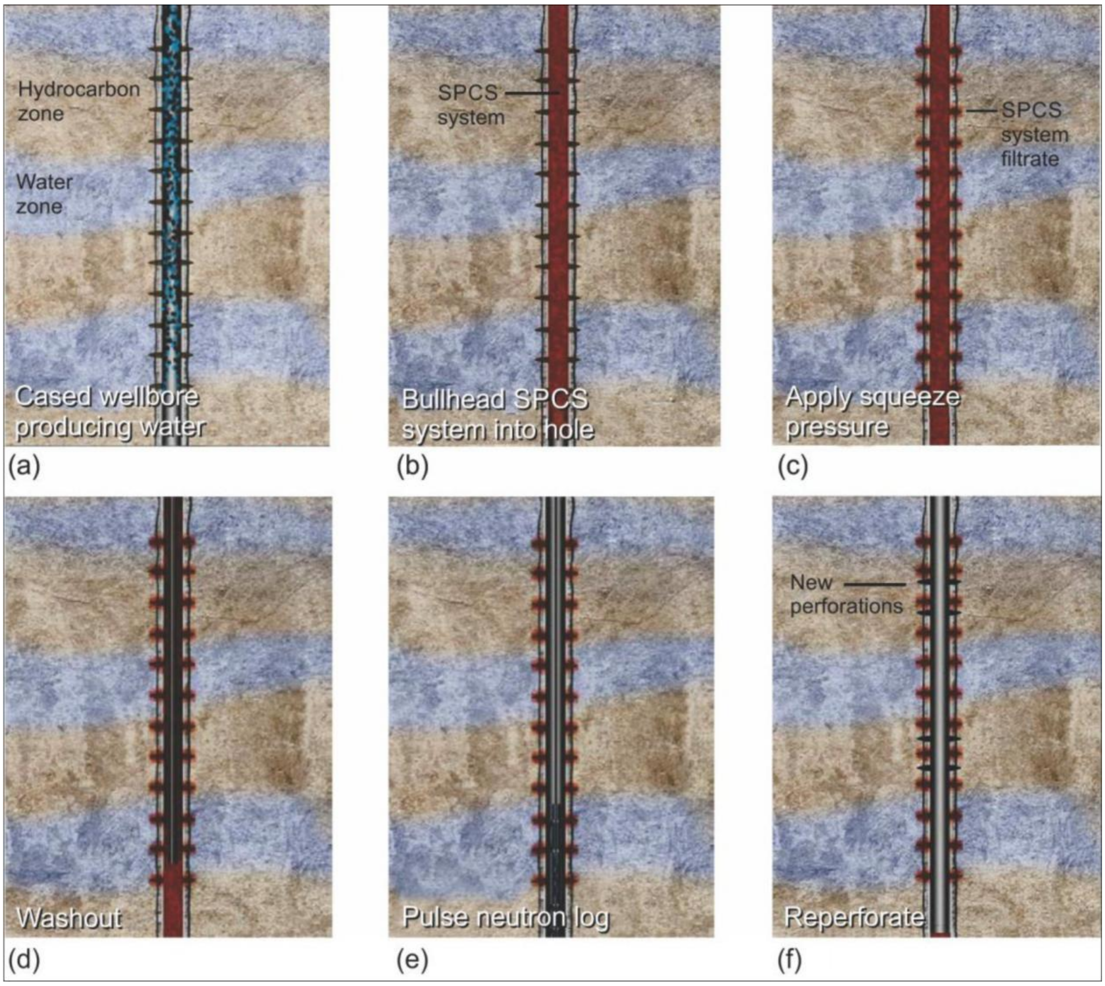

Figure 1. A typical sealant system (shallow penetration conformance sealant, SPCS) application. **(a)** cased hole and perforated wellbore producing at high water cut from multiple zones; **(b)** the SPCS system is bull-headed across all perforations; **(c)** once the SPCS system arrives at perforations, a squeeze pressure is applied so that the sealing polymer filtrate leaks off into the matrix with a controlled, shallow penetration; **(d)** after allowing the system to set up, excess SPCS system in the wellbore is washed/jetted out; **(e)** pay zones with economic hydrocarbon potential are identified with additional diagnostic tools (i.e., pulsed neutron logging tool); **(f)** new perforations are added with conventional perforation guns in the identified hydrocarbon-producing zones, bypassing SPCS [8].

2. Organically cross-linked porosity fill sealants

The sealant system is conventionally either polyacrylamide (PAM) or a copolymer of acrylamide (poly(acrylamide-co-t-butyl acrylate, PAtBA)), cross-linked with organic cross-linkers such as polyethyleneimine (PEI) [25,70,73–75]. The system's temperature range is from 40 to 400 °F (**Figures 2–5**) [76]. The borewell's temperature initiates the crosslinking process of the sealant formulation [77,78]. The cross-linking rate of the polymeric formulations depends on various factors, including the well's temperature, salinity, pH, polymer, cross-linker, and concentrations [79]. The significant advantages of the sealant systems are as follows:

- Due to the low viscosity of the polymeric formulation (20 to 30 cP), the solution can be easily injected deep into the formation without hydrolysis or precipitation. However, the chrome-based system tends to hydrolyze and precipitate at higher pH and elevated temperatures [80].

- Sufficient pumping times are required to properly place the polymeric formulations at high-temperature wells before the system forms a 3D-gel structure.
- Effective water and unwanted gas shutoffs depend on the gel's strength to resist drawdown pressure inside the formations to stop water and gas flow. The PAM-PEI systems provide sufficient strength to withstand differential pressures of at least 2600 psi.
- The overall thermal stability of the PAM-PEI gels is up to 400 °F (204 ℃).
- Moreover, the PAM-PEI sealant systems are not sensitive to formation fluids, lithology, and heavy metals. This system has been used globally in various applications, and Vasquez et al. summarized laboratory data and several case histories for both water and gas shutoffs [81].

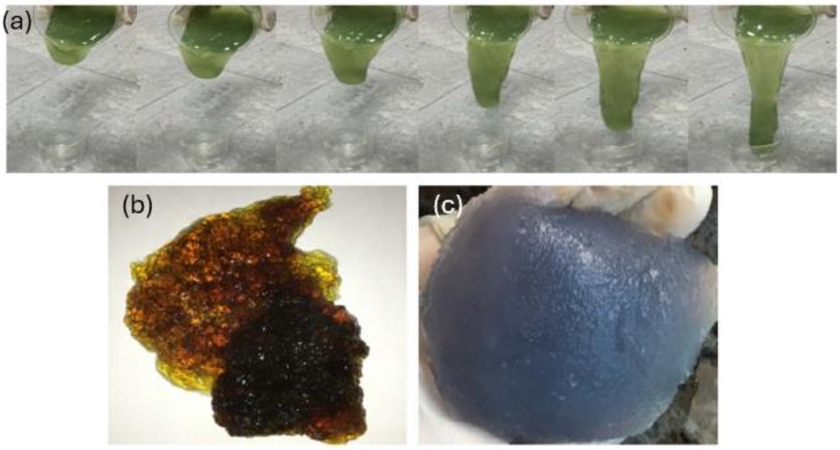

Figure 2. (a) Pre-crosslinked polyacrylamide gel; **(b)** and **(c)** cross-linked polymer gels with PEI at 150 ℃ [82].

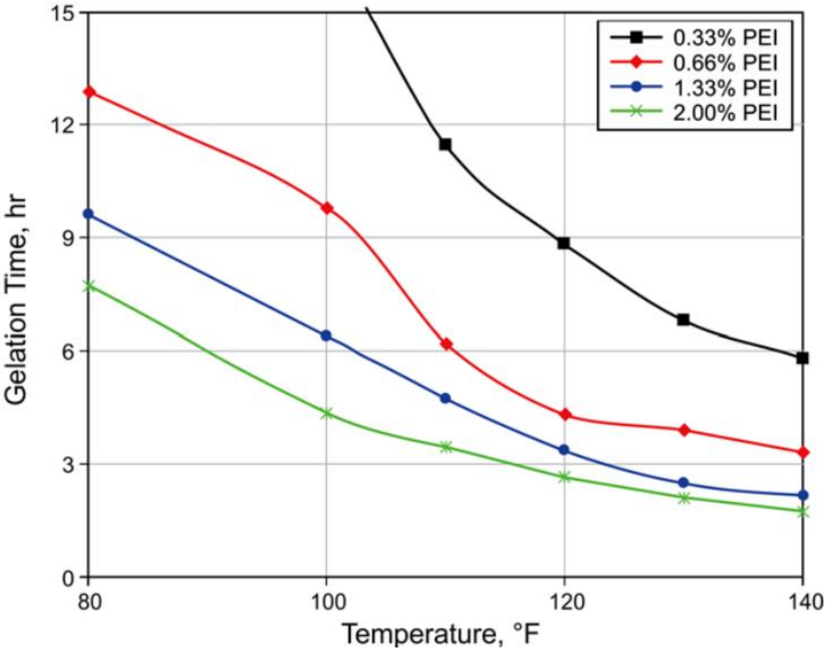

Figure 3. Gelation time of 5 wt.% of polyacrylamide in 2.0 wt.% of KCl with different PEI concentrations [81].

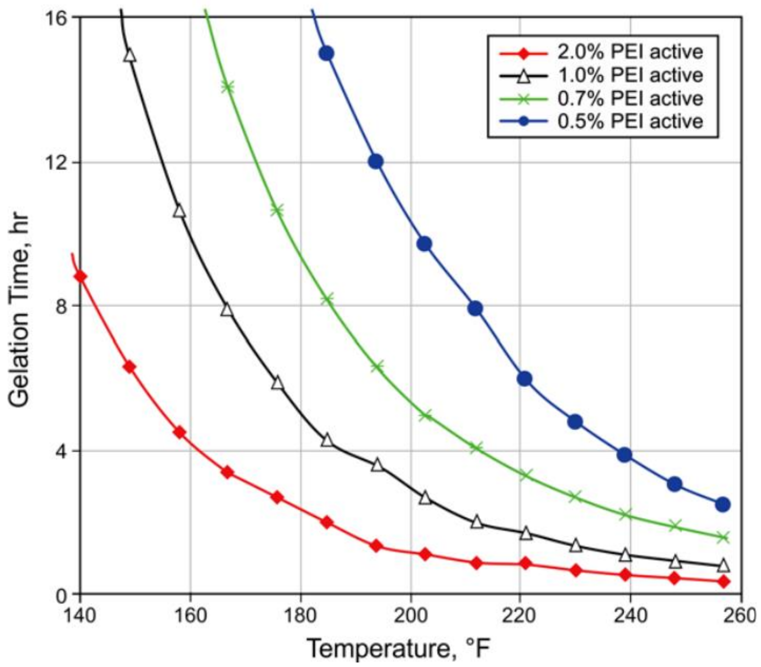

Figure 4. Gelation time of 7.0 wt.% of PAtBA in 2.0 wt.% of KCl with different PEI concentrations [81].

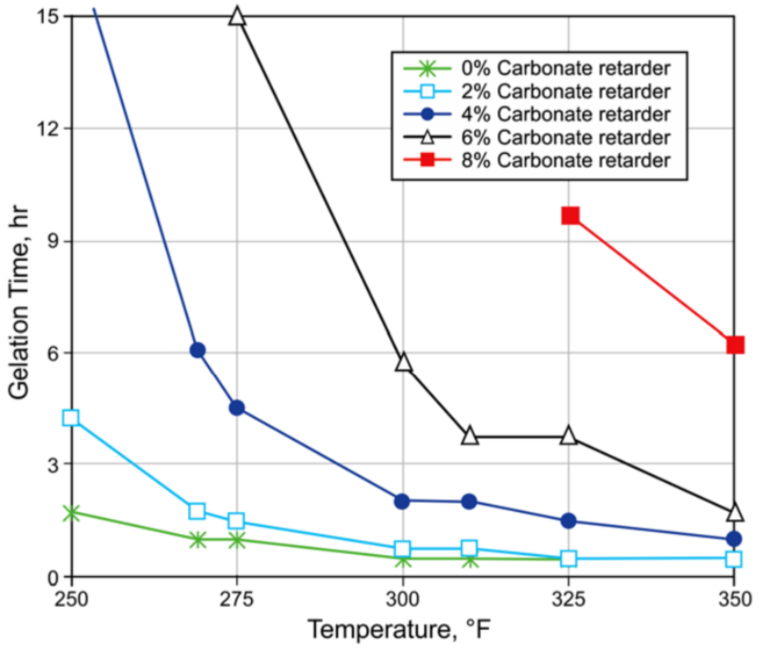

Figure 5. Gelation time of 7.0 wt.% of PAtBA with 0.66 wt.% of PEI and 2.0 wt.% of KCl with varied carbonate retarder concentrations [81].

2.1. Fluid loss control polymer

Polysaccharide-based biopolymers and their cross-linked gels (**Figures 6–9**) are usually added to the system for leak-off control to obtain a controlled, shallow penetration into the rock matrix [83–87]. Additionally, this polymer adds suspension properties to the inert solids present in the SPCS system formulation [88,89].

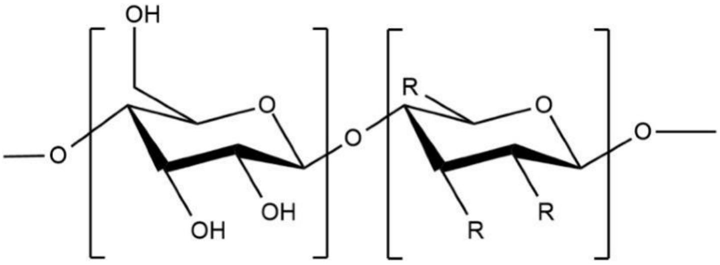

Figure 6. Chemical structure of Polysaccharide [84].

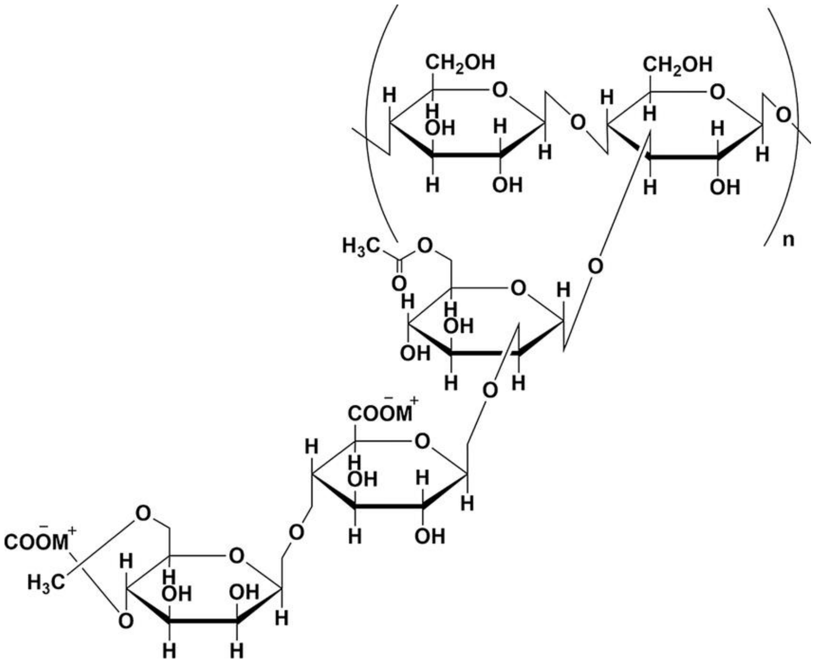

Figure 7. Chemical structure of Xanthan Gum [90].

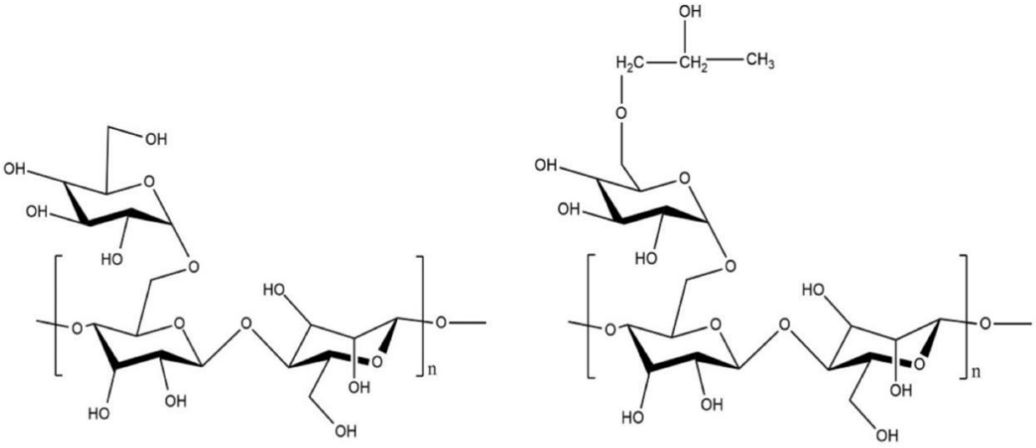

Guar

HydroxyPropyl Guar Gum (HPG)

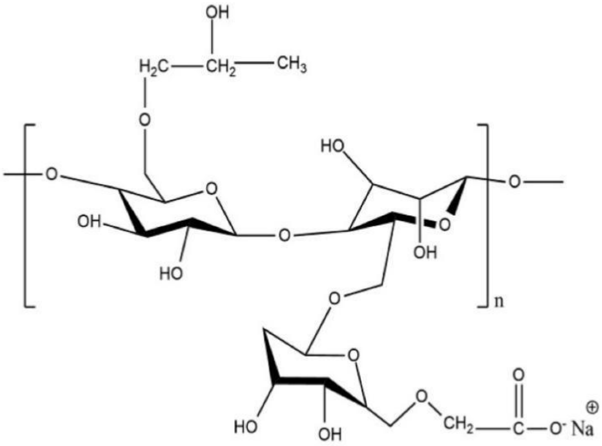

CarboxyMethyl HydroxyPropyl Guar (CMHPG)

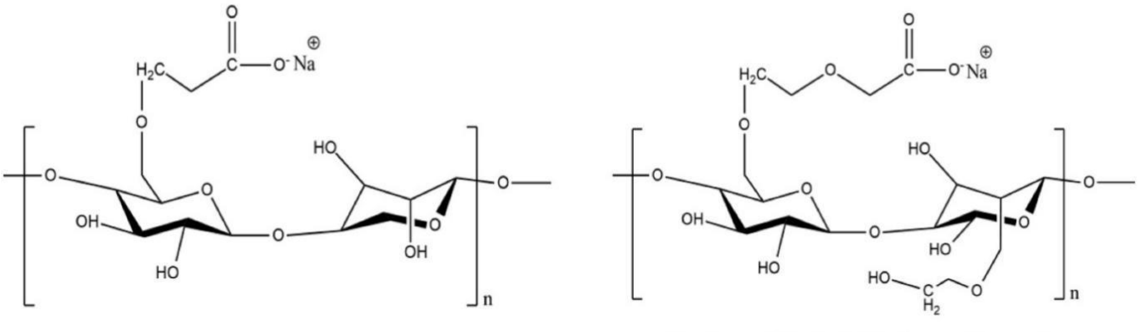

CarboxyMethyl Cellulose (CMC)

CarboxyMethyl HydroxyPropyl Cellulose (CMHEC)

Figure 8. Chemical structures of Guar and Guar derivatives [84].

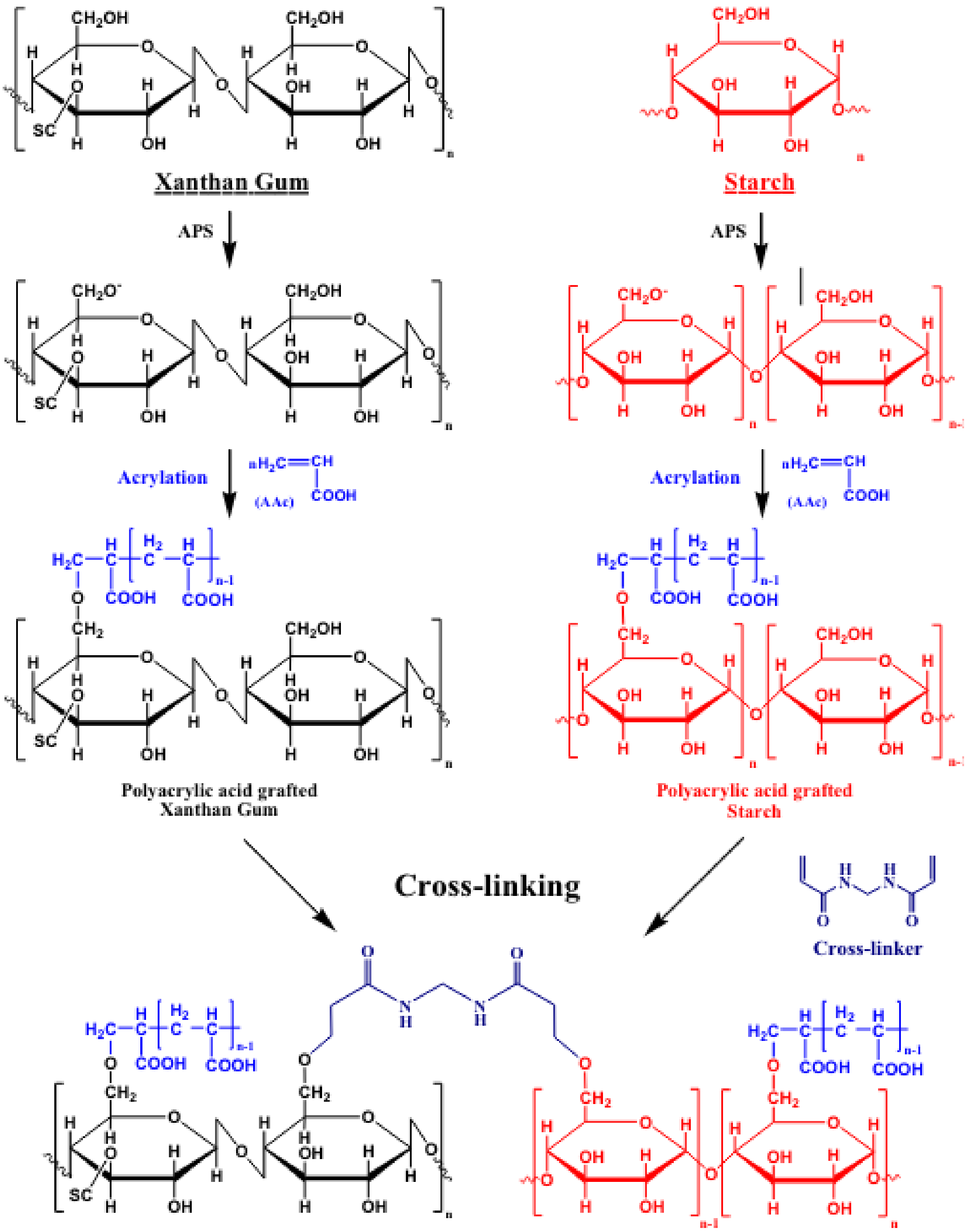

Figure 9. Chemical structures of Xanthun gum and starch and their respective cross-linking reactions [91].

2.2. Inert particulates

Inert particulates are added to the SPCS system for fluid-loss control [92,93]. These particulates synergize with the polysaccharide-based biopolymer to provide improved leak-off control. Various inert particulates, such as silica nanoparticles or cross-linked polymer gel-modified particulates, have been extensively employed to control fluid loss without changing the activation time of the sealant system. For most applications, silica flour [94] is used as the inert particulate (**Figures 10** and **11**); however, in some cases, nanosized calcium carbonate particulates [95] have been used (**Figure 12**) [96]. The major design criteria for the potential sealant systems are the gelation kinetics of the polymeric formulation for given down-hole conditions, such as temperature, salinity, and the squeezing time of the polymeric formulation before it gets completely gelled.

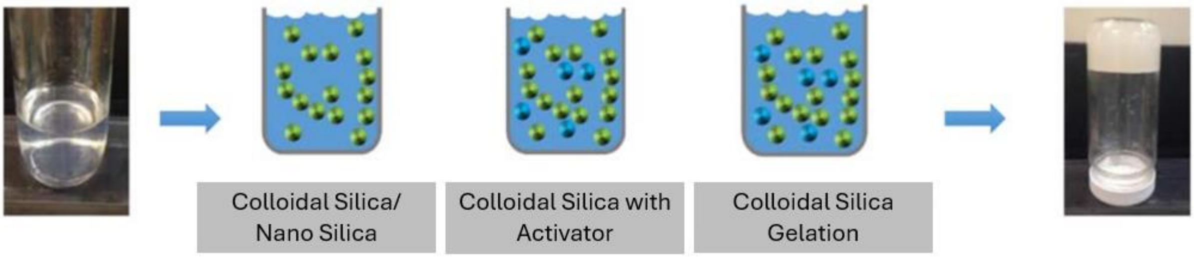

Figure 10. Schematic illustration of gelation of nano silica system [94].

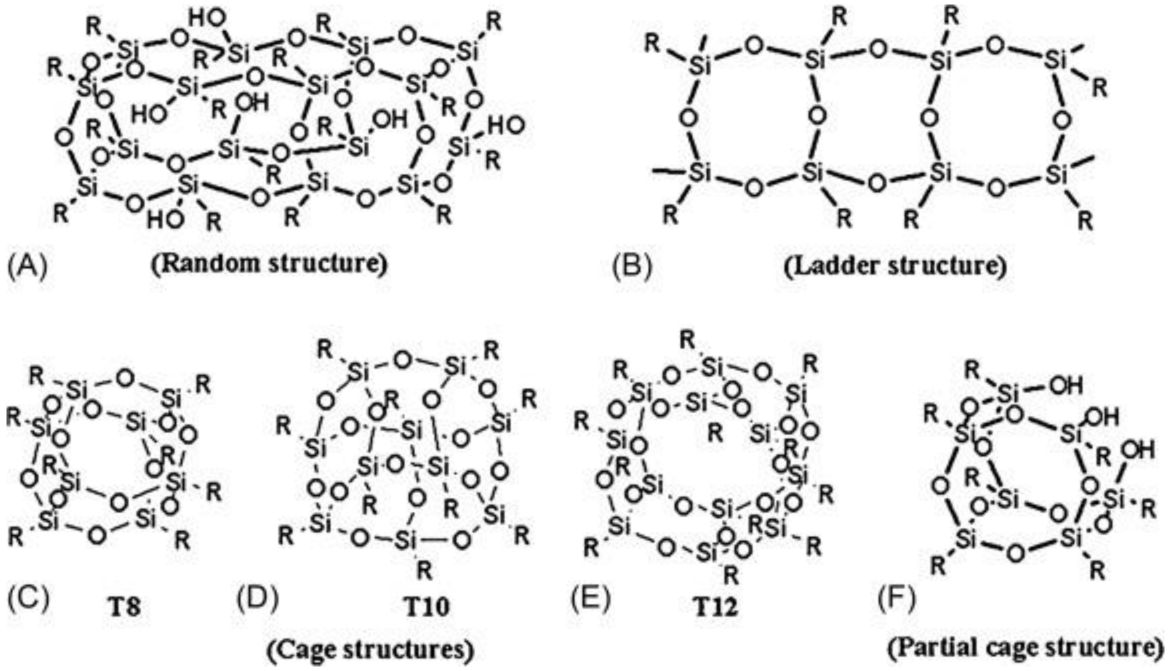

Figure 11. Chemical structures of silica nanoparticles [97].

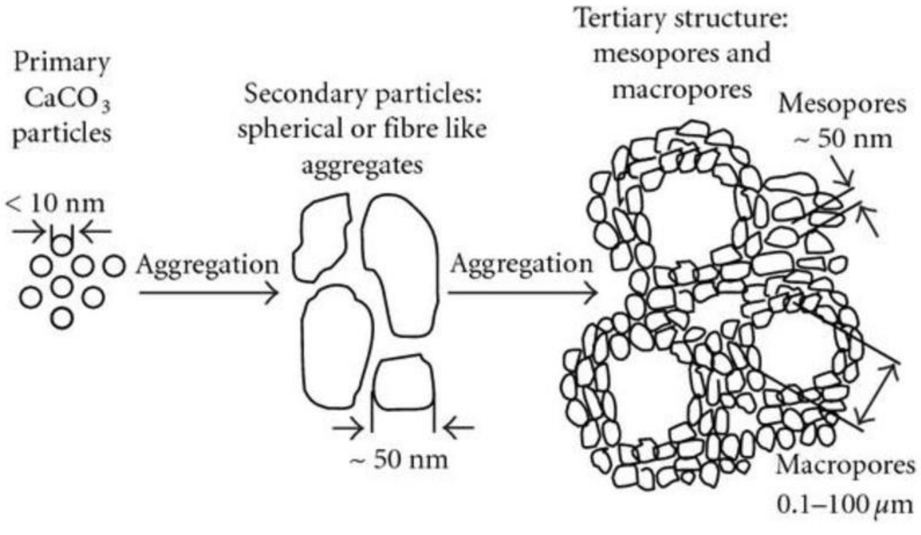

Figure 12. Schematic representation of gelation of calcium carbonate particles [96].

3. Summary and outlook

The general design for successful SPCS treatments is very similar to squeezing cement into a downhole in many aspects. Sufficient polymeric formulation is poured to cover all perforations, and approximately 10%–20% more is needed, considering the possible leak-off of the formulations into the perforations. After successfully filling all open perforations using the fluid, a squeeze operation is executed so that the polymeric formulations penetrate deep into the rock matrix. The squeezing operation is performed at a pressure just below the formation-parting pressure. The SPCS system provides an alternative to conventional cement squeeze treatments, offering the following advantages:

- There is no need for zonal isolation as with standard polymer gel sealant; the slurry can be bullheaded into all open perforations.
- Shallow penetration of the SPCS filtrate allows future reperforation of the hydrocarbon-producing zone(s), if applicable.
- Unlike cement, the SPCS slurry left inside the wellbore does not have to be drilled or milled out but can be easily jetted out the jointed pipe.
- Moreover, the SPCS formulation can be tailored and optimized for wellbore completion.

Based on prior experience, it is recommended to employ a sealant formulation with a cross-linking time similar to or comparable to the time required for the squeezing operation. This kind of sealant treatment provides a better and more complete sealing option. At the same time, premature gelation is considered a significant risk in these sealant formulations. After the SPCS plug is squeezed, the well is shut in to allow the base fluid to crosslink. Then, the set SPCS remaining in the wellbore is washed or jetted out to reperforate pay intervals. In these cases, preformed particle gels can be employed as a potential alternative to achieve a complete sealing solution, as shown in **Figure 13**.

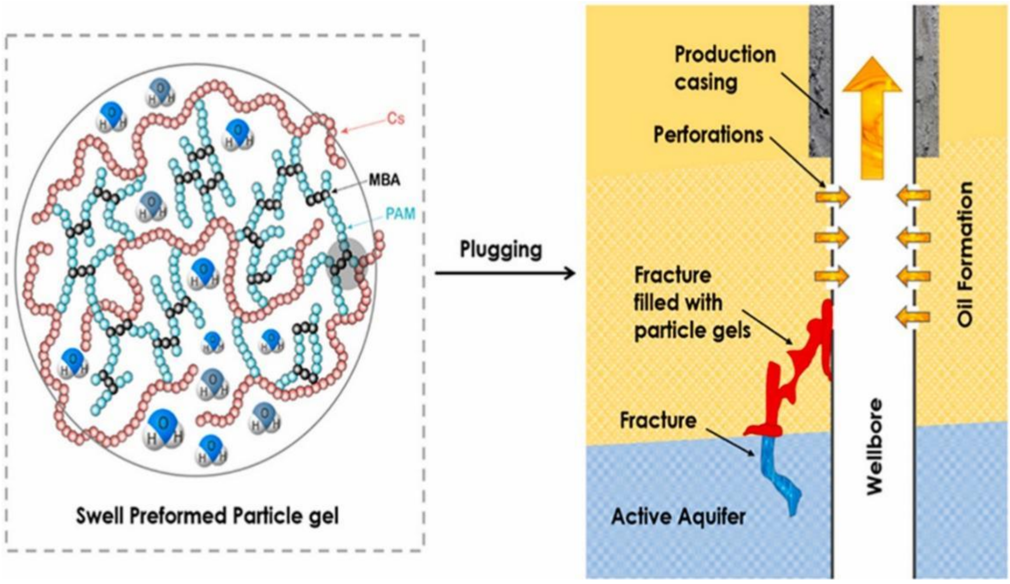

Figure 13. Preformed particle gel based on chitosan-g-polyacrylamide for conformance control in high-temperature, high-salinity (HT-HS) reservoirs [98].

Funding: This research was funded by Alfaisal University grant number 726174. The authors gratefully acknowledge Alfaisal University and its Office of Research and Innovation for their continuous support throughout this study.

Conflict of interest: The authors declare no conflict of interest.

References

1. Fathima A, Almohsin A, Michael FM, et al. Polymer nanocomposites for water shutoff application-A review. Materials Research Express. 2018; 6(3): 032001. doi: 10.1088/2053-1591/aaf36c
2. Michael FM, Krishnan MR, Fathima A, et al. Zirconia/graphene nanocomposites effect on the enhancement of thermo-mechanical stability of polymer hydrogels. Materials Today Communications. 2019; 21: 100701. doi: 10.1016/j.mtcomm.2019.100701
3. Michael FM, Krishnan MR, AlSoughayer S, et al. Thermo-elastic and self-healing polyacrylamide -2D nanofiller composite hydrogels for water shutoff treatment. Journal of Petroleum Science and Engineering. 2020; 193: 107391. doi: 10.1016/j.petrol.2020.107391
4. Almohsin A, Michal F, Alsharaeh E, et al. Self-healing PAM composite hydrogel for water shutoff at high temperatures: Thermal and rheological investigations. In: Proceedings of the SPE Kuwait Oil & Gas Show and Conference; 2019.
5. Krishnan M, Michal F, Alsoughayer S, et al. Thermodynamic and kinetic investigation of water absorption by PAM composite hydrogel. In: Proceedings of the SPE Kuwait Oil and Gas Show and Conference; 2019.
6. Keishnan MR, Michael FM, Almohsin AM, and Alsharaeh EH. Thermal and rheological investigations on N.N’ methylenebis acrylamide cross-linked polyacrylamide nanocomposite hydrogels for water shutoff applications. In: Proceedings of the Offshore Technology Conference Asia; 2020. p. 9.
7. Curtice RJ, Dalrymple ED. Just the cost of doing business. World Oil. 2004; 225: 77.
8. Vasquez JE, EofL Sf, Dalrymple ED, Van Eijden J. Shallow penetration particle-gel system for water and gas shutoff applications. In: Proceedings of the SPE Russian Oil and Gas Technical Conference and Exhibition; 2008.
9. Krishnan MR, Omar H, Almohsin A, and Alsharaeh EH. An overview on nanosilica-polymer composites as high-performance functional materials in oil fields. Polymer Bulletin. 2024; 81: 3883. doi: 10.1007/s00289-023-04934-y
10. Krishnan MR, Alsharaeh EH. Polymer gel amended sandy soil with enhanced water storage and extended release capabilities for sustainable desert agriculture. Journal of Polymer Science and Engineering. 2023; 6(1): 2892. doi: 10.24294/jpse.v6i1.2892
11. Almohsin A, Krishnan MR, Alsharaeh E, Harbi B. Preparation and properties investigation on sand-polyacrylamide composites with engineered interfaces for water shutoff application. Middle East Oil, Gas and Geosciences Show. 2023. doi: 10.2118/213481-MS
12. Krishnan MR, Li W, Alsharaeh EH. Ultra-lightweight Nanosand/Polymer Nanocomposite Materials for Hydraulic Fracturing Operations. SSRN Electronic Journal. 2022. doi: 10.2139/ssrn.4233321
13. Almohsin A, Alsharaeh E, Michael FM, Krishnan MR. Polymer-nanofiller hydrogels. U.S. Patent US20220112777A1, 2022.
14. Almohsin A, Alsharaeh E, Krishnan MR. Polymer-sand nanocomposite lost circulation material. U.S. Patent US20220290033A1, 2022.
15. Almohsin A, Alsharaeh E, Krishnan MR, Alghazali M. Coated nanosand as relative permeability modifier. U.S. Patent US11499092B2, 2022.
16. Sun XD and Bai BJ. Comprehensive review of water shutoff methods for horizontal wells. Petroleum Exploration and Development.2017; 44(6): 1022-1029. doi: 10.1016/S1876-3804(17)30115-5
17. El-Karsani KS, Al-Muntasheri GA, Hussein IA. Polymer Systems for Water Shutoff and Profile Modification: A Review Over the Last Decade. SPE Journal. 2013; 19(01): 135-149. doi: 10.2118/163100-pa
18. Duryagin V, Nguyen Van T, Onegov N, et al. Investigation of the Selectivity of the Water Shutoff Technology. Energies. 2022; 16(1): 366. doi: 10.3390/en16010366
19. Taha A, Amani M. Overview of Water Shutoff Operations in Oil and Gas Wells; Chemical and Mechanical Solutions. ChemEngineering. 2019; 3(2): 51. doi: 10.3390/chemengineering3020051
20. Sydansk RD and Seright RS. When and where relative permeability modification water-shutoff treatments can be successfully applied. In: Proceedings of the SPE/DOE Symposium on Improved Oil Recovery; 2006. p. 15.

21. Guo P, Tian Z, Zhou R, et al. Chemical water shutoff agents and their plugging mechanism for gas reservoirs: A review and prospects. Journal of Natural Gas Science and Engineering. 2022; 104: 104658. doi: 10.1016/j.jngse.2022.104658
22. Ali A, Alabdrabalnabi M, Ramadan MA, et al. A Review of Recent Developments in Nanomaterial Agents for Water Shutoff in Hydrocarbon Wells. ACS Omega. 2024; 9(13): 14728-14746. doi: 10.1021/acsomega.3c09219
23. Lu S, Bo Q, Zhao G, et al. Recent advances in enhanced polymer gels for profile control and water shutoff. Frontiers in Chemistry. 2023; 11: 1067094.
24. Lenji MA, Haghshenasfard M, Sefti MV, et al. Experimental study of swelling and rheological behavior of preformed particle gel used in water shutoff treatment. Journal of Petroleum Science and Engineering. 2018; 169: 739-747. doi: 10.1016/j.petrol.2018.06.029
25. Jia H, Pu WF, Zhao JZ, et al. Research on the Gelation Performance of Low Toxic PEI Cross-Linking PHPAM Gel Systems as Water Shutoff Agents in Low Temperature Reservoirs. Industrial & Engineering Chemistry Research. 2010; 49(20): 9618-9624. doi: 10.1021/ie100888q
26. Vasquez J, Dalrymple ED, Eoff L, et al. Development and evaluation of high-temperature conformance polymer systems in SPE international symposium on oilfield chemistry. Society of Petroleum Engineers; 2005.
27. Vasquez JE, Jurado I, Santillan A, and Hernandez R. Organically crosslinked polymer system for water reduction treatments in Mexico in SPE-104134-MS. Society of Petroleum Engineers; 2006.
28. Zhang L, Pu C, Cui S, et al. Experimental Study on a New Type of Water Shutoff Agent Used in Fractured Low Permeability Reservoir. Journal of Energy Resources Technology. 2016; 139(1). doi: 10.1115/1.4035146
29. Obino V, Yadav U. Application of Polymer Based Nanocomposites for Water Shutoff—A Review. Fuels. 2021; 2(3): 304-322. doi: 10.3390/fuels2030018
30. Yu Z, Li Y, Sha O,et al. Synthesis and properties of amphiprotic polyacrylamide microspheres as water shutoff and profile control. Journal of Applied Polymer Science. 2016; 133: 43366.
31. Ge J, Wu Q, Ding L, et al. Preparation and rheological Evaluation of a thixotropic polymer gel for water shutoff in fractured tight reservoirs. Journal of Petroleum Science and Engineering. 2022; 208: 109542. doi: 10.1016/j.petrol.2021.109542
32. Wu Q, Ge J, Ding L, et al. Insights into the key aspects influencing the rheological properties of polymer gel for water shutoff in fractured reservoirs. Colloids and Surfaces A: Physicochemical and Engineering Aspects. 2022; 634: 127963. doi: 10.1016/j.colsurfa.2021.127963
33. Sadeghnejad S, Ashrafizadeh M, Nourani M. Improved oil recovery by gel technology: Water shutoff and conformance control. Chemical Methods. 2022; 249-312. doi: 10.1016/b978-0-12-821931-7.00001-8
34. Cheng L, Qin Y, Gao K, et al. Experimental Investigation of a Novel Nanocomposite Particle Gel for Water Shutoff Treatment in Mature Oilfields. ACS Omega. 2022; 7(10): 8887-8895. doi: 10.1021/acsomega.1c07242
35. Samitsu S, Zhang R, Peng X, et al. Flash freezing route to mesoporous polymer nanofibre networks. Nature Communications. 2013; 4(1). doi: 10.1038/ncomms3653
36. Krishnan MR, Samitsu S, Fujii Y, et al. Hydrophilic polymer nanofibre networks for rapid removal of aromatic compounds from water. Chem Commun. 2014; 50(66): 9393-9396. doi: 10.1039/c4cc01786b
37. Krishnan MR, Chien YC, Cheng CF, et al. Fabrication of Mesoporous Polystyrene Films with Controlled Porosity and Pore Size by Solvent Annealing for Templated Syntheses. Langmuir. 2017; 33(34): 8428-8435. doi: 10.1021/acs.langmuir.7b02195
38. Chien YC, Huang LY, Yang KC, et al. Fabrication of metallic nanonetworks via templated electroless plating as hydrogenation catalyst. Emergent Materials. 2020; 4(2): 493-501. doi: 10.1007/s42247-020-00108-y
39. Krishnan MR, Chen HY, and Ho RM. Switchable structural colors from mesoporous polystyrene films. In: Proceedings of the 252nd Annual Meeting of American Chemical Society; 25-29 August 2016; Philadelphia, USA.
40. Lo TY, Krishnan MR, Lu KY, et al. Silicon-containing block copolymers for lithographic applications. Progress in Polymer Science. 2018; 77: 19-68. doi: 10.1016/j.progpolymsci.2017.10.002
41. Krishnan MR, Lu K, Chiu W, et al. Directed Self-Assembly of Star-Block Copolymers by Topographic Nanopatterns through Nucleation and Growth Mechanism. Small. 2018; 14(16). doi: 10.1002/smll.201704005
42. Cheng CF, Chen YM, Zou F, et al. Li-Ion Capacitor Integrated with Nano-network-Structured Ni/NiO/C Anode and Nitrogen-Doped Carbonized Metal-Organic Framework Cathode with High Power and Long Cyclability. ACS Applied Materials & Interfaces. 2019; 11(34): 30694-30702. doi: 10.1021/acsami.9b06354
43. Ho RM, Krishnan MR, Siddique SK, Chien YC. Method for fabricating nanoporous polymer thin film and corresponding

method for fabricating nanoporous thin film. U.S. Patent US11059205, 2021.

44. Krishnan MR, Alsharaeh E. Potential removal of benzene-toluene-xylene toxic vapors by nanoporous poly(styrene-r-methylmethacrylate) copolymer composites. Environmental Nanotechnology, Monitoring & Management. 2023; 20: 100860. doi: 10.1016/j.enmm.2023.100860
45. Krishnan MR, Alsharaeh EH. A review on polymer nanocomposites based high-performance functional materials. SSRN. 2022. doi: 10.2139/ssrn.4222854
46. Krishnan MR, Alsharaeh EH. Facile fabrication of thermos-mechanically reinforced polystyrene-graphene nanocomposite aerogel for produced water treatment. Journal of Porous Materials. 2024; 1. doi: 10.1007/s10934-024-01602-y
47. Krishnan MR, Alsharaeh EH. High-performance functional materials based on polymer nanocomposites—A review. Journal of Polymer Science and Engineering. 2023; 6(1): 3292. doi: 10.24294/jpse.v6i1.3292
48. Krishnan MR, Rajendran V. Sulfonated mesoporous polystyrene-1D multiwall carbon nanotube nanocomposite as potential adsorbent for efficient removal of xylene isomers from aqueous solution. Characterization and Application of Nanomaterials. 2023; 6(2): 3516. doi: 10.24294/can.v6i2.3516
49. Krishnan MR, Almohsin A, Alsharaeh EH. Syntheses and fabrication of mesoporous styrene-co-methyl methacrylate-graphene composites for oil removal. Diamond and Related Materials. 2022; 130: 109494. doi: 10.1016/j.diamond.2022.109494
50. Krishnan MR., Michael FM, Almohsin A, Alsharaeh EH. Polyacrylamide hydrogels coated super-hydrophilic sand for enhanced water storage and extended release. SSRN. 2022. doi: 10.2139/ssrn.4232876
51. Krishnan MR, Aldawsari YF, Alsharaeh EH. Three-dimensionally cross-linked styrene-methyl methacrylate-divinyl benzene terpolymer networks for organic solvents and crude oil absorption. Journal of Applied Polymer Science. 2020; 138(9). doi: 10.1002/app.49942
52. Krishnan MR, Aldawsari Y, Michael FM, et al. 3D-Polystyrene-polymethyl methacrylate/divinyl benzene networks-Epoxy-Graphene nanocomposites dual-coated sand as high strength proppants for hydraulic fracture operations. Journal of Natural Gas Science and Engineering. 2021; 88: 103790. doi: 10.1016/j.jngse.2020.103790
53. Krishnan MR, Aldawsari YF, and Alsharaeh EH. 3D-poly (styrene-methyl methacrylate)/divinyl benzene-2D-nanosheet composite networks for organic solvents and crude oil spill cleanup. Polymer Bulletin. 2021; 79: 3779-3802. doi: 10.1007/s00289-021-03565-5
54. Krishnan MR, Omar H, Aldawsari Y, et al. Insight into thermo-mechanical enhancement of polymer nanocomposites coated microsand proppants for hydraulic fracturing. Heliyon. 2022; 8(12): e12282. doi: 10.1016/j.heliyon.2022.e12282
55. Krishnan MR, Rajendran V, Alsharaeh E. Anti-reflective and high-transmittance optical films based on nanoporous silicon dioxide fabricated from templated synthesis. Journal of Non-Crystalline Solids. 2023; 606: 122198. doi: 10.1016/j.jnoncrysol.2023.122198
56. Krishnan MR, Omar H, Almohsin A, Alsharaeh EH. An overview on nanosilica-polymer composites as high-performance functional materials in oil fields. Polymer Bulletin. 2024; 81: 3883. doi: 10.1007/s00289-023-04934-y
57. Krishnan MR, Almohsin A, Alsharaeh EH. Mechanically robust and thermally enhanced sand-polyacrylamide-2D nanofiller composite hydrogels for water shutoff applications. Journal of Applied Polymer Science. 2024; 141(7): e54953. doi: 10.1002/app.54953
58. Michael FM, Krishnan MR, Li W, et al. A review on polymer-nanofiller composites in developing coated sand proppants for hydraulic fracturing. Journal of Natural Gas Science and Engineering. 2020; 83: 103553. doi: 10.1016/j.jngse.2020.103553
59. Aldosari MA, Alsaud KBB, Othman A, et al. Microwave Irradiation Synthesis and Characterization of Reduced-(Graphene Oxide- (Polystyrene-Polymethyl Methacrylate))/Silver Nanoparticle Nanocomposites and Their Anti-Microbial Activity. Polymers. 2020; 12(5): 1155. doi: 10.3390/polym12051155
60. Bongu CS., Krishnan MR., Soliman A, et al. Flexible and freestanding MoS_2/graphene composite for high-performance Supercapacitors. ACS Omega. 2023; 8(40): 36789-36800. doi: 10.1021/acsomega.3c03370
61. Tasleem S, Sekhar Bongu C, Krishnan MR, Alsharaeh EH. Navigating the hydrogen prospect: A comprehensive review of sustainable source-based production technologies, transport solutions, advanced storage mechanisms, and CCUS integration. Journal of Energy Chemistry. 2024; 97: 166-215. doi: 10.1016/j.jechem.2024.05.022
62. Krishnan MR, Alsharaeh EH. Mechanical strength investigation of chemically reinforced sandy soil using organic copolymers for geotechnical engineering applications. Journal of Polymer Science and Engineering. 2024; 7(1): 5170. doi: 10.24294/jpse.v7i1.5170

63. Krishnan MR, Li W, Alsharaeh EH. Cross-linked polymer nanocomposite networks coated nano sand light-weight proppants for hydraulic fracturing applications. Characterization and Application of Nanomaterials. 2023; 6(2): 3314. doi: 10.24294/can.v6i2.3314
64. Li W, Alsharaeh E, Krishnan MR. Proppant coatings and method of making. U.S. Patent US 11851614B2, 2023.
65. Li W, Alsharaeh E, Krishnan MR. Coated proppants and methods of making and use thereof. U.S. Patent US 11912938B2, 2024.
66. Li W, Alsharaeh E, Krishnan MR. Methods for making proppant coatings. U.S. Patent US 11459503B2, 2022.
67. Krishnan MR, Almohsin A, Alsharaeh EH. Thermo-Mechanically Reinforced Mesoporous Styrene-Co-Methyl Methacrylate-Graphene Composites for Produced Water Treatment. SSRN. 2022.
68. Alsharaeh EH, Krishnan MR. Method of making mutlilayer soil with property for extended release water for desert agriculture. U.S. Patent US 10772265B1, 2020.
69. Al-Shajalee F, Arif M, Machale J, et al. A Multiscale Investigation of Cross-Linked Polymer Gel Injection in Sandstone Gas Reservoirs: Implications for Water Shutoff Treatment. Energy & Fuels. 2020; 34(11): 14046-14057. doi: 10.1021/acs.energyfuels.0c02858
70. Bai Y, Xiong C, Wei F, et al. Gelation Study on a Hydrophobically Associating Polymer/Polyethylenimine Gel System for Water Shut-off Treatment. Energy & Fuels. 2015; 29(2): 447-458. doi: 10.1021/ef502505k
71. Shagiakhmetov A, Yushchenko S. Substantiation of In Situ Water Shut-Off Technology in Carbonate Oil Reservoirs. Energies. 2022; 15(14): 5059. doi: 10.3390/en15145059
72. Dai C, Zhao J, Yan L, et al. Adsorption behavior of cocamidopropyl betaine under conditions of high temperature and high salinity. Journal of Applied Polymer Science. 2014; 131(12). doi: 10.1002/app.40424
73. Jia H, Zhao JZ, Jin FY, et al. New Insights into the Gelation Behavior of Polyethyleneimine Cross-Linking Partially Hydrolyzed Polyacrylamide Gels. Industrial & Engineering Chemistry Research. 2012; 51(38): 12155-12166. doi: 10.1021/ie301818f
74. ElKarsani KSM, Al-Muntasheri GA, Sultan AS, et al. Performance of PAM/PEI gel system for water shut-off in high temperature reservoirs: Laboratory study. Journal of Applied Polymer Science. 2015; 132(17). doi: 10.1002/app.41869
75. Chen L, Wang J, Yu L, et al. Experimental Investigation on the Nanosilica-Reinforcing Polyacrylamide/Polyethylenimine Hydrogel for Water Shutoff Treatment. Energy & Fuels. 2018; 32(6): 6650-6656. doi: 10.1021/acs.energyfuels.8b00840
76. Ghriga MA, Grassl B, Gareche M, et al. Review of recent advances in polyethylenimine crosslinked polymer gels used for conformance control applications. Polymer Bulletin. 2019; 76(11): 6001-6029. doi: 10.1007/s00289-019-02687-1
77. Almeida AIAR, Carvalho LDO, Lopes RC, et al. Enhanced polyacrylamide polymer hydrogels using nanomaterials for water shutoff: Morphology, thermal and rheological investigations at high temperatures and salinity. Journal of Molecular Liquids. 2024; 405(1): 125041. doi: 10.1016/j.molliq.2024.125041
78. Sultan AS. Stability of PAM/PEI emulsified gels under HTHS conditions for water shut-off treatment. Journal of Petroleum Exploration and Production Technology. 2018; 9(3): 2027-2037. doi: 10.1007/s13202-018-0597-2
79. Tessarolli FGC, Souza STS, Gomes AS, et al. Influence of polymer structure on the gelation kinetics and gel strength of acrylamide-based copolymers, bentonite and polyethylenimine systems for conformance control of oil reservoirs. Journal of Applied Polymer Science. 2019; 136(22). doi: 10.1002/app.47556
80. Lockhart TP, Albonico P. New Chemistry for the Placement of Chromium(III)/Polymer Gels in High-Temperature Reservoirs. SPE Production & Facilities. 1994; 9(04): 273-279. doi: 10.2118/24194-pa
81. Vasquez J, Curtice R. Porosity-Fill Sealant for Water and Gas Shutoff: Case Histories and Lessons Learned after more than 1,000 Well Interventions. In: Proceedings of the SPE European Formation Damage Conference & Exhibition; 2013.
82. Jia H, Chen H, Guo S. Fluid loss control mechanism of using polymer gel pill based on multi-crosslinking during overbalanced well workover and completion. Fuel. 2017; 210: 207-216. doi: 10.1016/j.fuel.2017.08.032
83. Kabir A. Chemical water and gas shutoff technology- An overview. In: Proceedings of the SPE Asia Pacific Improved Oil Recovery Conference; 2001.
84. Hamza A, Shamlooh M, Hussein IA, et al. Polymeric formulations used for loss circulation materials and wellbore strengthening applications in oil and gas wells: A review. Journal of Petroleum Science and Engineering. 2019; 180: 197-214. doi: 10.1016/j.petrol.2019.05.022
85. Crowe CW, Hutchinson BH, Trittipo BL. Fluid-Loss Control: The Key to Successful Acid Fracturing. SPE Production Engineering. 1989; 4(02): 215-220. doi: 10.2118/16883-pa

86. Bouts MN, Trompert RA, Samuel A. Time delayed and low impairment fluid-loss control using a succinoglycan biopolymer with an internal acid breaker. In: Proceedings of the SPE Formation Damage Control Symposium; 1996.
87. Song K, Wu Q, Li M, et al. Water-based bentonite drilling fluids modified by novel biopolymer for minimizing fluid loss and formation damage. Colloids and Surfaces A: Physicochemical and Engineering Aspects. 2016; 507: 58-66. doi: 10.1016/j.colsurfa.2016.07.092
88. Ali I, Ahmad M, Ganat T. Biopolymeric formulations for filtrate control applications in water-based drilling muds: A review. Journal of Petroleum Science and Engineering. 2022; 210: 110021. doi: 10.1016/j.petrol.2021.110021
89. Akpan EU, Enyi GC, Nasr GG. Enhancing the performance of xanthan gum in water-based mud systems using an environmentally friendly biopolymer. Journal of Petroleum Exploration and Production Technology. 2020; 10(5): 1933-1948. doi: 10.1007/s13202-020-00837-0
90. Gadhave RV, Vineeth SK. Synthesis and characterization of xanthan gum stabilized polyvinyl acetate-based wood adhesive. Polymer Bulletin. 2023; 81(8): 7423-7440. doi: 10.1007/s00289-023-05064-1
91. Sethi S, Saruchi, Kaith BS, et al. Cross-linked xanthan gum-starch hydrogels as promising materials for controlled drug delivery. Cellulose. 2020; 27(8): 4565-4589. doi: 10.1007/s10570-020-03082-0
92. Nasiri A, Ghaffarkhah A, Keshavarz Moraveji M, et al. Experimental and field test analysis of different loss control materials for combating lost circulation in bentonite mud. Journal of Natural Gas Science and Engineering. 2017; 44: 1-8. doi: 10.1016/j.jngse.2017.04.004
93. Calçada LA, Duque Neto OA, Magalhães SC, et al. Evaluation of suspension flow and particulate materials for control of fluid losses in drilling operation. Journal of Petroleum Science and Engineering. 2015; 131: 1-10. doi: 10.1016/j.petrol.2015.04.007
94. Alabdrabalnabi M, Almohsin A, Huang J, Sherief M. Experimental investigation of a novel nanosilica for blocking unwanted water production. In: Proceedings of the SPE/IATMI Asia Pacific Oil & Gas Conference and Exhibition; October 2021.
95. Tock RW, Keshavaraj R. Physical-chemical changes in silicone elastomers used for building sealants. Astm special technical publication. 1996; 1271: 113-125.
96. Plank J, Hoffmann H, Schölkopf J, et al. Preparation and Characterization of a Calcium Carbonate Aerogel. Advances in Materials Science and Engineering. 2009; 2009(1). doi: 10.1155/2009/138476
97. Barua S, Gogoi S, Khan R, et al. Silicon-Based Nanomaterials and Their Polymer Nanocomposites. Nanomaterials and Polymer Nanocomposites. 2019; 261-305. doi: 10.1016/b978-0-12-814615-6.00008-4
98. Elaf R, Ben Ali A, Saad M, et al. Development of eco-friendly chitosan-g-polyacrylamide preformed particle gel for conformance control in high-temperature and high-salinity reservoirs. Geoenergy Science and Engineering. 2023; 230: 212136. doi: 10.1016/j.geoen.2023.212136

Journal of Polymer Science and Engineering 2024, 7(2), 8211.
https://doi.org/10.24294/jpse8211

Review

Synthetic composite membranes and their manifold applications: A comprehensive review

Mohd Arsalan[1,*], Suzain Akhtar[1], Mohammad Ehtisham Khan[2,*]

[1] Department of Applied Chemistry, Aligarh Muslim University, Aligarh 202001, India
[2] Department of Chemical Engineering Technology, College of Applied Industrial Technology, Jazan University, Jazan 45142, Saudi Arabia
*** Corresponding authors:** Mohd Arsalan, mohdarsalan.chem@gmail.com; Mohammad Ehtisham Khan, mekhan@jazanu.edu.sa

CITATION

Arsalan M, Akhtar S, Khan ME. (2024). Synthetic composite membranes and their manifold applications: A comprehensive review. Journal of Polymer Science and Engineering. 7(2): 8211. https://doi.org/10.24294/jpse8211

ARTICLE INFO

Received: 26 July 2024
Accepted: 18 October 2024
Available online: 19 November 2024

Abstract: Synthetic membranes play a crucial role in a wide range of separation processes, including dialysis, electrodialysis, ultrafiltration, and pervaporation, with growing interest in synthetic emulsion membranes due to their precision, versatility, and ion exchange capabilities. These membranes enable tailored solutions for specific applications, such as water and gas separation, wastewater treatment, and chemical purification, by leveraging their multi-layered structures and customizable properties. Emulsion membrane technology, particularly in pressure-driven methods like reverse osmosis (RO) and nanofiltration (NF), has shown great potential in overcoming traditional challenges, such as fouling and energy inefficiency, by improving filtration efficiency and selectivity. This review explores the latest advancements in emulsion membrane development, their adaptability to various industrial needs, and their contribution to addressing long-standing limitations in membrane separation technologies. The findings underscore the promise of emulsion membranes in advancing industrial processes and highlight their potential for broader applications in water treatment, environmental management, and other key sectors.

Keywords: synthetic composite membranes; membrane stability; emulsion membrane manufacturing; water and wastewater treatment; medicinal and medical operations; membrane filtering technology

1. Introduction

Membrane technology is very important to medical operations, especially for several life-saving treatment modalities. Membranes are employed in bio separations, individual bias, tissue regeneration, artificial organs, medicine distribution, and coatings for medical bias [1]. The total membrane area generated during medical procedures is almost equal to the entire area of all artificial membrane procedures combined. Medical membrane products actually have a significantly higher financial value than all of the other combined operations [2]. For example, the medical membrane request grows rapidly and exceeds 1.5 billion bones per time only in the US. The majority of medical requests concern membranes used in tissue engineering, hem dialysate, artificial organs (pancreas, oxygenators, etc.), and medicine distribution [3,4]. This review will go into great detail on these topics. For the production of the membranes, biocompatible and, in certain situations, biodegradable accessories are required. Therefore, we compactly bind the biocompatibility and biodegradability difficulties prior to the specified operations [5].

Medical implants have well-defined and controlled interfaces, as biomedical engineers have realised recently. A significant hindrance to the clinical implementation of active bias devices carrying out physiologically beneficial tasks has been the decline in function upon implantation as a result of inadequate comprehension of the implantation interface [6]. Even in cases where a medical implant device exhibits satisfactory in vitro performance for extended periods of time, long-term in vivo functionality is still unattainable. Due to its ability to be formed from a variety of materials and having multiple layers, composite membranes have garnered a lot of attention [7]. This will make it possible for researchers and businesses to create customised membranes for certain uses. Because of their synthesis's flexibility, composite membranes can be employed in a variety of advantageous methods for both liquid and gaseous applications. Nowadays, most commercial membranes are made of thin composite materials, such those used in reverse osmosis and nanofiltration [8,9].

Developing energy storage systems that are efficient and reliable is crucial for the global effort to transition away from conventional energy sources. In addition to bacterial batteries, hybrid batteries, and hybrid redox flow cells, new electrochemical energy storage technologies are on the horizon. As an alternative to traditional electrochemical cells, these alternative architectures offer a high degree of energy conversion efficiency. They are also highly modular in terms of the design of devices and flexible in terms of material and operating conditions [10]. These various gadgets have power outputs ranging from several megawatts to a few milliwatts. Now that solid-state batteries with extended cycling capabilities and high energy density are available, sustainable electronic devices and point-of-care equipment can be manufactured. In recent years, lithium-ion batteries have approached the capacity of new batteries utilizing earth-abundant metal ions [11].

2. Major classification of composite membrane

Composite membranes are classified into major categories based on their composition, structure, and functional design. The following are the major classifications of composite membranes:

2.1. Polymeric composite membranes

These membranes are composed of two or more polymeric materials that are combined to create a membrane with enhanced performance characteristics. By blending polymers, the resulting membrane benefits from the desirable properties of each polymer, such as flexibility, mechanical strength, and chemical resistance. Polymeric composite membranes are typically used in applications like microfiltration (MF), ultrafiltration (UF), and nanofiltration (NF). Examples include blending materials like polyvinylidene fluoride (PVDF) with other polymers to improve hydrophilicity and fouling resistance in water treatment processes [12].

2.2. Inorganic composite membranes

Inorganic composite membranes are made from materials like ceramics, metals, or carbon-based materials. These membranes are known for their thermal stability, chemical resistance, and mechanical strength, making them suitable for extreme conditions such as high temperatures, aggressive chemical environments, and high-pressure systems [13]. Ceramic composite membranes, for example, are commonly used in industrial processes like gas separation, catalytic reactions, and water treatment due to their durability and resistance to fouling. They can also handle harsh solvents, making them valuable in chemical and pharmaceutical industries [14].

2.3. Polymer-inorganic hybrid membranes

These membranes combine organic polymers with inorganic materials, such as metal oxide nanoparticles (e.g., zinc oxide or titanium dioxide) or carbon nanotubes, to create hybrid structures that merge the flexibility and ease of fabrication of polymers with the robustness and high separation performance of inorganic materials [15]. Polymer-inorganic hybrid membranes are engineered to enhance properties like selectivity, mechanical stability, and fouling resistance. These hybrid membranes are often used in advanced water treatment processes, gas separation, and membrane distillation, where high performance is needed under challenging operating conditions [15].

2.4. Thin-film composite (TFC) membranes

Thin-film composite membranes are widely used in pressure-driven membrane processes like reverse osmosis (RO), nanofiltration (NF), and forward osmosis (FO). TFC membranes consist of a thin selective layer, often made of a polymer such as polyamide, that is cast onto a porous support substrate [16]. The thin selective layer governs the separation properties, while the porous support provides mechanical strength. TFC membranes are prized for their high permeability and selectivity, which makes them highly effective in applications like desalination, wastewater treatment, and brine concentration. The thin selective layer can be further modified to enhance specific separation characteristics, such as salt rejection or pollutant removal [17].

2.5. Mixed-matrix membranes (MMMs)

Mixed-matrix membranes are composite membranes where inorganic fillers, such as zeolites, metal-organic frameworks (MOFs), silica, or carbon nanotubes, are dispersed within a polymer matrix [18]. The incorporation of these fillers enhances the membrane’s separation capabilities by improving selectivity, permeability, and resistance to physical degradation. MMMs are designed to combine the advantages of both inorganic and organic components, offering higher performance than pure polymeric membranes. They are particularly useful in gas separation applications, such as carbon dioxide capture, natural gas processing, and the separation of organic solvents. By fine-tuning the dispersion and interaction between the fillers and the polymer matrix, MMMs can be optimized for specific separations and challenging environments [19].

3. Characteristics of composite membranes

Composite membranes are characterized by enhanced selectivity and high permeability, allowing for efficient separation of specific particles or molecules in various applications [20]. Their multi-layered structure, typically featuring a thin selective layer atop a robust support, provides excellent mechanical strength and thermal and chemical stability, making them suitable for high-pressure and harsh industrial environments [21]. Many composite membranes exhibit improved fouling resistance through the incorporation of hydrophilic materials or nanoparticles, extending their operational lifespan and reducing maintenance needs [22]. Customizability is a key feature, enabling tailored properties to meet specific application requirements, which, coupled with their scalability, makes them ideal for large-scale processes like water treatment and gas separation. Additionally, composite membranes contribute to energy efficiency by reducing hydraulic resistance and optimizing performance, further enhancing their value across diverse industries such as pharmaceuticals, food processing, and environmental management [23].

4. Composite membrane and their applications

Generally, synthetic membranes are used in laboratory separations for separation purposes since they are synthetically created. The use of synthetic membranes in artificial processes has been successful for a long time now, on a small and large scale [24,25]. Synthetic membranes can be found in a wide variety. Most synthetic membranes in the laboratory are composed of polymeric structures, but they can also be made from inorganic materials such as liquids or polymers [26]. On the basis of the chemistry of the face, the bulk structure, the morphology, and the product system, they can be classified. Synthetic membranes and patches are chemically and physically characterized by their physical parcels, as well as the driving force that determines how they are separated [27]. An in-vitro membrane process is primarily driven by pressure and grade of attention. The separate membrane process is thus known as filtration. It is possible to utilize synthetic membranes with different figures and inflow configurations in a separation process [28]. As well as disseminating and governing them, they can also be grouped based on their operations and separations. In addition to water sanctification, reverse osmosis, dehydrogenation of natural gas, microfiltration and ultrafiltration, and junking of microorganisms from dairy products, dialysis also uses synthetic membranes to separate matter [29]. Following is a list of some of the most important applications of membrane processes **Figure 1**.

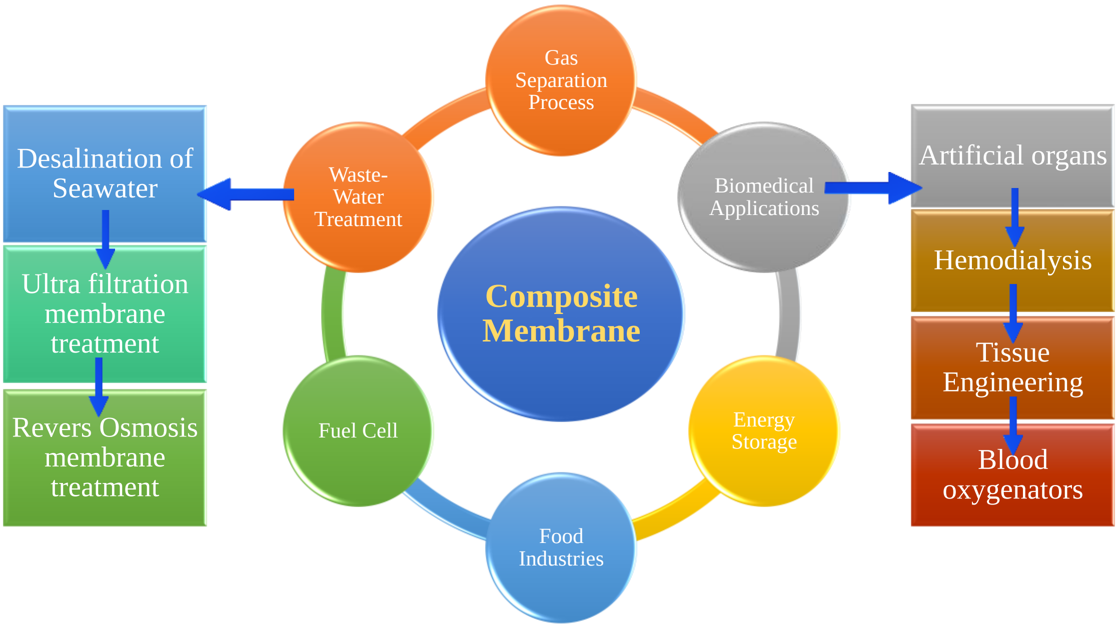

Figure 1. Flow chart of various important composite membrane applications.

4.1. Composite membrane in water treatment

Membrane technology has emerged as a crucial solution for addressing the global water crisis by purifying seawater and treating wastewater. This technology leverages various types of membranes, including reverse osmosis (RO), ultrafiltration (UF), nanofiltration (NF), and microfiltration (MF), each tailored for specific applications based on their unique properties. RO utilizes a semi-permeable membrane that effectively separates dissolved salts and organic molecules, making it widely used in desalination and producing high-purity water, despite its challenges of high energy consumption and membrane fouling. UF membranes, with larger pore sizes, are effective in removing larger particles, colloids, and bacteria, often serving as a pre-treatment step for RO systems and in wastewater treatment, while also facing issues related to organic fouling. NF membranes bridge the gap between UF and RO by selectively allowing the passage of divalent ions and organic molecules, making them suitable for water softening and polishing processes, though they can also suffer from fouling and limitations in monovalent ion rejection. MF membranes, the largest in pore size, are effective in removing large particles and microorganisms from water, commonly used in water treatment and beverage clarification, but they are limited in their ability to remove dissolved substances. A significant drawback of membrane technology is membrane fouling, caused by the accumulation of particles, colloids, and microorganisms that impede water flow, categorized into organic, inorganic, and biofouling. To mitigate fouling, strategies such as pre-treatment, membrane surface modification, and regular cleaning are employed. Despite advancements in material science and membrane chemistry enhancing performance, ongoing research focuses on developing innovative membrane structures and materials, optimizing device designs to improve flow dynamics, and reducing costs to make membrane technology more accessible. By enhancing the efficiency and performance of composite membranes while addressing existing challenges, membrane technology is positioned to play a pivotal role in sustainable water management, crucial for meeting the growing demand for clean water in a world increasingly facing water scarcity. The treatment of water is divided into several subcategories:

4.1.1. Waste-water treatment

The treatment of wastewater is one of the most important applications for membranes. In the early stages of its manufacture, ultra-modern UF was used to treat sewage and wastewater in order to remove particulate matter and macromolecular constituents [30]. There have been many applications developed for this technology, including water treatment and replicas handling as well as biotechnology and food processing. There are many methods for treating conventional wastewater, including chemical addition (aluminium sulphate, polymers, and lime), coagulation, and flocculation [31]. Sedimentation, filtration, and chlorine- grounded disinfection unfortunately; chlorine must be removed if chlorine-sensitive RO or NF is performed latterly. Trihalomethane (THM) and synthetic organic chemicals may also need to be removed in agreement with fresh regulations. In relevance of micro-organisms that could be dangerous to one’s health, MF (Microfiltration) and UP are especially helpful [32]. The conformation of microfilms on the membrane’s percolate side is one implicit issue. Strong boluses of chlorine, a detergent, can be used to treat this reverse flushable membrane systems (concave filaments) pottery. In the long run, UF membranes may be superior to MF membranes because they are more at removing contagious. These membranes generally last for about five times. Devilish hardness might bear water mellowing, which should likewise be possible by NF. In order to ensure a long reverse osmosis membrane life, pre-treatment is required, but it is costly and accounts for one third of operating costs [33].

In recent decades, environmental concerns about the wide application of petroleum-based synthetic polymers have pushed naturally occurring polymers to gain prominence [34]. In medicine delivery systems, tissue engineering, membrane technology, biosensor bias, etc., bio-based polymers are constantly gaining new disciplines of application in biocompatible and environmentally friendly ways. In order to fabricate fully or semi-biodegradable wastewater treatment membranes, scientists are applying colourful kinds of biopolymers, like cellulose, chitin, bounce, and alginate [35]. Biopolymers, in addition to being biocompatible, possess a number of desirable characteristics, like hydrophilicity and functionality, that make them ideal candidates for improving the effectiveness of compound membranes in purifying water. The introduction of organic and inorganic complements is also a key focus in elevating the thermo-mechanical and chemical stability of these bio-based accoutrements.

The following issues are addressed in this review:

1) The potential use of biopolymers as raw materials for the synthesis of water treatment membranes is explored here.
2) The structural characteristics of these membranes are considered in developing a comprehensive categorization.
3) Examining the effectiveness of these membranes at barring various types of pollutants from backwaters, as well as their strengths and weaknesses.

4.1.2. Desalination of seawater or brackish water

About half of the presently installed reverse osmosis systems desalinate seawater or brackish water. The salt content of harsh water is higher than that of new water, but lower than that of ocean water [36]. In fact, bitter water contains somewhere in the range of 0.5 and 30 grams of salt for every liter or 0.5 to 30 sections for each thousand, the near expenses of the significant desalination advances are as an element of salt focus. Desalination can also be accomplished using competing techniques like ion exchange, electro-dialysis, and multi-effect evaporation. In any case, the utilization of these three techniques relies upon the degree of salt fixation. 500 mg/L is the concentration that the World Health Organization (WHO) recommends for salt in drinking water [37]. Thus frequently 90% of salt in bitter water must be eliminated. Reverse osmosis’s first application was a membrane made of cellulose acetate, which is easy to make and meets this requirement [38]. Seawater has a salt centralization of 3.2%–4.0% and membrane with higher salt dismissals is wanted. Cellulose acetic acid derivation films accomplish a salt dismissal of 97 close to 100% which was somewhat beneath the ideal level. Poly amide empty fine strands and inter facial composites then evolved to meet the ideal necessity [39].

Technologies of desalination and water exercise have been developed rapidly over the past few decades throughout the world to provide safe, clean water to address these grand challenges [40]. Water pollution has become a major concern as we strive to supply affordable and safe drinking water. Water treatment has emerged as a promising solution to overcome water pollution and to meet the ever-growing demand for water. A wide range of membrane and non-membrane approaches to water treatment styles have been developed over the past decades as a result of technological advances in material engineering. For example, adsorption, multistep coagulation, flocculation, ozone treatment, rush, sedimentation, and filtration have been developed. The process of desalinating water involves removing salty water and producing fresh water by removing swabs of it. There is a wide variation in the description of fresh water depending on the country [41]. Two methods of desalination are available: thermal (multi-stage flash) and membrane (RO). According to the US Environmental Protection Agency, water for fresh purposes should contain no more than 250 milligrams per liter of chloride and 500 milligrams per liter of total dissolved solids (TDS) [42].

Thermal (multi-stage flash), this type of technology is used to evaporate water and generate steam, which is then used to power turbines to generate electricity. It is an efficient and cost-effective method for producing electricity [43]. Reverse osmosis (RO) is a process in which water is forced through a membrane under pressure, leaving behind impurities. It is an effective method for purifying water and removing contaminants. Reverse osmosis is a common method for treating drinking water [44].

4.1.3. Reverse osmosis membrane treatment process

The process of osmosis describes the passing of a detergent (generally water) through a semi-permeable hedge from one side with lower solute attention to the other side with higher solute attention. Water inflow continues until chemical implicit equilibrium of the detergent is achieved. Since RO membranes are able to perform the RO processes efficiently, they are of great interest because they consume little energy, require a small space, and emit little carbon dioxide when they are used [45]. A further benefit of RO membranes is that they are non-porous and, thus, they are capable of blocking patches, ions, and organic substances. As with total dissolved solids (TDS), RO membranes can reject 90–99 percent of pollutants. Depending on the size and charge of the charge, as well as the relationship between solute, detergent, and membrane, their rejection performance will vary. It is also important to consider operating conditions and membrane parcels as well as the quality of the feed water in order to increase the efficiency of this process [46].

The bibulous pressure represents the difference in pressure between the two sides of a membrane at equilibrium [47]. In the present invention, the goal is to provide a rear osmosis compound membrane that is highly swab rejection resistant, highly water permeable, and fouling tolerant, which can be used in practical desalination at a low pressure, as well as a reverse osmosis treatment system for water provides a reverse osmosis compound membrane comprising a spongy sub caste, and a separation sub caste (also appertained to as a skin sub caste) formed on a face of the spongy sub caste, At least one substance belonging to the group consisting of electrically neutral organic substances and electrically neutral polymers is present in the separation sub caste, or at least one substance belonging to the group consisting of electrically neutral organic substances and electrically neutral polymers is carpeted over one of the faces of the separation sub caste. The subcaste or the separation subcaste before the face coating contains a limited range of specific face areas with at least one substance present.

It was investigated whether HT (high temperature) objectification and the use of 3-3-(trimethoxy silyl) propyl ammonium chloride (DMOTPAC) called the (VENUS-5700) graft enhanced membrane selectivity [48]. It was measured how much water was flowing through a swab and how much was rejected. It is believed that HT objectification improved the water flux of RO membranes, which may have been due to the increase of the face roughness, the improvement of hydrophilicity, and the construction of water channels [49]. The incorporation of HT led to significant face roughness, thus allowing water to flow more freely, since a smaller area was available for filtration. As a result of the hydrophilic surface of Dad-HT-0, it had a greater ability to relate to water and improved the flow of water. As a result of the pores in the HT matrix and the gaps between the nanoparticles and the matrix of PA, water could move at a high speed, thereby increasing the flow of water. A gradual decrease in the water flux was observed after DMOTPAC grafting after DMOTPAC paid attention to the grafting outcome. In the presence of DMOTPAC grafted on the skin membrane, water transfer through the membrane is hindered, causing a drop in pressure. It appears that many DMOTPAC have been grafted onto the membrane surface, resulting in a further decrease in water flux. When the DMOTPAC attention was not more than 0.06 wt, the modified membranes showed an advantage in water flux. In Dad-HT-0.06, the water flux was 49.8 gonnecm2/h, which represents a forward progress of 16.4 gonnecm2/h compared to PA-pristine (42.8 gonnecm2/h). It might be possible to compensate to some extent the mass transfer resistance recouped from the grafting subcaste with the preface of HT nano particles. It is evident that the modified membranes exhibit analogous swab rejection as PA-pristine, which means that HT objectification and DMOTPAC grafting have not damaged the PA skin subcaste. In comparison with the pristine membrane, Dad-HT-0.06 showed a rejection rate of 99.1 in swabs [50]. Due to this, it is possible for nano particle objectification to maintain the relatively high-water flux while fictionalizing membranes based on grafting. It was physically clicked that HT nanoparticles attached to the PA matrix, and then it was covalently clicked that DMOTPAC attached to HT nanoparticles [51]. This revision system, which incorporates anti-fouling grafting and nanoparticle objectification, proved effective in achieving excellent selectivity [52].

4.1.4. Ultra-filtration membrane treatment process

UF (ultrafiltration) is the process of purifying macromolecules, colloids, and suspended patches from various results by using pressurized membrane filtration. It is also used in a number of artificial processes, such as water treatment, wastewater treatment, chemical manufacturing, and food processing, etc. [53,54]. For those who would rather have minerals in their water but still wish to remove minute impurities, ultrafiltration is the preferred filtration method. Ultrafiltration (UF) is a process that employs the same water pressure seen in a home to force water through a semipermeable membrane and eliminate impurities. Ultrafiltration, as opposed to reverse osmosis, removes bacteria, viruses, and parasites from water while retaining minerals in the water. Because a UF system uses less water to drain than a RO system, it might be chosen. After filtering, effluent water is occasionally recycled using ultrafiltration so that it can be utilized again for irrigation. In most cases, UF membranes are used to eliminate harmful organisms and nearly all colloidal particles. It is expected that the majority of the dissolved solids will pass through the membrane without causing any problems later or in the final product water. Water turbidity will be eliminated by UF for most cases. The contamination of membranes, also known as membrane fouling, is a big problem for UF. In addition to morphology, porosity, and hydrophilicity, membrane fouling depends on the face parcels of the membrane. It is becoming increasingly common to use sweats to enhance the effectiveness of UF processes [55].

In addition to their outstanding hydrolytic and thermal stability, sulfone-containing polymers, such as polyether sulfone and polysulfides (PESU), are often used in nanofiltration (NF) and UF membranes for water operation, due to their strong mechanical parcels and chemical stability [56]. It is still a major concern for real-time operations that PESU fouling, as well as the fouling of the general polymer membranes, will lead to lower flux, an increase in energy consumption, and a reduction in separation efficiency. Researchers have linked fouling to the membrane material’s natural hydrophobicity. The organic foulants that are present in artificial wastewater have a natural origin. These foulants adhere to the hydrophobic membrane shells and holes and are therefore absorbed [57].

5. Role of membrane in gas separation process

The process of gas separation via a membrane is propelled by pressure, specifically the differential in pressure between the raw materials intake and the product’s output. Since the membrane employed in the procedure is typically non-porous, there won’t be a significant gas loss through it. The vapor/air combination can be split using selective membranes into two phases: a hydrocarbon-depleted phase (retentate) and a hydrocarbon-enriched phase (permeate), which is then condensed. Cellulose acetate (CA) compound membranes are acclimatized for implicit gas-transportation and antibacterial exertion by incorporating colourful rates (0–8wt.) of zeolite-CuO (101, ZC) compound [58]. The end behind this is to develop an anti-fouling membrane with enhanced CO_2 saturation and selection parcels. It is selective to separate gases using polymeric membranes since they are not precious and can easily be fabricated. Despite this, polymeric membranes still face limitations in terms of gas permeability versus selected gas flow [59]. The previous inorganic membranes are highly selective, permeabilise, chemically stable, and thermally stable, but have high fabrication costs and poor mechanical stability. In mixed matrix membranes (MMMs), previous inorganic components are dispersed in a polymeric matrix, combining the advantages of padding patches and polymer membranes. As part of the United States’ renewable energy program enacted encyclopaedically by the Renewable Energy Standard (RES), hydrogen is given further attention as a green energy source that can be produced from natural gas, coal, and biomass. As the largest on-going bioenergy program, it is enforced encyclopaedically through the Renewable Energy Standard. The separation and/or sanctification of hydrogen from carbon dioxide can be done with an environmentally friendly membrane module designed for an airman membrane-grounded separation [60]. In light of the previous description, it is clear that mixed matrix membranes (MMMs) are utilized largely implicitly when separating hydrogen gas from carbon dioxide gas.

We investigated several inorganic membranes to get MMM with charming gas separation performance in relation to inorganic and polymeric membranes, with a few of them proving a good fit in membrane operations. A zeolitic pudding, a silica nanoparticle pudding, and a CMS pudding are probably the most extensively examined inorganic puddings [61]. As far as the shape of fly specks and chemical composition are concerned, these puddings are exaggeratedly rigid. Gas separation and sanctification are Mixed matrix membranes comprise polymeric accoutrements and puddings; they enhance membrane separation performance. By using them, sustainable development goals can be achieved, especially those related to essence-organic fabrics, since they are more environmentally friendly and require less energy than other options [62].

The membrane technology has recently emerged as an innovative and promising approach for distant chemical engineering processes such as the production of H2 products, the enrichment of oxygen, the production of biogas, the separation of hothouse feasts and the treatment of wastewater due to its innovative performance, environmental friendliness, and ease of operation. The membrane-ground gas separation (MGS) fashion for gassy fusion has been of great interest despite its modest maturity in artificial conditioning due to its colourful functional/functional advantages including simplicity, cost effectiveness, environmental friendliness, versatility, ease of scaling up, inflexibility, and modularity [63]. A considerable amount of research has been conducted on how mongrel compound membranes, which have both organic and inorganic properties, perform efficiently and cost effectively.

It is the role of the membrane employed in MGS to function as a passable pervious hedge, permitting motes of a given gas to pass through its nano/microspores, but prohibiting motes of other specific gases from entering based on their size, diffusivity, or solubility [64]. Considering the feasibility of applying these components for gas separation (especially CO2) depends primarily on their cost and effectiveness. Due to their brilliant advantages, such as negligible costs and ease of processing, polymeric membranes have become an irrefutable material for gas separation. In general-applied polymeric membranes, the permeability and selectivity of gases must be high so that the separation will be effective, and the membrane area will be reduced [65]. As a consequence of a trade-off between the two previously mentioned parameters (permeability and selectivity), new polymeric membranes are no longer developing as fast. In recent years, nanomaterials (particularly nanofibers and carbon nano tubes) have been successfully utilized for improving and optimizing the performance of various membranes [66].

5.1. Membrane in energy storage and conversion

The implementation of effective, efficient energy storage devices has become increasingly important as the world strives to move away from traditional energy sources [67]. In order to address this problem, unconventional energy storage devices like hybrid batteries, redox flow cells, and bacterial batteries are emerging. Electrochemical devices designed using these alternative cell configurations offer high energy conversion efficiency and modularity while providing flexibility in materials and operating conditions. There are a wide range of power levels among these diverse devices, ranging from a few milliwatts to several megawatts. Developing all-solid-state batteries that can cycle for long periods of time and have a high energy density makes it possible to manufacture durable electronic and point-of-care devices. In the future, earth-abundant metal ions could replace lithium-ion batteries in terms of capacity [68].

5.1.1. Membrane process in fuel cell

The term "energy cell" refers to an electrochemical device that continuously converts the chemical energy of an energy source and an oxidizing agent into electrical energy by changing the electrodes within the electrolyte" [69]. Electrochemical batteries work on similar principles to energy cells. The only difference is that chemical energy is stored outside of the cell of an energy cell, while chemical energy is stored inside the cell of an electrochemical battery. It is more efficient to generate electrical power from energy cells than through conventional approaches, which undergo multitudinous conversions before they produce actual electricity. Through the conversion of chemical energy directly into usable power and thermal energy, energy cells can achieve up to 60 effective conversions. Types of electrolyte and operating temperatures can determine how energy cells are distributed [70]. There are several types of low temperature energy cells, including alkaline energy cells (AFCs), phosphoric acid energy cells (PAFCs), polymer electrolyte energy cells (PEFCs), and direct methanol energy cells (DMFCs). The two most common forms of high temperature energy cells are solid oxide fuel cells (SOFCs) and molten carbonate fuel cells (MCFCs). In order for fuel cells to perform efficiently, proton conductivity becomes one of their backups. Proton conductivity is needed to allow the protons to move freely through the fuel cell. It also helps to minimize energy losses due to electrochemical processes. Proton conductivity is essential for fuel cell performance. Therefore, proton conductivity must be optimized to ensure optimal performance of a fuel cell. This can be done through material selection and proper design [71,72].

Electrolyte membrane continuation is not yet compatible with target applications [73]. Energy cell systems for automotive operations, for instance, require high-performance membranes that operate under conditions of low relative humidity and temperatures beyond the boiling point of water. As a result of these conditions, energy cell membrane electrode assemblies (MEA) cannot maintain a significant amount of water, limiting conductivity, among other things. In addition to their strength and stability, membranes must also be compatible with electrodes and perform well as energy cells for automotive operations across the entire temperature range: from subzero to full power (up to 120 °C–130 °C); for stationary operations at advanced temperatures > 150 °C, over periods of 5000 to 50,000 h (automotive) [74].

5.1.2. Membrane process in redox flow batteries

The redox inflow battery stores energy by oxidizing and reducing two redox couples as electroactive components [75]. An electrochemical cell mound is comprised of a number of cells connected in series or parallel so that response occurs at inert electrodes in a typical redox inflow battery with 2 electrolyte budgets and electrolytes circulated by pumps through an electrochemical cell mound. It is usually anode, cathode, and ion exchange membrane that provide prolixity of ions across the membrane as well as preventing cross-mixing of electrolyte results between these two budgets of electrolytes [76]. In a half cell electrolyte, the discharged state of the redox species is converted into the charged state during charging by applying power from an external source. The chemical energy is transformed into electricity during discharge by electrons flowing between redox species. Accordingly, the number of active redox species in the mound and electrolyte volume will determine the energy capacity of the system and the power of the system is determined by the number of cells. Therefore, a redox inflow battery behaves more like a regenerative energy cell than a conventional battery [77].

In a redox flux cell, the membrane plays an important role. A suitable membrane for redox flux systems generally requires a great deal of effort. It is ideal to have good chemical stability under acidic conditions, resistance to the highly oxidizing terrain of the positive half-cell electrolyte, low electrical resistance, low permeability to vanadium or polyhalide ions, high permeability to hydrogen ions, good mechanical parcels, and low cost in vanadium redox systems [78]. By allowing ions to transfer from one electrode to the other during current flow, the membrane of redox flux cells assists the cross-mixing of the positive and negative electrolytes. In order to commercialize multitudinous redox flux cells, the membrane has proven to be a major obstacle. A membrane used for ion exchange can be a waste product, a list, or a tube that separates two fluids and enables ions to move between them. These membranes are made up of a three-dimensional network of cross-linked direct polymer chains [79]. Water would dissolve the membrane in the absence of the cross-linking, leaving a polyelectrolyte in place. There are fixed ion functional groups on ion exchange membranes; these are combined with counterions in sufficient numbers to render the exchanger electrically neutral [80].

The number of review papers which addressed membranes in the battery system is certainly quite large, but many of these focused on the details of membrane manufacturing styles, which is not a desirable process in the exploration of membranes. Consequently, fabrication of membrane products has received relatively little attention. Microstructure and lading additions in membrane products are affected not only by the manufacturing styles but also by their cost [81]. The first section of the article introduces the bracket of membranes and their operating principles. Additionally, these membrane types are studied from a medication standpoint. A description of typical membrane medication styles follows. In the end, membrane medications are epitomized by their environmental impacts.

5.1.3. Super capacitor for electrode fabrication

When compared to other energy storage technologies like fuel cells, capacitors, and batteries, supercapacitors have several important advantages. Supercapacitors' efficiency is dependent on a number of factors that are dependent on its constituent parts. Electrolyte, separator, current collectors, and electrodes are some of these parts. A separator prevents the electrical circuit from shorting out, an electrode stores the charge, and an electrolyte supplies the necessary ions, all of which are transmitted from the electrode to an external circuit. A supercapacitor's design is greatly influenced by the material selection for the separator. Its primary job in supercapacitors is to keep the anode and cathode electrode materials apart to avoid short circuits. It primarily exists as a porous membrane to facilitate simple ion transport. Materials such as glass fibre, cellulose, ceramic fibres, or polymeric film materials are frequently utilised as separators.

A major drawback of polyvinylidene difluoride (PVDF) is that it is more prone to list action when used to manufacture electrodes for super capacitors. Binders are designed to bind active materials in electrodes and improve adhesion between electrodes and current collectors [82]. The selection of suitable binders has been guided by the quality parameters of adhesion strength, hydrophilicity, thermal and electrochemical stability, as well as non-bane properties. In addition to enhancing electrical communication between active apparatus, binders could make electrodes compact, thus facilitating a more compact arrangement. There is an enormous impact on the electrode drug and overall electrochemical performance of a super capacitor depending on physical parameters such as the attention of the binder, its cleaner, and its drying temperature [83].

These physical parameters need to be kept in mind for a nanomaterial to have a voguish electrochemical performance or to produce the maximum electrochemical parcels possible. In the case of adding a binder, attention must be paid to the rate at which the active material is added to the polymer binder, as there is an optimum rate. An excess of binder can block the pores of an active material and minimize its compact capability if the volume of binder is too low [84]. By reducing electron-transfer resistance, enhancing pseudo capacitive charging, allowing electrolyte ions to diffuse faster inside nano porous materials and reducing ion diffusion resistance, proper attention can be paid to the binding agent and active material [85].

5.1.4. Membrane process in nuclear industry

Membrane processes are thought to be promising techniques for clean technologies that minimize raw material use, optimize energy utilization, and lower waste generation. They are competent to address a wide range of environmental issues, including those pertaining to nuclear technology [86]. Many nuclear facilities around the world have used membrane methods to process liquid radioactive waste. High levels of chemical, thermal, and radiation resistance are exhibited by ceramic or composite membranes. For the concentration of radioactive waste, a thermal method known as membrane distillation using resistant porous membranes was proposed and tested [87]. Additional techniques, such as electric processes utilizing ion-exchange membranes and liquid membranes, are being developed for potential use in the nuclear sector [86]. Membrane techniques were taken into consideration as substitute approaches for recovering various recyclable and reusable materials.

5.1.5. Soil science and membrane technology

Cleaning up soils contaminated with hazardous organic and metals substances is necessary to comply with regulations. When pollutants are transferred from the solid matrix to the wash liquor during soil washing with aqueous solutions, further treatment is required [88]. These wash liquors have not been concentrated substantially using membranes. Nonetheless, a number of membrane approaches seem promising. The primary goal of these methods is to identify strategies to reduce the volume of the pollutants while still concentrating them. Acid leaching was used in conjunction with microfiltration and nanofiltration membrane techniques to improve heavy metal removal from polluted soil. Soil particles were separated from the metal-containing leachate by microfiltration. Subsequently, the leachate underwent nanofiltration processing to extract wasted acid from the slurry and decrease its volume. The bench size study's findings illustrated the benefits of using membrane processes in soil treatment procedures, which should remove metals more quickly and completely and produce less waste products overall.

5.1.6. Membrane process in food and beverage industry

Membrane technology is becoming widely used in the food sector as a processing and separation technique. Processing novel components and foods can be done with innovative technologies like membrane separations. One green technique that is being used is membrane separation [89]. Reverse osmosis and ultrafiltration membranes use energy efficiently because there is no phase change, which is one of the technology's main advantages [90]. Furthermore, high pressure can be used to reverse the flow direction of the food solution to obtain the desired concentration without compromising nutrition quality. Low molecular weight solutes such as salts, monosaccharides, and fragrance chemicals are extracted from food products using this approach. This membrane technology can be used to concentrate and purify fruit juices, enzymes, fermented liquors, and vegetable oils, among others. Membrane processes driven by pressure make it easier to separate components with a wide variety of particle sizes. This explains why the food processing sector uses them in a variety of ways [91].

6. Role of composite membrane in biomedical applications

In the clinical field, manufactured membranes play a crucial role across various applications, showcasing their versatility and importance in medical technology [92]. Five key applications include haemodialysis, where membranes function as artificial kidneys to remove waste products and excess fluid from the blood of patients with renal failure [93]. These membranes must possess high permeability to small solutes while selectively retaining larger molecules like proteins. Blood oxygenators utilize membranes to facilitate the transfer of oxygen into the bloodstream while removing carbon dioxide, making them essential in cardiac surgeries and during organ transplants [94]. Another significant application is in controlled drug delivery systems, where membranes regulate the release of therapeutic agents, ensuring sustained and targeted delivery, thereby enhancing the efficacy of treatments and minimizing side effects. Artificial organs, such as heart valves and vascular grafts, often rely on specialized membranes to mimic the function of natural organs, requiring biocompatibility and mechanical strength to withstand physiological conditions [94]. Lastly, in tissue engineering, membranes serve as scaffolds for cell growth and tissue regeneration, necessitating specific characteristics such as porosity and biocompatibility to support cell attachment and proliferation. Each of these applications necessitates a thorough understanding of membrane types, their performance characteristics, and the challenges they face, such as fouling, biocompatibility issues, and long-term stability [95]. Addressing these challenges is essential for advancing the field of medical membranes and improving patient outcomes in various therapeutic contexts. Following are some important applications in medical fields **(Figure 2)**.

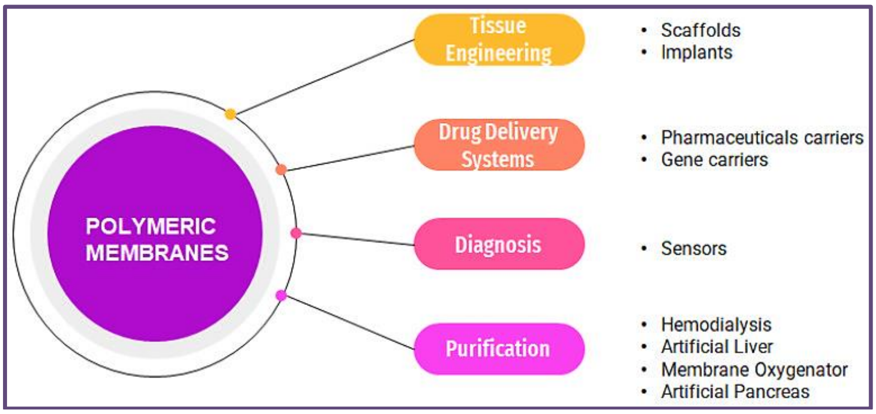

Figure 2. Applications of polymeric membranes in biomedicine [96].

6.1. Haemodialysis through membrane

Because of the continually evolving criteria for selectivity and the upgrading of materials developed to meet these objectives, the field of membrane materials is among the most dynamic. Artificial kidneys are made of membrane materials such as polyacrylonitrile (PAN), polysulfone derivatives (PSU), and cellulose derivatives. Desalination and hemodialysis are the two membrane processes that are currently necessary for daily living rather than for development. Tens of millions of people with chronic renal disease have benefited from hemodialysis during the past 60–70 years, both in terms of life preservation and enhanced longevity. It is fundamental for those whose kidney has fizzled and are as of now not ready to control the body's garbage removal [97]. Failure of the kidneys to remove harmful wastes may result in elevated blood pressure, excessive fluid retention, and insufficient red blood cells.

It can provide electrolyte replacement and re-establish pH levels and remove side effects associated with kidney disease. Dialysis is an effective way to replace a portion of the elements found in the kidneys. A semi-permeable dialysis film is used to collect blood from the patient, which is then flooded with saline that has salt, potassium, and calcium concentrations comparable to the patient's blood. A concentration gradient across the membrane transports urea and other low-molecular-weight metabolites to the dialysate. Proteins and blood cells, which are larger components in the blood, are prevented from diffusing. The dialysis membrane underwent various module design phases. The empty fiber frameworks are the most ruling on the lookout and the cost for these dialyzers are generally low since they are made in mass. The dialyzer can be easily refilled with as little as 60to 100 milliliters of blood, which is an appealing feature of this design. Significant metabolic products such as urea and creatinine are efficiently eliminated by the cellulose layer, while metabolites with sub-atomic loads exceeding 1000 are less successfully removed [98]. In the following years, there has been a need to view such material as elective. It has become more common to replace cellulose with synthetic polymers due to their tendency to stimulate normal kidney function more closely. There are a number of substances that can be substituted for cellulose, including polyacrylonitrile, polysulfide, polycarbonate, polyamide, and polysulfide. Synthetic Fiber membranes are composed of finely micro porous skin layers on their inner surface that contact the blood. Membranes made from these fibres have a tenfold increase in hydraulic permeability compared to those made from cellulose [99].

6.2. Blood oxygenators through membrane

Blood oxygenators are utilized during a medical procedure when the patient's lungs can't work regularly. In the 1930s, pioneering work on these devices was done. This mechanical device was made to look like the heart and lungs so that it can be used for surgery on the heart and its great vessels [99,100]. Artificial lungs, or blood oxygenators, have long been recognized as a potential use for membrane contactors. In fact, the ability to exchange gases without the production of bubbles is vital to avoid surgical complications. The oxygenator's lung-like function is to remove carbon dioxide from the blood and expose it to oxygen. It is disposable and has 2–4 square meters of hollow fiber-shaped membrane that is permeable to gas but impenetrable to blood. Within the hollow fibers, oxygen travels in the opposite direction from that of blood on the outside. Blood oxygenators have a special design, and materials must meet strict requirements for their suitability for use in medicine. Dense or porous hydrophobic membranes are suggested as alternatives.

In the human lung, the all-out trade film region between the blood vessels and the air attracted and out is around 80 m^2. The membrane of the human lung is thought to be about 1 mm thick, and the lungs, total exchange capacity is much greater than what is typically required. This permits individuals with debilitated lung ability to have generally typical existences. Micro porous poly-olefin fibers are now utilized, whereas silicone rubber membranes were utilized in the initial membrane oxygenators. Drop through the device to maintain good mass transfer with minimal pressure. Most of the time, the outside of the fibers is where blood circulates. This method, on the other hand, does more harm than good when used for extended periods of time. Generalized enema, thrombocytopenia, coagulopathy, hemolysis, and impairment of organ function occur [101].

6.3. Controlled discharge drugs through membrane

Every osmotic medication delivery method has an osmotic core and a semi-permeable membrane that regulates water flow. The medicine is exclusively discharged in solution form, and it has a single orifice. Only works with medications that dissolve in water. The composite membrane may successfully encourage PC-12 cells to develop into neurons and has good biocompatibility [102]. Furthermore, there would not be any more harm done when the composite membrane is placed directly to the damaged areas [102]. A medicine should be delivered to a specified location at a given time with a certain release pattern in an ideal medicine delivery system. The pharmaceutical supply provided by conventional medical forms (tablets, injection outcomes, etc.) often soars over the required cure. The primary hurdles for all delivery systems are maintaining medication positions in the bloodstream or releasing medication gradually to prevent repeated doses and hepatic "first-pass" processing around the medication [103].

In control drug delivery systems, a membrane controls the rate at which the drug is delivered to the body. In certain gadgets the film controls penetration of the medication from a supply to accomplish the expected medication conveyance rate. Different gadgets utilize the osmotic strain created by dispersion of water across a layer to control smaller than usual siphons. In other devices, the drug is embedded in the material of the membrane, whereupon it slowly dissolves or breaks down in the body. After that, a combination of diffusion and biodegradation is used to control drug delivery. The target of these gadgets is to convey a medication to the body at a rate foreordained by the plan of the gadget and free of the changing climate of the body. Only the total amount of medication administered to a patient is controlled in conventional medications [104].

6.4. Artificial organs through composite membranes

The amazing advances in artificial organs (AO) technology are becoming more and more significant in today's medical procedures. By keeping physiochemical gradients within a safe range, AO technology can now partially enhance the activities of human organs. To support the failing organs' chemical and physical activities, many of these artificial organ replacements use synthetic polymeric membranes. Artificial kidney, liver, pancreas, and lung are among the specific AOs that use membrane technology. While the technology for artificial kidneys is clinically mature, there are still numerous unresolved technical issues with other membrane-based AOs such pancreas, liver, and lung. Such problems are undoubtedly extremely complicated and call for multidisciplinary cooperation within the domains of chemistry, biology, materials science, and engineering. Furthermore, even with improvements, the quality of life remains low for people with organ failure. To enhance patient well-being and quality of life, AO technology needs to be continuously improved from both a membrane and a biocompatibility standpoint [105].

In the early 1900s, the bubble oxygenator was a popular artificial lung bias. The use of membranes prevented unintended haemolysis and air emboli, which were induced by bubble oxygenators. In addition to continuously improving permeance performance, multilayer flat distance membranes were reduced to about 2 m^2 per concave fibre membrane as a result of continuous improvement in membrane permeance performance. As of now, blood oxygenation effectiveness is limited by blood side mass transfer resistance rather than membrane gas transport performance [94]. In general, there are two types of artificial lung technology: short-term and long-term respiratory aids. Approximately 1.5 million open heart bypass surgeries are performed every year as short-term support. A cardiopulmonary bypass device, also known as a heart-lung machine, circulates venous blood from the case extra-corporeally, or outside the body [106]. During the oxygenation process, the blood is put back into the shell after having been oxygenated inside an oxygenator. It is aimed at temporarily integrating the functions of the heart and lungs during the approximately six-hour procedure [107]. A long-term respiratory support system called extracorporeal membrane oxygenation (ECMO) is used to provide this support. This medication is only approved for patients with severe lung failure caused by advanced age, long-term lung illnesses, or recent viral infections. As a primary objective, ECMO systems are intended to sustain the patient until their own bodies can heal. The fact that it can raise patient survival rates by as much as 75%, when compared to traditional treatments, has repeatedly demonstrated its efficacy.

6.5. Tissue engineering through membrane

The field of tissue engineering is expanding in order to create novel technologies aimed at effectively treating degenerative disorders that impact various kinds of connective tissues [108]. In recent years, there has been a tremendous increase in the search for materials that are biocompatible, bioactive, biodegradable, and multifunctional [109]. Because of their high-water retention capacity, biocompatibility, and degradability, natural polymers including hyaluronic acid, collagen, and chitosan provide excellent materials for tissue engineering composites. The combination of chitosan, collagen, and calcium phosphates as composite materials satisfies the necessary requirements and may produce bio stimulation for tissue regeneration [109,110]. After 48 hours, the chitosan membranes with the largest amounts of collagen and hydroxyapatite showed the highest levels of cell attachment. Good cell adhesion and little cytotoxicity were demonstrated by all composite membranes, indicating a high degree of potential for these materials as biomaterials for tissue engineering [111–113].

7. Challenges of composite membranes

Synthetic composite membranes face significant challenges that impede their performance and widespread adoption across various applications, including water treatment and pharmaceuticals [114]. One of the primary issues is membrane fouling, which occurs when particles, organic matter, or microorganisms accumulate on the membrane surface, leading to reduced permeability, increased energy consumption, and the need for frequent cleaning. Fouling can be categorized into organic, inorganic, and biofouling, each requiring specific mitigation strategies such as pre-treatment, surface modification, and advanced cleaning protocols [115]. Stability is another critical challenge, with membranes needing to maintain chemical, thermal, and mechanical integrity under operational conditions. Degradation from aggressive chemicals or varying temperatures can compromise membrane performance, while long-term use may lead to changes in permeability and selectivity [116]. Additionally, scalability presents hurdles in transitioning from laboratory-scale to industrial applications, as achieving consistent manufacturing quality, controlling production costs, integrating new technologies into existing systems, and complying with regulatory standards are all vital considerations [116]. Addressing these challenges through ongoing research and innovation in membrane materials, designs, and production methods is essential to unlocking the full potential of synthetic composite membranes in various industries [117]. So, the composite membranes should focus on developing novel polymers, nanocomposites, and hybrid structures to enhance permeability, selectivity, and fouling resistance. Advanced surface modification techniques and innovative coatings can improve hydrophilicity and anti-fouling properties, while 3D-structured and layered designs may facilitate better mass transfer. Exploring scalable manufacturing methods and efficient fouling mitigation strategies, such as intelligent membranes with real-time detection, will be crucial for extending membrane lifetimes [23]. Integrating membranes with renewable energy and biological processes can enhance sustainability. Additionally, conducting life cycle assessments and tailoring membranes for specific applications will optimize performance and meet the growing demands in water treatment and healthcare.

8. Future perspectives

Water treatment applications have proven to be successful with membranes, and membrane technology continues to advance. Fouling and chemical stability of membranes are two major problems that still need to be addressed [118]. As membranes' operational lifetimes are extended and their energy requirements are reduced, they will become even more cost-effective. This area of research has focused on the modification of membrane surfaces and improving pretreatment of the feed water before it reaches the membranes. Additionally, membranes are being studied for chemical stability. Through improved tolerance to chlorine, the poly amide TFC membrane could be operated at lower costs by eliminating pretreatment dichlorination. There are new applications of membranes for water purification in addition to wastewater treatment and desalination. In the oil and gas industry, produced water is purified, which is water that is generated during production. Many of these waters are contaminated with oils and salts, so they cannot be used for beneficial purposes [119]. Water produced from oil and gas production often occurs in arid regions, making membranes capable of removing hydrocarbons and salt an excellent source of water. There has been an enormous advance in the membrane field as a whole. The advantages of membranes for water purification applications include being economical, environmentally friendly, versatile, and easy to use [57].

In terms of desalination, nano-based composite membranes can be a promising option; however, there are still many research requirements to be addressed. Toxicology of nanoparticles and health risks associated with adding nanoparticles during manufacturing must be fully understood [39]. It is a demanding concern to address the durability of fillers inside membranes, despite various nanoparticles being incorporated as fillers inside the polymer matrix. In the future, nanomaterial-based composite membranes may be a promising option for seawater pre-treatment, but mechanisms and technologies need to be developed so that nanomaterial toxicity can be estimated cost-effectively on living and non-living organisms.

Due to the very thin graphene-based composite membranes, separating the membrane from the substrate is challenging. In order to improve the permeation of graphene-based membranes, a lot of research is required [120]. The best material for making composite membranes is polymeric-based membranes for desalination. It is essential to continuously research and develop polymeric membranes to address bio fouling and chlorine resistance. The resistance to chlorides of TFC membranes needs to be improved through research and development [121]. In order to improve chlorine resistance, the di-chlorination step can be eliminated to decrease overall costs. The mass production of graphene oxides and the ease of functionalizing graphene oxides make graphene-based composite membranes inexpensive [122]. Although the use of composite membranes has been widespread, still the issues stated in the manuscript need attention for these to serve as perfect alternatives for seawater pre-treatment [39].

9. Conclusions

Finally, it has been determined that composite membranes have a wide range of contemporary uses that are amazing and still expanding. Utilising membranes to create process water from surface water, groundwater, or wastewater is becoming more and more common. Nowadays, membranes are competitive with traditional methods. Membranes can be employed as catalysts in syntheses or for gas storage in biogas plants in addition to being utilised for filtering, extraction, and distillation. Among the industries that heavily rely on membrane filtering technology are the ones treating water and wastewater, processing food and beverages, pharmaceuticals, and medical applications. This review article has covered a wide range of membrane application processes, with a classification of these applications based on the characteristics of the membrane.

Pharmaceuticals, chemicals, medicines, and industrial processes need clean water, which can be achieved with water filtration. There are a few most popular and simple techniques for purifying water. These include solar purification, UV radiation, iodine addition, gradual sand filtration, water purification, water chlorination, boiling water, and more. There have been many different techniques used to purify water throughout history. There are many techniques used in wastewater treatment, including physical processes like filtration, sedimentation, and distillation, biological processes like biologically active carbon and slow sand filters, chemical processes including flocculation and chlorination, and the use of electromagnetic radiation, including ultraviolet light. It is possible to lower dissolved and particulate matter, as well as parasites, bacteria, algae, viruses, and fungus concentrations by purifying water.

Acknowledgments: The authors are greatly acknowledged to the chairman, Department of Applied Chemistry AMU Aligarh for providing all the necessary literatures and related materials required to execute this great review work.

Conflicts of interest: The authors declare no conflict of interest.

References

1. Li Q, Wen C, Yang J, et al. Zwitterionic Biomaterials. Chemical Reviews. 2022; 122(23): 17073-17154. doi: 10.1021/acs.chemrev.2c00344
2. Drioli E, Romano M. Progress and New Perspectives on Integrated Membrane Operations for Sustainable Industrial Growth. Industrial & Engineering Chemistry Research. 2001; 40(5): 1277-1300. doi: 10.1021/ie0006209
3. De Bartolo L, Curcio E, Drioli E. Membrane systems: for bioartificial organs and regenerative medicine. Walter de Gruyter GmbH & Co KG; 2017.
4. Legallais C, Kim D, Mihaila SM, et al. Bioengineering Organs for Blood Detoxification. Advanced Healthcare Materials. 2018; 7(21). doi: 10.1002/adhm.201800430
5. Chorsi MT, Curry EJ, Chorsi HT, et al. Piezoelectric Biomaterials for Sensors and Actuators. Advanced Materials. 2018; 31(1). doi: 10.1002/adma.201802084
6. Salatino JW, Ludwig KA, Kozai TDY, et al. Glial responses to implanted electrodes in the brain. Nature Biomedical Engineering. 2017; 1(11): 862-877. doi: 10.1038/s41551-017-0154-1
7. Nunes SP, Culfaz-Emecen PZ, Ramon GZ, et al. Thinking the future of membranes: Perspectives for advanced and new membrane materials and manufacturing processes. Journal of Membrane Science. 2020; 598: 117761. doi: 10.1016/j.memsci.2019.117761

8. Yang Z, Zhou Y, Feng Z, et al. A Review on Reverse Osmosis and Nanofiltration Membranes for Water Purification. Polymers. 2019; 11(8): 1252. doi: 10.3390/polym11081252
9. Osada Y, Nakagawa T. Membrane science and technology. CRC Press; 1992.
10. Dell RM, Rand DAJ. Energy storage—a key technology for global energy sustainability. Journal of power sources. 2001; 100: 2-17.
11. Dudchenko N, Pawar S, Perelshtein I, et al. Magnetite Nanoparticles: Synthesis and Applications in Optics and Nanophotonics. Materials. 2022; 15(7): 2601. doi: 10.3390/ma15072601
12. Baker RW. Membrane technology and applications. John Wiley & Sons; 2023.
13. Goh PS, Ismail AF. A review on inorganic membranes for desalination and wastewater treatment. Desalination. 2018; 434: 60-80. doi: 10.1016/j.desal.2017.07.023
14. Kayvani Fard A, McKay G, Buekenhoudt A, et al. Inorganic Membranes: Preparation and Application for Water Treatment and Desalination. Materials. 2018; 11(1): 74. doi: 10.3390/ma11010074
15. Agboola O, Fayomi OSI, Ayodeji A, et al. A Review on Polymer Nanocomposites and Their Effective Applications in Membranes and Adsorbents for Water Treatment and Gas Separation. Membranes. 2021; 11(2): 139. doi: 10.3390/membranes11020139
16. Lau WJ, Lai GS, Li J, et al. Development of microporous substrates of polyamide thin film composite membranes for pressure-driven and osmotically-driven membrane processes: A review. Journal of Industrial and Engineering Chemistry. 2019; 77: 25-59. doi: 10.1016/j.jiec.2019.05.010
17. Alihemati Z, Hashemifard SA, Matsuura T, et al. Current status and challenges of fabricating thin film composite forward osmosis membrane: A comprehensive roadmap. Desalination. 2020; 491: 114557. doi: 10.1016/j.desal.2020.114557
18. Goh PS, Ismail AF, Sanip SM, et al. Recent advances of inorganic fillers in mixed matrix membrane for gas separation. Separation and Purification Technology. 2011; 81(3): 243-264. doi: 10.1016/j.seppur.2011.07.042
19. Yazid AF, Mukhtar H, Nasir R, et al. Incorporating Carbon Nanotubes in Nanocomposite Mixed-Matrix Membranes for Gas Separation: A Review. Membranes. 2022; 12(6): 589. doi: 10.3390/membranes12060589
20. Li Y, He G, Wang S, et al. Recent advances in the fabrication of advanced composite membranes. Journal of Materials Chemistry A. 2013; 1(35): 10058. doi: 10.1039/c3ta01652h
21. Aziz T, Li W, Zhu J, et al. Developing multifunctional cellulose derivatives for environmental and biomedical applications: Insights into modification processes and advanced material properties. International Journal of Biological Macromolecules. 2024; 278: 134695. doi: 10.1016/j.ijbiomac.2024.134695
22. Li C, Sun W, Lu Z, et al. Ceramic nanocomposite membranes and membrane fouling: A review. Water Research. 2020; 175: 115674. doi: 10.1016/j.watres.2020.115674
23. Osman AI, Chen Z, Elgarahy AM, et al. Membrane Technology for Energy Saving: Principles, Techniques, Applications, Challenges, and Prospects. Advanced Energy and Sustainability Research. 2024; 5(5). doi: 10.1002/aesr.202400011
24. Wang LK, Chen JP, Hung YT, et al. Membrane and Desalination Technologies. Humana Press; 2011. doi: 10.1007/978-1-59745-278-6
25. Khulbe K, Matsuura T. Synthetic membrane characterisation–a review: part I. Membrane Technology. 2017; 7-12.
26. Khulbe KC, Feng C, Matsuura T. The art of surface modification of synthetic polymeric membranes. Journal of Applied Polymer Science. 2009; 115(2): 855-895. doi: 10.1002/app.31108
27. Wang H, Wang M, Liang X, et al. Organic molecular sieve membranes for chemical separations. Chemical Society Reviews. 2021; 50(9): 5468-5516. doi: 10.1039/d0cs01347a
28. Bohr SJ, Wang F, Metze M, et al. State-of-the-art review of porous polymer membrane formation characterization—How numerical and experimental approaches dovetail to drive innovation. Frontiers in Sustainability. 2023; 4. doi: 10.3389/frsus.2023.1093911
29. Adu-Ahyiah M, Anku RE. Small scale wastewater treatment in Ghana (a scenerio). Retrieved; 2010.
30. Al Aani S, Mustafa TN, Hilal N. Ultrafiltration membranes for wastewater and water process engineering: A comprehensive statistical review over the past decade. Journal of Water Process Engineering. 2020; 35: 101241. doi: 10.1016/j.jwpe.2020.101241
31. Iwuozor KO. Prospects and Challenges of Using Coagulation-Flocculation method in the treatment of Effluents. Advanced Journal of Chemistry-Section A. 2019: 105-127. doi: 10.29088/sami/ajca.2019.2.105127
32. de Peón CM. Organic micropollutants in reverse osmosis water treatments, presence and rejection. Universitat Rovira i Virgili;

2015.

33. Fritzmann C, Löwenberg J, Wintgens T, et al. State-of-the-art of reverse osmosis desalination. Desalination. 2007; 216(1-3): 1-76. doi: 10.1016/j.desal.2006.12.009
34. Azapagic A, Emsley A, Hamerton L. Polymers, the Environment and Sustainable Development. Published online February 14, 2003. doi: 10.1002/0470865172
35. Maranchi JP, Trexler MM, Guo Q, et al. Fibre-reinforced hydrogels with high optical transparency. International Materials Reviews. 2014; 59(5): 264-296. doi: 10.1179/1743280414y.0000000032
36. Darwish M, Hassabou AH, Shomar B. Using Seawater Reverse Osmosis (SWRO) desalting system for less environmental impacts in Qatar. Desalination. 2013; 309: 113-124. doi: 10.1016/j.desal.2012.09.026
37. Najib S, Fadili A, Mehdi K, et al. Salinization process and coastal groundwater quality in Chaouia, Morocco. Journal of African Earth Sciences. 2016; 115: 17-31. doi: 10.1016/j.jafrearsci.2015.12.010
38. Ghernaout D. Short Communication: Requiring Reverse Osmosis Membranes Modifications – An Overview. American Journal of Chemical Engineering. 2017; 5(4): 81. doi: 10.11648/j.ajche.20170504.1
39. Jaspal D, Malviya A, El Allaoui B, et al. Emerging advances of composite membranes for seawater pre-treatment: a review. Water Science & Technology. 2023; 88(2): 408-429. doi: 10.2166/wst.2023.220
40. Liu G. A study on sustainable urban water management in small and medium sized cities in China. Dortmund Technische Universität, Diss; 2012.
41. Prest EI, Hammes F, van Loosdrecht MCM, et al. Biological Stability of Drinking Water: Controlling Factors, Methods, and Challenges. Frontiers in Microbiology. 2016; 7. doi: 10.3389/fmicb.2016.00045
42. Schaefer DH, Thiros SA, Rosen MR. Ground-water quality in the carbonate-rock aquifer of the Great Basin, Nevada and Utah, 2003. Scientific Investigations Report. 2005. doi: 10.3133/sir20055232
43. Tareemi AA, Sharshir SW. A state-of-art overview of multi-stage flash desalination and water treatment: Principles, challenges, and heat recovery in hybrid systems. Solar Energy. 2023; 266: 112157. doi: 10.1016/j.solener.2023.112157
44. Faroon M, ALSaad Z, Albadran F, et al. Review on Technology-Based on Reverse Osmosis. Anbar Journal of Engineering Sciences. 2023; 14(1): 89-97. doi: 10.37649/aengs.2023.139414.1047
45. Buonomenna MG. Membrane processes for a sustainable industrial growth. RSC Advances. 2013; 3(17): 5694. doi: 10.1039/c2ra22580h
46. Judd S, Jefferson B. Membranes for industrial wastewater recovery and re-use. Elsevier; 2003.
47. Zhang S, Zhang W, Zhou X, et al. Interaction of water mists with bibulous filter media and hygroscopic particles in pressure drop jump of fibrous filter media. Chemical Engineering Science. 2024; 285: 119544. doi: 10.1016/j.ces.2023.119544
48. Tian X, Yu H, Yang J, et al. Preparation of reverse osmosis membrane with high permselectivity and anti-biofouling properties for desalination. Frontiers of Environmental Science & Engineering. 2021; 16(7). doi: 10.1007/s11783-021-1497-0
49. Milad G, Kijoon L, Yujuan H, et al. Selective laser melting of 304L stainless steel: Role of volumetric energy density on the microstructure, texture and mechanical properties. Additive Manufacturing. 2020; 32: 101011Kearns VR. Surface engineering of dental implants using a deposition of nano-features. The University of Liverpool (United Kingdom); 2007.
50. Jafari M, Rezvanpour A. Upconversion nano-particles from synthesis to cancer treatment: A review. Advanced Powder Technology. 2019; 30(9): 1731-1753. doi: 10.1016/j.apt.2019.05.027
51. Kumar S, Ye F, Dobretsov S, et al. Nanocoating Is a New Way for Biofouling Prevention. Frontiers in Nanotechnology. 2021; 3. doi: 10.3389/fnano.2021.771098
52. Shi X, Tal G, Hankins NP, et al. Fouling and cleaning of ultrafiltration membranes: A review. Journal of Water Process Engineering. 2014; 1: 121-138. doi: 10.1016/j.jwpe.2014.04.003
53. Goosen MFA, Sablani SS, Al-Hinai H, et al. Fouling of Reverse Osmosis and Ultrafiltration Membranes: A Critical Review. Separation Science and Technology. 2005; 39(10): 2261-2297. doi: 10.1081/ss-120039343
54. Yuan Z, Olsson G, Cardell-Oliver R, et al. Sweating the assets – The role of instrumentation, control and automation in urban water systems. Water Research. 2019; 155: 381-402. doi: 10.1016/j.watres.2019.02.034
55. Liu R. Synthesis and Characterization of Novel Polybenzimidazoles and Post-modifications for Membrane Separation Applications. Virginia Tech; 2018.
56. Zhang R, Liu Y, He M, et al. Antifouling membranes for sustainable water purification: strategies and mechanisms. Chemical Society Reviews. 2016; 45(21): 5888-5924. doi: 10.1039/c5cs00579e
57. Mohammad AW, Teow YH, Ang WL, et al. Nanofiltration membranes review: Recent advances and future prospects.

Desalination. 2015; 356: 226-254. doi: 10.1016/j.desal.2014.10.043

58. Zhu L, Liu X, Lund R. Graduate Research and Discovery Symposium (GRADS). Clemson University; 2018.
59. He X, Hägg MB. Membranes for Environmentally Friendly Energy Processes. Membranes. 2012; 2(4): 706-726. doi: 10.3390/membranes2040706
60. Vallet-Regí M. Mesoporous Silica Nanoparticles: Their Projection in Nanomedicine. ISRN Materials Science. 2012; 2012: 1-20. doi: 10.5402/2012/608548
61. Roorda N. Fundamentals of Sustainable Development. Routledge; 2020. doi: 10.4324/9781003052517
62. Kertik A, Wee LH, Pfannmöller M, et al. Highly selective gas separation membrane using in situ amorphised metal–organic frameworks. Energy & Environmental Science. 2017; 10(11): 2342-2351. doi: 10.1039/c7ee01872j
63. Kimble MC, White RE, Tsou Y, et al. Estimation of the Diffusion Coefficient and Solubility for a Gas Diffusing Through a Membrane. Journal of The Electrochemical Society. 1990; 137(8): 2510-2514. doi: 10.1149/1.2086977
64. Lau CH, Li P, Li F, et al. Reverse-selective polymeric membranes for gas separations. Progress in Polymer Science. 2013; 38(5): 740-766. doi: 10.1016/j.progpolymsci.2012.09.006
65. Goh PS, Wong KC, Ismail AF. Nanocomposite Membranes for Liquid and Gas Separations from the Perspective of Nanostructure Dimensions. Membranes. 2020; 10(10): 297. doi: 10.3390/membranes10100297
66. Olabi AG, Onumaegbu C, Wilberforce T, et al. Critical review of energy storage systems. Energy. 2021; 214: 118987. doi: 10.1016/j.energy.2020.118987
67. Xu J, Cai X, Cai S, et al. High-Energy Lithium-Ion Batteries: Recent Progress and a Promising Future in Applications. Energy & Environmental Materials. 2023; 6(5). doi: 10.1002/eem2.12450
68. Badwal SPS, Giddey SS, Munnings C, et al. Emerging electrochemical energy conversion and storage technologies. Frontiers in Chemistry. 2014; 2. doi: 10.3389/fchem.2014.00079
69. Rashidi S, Karimi N, Sunden B, et al. Progress and challenges on the thermal management of electrochemical energy conversion and storage technologies: Fuel cells, electrolysers, and supercapacitors. Progress in Energy and Combustion Science. 2022; 88: 100966. doi: 10.1016/j.pecs.2021.100966
70. Ogungbemi E, Wilberforce T, Ijaodola O, et al. Review of operating condition, design parameters and material properties for proton exchange membrane fuel cells. International Journal of Energy Research. 2020; 45(2): 1227-1245. doi: 10.1002/er.5810
71. Jiao K, Xuan J, Du Q, et al. Designing the next generation of proton-exchange membrane fuel cells. Nature. 2021; 595(7867): 361-369. doi: 10.1038/s41586-021-03482-7
72. Wang Y, Chen KS, Mishler J, et al. A review of polymer electrolyte membrane fuel cells: Technology, applications, and needs on fundamental research. Applied Energy. 2011; 88(4): 981-1007. doi: 10.1016/j.apenergy.2010.09.030
73. de Bruijn FA, Makkus RC, Mallant RK, et al. Materials for state-of-the-art PEM fuel cells, and their suitability for operation above 100 C. Advances in fuel cells. 2007; (1): 235-336.
74. Zahid M, Savla N, Pandit S, et al. Microbial desalination cell: Desalination through conserving energy. Desalination. 2022; 521: 115381. doi: 10.1016/j.desal.2021.115381
75. Prifti H, Parasuraman A, Winardi S, et al. Membranes for Redox Flow Battery Applications. Membranes. 2012; 2(2): 275-306. doi: 10.3390/membranes2020275
76. He X, Bresser D, Passerini S, et al. The passivity of lithium electrodes in liquid electrolytes for secondary batteries. Nature Reviews Materials. 2021; 6(11): 1036-1052. doi: 10.1038/s41578-021-00345-5
77. Cunha Á, Martins J, Rodrigues N, et al. Vanadium redox flow batteries: a technology review. International Journal of Energy Research. 2014; 39(7): 889-918. doi: 10.1002/er.3260
78. Zagorodni AA. Ion exchange materials: properties and applications. Elsevier; 2006.
79. SenGupta AK. Ion exchange in environmental processes: Fundamentals, applications and sustainable technology. John Wiley & Sons; 2017.
80. Liu H, Zhang X, Xu N, et al. Progress of One-Dimensional SiC Nanomaterials: Design, Fabrication and Sensing Applications. Nanomaterials. 2024; 14(2): 187. doi: 10.3390/nano14020187
81. Zhang Y, Li L, Su H, et al. Binary metal oxide: advanced energy storage materials in supercapacitors. Journal of Materials Chemistry A. 2015; 3(1): 43-59. doi: 10.1039/c4ta04996a
82. Saikia BK, Benoy SM, Bora M, et al. A brief review on supercapacitor energy storage devices and utilization of natural carbon resources as their electrode materials. Fuel. 2020; 282: 118796. doi: 10.1016/j.fuel.2020.118796
83. Schnell J, Günther T, Knoche T, et al. All-solid-state lithium-ion and lithium metal batteries—paving the way to large-scale

production. Journal of Power Sources. 2018; 382: 160-175. doi: 10.1016/j.jpowsour.2018.02.062
84. Yan J, Li S, Lan B, et al. Rational Design of Nanostructured Electrode Materials toward Multifunctional Supercapacitors. Advanced Functional Materials. 2019; 30(2). doi: 10.1002/adfm.201902564
85. Zakrzewska-Trznadel G. Membrane processes for environmental protection: applications in nuclear technology. Nukleonika. 2006; (51): 101-111.
86. Khayet M. Treatment of radioactive wastewater solutions by direct contact membrane distillation using surface modified membranes. Desalination. 2013; 321: 60-66. doi: 10.1016/j.desal.2013.02.023
87. Liu L, Li W, Song W, et al. Remediation techniques for heavy metal-contaminated soils: Principles and applicability. Science of The Total Environment. 2018; 633: 206-219. doi: 10.1016/j.scitotenv.2018.03.161
88. Nazir A, Khan K, Maan A, et al. Membrane separation technology for the recovery of nutraceuticals from food industrial streams. Trends in Food Science & Technology. 2019; 86: 426-438. doi: 10.1016/j.tifs.2019.02.049
89. Anis SF, Hashaikeh R, Hilal N. Reverse osmosis pretreatment technologies and future trends: A comprehensive review. Desalination. 2019; 452: 159-195. doi: 10.1016/j.desal.2018.11.006
90. Sarbatly R, Sariau J, Krishnaiah D. Recent Developments of Membrane Technology in the Clarification and Concentration of Fruit Juices. Food Engineering Reviews. 2023; 15(3): 420-437. doi: 10.1007/s12393-023-09346-2
91. Davies M, Hamilton C, Murphy S, et al. Polymer membranes in clinical sensor applications: I. An overview of membrane function. Biomaterials. 1992; (13): 971-978.
92. Said N, Lau WJ, Ho YC, et al. A Review of Commercial Developments and Recent Laboratory Research of Dialyzers and Membranes for Hemodialysis Application. Membranes. 2021; 11(10): 767. doi: 10.3390/membranes11100767
93. Mostafavi AH, Mishra AK, Ulbricht M, et al. Oxygenation and membrane oxygenators: emergence, evolution and progress in material development and process enhancement for biomedical applications. Journal of Membrane Science and Research. 2021; (7): 230-259.
94. Hernandez JL, Woodrow KA. Medical Applications of Porous Biomaterials: Features of Porosity and Tissue-Specific Implications for Biocompatibility. Advanced Healthcare Materials. 2022; 11(9). doi: 10.1002/adhm.202102087
95. Radu ER, Voicu SI, Thakur VK. Polymeric Membranes for Biomedical Applications. Polymers. 2023; 15(3): 619. doi: 10.3390/polym15030619
96. Satel S. Desperately seeking a kidney. The New York Times. 2007; 16.
97. Das R, Nag S, Banerjee P. Electrochemical Nanosensors for Sensitization of Sweat Metabolites: From Concept Mapping to Personalized Health Monitoring. Molecules. 2023; 28(3): 1259. doi: 10.3390/molecules28031259
98. Pusch W, Walch A. Synthetic Membranes—Preparation, Structure, and Application. Angewandte Chemie International Edition in English. 1982; 21(9): 660-685. doi: 10.1002/anie.198206601
99. Cooley DA. Con: beating-heart surgery for coronary revascularization: is it the most important development since the introduction of the heart-lung machine? The Annals of thoracic surgery. 2000; (70): 1779-1781.
100. Sweetser S. Gastrointestinal manifestations of systemic diseases. Yamada's Textbook of Gastroenterology. Published online February 18, 2022: 2231-2273. doi: 10.1002/9781119600206.ch111
101. Oprea D, Sanz CG, Barsan MM, et al. PC-12 Cell Line as a Neuronal Cell Model for Biosensing Applications. Biosensors. 2022; 12(7): 500. doi: 10.3390/bios12070500
102. Goodman LS. Goodman and Gilman's the pharmacological basis of therapeutics. McGraw-Hill New York; 1996.
103. Herman PM, Craig BM, Caspi O. Is complementary and alternative medicine (CAM) cost-effective? a systematic review. BMC Complementary and Alternative Medicine. 2005; 5(1). doi: 10.1186/1472-6882-5-11
104. Duy Nguyen BT, Nguyen Thi HY, Nguyen Thi BP, et al. The Roles of Membrane Technology in Artificial Organs: Current Challenges and Perspectives. Membranes. 2021; 11(4): 239. doi: 10.3390/membranes11040239
105. Hafez T, Fuller B. Applications. Advances in Biopreservation. 2006: 197-270. doi: 10.1201/9781420004229.ch9.
106. Fabrizio M. Management of Challenging Cardiopulmonary Bypass Separation. National Institution of Health; 2020.
107. Salgado AJ, Oliveira JM, Martins A, et al. Tissue Engineering and Regenerative Medicine. Tissue Engineering of the Peripheral Nerve: Stem Cells and Regeneration Promoting Factors. Published online 2013: 1-33. doi: 10.1016/b978-0-12-410499-0.00001-0
108. Khan A, Alamry KA, Asiri AM. Multifunctional Biopolymers-Based Composite Materials for Biomedical Applications: A Systematic Review. ChemistrySelect. 2021; 6(2): 154-176. doi: 10.1002/slct.202003978
109. Morsada Z, Hossain MM, Islam MT, et al. Recent progress in biodegradable and bioresorbable materials: From passive

implants to active electronics. Applied Materials Today. 2021; 25: 101257. doi: 10.1016/j.apmt.2021.101257

110. Sharma A, Kokil GR, He Y, et al. Inorganic/organic combination: Inorganic particles/polymer composites for tissue engineering applications. Bioactive Materials. 2023; 24: 535-550. doi: 10.1016/j.bioactmat.2023.01.003
111. Mrzljak A, Novak R, Pandak N, et al. Emerging and neglected zoonoses in transplant population. World Journal of Transplantation. 2020; 10(3): 47-63. doi: 10.5500/wjt.v10.i3.47
112. Gao X, Han S, Zhang R, et al. Progress in electrospun composite nanofibers: composition, performance and applications for tissue engineering. Journal of Materials Chemistry B. 2019; 7(45): 7075-7089. doi: 10.1039/c9tb01730e
113. Yusuf A, Sodiq A, Giwa A, et al. A review of emerging trends in membrane science and technology for sustainable water treatment. Journal of Cleaner Production. 2020; 266: 121867. doi: 10.1016/j.jclepro.2020.121867
114. Gkotsis P, Banti D, Peleka E, et al. Fouling Issues in Membrane Bioreactors (MBRs) for Wastewater Treatment: Major Mechanisms, Prevention and Control Strategies. Processes. 2014; 2(4): 795-866. doi: 10.3390/pr2040795
115. Aristizábal SL, Lively RP, Nunes SP. Solvent and thermally stable polymeric membranes for liquid molecular separations: Recent advances, challenges, and perspectives. Journal of Membrane Science. 2023; 685: 121972. doi: 10.1016/j.memsci.2023.121972
116. Karki S, Hazarika G, Yadav D, et al. Polymeric membranes for industrial applications: Recent progress, challenges and perspectives. Desalination. 2024; 573: 117200. doi: 10.1016/j.desal.2023.117200
117. Goh PS, Matsuura T, Ismail AF, et al. Recent trends in membranes and membrane processes for desalination. Desalination. 2016; 391: 43-60. doi: 10.1016/j.desal.2015.12.016
118. Ghafoori S, Omar M, Koutahzadeh N, et al. New advancements, challenges, and future needs on treatment of oilfield produced water: A state-of-the-art review. Separation and Purification Technology. 2022; 289: 120652. doi: 10.1016/j.seppur.2022.120652
119. Liu G, Jin W, Xu N. Graphene-based membranes. Chemical Society Reviews. 2015; 44(15): 5016-5030. doi: 10.1039/c4cs00423j
120. Ismail AF, Padaki M, Hilal N, et al. Thin film composite membrane—Recent development and future potential. Desalination. 2015; 356: 140-148. doi: 10.1016/j.desal.2014.10.042
121. Han Z yang, Huang L jun, Qu H jiao, et al. A review of performance improvement strategies for graphene oxide-based and graphene-based membranes in water treatment. Journal of Materials Science. 2021; 56(16): 9545-9574. doi: 10.1007/s10853-021-05873-7
122. Sabih Q, Naveed R, Waqas A. Graphene dispersion, functionalization techniques and applications: A review. Synthetic Metals. 2024; 307: 117697-117710. doi: 10.1016/j.synthmet.2024.117697

EnPress Publisher, LLC

Add: 9650 Telstar Avenue, Unit A, Suite 121, El Monte, CA 91731, USA.
Email: contact@enpress-publisher.com
Web: https://systems.enpress-publisher.com

ISSN 2578-1855
9 772578 185076 02